Amphiphilic and Random Copolymers: Self Assembly and Application in Drug Delivery Formulations

DISSERTATION
SUBMITTED TO THE FACULTY OF
UNIVERSITY OF MINNESOTA, TWIN CITIES
BY

Swapnil Tale

IN PARTIAL FULFILLMENT OF THE REQUIREMENTS
FOR THE DEGREE OF
DOCTOR OF PHILOSOPHY
IN
CHEMISTRY

Advisor: Theresa M. Reineke

Acknowledgements

Today, I gratefully thank my respected and admirable advisor Prof. Theresa M. Reineke, for her guidance, critical suggestions and comments, timely encouragement, and her unlimited patience throughout my research work. She not only helped me to think scientifically but also taught me a systematic approach to solve problems. She is very open-minded, passionate about her group, and always ready to help her students. She granted me permission to explore different areas of chemistry to broaden my horizon, which really helped to learn new skills and pursue areas of science I am passionate about. It's been a great learning experience at University of Minnesota and I will truly miss all of the group members.

I express my gratitude to Prof. Marc Hillmyer, Prof. Frank Bates, and Prof. Timothy Lodge for all their suggestions, questions, and comments at monthly Dow meetings. I also extend my thankfulness to the Dow Team for their ideas and fun times that we all shared together. In particular, I would like to thank Dr. Ligeng Yin for teaching me different analytical techniques and providing me with PEP-CTA.

I wish to convey my sincere thanks to Dr. Steve Guillaudeu, Dr. Li Guo, Dr. Bob Schmitt, Tom Jurek, Sara Oueland, and Dr. Trey Porter at The Dow Chemical Company for helpful discussions and feedback, which really helped me to excel in my projects.

A special thanks to all staff members, non-teaching staff, technicians for maintaining all instruments in working conditions, librarians, all students in the Polymer

Group at the University of Minnesota for their help, fun times, and support, which helped me to finish my thesis.

I also thank my wife, Shivani Mete, my parents, my brother, my parents-in-law and all my friends for their continuous support and love during my doctorate degree. Shivani was always there when I needed her. She is been very supportive about my career and always encouraged me to follow my dreams. I never talk chemistry with her since she does not understand it ☹. However, few times she makes me learn computer programming. I am really excited for the next phase of my life. This thesis is dedicated to my wife, parents, and all my close friends.

Abstract

One of the biggest challenges in the field of drug delivery is the development of a system that can deliver cargo to a specific organ or cell and improve the aqueous solubility of poorly water soluble drugs. Recently, amphiphilic and random polymers have attracted considerable attention from researchers in order to elucidate these issues. Amphiphilic polymers consist of both hydrophilic and hydrophobic segments. Amphiphilic polymers are not only limited to drug delivery applications but also have utility in products such as food, detergents, paints, and cosmetics etc. Random copolymers consist of two or more monomers, the chain can add these monomers in any order. The incorporation on monomers into chain based on numerous factors such as conditions used for polymerization, reactivity of one monomer towards another etc. which can follow order depend on reactivity of one monomer towards another. Random polymers are continuously finding applications in the formulation industry due to their ability to improve aqueous solubility of poorly water soluble drugs. This thesis highlights my work on 1) the self-assembly of amphiphilic polymers to form micelles, 2) the application of micelles in pharmaceutical formulation, 3) the use of amphiphilic polymers as excipients, and 4) the use of random copolymers to enhance aqueous solubility of model drugs. Initial efforts are focused on amphiphilic polymers to leverage their ability to form micelles, and study the effects of micelles in pharmaceutical formulations. Toward this end, we synthesized trehalose-containing amphiphilic diblock terpolymers with increasing trehalose content in the hydrophilic segment of the terpolymers. A poly(ethylene-alt-propylene)–poly[(N,N-dimethylacrylamide)-*grad*-poly(6-deoxy-6-methacrylamido trehalose)] (PEP-P(DMA-*g*-

MAT)) polymer was chosen as a model system. The PEP content of the system was deliberately kept low to trigger formation of micelles in solution. PEP-P(DMA-*g*-MAT) successfully self-assembled into micelles in water. When incubated in various salt and serum-containing media, these micelles exhibited excellent stability from aggregation. Due to their excellent stability, these nanocarriers can be further optimized for potential systemic drug delivery applications. To further expand our work on micelles, we studied role of solution state polymer assemblies (prior to spray drying) on drug dissolution and supersaturation maintenance of poorly water soluble drugs. Herein, we synthesized four model polymer excipients (amphiphilic diblock ter- and copolymers): PEP-P(DMA-grad-MAG) and PEP-PDMA, and their respective hydrophilic analogues, P(DMA-grad-MAG) and PDMA. Our study confirmed that formation of micelles prior to spray drying enhanced the dissolution of poorly water soluble drugs. Therefore, using micelle structures in excipient formulations is a simple and controlled platform for oral drug delivery. To study effect of hydrogen bonding in excipient formulations, we decide to explore a new synthetic platform with Trehalose-based diblock terpolymers to increase the solubility of poorly water soluble drug candidates. This study reveals that the solubility of polymer matrices in dissolution media and increase in hydrogen bonding sites in polymer matrices are critically important to decrease drug crystallinity & maintaining super saturation concentration in dissolution media. The diblock copolymers synthesized so far failed to enhance solubility of a highly lipophilic drug, phenytoin. In our quest for finding right excipient for phenytoin, we synthesized random copolymers of poly(*N*-isopropylacrylamide-*co*-vinylpyrrolidone) (P(NIPAAm-*co*-VP)). The results of this study indicate that balance between the VP and

NIPAAm content is key to improve phenytoin solubility. We also proposed that it is essential to incorporate similar chemical groups in the polymer backbone that are also present in drug molecular structure, which can interfere with the drug crystallization mechanism. Finally, we developed a systematic approach to understand structure-property relationships between drugs and excipients. In this study, we synthesized libraries of random copolymer of poly(*N*-isopropylacrylamide-*co*-*N*,*N*-dimethylacrylamide) P(NIPAAm-co-DMA) with varying mole ratios and molecular weights. This study illustrates that the first step to design a new excipient for a drug is to study the crystallization mechanism of that drug. When the drug crystallization mechanism is known, it is necessary to incorporate groups in the excipient formulation that can interact and interfere with the drug crystallization process to increase and maintain its aqueous solubility.

Table of Contents

List of Tables

List of Figures

1 Background

1.1 Challenges in drug delivery

Contrary to popular belief, developing a potent and non-toxic drug molecule doesn't translate into a cure.[1] A majority of free drug molecules cannot be delivered directly to humans, animals, or plants.[2,3] The most fundamental challenges to drug delivery are solubility of the drug in aqueous media, degradation of the drug molecule prior to reaching the target tissue, and undesired side effects caused by non-specific uptake.[3,4] A common example of a targeted drug is aspirin, which has an irritant effect on the stomach and is coated with a polymer that will only dissolve in the small intestine. This delivery formulation allows the release of active ingredient aspirin only in the small intestine. Development of an appropriate drug delivery method is of paramount importance to overcome the barriers associated with the transport of a free drug.[5] Drug delivery can be defined as a process or method of administering a pharmaceutical compound to humans, animals, or plants in order to achieve a desired therapeutic effect. At the heart of any drug delivery system is a carrier, which encapsulates, entraps, or is covalently attached to a drug molecule, and alleviates problems such as poor water solubility and enzymatic degradation of the free drug.[6]

Additionally, the vast majority of newly discovered active pharmaceutical ingredients (APIs) today are poorly water-soluble and consequently, limited in bioavailability for intended therapeutic targets. In drug discovery, it takes approximately 12-15 years to bring a new drug to the market. The statistics says that of about every 20,000 compounds tested on animals, 10 get approved for clinical trials out of which one enters into the market (see Figure 1.1).[7] This data indicates that drug discovery is a painful and

arduous process. Therefore, the use of polymeric excipients/carriers to increase drug solubility and bioavailability is of great importance across the pharmaceutical industry.

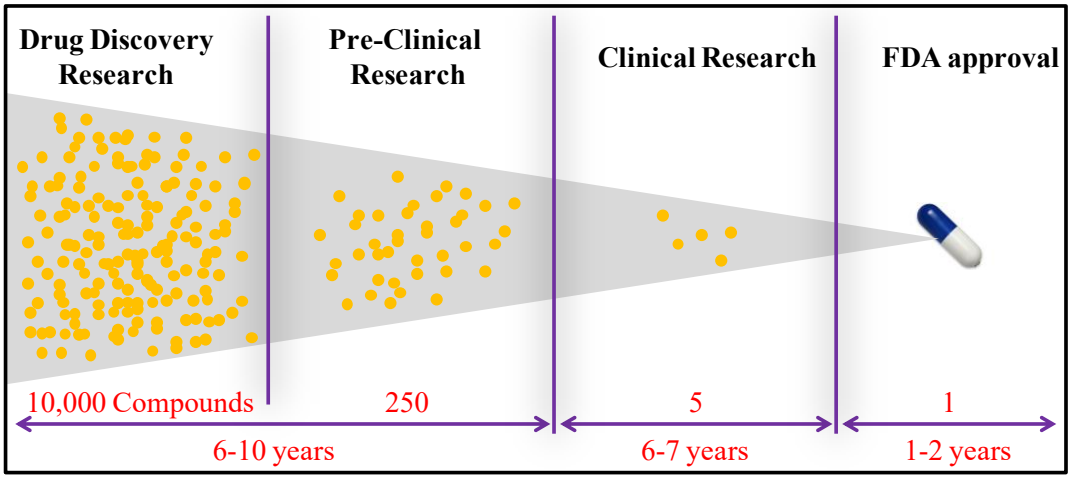

Total
Cost: $800 million - $1 billion
Time: 13-20 years

Figure 1.1 The drug discovery process and barriers to FDA approval.

Commonly used drug carriers include microspheres,[8] hydrogels,[9] surfactants, cyclodextrins,[10] amphiphilic polymer-based micellar systems,[11] liposomes,[12] and amorphous solid dispersions.[13] The combination of these carriers with drugs can often be adapted into an appropriate dosage form (e.g. pill, tablet, capsule), depending on the route of administration (e.g. oral, intravenous). The route of administration depends on the systemic pharmacokinetics of the drug delivery system such as targeting concerns or time required for the onset action and stability of the drugs.[14] In addition, systems can be developed for controlled or targeted delivery of the drug. To overcome severe side effects of drugs such as hair loss, immune reactions and cardiovascular problems, scientists are trying to optimize targeted drug delivery vehicles in order to provide controlled doses to patients at specific biological sites.[15]

1.2 Drug Delivery Systems

1.2.1 Cyclodextrin Polymers

Cyclodextrins are cyclic oligosaccharides that are commonly used as drug carriers due to their ability to improve the solubility and bioavailability of a drug by forming an inclusion complex.[16,17] Cyclodextrin structures with 6, 7, or 8 glucose units are subsequently named α-, β-, or γ-cyclodextrin, respectively. These compounds are biocompatible and non-toxic. β-Cyclodextrin in particular has several advantages in drug delivery applications since its exterior is hydrophilic and its interior is a hydrophobic cavity which has the ability to encapsulate drugs. While β-cyclodextrin forms inclusion complexes with aromatic molecules such as paclitaxel,[18] this molecule also has affinity towards cholesterol and can extract it from cells. β-cyclodextrin has a lower solubility in water because of the secondary hydrogen bonding which makes it difficult for parenteral administration. However, high dosing rates of β-cyclodextrin can result in the hemolysis of erythrocytes.[18] Figure 1.2 shows how cyclodextrins form complexes with drugs.

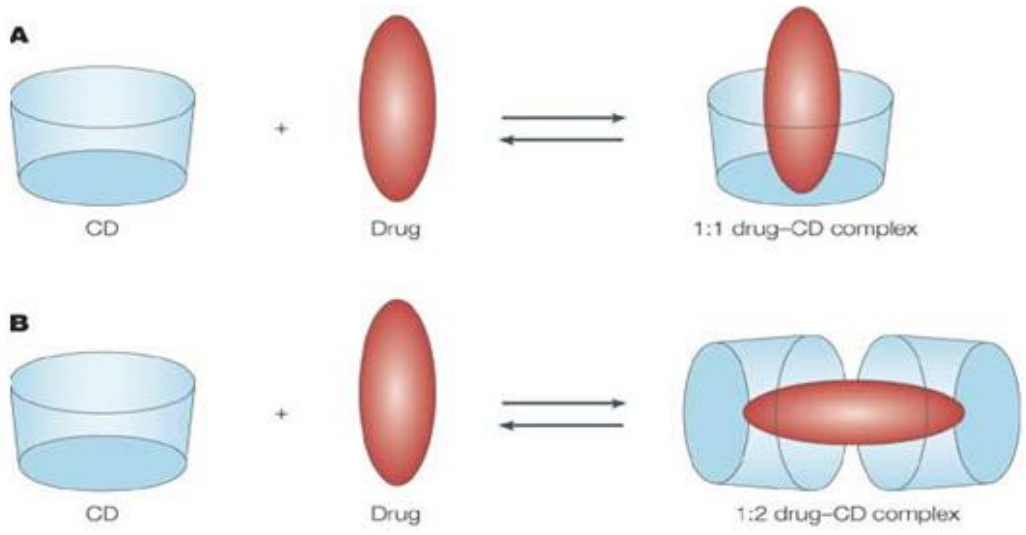

Figure 1.2 Cyclodextrins forming complexes with drugs adapted from Davis, M. E.; Brewster, M. E. *Nat. Rev. Drug Discov.* 2004, *3*, 1023-1035.[18]

1.2.2 Amphiphilic polymers

The use of amphiphilic block copolymers, which are known to assemble into micelles in aqueous solutions are of high interest for drug delivery applications. Micelles exhibit core-shell morphologies with diameters typically between 20 and 50 nm and usually consist of several hundred block copolymers. The densely packed core consists of hydrophobic blocks and the shell consists of hydrophilic blocks.[11,19] Utilizing techniques such as nanoprecipitation or direct dissolution, a poorly water-soluble drug can be entrapped in the core of micelles. This system allows the delivery of poorly water-soluble drugs in desired quantities.[20] The outer hydrophilic block (corona) not only protects the contents of the micelle core against hydrolysis and enzymatic degradation,[21] but also can serve as a targeting ligand to specific receptors; for example, if the hydrophilic block contains D-galactose or N-acetyl-D-galactosamine moieties, the polymer can target the asialoglycoprotein receptors on hepatocytes.[22,23] The corona may also mask the micelles from the reticuloendothelial system (RES), thereby preventing their early elimination from the body. RES system is a network of cells throughout the body that assist to eliminate foreign particles & toxic substances from the body. Functionalizing the block copolymers with crosslinkable groups can further enhance the stability of the micelles.[24] The drawbacks of using polymer-based micelles as drug carriers include non-specific interactions with serum proteins, aggregation, and clearance by the reticuloendothelial system (RES).[25] Therefore, the stability of micelles in serum-containing media is vitally important. Unfortunately, aggregation or thermodynamic instability of micelles *in vivo* can trigger the premature release of the drug and lead to side effects. Therefore, it is important to exhaustively study the stability of micelles *in vitro* prior to performing animal studies.[26]

Poly(ethylene oxide) (PEO)-based amphiphilic polymers have been exhaustively studied as micelle precursors for the design of non-immunogenic carriers.[27] The corona of these micelles is composed of a dense brush of hydrophilic PEO, which has been shown to prevent aggregation, protein absorption, and cellular adhesion. PEO nanoparticles exhibit a drastic increase in blood circulation time, higher stability of formulation upon storage, and reduced renal filtration. Additionally, PEO is soluble in both organic and aqueous solvents, making it an ideal candidate for chemical functionalization.[28,29] For example, poly(ethylene glycol) methyl ether can be converted into a trithiocarbonate-based chain transfer agent, which can then be applied toward reversible addition fragmentation chain transfer (RAFT) polymerization.[30] Unfortunately, PEO-based nanoparticles do not have a well-characterized biodegradation pathway,[31] and in some cases have caused hypersensitive reactions upon oral, dermal, and intravenous administration. For these reasons, alternative polymers that stabilize colloidal particles from aggregation are of strong interest to the biomaterials community. Irrespective of the composition of the corona and the core of the micelle, it is important to understand the concepts related to micelle stability, drug loading, and the release of the drug from micellar complexes.[32,33]

1.2.3 Amorphous Solid Dispersions

Amorphous solid dispersions (ASD) have been developed as a platform to increase apparent drug solubility and bioavailability using polymeric excipients. This type of dispersion refers to solid mixtures consisting of at least two components, a polymer matrix and a drug.[34] In ASDs, the drugs are kinetically trapped in a high-energy amorphous state, which increases the drug bioavailability and therapeutic effect. However, the drug may recrystallize, reverting to the more thermodynamically stable state, which negates any

solubility increase and significantly decreases bioavailability. Stabilization of the amorphous state of the drug during the manufacturing process and long-term storage are critical issues in improving oral therapeutic efficacy. These issues are typically solved by reducing molecular mobility through the utilization of a polymer exhibiting a high glass transition temperature (T_g), optimizing drug-polymer interactions (such as hydrogen bonding and van der Waals), and creating a homogenous mixture of drug and polymer. Further, it is of equal importance to utilize an excipient that will solubilize the drug upon dissolution into aqueous media and maintain drug supersaturation by inhibiting crystal nucleation and growth, which is of particular importance for enhancing *in vivo* pharmaceutical performance. Several commercial examples of pharmaceutical products that use the solid dispersion method to enhance the solubility of APIs are shown in Table 1.1.[17]

Table 1.1 Commercially available examples of solid dispersions.

Drug	Polymer Excipients
Itraconazole	Hydroxypropyl methylcellulose (HPMC)
Telaprevir	Hydroxypropyl methylcellulose acetate succinate (HPMCAS)
Ritonavir	Copolymers of vinylpyrrolidone (VP)/vinyl acetate (VA) (PVPVA)
Griseofulvin	Polyethylene glycol (PEG)

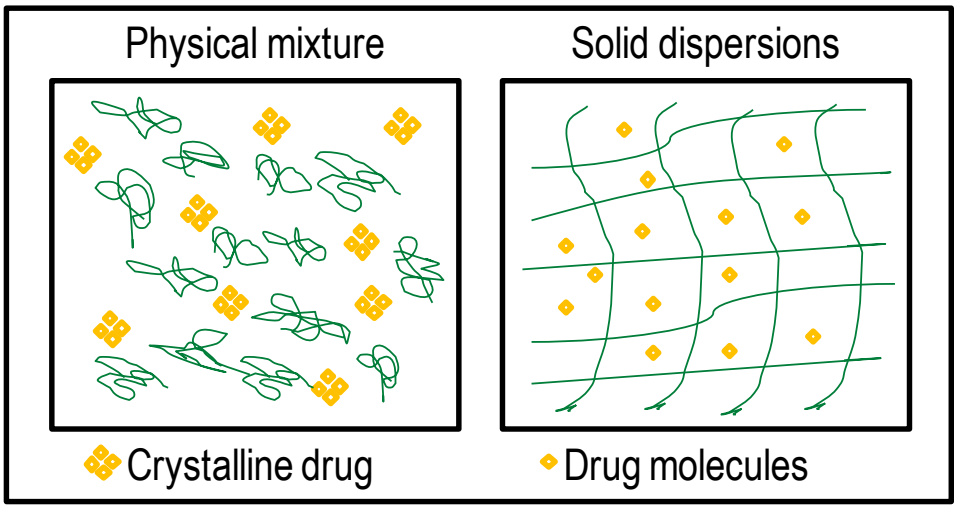

Figure 1.3 Cartoon illustrating the differences between physical mixtures and amorphous solid dispersions of drugs and polymers.

1.2.4 Hydroxypropyl methylcellulose acetate succinate (HPMCAS)

The polymer matrix plays an important role in determining the performance of an amorphous dispersion (ASD) in bulk and in solution. The polymer matrix also dictates shelf life stability and is responsible for enhancing bioavailability.[34] Hydroxypropyl methyl cellulose acetate succinate (HPMCAS) is one of the top performing excipients on the market for increasing the solubility of crystalline hydrophobic drugs in aqueous solution.[35-38] The superior performance of HPMCAS in ASDs is attributed to its multifunctional molecular structure. HPMCAS is a cellulosic ether of mixed esters. It contains two esters, acetate (Ac) and succinate (Su), and two ethers, methoxy (MeO) and hydroxypropoxy (HPO). It is believed that HPMCAS tends to form nanoaggregates during the dissolution process, which are hypothesized to aid in the supersaturation maintenance of the drug.[37,39] Friesen and coworkers believe that hydrophobic drug molecules interact with the hydrophobic portions (acetate) of the polymer, inducing the formation of nanoaggregates. The hydrophilic portions (unreacted hydroxyls) are then likely exposed on the surface, yielding a pseudo micelle-like structure and allowing the aggregates to remain stable in

aqueous media.[35] However, it is difficult to understand the role of each functional group of HPMCAS due to the excipient's extremely complicated structure.

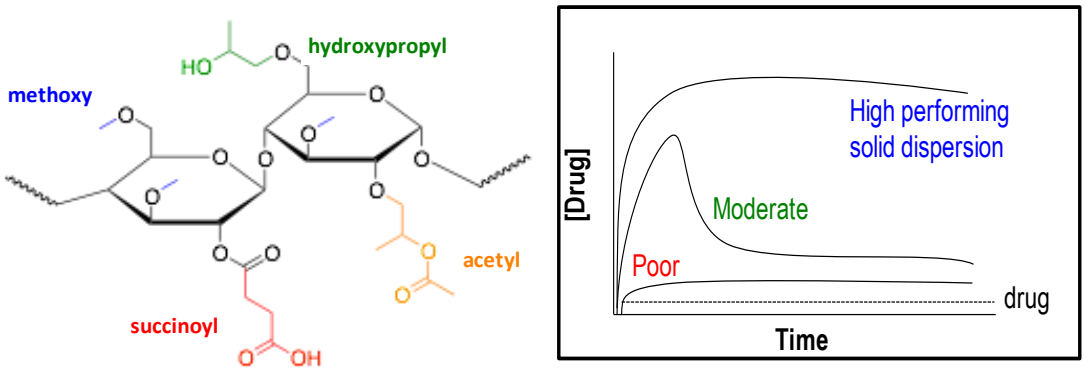

Figure 1.4[35-38] Structure of HPMCAS and example graph of the dissolution profiles of solid dispersions.

1.3 Methods to prepare amorphous solid dispersions

Numerous reports have been published in the literature on preparation methods for solid dispersions. However, three methods have been primarily used to obtain solid dispersions that can enhance bioavailability of poorly water-soluble drugs. [34-36]

1.3.1 Fusion Method

The fusion method for preparing solid dispersions is based on the melting of a physical mixture at its eutectic composition. The eutectic composition is chosen to obtain simultaneous crystallization of drug and matrix during cooling. This was the first method ever to be used for preparing solid dispersions for pharmaceutical applications. The first dispersion consisted of sulfathiazole in a urea matrix.[33] The drug may be molecularly dissolved in the solid excipient matrix (solid solution), or dispersed as crystalline or amorphous particles (solid dispersion). If dissolved, the API could, in principle, be miscible with the excipient over the entire composition range. However, in practice the API and excipients are miscible over a limited range, as illustrated by the phase diagram in Figure

1.5. The eutectic composition has the lowest melting point, called the eutectic temperature, and the eutectic point is at the intersection of the eutectic composition and the eutectic temperature in the phase diagram. Examples of polymers used as excipients include poly(ethylene glycol) (PEG) and poly(vinyl pyrrolidone) (PVP). The experimental technique employed and the type of solid dispersion formed depends on the excipient and drug. For example, polyethylene glycols melt at 70 °C and are hydrophilic polymers; in this case, the drug amalgamates as individual molecules in the helices of crystalline PEG. On the other hand, PVP that is supplied in the amorphous state needs to be heated above its glass transition temperature (T_g). The drug needs to be fused or dissolved in the rubbery matrix, which is subsequently cooled to vitrify the solid dispersion. The nature of the drug dispersion depends on the polymer-drug miscibility and the method of preparation.

The fusion method, although popular, has its share of drawbacks. The most obvious disadvantage is the use of temperature-sensitive drugs. For example PVP needs to be heated to 170 °C in order to convert a glassy PVP into rubbery PVP. Most of the drugs are degradable at this temperature. Therefore, polyethylene glycols are popular as they melt at a moderate 70 °C. The second major disadvantage is that the method can only be applied if the drug and matrix mix well at the heating temperature. If the drug and polymer are immiscible, this leads to the formation of a biphasic system or suspension, which ultimately results in an inhomogeneous solid dispersion. This issue can sometimes be addressed by the use of a surfactant. Similarly, the problem of immiscibility can also arise during the cooling cycle.

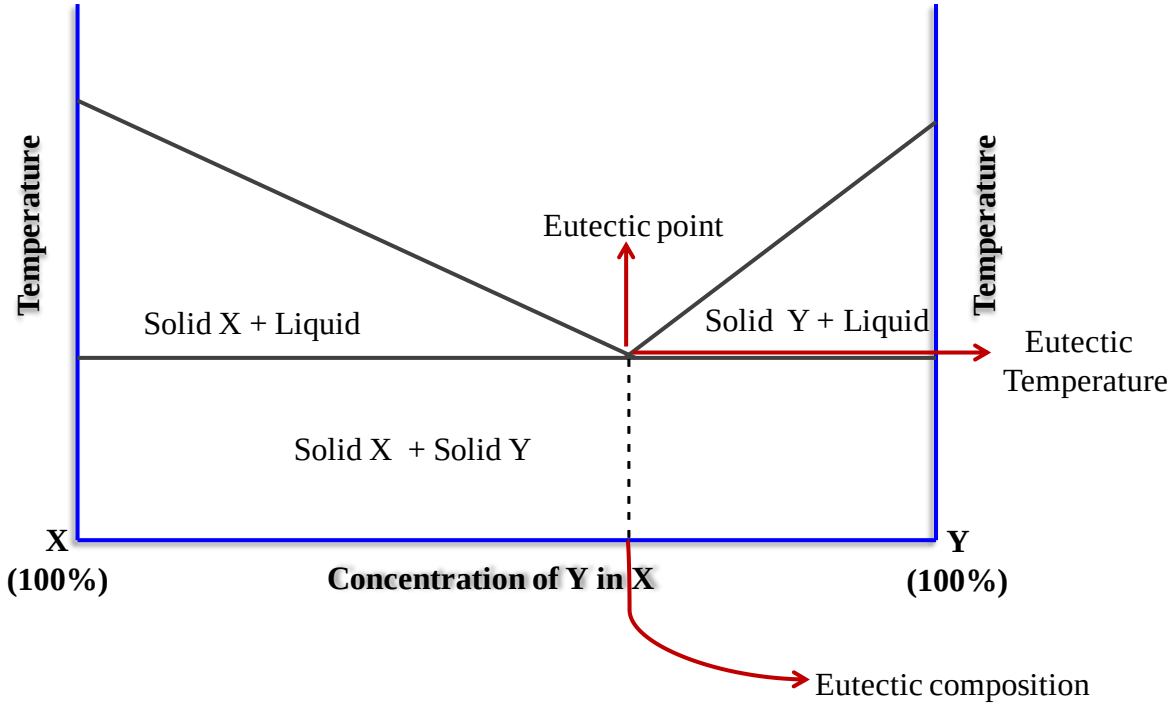

Figure 1.5 Phase diagram illustrating the eutectic composition, point, and temperature of a binary mixture.

1.3.2 Hot Melt Extrusion (HME)

HME is the most extensively used process in the plastic, rubber, and food industries. This method is used to prepare plastic bags, foams, and pipes. Recently, HME has been applied to the formulation of active pharmaceutical ingredients (APIs) with polymers to enhance API bioavailability. Typically, HME consist of an extruder containing one or two rotating screws which conveys material (mix of polymer and API) down the extruder. Single screw extruders are usually used to melt and transport polymers into continuous shapes. Twin screw extrusion technology is widely used to create melt-mix of polymers with additional materials such as APIs. Therefore, twin screw extrusion technology is largely utilized in the pharmaceutical industry which demands uniformly distributed APIs in polymers to improve the dissolution rate. The material is melted using

frictional heating (rotation between the twin screws and between the screws and wall) in the extruder as the material is conveyed down the barrel. This leads to homogenous mixing of APIs with polymer. Several examples of FDA-approved products developed using the HME process are shown in Table 1.2. [33, 34]

Table 1.2 Examples of FDA-approved products developed using the HME process.

Product Name	API	Polymer Matrix	Year of approval
Kaletra	Ritonavir	PVPVA	2005
Onmel	Itraconazole	HPMC	2010

1.3.3 Spray drying

Spray drying is the widely accepted process to prepare spray dried dispersions (SDDs) from a feed solution in the food and pharmaceutical industries. The feed solution can be a liquid slurry, solutions, suspensions, or emulsions. Spray drying has gained considerable attention in research and development due to its ability to make a consistent particle size distribution and morphology in a one step process. Ideal spray dried dispersions in the pharmaceutical industry are mixtures of drug molecularly dispersed in polymer matrix. The first step of this process involves dissolving drug and polymer in an organic solvent and spray drying this solution using a spray dryer. This technique is based on the principle of rapid evaporation of solvents from small droplets, permitting inadequate time for crystallization or phase separation. The drug molecules are kinetically trapped in the polymer matrix, which results in long term stability of SDDs.

A conventional laboratory-scale mini spray dryer is typically composed of the following key components (see Figure 1.6):

1. *Feed system* – Syringe Pump

2. *Hot air or gas inlet* – Nitrogen or air is used as a heating source
3. *Atomizer or spray nozzle* – Pressure spray nozzle
4. *Drying Chamber* – Cylindrical in shape

During the spray drying process, the feed solution is pumped into the spray nozzle using the feed system. The atomizer or spray nozzle then atomizes liquid feed solution into a spray of fine droplets in a drying chamber, which is provided with hot air or a heated gas stream. The purpose of the atomizer is to create a high surface area for faster evaporation rates and to produce particles with a consistent size distribution. The smaller droplets create large surface area, which is better for thermal efficiency of the spray dryer. The drying chamber is generally cylindrical in shape. In the drying chamber, a huge amount of heat and mass transfer takes place within a short period of time. The small droplets are exposed to the hot air/gas stream for a very short period of time, the solvents are evaporated, and the cooled particles are collected from the bottom of the drying chamber.

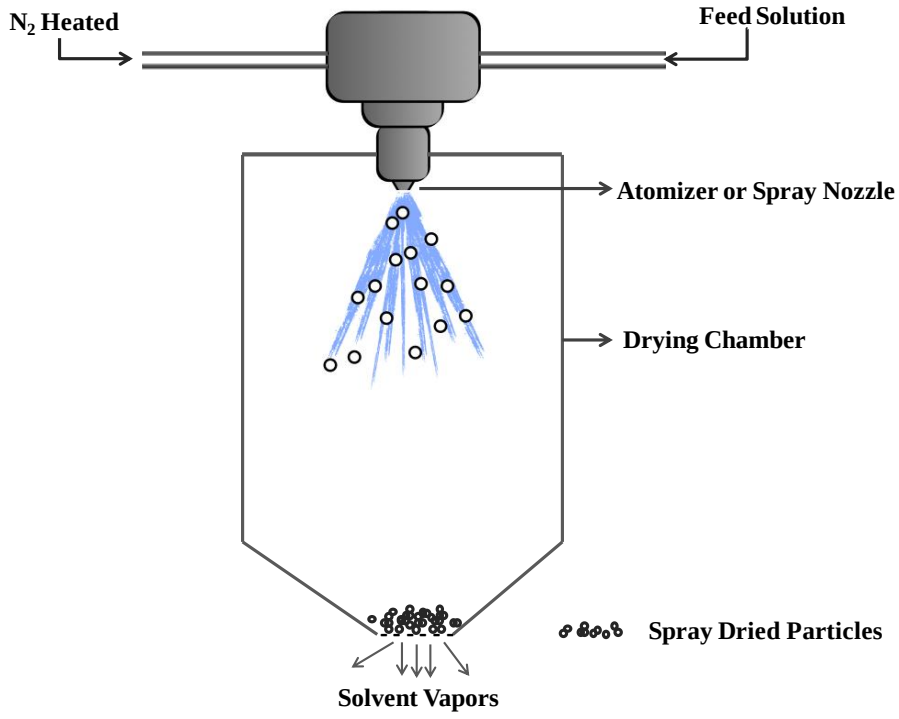

Figure 1.6 Cartoon of laboratory scale mini spray drying system.

Table 1.3 FDA-approved medicines prepared using the spray drying method.[34]

Product Name	API	Polymer Matrix	Year of approval
Sporanox	Itraconazole	HPMC	1992
Intelence	Etravirine	HPMC	2008
Incivek	Telaprevir	HPMCAS	2011
Kalydeco	Ivacaftor	HPMCAS	2012

Spray drying equipment is available in different scales starting from the lab scale (mg) to commercial scale (metric tons of SDDs). The milligrams scale mini spray dryer is ideal for early stage testing of SDDs as it requires a lower amount of drug and polymer. Additionally, spray drying is ideal for heat-sensitive active pharmaceutical ingredient (APIs) due to its relatively short exposure time to high heat during the manufacturing of amorphous solid dispersions. Most of the APIs are soluble in volatile organic solvents; therefore spray drying is more applicable for broader chemical space.

1.4 References

(1) Silverman, R. B. *The Organic Chemistry of Drug Design and Drug Action*; Second Edition ed.

(2) Watt, A.; Morrison, D. *Drug Discov. Today* **2001**, *6*, 290-292.

(3) Khanna, I. *Drug Discov. Today* **2012**, *17*, 1088-1102.

(4) Jain, K. K. *Curr. Opin. Mol. Ther.* **2006**, *8*, 487-492.

(5) Guido, R. V.; Oliva, G.; Andricopulo, A. D. *Comb. Chem. High Throughput Screen.* **2011**, *14*, 830-839.

(6) Mudshinge, S. R.; Deore, A. B.; Patil, S.; Bhalgat, C. M. *Saudi Pharm. J.* **2011**, *19*, 129-141.

(7) Gupta, S.; Kesarla, R.; Omri, A. *ISRN Pharm.* **2013**, *2013*, 848043.

(8) Davis, S. S.; Illum, L. *Biomaterials* **1988**, *9*, 111-115.

(9) Kim, S. W.; Bae, Y. H.; Okano, T. *Pharmaceut. Res.* **1992**, *9*, 283-290.

(10) Uekama, K.; Otagiri, M. *Crit. Rev. Ther. Drug Carrier Syst.* **1987**, *3*, 1-40.

(11) Kwon, G. S.; Okano, T. *Adv. Drug Deliv. Rev.* **1996**, *21*, 107-116.

(12) Torchilin, V. P. *Nat. Rev. Drug Discov.* **2005**, *4*, 145-160.

(13) Lee, T. W.; Boersen, N. A.; Hui, H. W.; Chow, S. F.; Wan, K. Y.; Chow, A. H. *Curr. Pharm. Des.* **2014**, *20*, 303-324.

(14) Jitendra; Sharma, P. K.; Bansal, S.; Banik, A. *Indian J. Pharm. Sci.* **2011**, *73*, 367-375.

(15) Siepmann, J.; Siepmann, F. *J. Control. Release* **2012**, *161*, 351-362.

(16) Brewster, M. E.; Loftsson, T. *Adv. Drug Deliv. Rev.* **2007**, *59*, 645-666.

(17) Williams, H. D.; Trevaskis, N. L.; Charman, S. A.; Shanker, R. M.; Charman, W. N.; Pouton, C. W.; Porter, C. J. *Pharmacol. Rev.* **2013**, *65*, 315-499.

(18) Davis, M. E.; Brewster, M. E. *Nat. Rev. Drug Discov.* **2004**, *3*, 1023-1035.

(19) Jones, M. C.; Leroux, J. C. *Eur. J. Pharm. Biopharm.* **1999**, *48*, 101-111.

(20) Xu, W.; Ling, P.; Zhang, T. *J. Drug Deliv.* **2013**, *2013*, 15.

(21) Jhaveri, A. M.; Torchilin, V. P. *Front. Pharmacol.* **2014**, *5*, 77.

(22) Wu, Y. T.; Jiaang, W. T.; Lin, K. G.; Huang, C. M.; Chang, C. H.; Sun, Y. L.; Fan, K. H.; Hsu, W. C.; Wang, H. E.; Lin, S. B.; Chen, S. T. *Curr. Drug Deliv.* **2004**, *1*, 119-127.

(23) Kim, S. H.; Goto, M.; Akaike, T. *J. Biol. Chem.* **2001**, *276*, 35312-35319.

(24) Tiwari, G.; Tiwari, R.; Sriwastawa, B.; Bhati, L.; Pandey, S.; Pandey, P.; Bannerjee, S. K. *Int. J. Pharm. Investig.* **2012**, *2*, 2-11.

(25) van Vlerken, L. E.; Vyas, T. K.; Amiji, M. M. *Pharmaceut. Res.* **2007**, *24*, 1405-1414.

(26) Ahmad, Z.; Shah, A.; Siddiq, M.; Kraatz, H. B. *R. Soc. Chem. Adv.* **2014**, *4*, 17028-17038.

(27) Lavasanifar, A.; Samuel, J.; Kwon, G. S. *Adv. Drug Deliv. Rev.* **2002**, *54*, 169-190.

(28) Kadajji, V. G.; Betageri, G. V. *Polymers* **2011**, *3*, 1972-2009.

(29) Osada, K.; Christie, R. J.; Kataoka, K. *J. R. Soc. Interface* **2009**, *6 Suppl 3*, S325-339.

(30) Zhao, W.; Gody, G.; Dong, S. M.; Zetterlund, P. B.; Perrier, S. *Polym. Chem.* **2014**, *5*, 6990-7003.

(31) Zhang, N.; Wardwell, P. R.; Bader, R. A. *Pharmaceutics* **2013**, *5*, 329-352.

(32) Knop, K.; Hoogenboom, R.; Fischer, D.; Schubert, U. S. *Angew. Chem. Int. Ed.* **2010**, *49*, 6288-6308.

(33) Hatakeyama, H.; Akita, H.; Harashima, H. *Biol. Pharm. Bull.* **2013**, *36*, 892-899.

(34) Huang, Y.; Dai, W. G. *Acta Pharm. Sin. B* **2014**, *4*, 18-25.

(35) Friesen, D. T.; Shanker, R.; Crew, M.; Smithey, D. T.; Curatolo, W. J.; Nightingale, J. A. *Mol. Pharm.* **2008**, *5*, 1003-1019.

(36) Konno, H.; Handa, T.; Alonzo, D. E.; Taylor, L. S. *Eur. J. Pharm.Biopharm.* **2008**, *70*, 493-499.

(37) Curatolo, W.; Nightingale, J. A.; Herbig, S. M. *Pharmaceut. Res.* **2009**, *26*, 1419-1431.

(38) Tajarobi, F.; Larsson, A.; Matic, H.; Abrahmsen-Alami, S. *Eur J Pharm Biopharm* **2011**, *78*, 125-133.

(39) Ilevbare, G. A.; Liu, H. Y.; Edgar, K. J.; Taylor, L. S. *Cryst. Growth Des.* **2012**, *12*, 3133-3143.

2 CHAPTER TWO

Trehalose-functionalized block copolymers form serum-stable micelles

Adapted from:

Tale S. R.; Yin L.; Theresa T.M., Trehalose-functionalized block copolymers form serum-stable micelles, *Polym. Chem.* **2014**, 5, 5160-5167.

This work was a joint venture by this author who is responsible for synthesis and characterization of TMS-MAT, Trehalose-functionalized block copolymers, formation of micelles, characterization and data analysis of micelles by DLS. Ligeng Yin synthesized PEP-CTA as a hydrophobic component of the block copolymer systems and responsible for cryo-TEM images.

2.1 Introduction

Amphiphilic block copolymers are known to assemble into micelles that are of high interest for actives delivery applications. For example, micellar systems aid in improving the aqueous solubility of hydrophobic drugs via encapsulation within the micelle core.[1] For systemic delivery, the payload must be transported intact to the target site. For tumors, one method is via passive targeting known as the enhanced permeability and retention (EPR) effect.[2,3] While in circulation, polymer-based micelle carriers encounter numerous biological barriers. Therefore, *in vivo* delivery systems should possess hydrophilic regions that shield their payload from non-specific interactions with serum proteins, aggregation, and clearance by the reticuloendothelial system (RES) to increase circulation lifetime.[4] Polymeric micelles can also lose their payload upon dilution. Biologically, premature release and aggregation can provoke severe side effects, including an acute immunological response,[5] signifying the need to examine the stability and aggregation behavior of micelles *in vitro*.[6]

Polyethylene glycol (PEG) is a widely studied polymer for the design of non-immunogenic carriers. A PEG hydrophilic shell has been shown to prevent aggregation and RES clearance of micelle-based carriers.[7] PEGylated nanoparticles exhibit a drastic increase in blood circulation time, higher stability of formulation upon storage, and reduced renal filtration.[8]

In addition, the chemical modification of PEG is generally straightforward due to its versatile solubility in both aqueous and organic solvents. Considering these advantages, PEG does not have a well-characterized biodegradation pathway and in some cases, has been shown to cause hypersensitive reactions upon oral, dermal, and intravenous administration.[9] For these reasons, other polymers that stabilize colloidal particles from aggregation with other added benefits such as targeting are of potential interest to the biomaterials community. In one approach, Mancini, *et al.* demonstrated that trehalose glycopolymers, when covalently attached to proteins, helped retain protein activity and significantly increased stability following lyophilization.[10] Our lab has also examined trehalose polymers for nucleic acid delivery; Sizovs, *et al.* demonstrated that cationic polytrehalose block copolymers assemble with siRNA in a core (cationic block + siRNA) shell (polytrehalose) structure, which aided colloidal stability and allowed the resulting polyplexes to internalize into glioblastoma cells.[11] Carbohydrates also have the added benefit of offering receptor recognition. For example, K. Yasugi, *et al*. formulated polymeric micelles with a glucose or galactose residue on their surface offering a sugar-bearing poly(ethylene glycol)-poly(D,L-lactide) [PEG-PLA] block copolymer. In that study, the galactose-bearing PEG−PLA micelles were shown to selectively attach to the RCA-1 lectin, which is known to recognize D-galactose residues.[12] These and related strategies may help researchers develop intelligent micelles for receptor-mediated endocytosis, while maintaining hydrophilic shells to prevent aggregation. Thus, there exists a need to investigate synthetic approaches to install carbohydrates as hydrophilic components in assembled nanosystems such as polymeric micelles.

Herein, we explore a terpolymer design containing polymerized trehalose moieties within the hydrophilic shell for constructing polymeric micelles that are soluble and colloidally stable in aqueous salt and serum conditions.[13] Trehalose is a 1,1- α,α- linked disaccharide of two glucopyranose units and has interesting properties to be exploited for this purpose. This disaccharide offers a higher glass-transition temperature than other related disaccharides,[14] which allows freeze-drying of biological macromolecules for preservation.[15] Trehalose is currently utilized in food preservation,[16] is not harmful when present in high concentrations in serum,[17] and has useful properties as an excipient and for cryopreservation for cells and organs.[18] Crow and Clegg showed that high concentrations of polyhydroxyl carbohydrates (sucrose, trehalose) in cells prevents organism dehydration.[19-21]

The first report describing trehalose-based polymers was published in 1979, where Kurita *et al*. synthesized trehalose-based polyurethanes using step polymerization. By condensing the two primary hydroxyl groups on trehalose with diisocyanate monomers, carbohydrate-based linear polyurethanes were formed (it was mentioned that with this polymerization method, there was the possibility of chain branching).[22] In 1994, the same group established an efficient procedure to synthesize diamino-trehalose, which was converted to a diisothiocyanate to afford polyureas with high aqueous solubility and biodegradability.[23] In 2002 and 2004, Teramoto *et al*. reported the synthesis of a trehalose-based polyacetal using an acid catalyst for use as a thermoplastic.[24,25] The step-growth synthesis of trehalose-based polymers has also been reported by our group using Huisgen (3+2) cycloaddition (click reaction); a 6,6'-diazido-6-6'-dideoxy trehalose monomer was

created and reacted with dialkyne-oligoamine compounds to yield a series of polymers that were examined for plasmid DNA delivery to cells.[26,27]

Herein, we report the synthesis of a trimethylsilyl (TMS)-protected trehalose monomer, 6-deoxy-6-methacrylamido-2,3,4,2',3',4',6'-hepta-O-trimethylsilyl trehalose (TMS-MAT), for creation of amphiphilic block copolymers via RAFT polymerization. A family of polytrehalose (PT)-functionalized diblock terpolymers composed of three different units have been synthesized to create a diblock structure with distinct solubility profiles. An aliphatic hydrocarbon chain, poly(ethylene-alt-propylene) (PEP), has been incorporated as the hydrophobic fragment and a polytrehalose-functionalized gradient block copolymerized with dimethyl acrylamide (DMA) was combined in the hydrophilic unit in the amphiphilic structure. DMA has demonstrated a wide range of solubility from aqueous to organic solvents,[28] and in the current system it serves to decrease the difference in polarity of the PEP and PT blocks. PEP (T_g= -65 ^{o}C) has served as a hydrophobic block to promote micelle core formation in macromolecular carriers.[29] In addition to providing a hydrophilic shell with possible stealth-like properties,[17] the polytrehalose-DMA block was added to increase the overall glass transition temperature of the synthesized diblock terpolymers. A control system lacking trehalose was also synthesized through copolymerization of a PEP macromolecular chain transfer agent (created through anionic polymerization) with DMA in a diblock fashion.[29] The PEP chain transfer agent was then used to generate a family of PT diblock terpolymers through RAFT polymerization with both DMA and TMS-MAT. The composition of TMS-MAT was varied from 0.05 to 0.14 mole fraction in the hydrophilic block of the diblock terpolymers. Reactivity ratio studies between DMA and TMS-MAT suggested that the hydrophilic block was a gradient

copolymer.[30,31] Micellar dispersions of the PT diblock terpolymers in water were prepared using both nanoprecipitation and direct dissolution techniques. The resulting nanostructures were characterized for size and stability with dynamic light scattering (DLS) and cryo-transmission electron microscopy (Cryo-TEM). The micelle structures were shown to remain stable from aggregation in a variety of media types.[32]

2.2 Results and Discussion

2.2.1 Synthesis of 6-deoxy-6-methacrylamido-2,3,4,2´,3´,4´,6´-hepta-O-trimethylsilyl trehalose (TMS-MAT) (7)

The synthesis of TMS-MAT (**7**) was achieved in six steps according to a previously published procedure.[11] The first step involved breaking the *C2* symmetry of trehalose (**1**), which was accomplished by reacting anhydrous trehalose with iodine in the presence of triphenylphosphine in dry dimethyl formamide (DMF) at 80 °C. The crude product was taken to the next step without further purification and reacted with acetic anhydride in the presence of pyridine to yield a mixture of three products; acetylated mono-iodo trehalose, acetylated di-iodo trehalose, and acetylated trehalose. This mixture of products was purified using silica column chromatography to yield acetylated mono-iodo trehalose (**2**).[26,33,34] The second step involved the reaction of (**2**) with sodium azide in an S_N2 fashion in DMF at 80 °C for 4 hours to yield acetylated mono-azido trehalose (**3**), which was purified by recrystallization. Deprotection of the acetyl groups was achieved with sodium methoxide in methanol yielding (**4**). Hydrogenation with palladium on carbon reduced the azide to the primary amine (**5**).[34] Subsequent protection of the hydroxyls with trimethylsilyl (TMS) groups provided the TMS-protected aminotrehalose derivative (**6**)**.** In the final step,

6 was reacted with methacryloyl chloride in DMF/dichloromethane (DCM) to yield the methacrylamide trehalose monomer (**7**) confirmed by ^{1}H NMR (see Figure 2.8).

Scheme 2.1 Synthesis of 6-deoxy-6-methacrylamido-2,3,4,2´,3´,4´,6´-hepta-O-trimethylsilyl trehalose (TMS-MAT) (7)

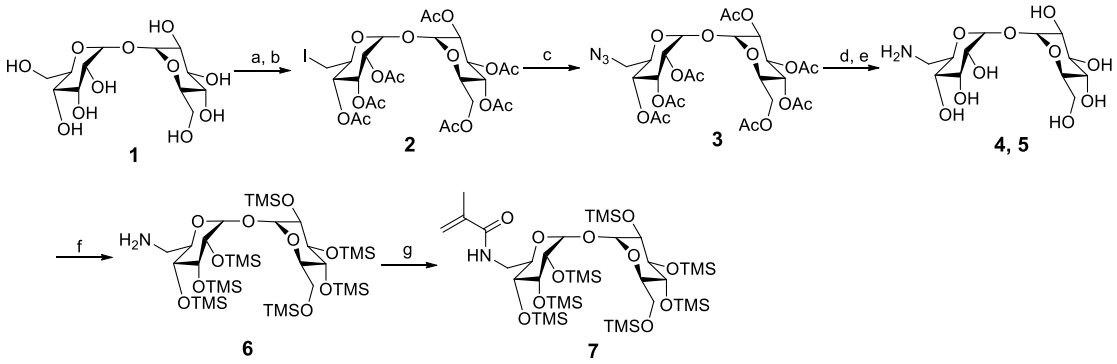

Reagents, conditions, and yields: a) I_2, PPh_3, 80 ^oC, 4 h, b) Ac_2O, pyridine, r.t., 12 h, 20%, c) NaN_3, DMF, 80 ^oC, 4 h, 82%, d) MeONa, MeOH, r.t., 3 h, e) H_2, Pd(C), MeOH, r.t., 20 h, 70 %, f) TMSCl, pyridine, r.t., 15 h, 90%, g) methacryloyl chloride, DMF, CH_2Cl_2, Et_3N, r.t., 4 h, quantitative.

2.2.2 Reactivity Ratios of DMA and TMS-MAT by Non-linear Fitting

The reactivity ratios for the copolymerization of DMA and TMS-MAT were studied in toluene at 70 ^oC using AIBN as the initiator by free radical polymerization (Scheme 2.2). We varied the monomer feed (mole fraction) of TMS-MAT (monomer 1) from 0.11 to 0.91 and ran seven experimental runs to calculate the reactivity ratios of copolymerization. The conversions of each monomer were kept less than 20 percent, in order to maintain the monomer feed composition during polymerization. These results are tabulated in Table 2.4.

Scheme 2.2 Reactivity ratios of TMS-MAT (monomer 1) and DMA (monomer 2) were determined by varying the feed ratio of each monomer in free radical polymerizations. x & 1-x are mole fraction of TMS-MAT and DMA respectively.

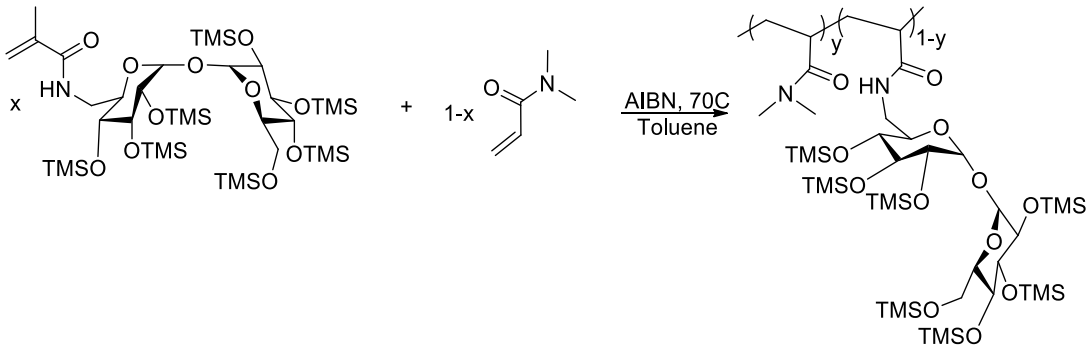

Conditions: AIBN : monomer =500-1000 : 1 mole fraction, total conc. = 0.5 M, the conversion was kept below 15 mole %, temp = 70 °C.

We used a non-linear fitting model to analyze the reactivity ratios for copolymerization of TMS-MAT and DMA. Using the equation $F_1 = (r_1 f_1^2 + f_1 f_2) / (r_1 f_1^2 + 2 f_1 f_2 + r_2 f_2^2)$, the data in Table 2.4 was fit and calculated to be $r_1 = 0.09 \pm 0.01$ and $r_2 = 1.6 \pm 0.1$. Figure 2.1 shows the non-linear fit used to determine the reactivity ratios.[30,35]

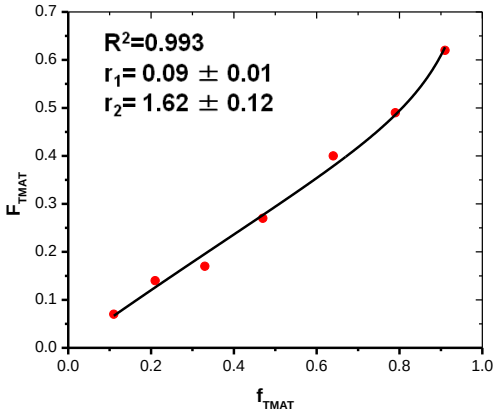

Figure 2.1 The non-linear fitting model used to determine the reactivity ratios for the copolymerization of TMS-MAT (monomer 1) and DMA (monomer 2). Seven experimental runs were carried out in toluene at 70 ^{o}C using AIBN as the initiator. **(Table 2.4)**

The reactivity ratio data (i.e. $r_1 = 0.09$) indicates that homopolymerization of TMS-MAT is exceedingly slow. We attribute this fact to the bulky TMS groups that are used to protect the trehalose monomer, whereby the propagating radical site is sterically hindered. The reactivity ratio ($r_1 r_2 = 0.15$) indicates that TMS-MAT and DMA can be effectively

copolymerized. However, there will be a gradual change in one monomer composition over the other. Thus, it can be concluded that the trehalose blocks are likely gradient copolymers. As polymerization proceeds, the DMA feed composition decreases due to the greater r_2. Therefore, the TMS-MAT monomer will be added towards the end of the hydrophilic block of each of the diblock terpolymers.

2.2.3 Synthesis of Poly (ethylene-*alt*-propylene)−poly[(*N*,*N*-dimethylacrylamide)-*grad*-poly(6-deoxy-6-methacrylamido trehalose)] (PEP-poly(DMA-*grad*-MAT)

Scheme 2.3 Synthesis of PT diblock terpolymers.

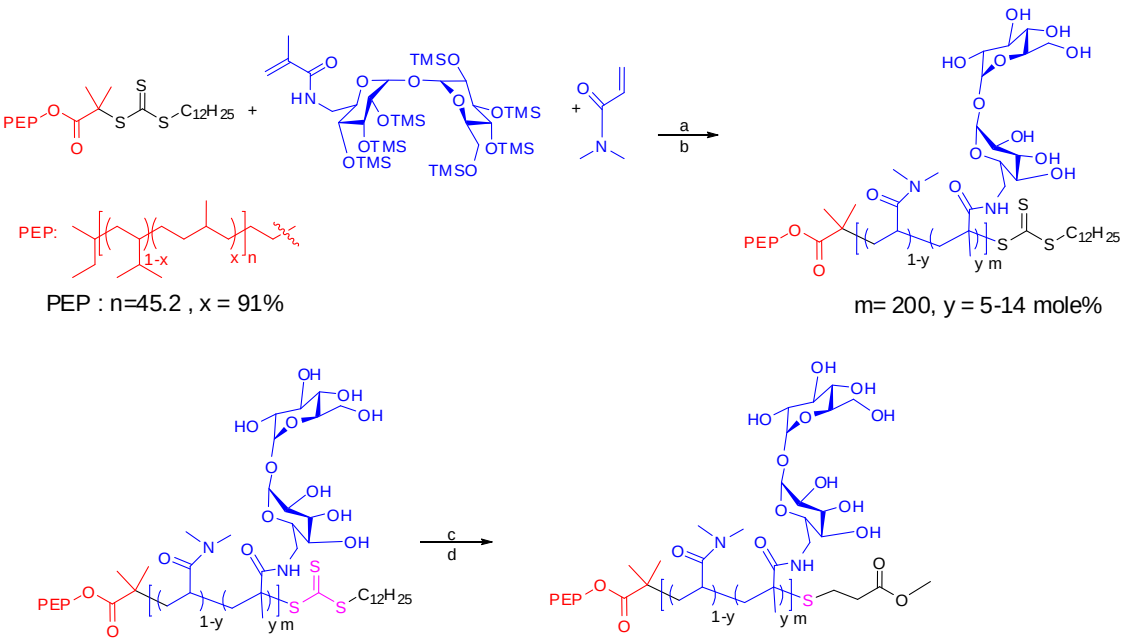

Reagents and conditions: a) AIBN, toluene, 70 °C, b) HCl in methanol, r.t., 5 min., c) n-butyl amine, TCEP, THF/methanol, 25 °C, 24 h., d) methyl acrylate, r.t., 24 h.

The macromolecular chain transfer agent, PEP-CTA, was synthesized as reported in the literature.[29,32] The number-average molar mass (M_n) of the PEP-CTA was 3.6 kg mol^{-1} (by end-group analysis using ^{1}H NMR spectroscopy), and the dispersity ($Đ$) was

1.05 (by SEC, relative to PS standards).[36] Three PT diblock terpolymers were prepared by copolymerizing DMA and TMS-MAT in toluene at 70 ^{o}C using AIBN as an initiator. Characterization details (M_n and $Đ$) of the PT diblock terpolymers are provided in Table 2.1. SEC chromatograms of the PEP-CTA, PEP-DMA, and PT (3.6-24.5-0.11) polymers (Figure 2.10) revealed monomodal elution curves. As previously discussed, the reactivity ratios of TMS-MAT (monomer 1) and DMA (monomer 2) were found to be r_1= 0.09 and r_2 = 1.59 by free radical polymerization using the nonlinear as well as the linear Fineman and Ross fitting model (Table 2.5, Table 2.6, Figure 2.7). Based on these ratios, we believe the TMS-MAT blocks are gradient in nature. The obtained reactivity ratio data was compared with the DMA and TMS-MAG pair, and found to be similar to the published results by Yin et al. for the DMA and TMS-glucose monomer pair.[32] TMS deprotection was achieved using HCl in methanol to yield amphiphilic diblock terpolymers. Finally, the trithiocarbonate RAFT fragment was removed by aminolysis and complete removal was supported by UV-Vis spectroscopy (Figure 2.11). The glass transition temperature of the amphiphilic polymers and the observed increase in glass transition temperature with increasing content of MAT was determined using DSC (Figure 2.12).

Table 2.1 Experimental details of RAFT copolymerizations with DMA and TMS-MAT to obtain PD and PT diblock terpolymers with different compositions. The molecular weight of the PEP-CTA was 3.6 kg/mol in all cases (mass includes the $C_{12}H_{25}$ RAFT fragment).

Sample[a]	[AIBN] : [PEP-CTA]: [DMA] : [TMS-TMAT][b]	[M_0]	Time (hr)	Conv. of DMA[c]	Conv. of TMS-MAT[c]	M_n kg/ mole [d]	$Đ$[e]
PD (3.6 -23.5)	0.05 : 1 : 199 : 0	4.5	4.3	99.5%	0	23.5	1.13
PT (3.6 -21.1-0.05)	0.05 : 1: 174.8 : 9.2	1.67	6	92%	92%	24.7	1.19
PT (3.6 -24.5-0.11)	0.05 : 1: 179.1 : 18.3	1.68	10	99.5%	91.5%	28.1	1.23
PT (3.6 -26.4-0.14)	0.05 : 1 : 158.1 : 26.1	1.7	10	93%	87%	30.0	1.28

[a]The first value in parentheses indicates the number average molecular weight of PEP in kg/mole (hydrophobic component of diblock terpolymers) and the second value indicates the number average molecular weight of the PDMA or PDMA and PMAT block in kg/mole (hydrophilic components of diblock terpolymers). The third value indicates the mole fractions of MAT (trehalose) repeat units in the hydrophilic block of the terpolymers. [b]Initial composition of AIBN (initiator), PEP-CTA, and monomers in the feed. [c]Conversion of DMA and TMS-MAT as monitored by ^{1}H NMR spectroscopy. [d]Number average molecular weight of the diblock terpolymers after deprotection of TMS groups. [e]Polydispersity of diblock terpolymers before the removal of the trimethylsilyl protecting groups.

2.2.4 Formation of PT Terpolymer Micelles in Water

As reported in Table 2.1, four amphiphilic polymers were synthesized for this study: PD (3.6 – 23.5), PT (3.6 – 21.5 - 0.05), PT (3.6 – 24.5 – 0.11), and PT (3.6 – 26.4 – 0.14). The hydrophobic block (T_g = -65^{o}C) in the terpolymer was kept small (3.2 kg/mol) to avoid complication from nonergodicity effects.[37,38] Micellar dispersions of PT terpolymers were prepared by using both nanoprecipitation and direct dissolution methods.[32] Nanoprecipitation was used in conjugation with dialysis against water to form micelles from PD (3.6 – 23.5), PT (3.6 – 21.5 - 0.05), and PT (3.6 – 24.5 – 0.11). PD (3.6 – 23.5) was readily soluble in THF, but we found a binary mixture of THF:methanol (15:2 v/v) to be the most suitable solvent for dissolving the synthesized terpolymers containing

polytrehalose (PMAT).[32] Due to the large difference in polarity of the two blocks, we were unable to find a solvent system that dissolved PT (3.6 – 26.4 – 0.14), which had the highest PMAT content. Direct dissolution was employed to make micellar dispersions (by heating each sample to 60 ºC for two weeks) with PT (3.6 – 21.5 - 0.05), PT (3.6 – 24.5 – 0.11), and PT (3.6 – 26.4 – 0.14).

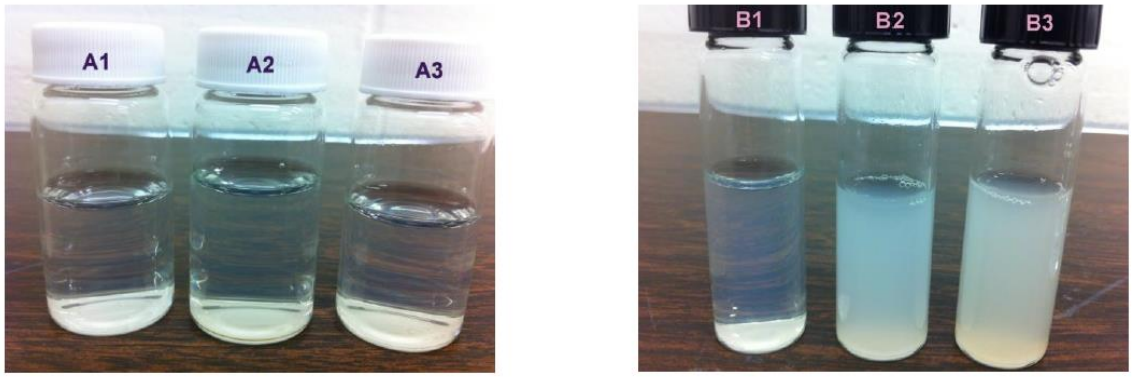

Figure 2.2 a) Image of micellar dispersions (1 wt percent) prepared by nanoprecipitation (NP) in water. Vial labels are as follows: A1: PD ((3.6 – 23.5), A2: PT (3.6 – 21.5 - 0.05), A3: PT (3.6 – 24.5 – 0.11). b) Image of micellar dispersions (1 wt percent) prepared by direct dissolution (DD) in water. Vial labels are as follows: B1: PT (3.6 – 21.5 – 0.05), B2: PT (3.6- 24.5 – 0.11), B3: PT (3.6 – 26.4 – 0.14).

Visual analysis of the samples showed that the micellar dispersions prepared by nanoprecipitation (NP) were clear and transparent with no signs of micellar aggregation. We attempted to find a solvent system that could dissolve PT (3.6 – 26.4 – 0.14) by trying different solvent systems of THF with methanol, DMF, and DMSO. However, no solvent combination successfully dissolved the polymer due to the extreme differences in polarity between the hydrophilic and hydrophobic blocks. Direct dissolution (DD) was used to create micellar dispersions from all of the PT terpolymers to compare the size of the nanoparticles formed by each technique. The micellar dispersions formed by DD were white and cloudy indicating the presence of large aggregates. Micellar dispersions prepared by both techniques were first analyzed by DLS to obtain information about the average

particle size and distribution in aqueous medium. Micelles formed by NP exhibited hydrodynamic radii of ca. 14 nm, with narrow dispersity in the cases of PD (3.6-23.5), PT (3.6-21.5-0.05), and PT (3.6-24.5-0.11). Large aggregates were absent according to REPES analysis (Figure 2.3A). The obtained results were verified with the correlation function using the cumulant expansion (Figure 2.13, Figure 2.14, Figure 2.15). These results are tabulated in Table 2.2 and Figure 2.3A. Micelles formed by DD showed the presence of large aggregates in the case of the three PT formulations: (3.6-21.5-0.05), (3.6-24.5-0.11), and (3.6-26.4-0.14) by REPES analysis (Table 2.2, Figure 2.3B). A double exponential correlation function was used to verify the data, which was consistent with our previous result (Figure 2.16, Figure 2.17, Figure 2.18). Bimodal hydrodynamic radii (R_h) of 12/52 and 21/129 nm were observed for the micellar dispersions prepared from PT (3.6-21.5-0.05) and PT (3.6-24.5-0.11) by DD, respectively. When the same diblock terpolymers were used to form micellar dispersions via the NP method, hydrodynamic radii ca. 15nm were found to be prevalent for each sample with a narrow dispersity.

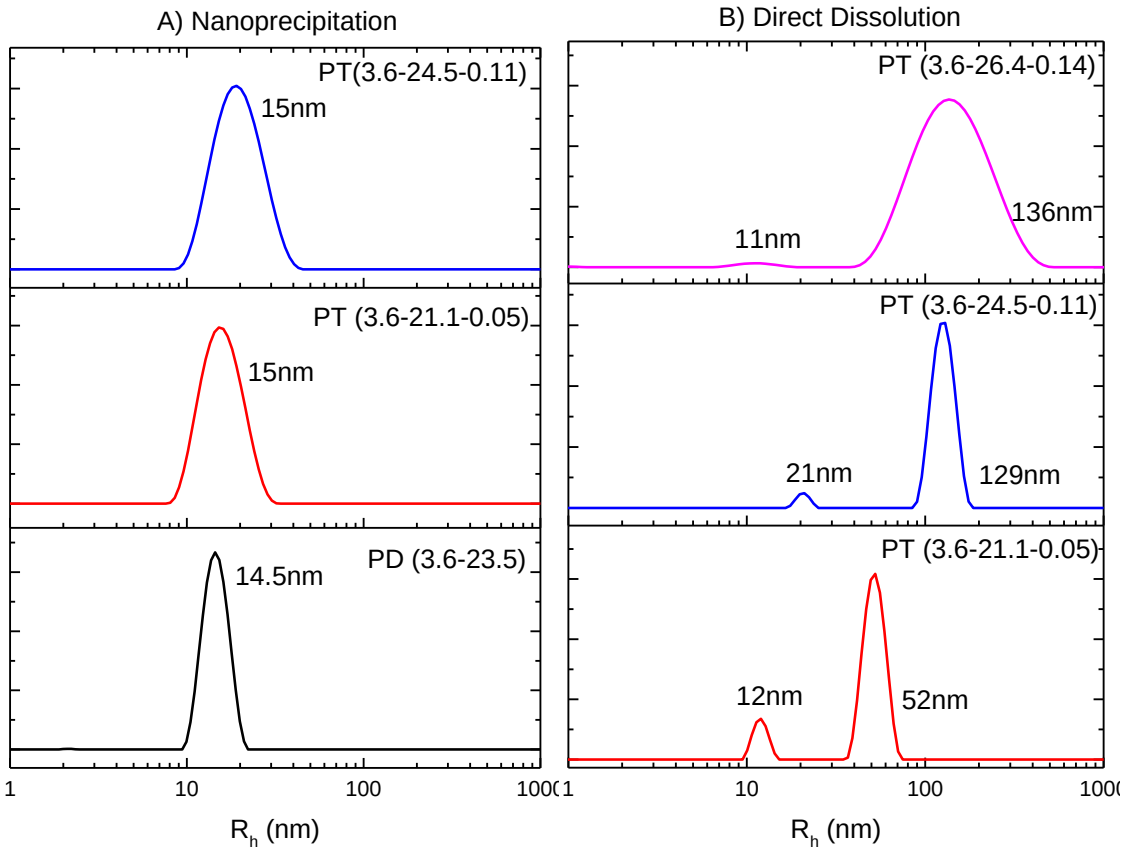

Figure 2.3 DLS characterization of the micellar dispersions (1 wt percent) formed by A) NP and B) DD by REPES analysis. The scattering angle was 90°. Peak positions are shown in Table 2.2.

Table 2.2 DLS characterization of micellar dispersions formed by the terpolymers in water.

Sample	Conc.	Method	R_h1 (nm)	R_h2 (nm)
PD(3.6-23.5)[a]	**1wt%**	**NP**	**14.7±0.2**	
PT(3.6-21.1-0.05)[a]	**1wt%**	**NP**	**14.4±0.4**	
PT(3.6-24.5-0.11)[a]	**1wt%**	**NP**	**14.3 ±0.2**	
PT(3.6-21.1-0.05)[b]	**1wt%**	**DD**	**13.6 ±0.3**	**55± 1.3**
PT(3.6-24.5-0.11)[b]	**1wt%**	**DD**	**21.3±0.7**	**130± 3.7**
PT(3.6-26.4-0.14)[b]	**1wt%**	**DD**	**16.7±0.4**	**174 ± 7.2**

[a]A cumulant expansion function was used to determine the hydrodynamic radii by fitting the data into the correlation function. A linear regression of Γ vs. q^2 was performed over 5 angles between 60° to 120° in increments of 15° (for further information see Figure 2.13, Figure 2.14, Figure 2.15). [b]A double exponential function was used to determine the hydrodynamic radii by fitting the data into the correlation function. Linear regression of Γ vs. q^2 was performed over 5 angles between 60° to 120° in increment of 15° (for further information see Figure 2.16, Figure 2.17, Figure 2.18).

The T_g of each synthesized PT terpolymer was also determined. Figure 2.12 reveals that as more trehalose content is introduced into the hydrophilic blocks, the T_g increases. Nanoprecipitation followed by dialysis was found to be the preferred technique for these high T_g polymers to form nanostructures in solution (direct dissolution technique resulted in larger aggregates).[39-41]

Cryo-TEM was used to image the micelles. Figure 2.4 shows micrographs of the dispersions of PT (3.6-21.5-0.05) and PT (3.6-24.5-0.11) micelles in water, and both samples were shown to be spherical micelles with narrow dispersity in particle size. The micelle cores were shown as the dark circles in the images and their radii were determined to be 8 ± 1 nm in both cases. The existence of micelle coronae were revealed by grey halos around the dark cores as highlighted by black arrows in Figure 2.4B. Similar to our previous results with glucose-functionalized micelles,[32] the electron-rich trehalose moieties greatly enhanced the contrast of micelle coronae and made them visible even in a water-swollen state. For example, the electron density of micelle coronae was calculated to be 412 e nm^{-3} in PT (3.6-24.5-0.11) micelles and 427 e nm^{-3} in PT (3.6-24.5-0.11) micelles, compared to 397 e nm^{-3} in PEP-PDMA ones and 314 e nm^{-3} of amorphous ice.[42]

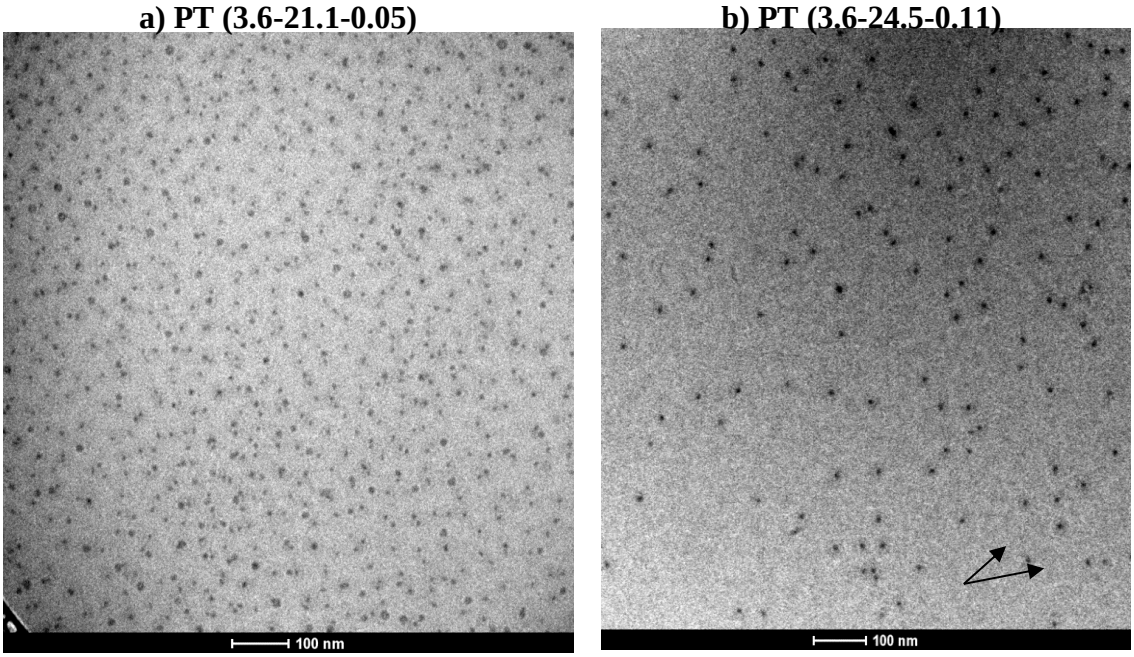

Figure 2.4 Cryo-TEM images of a 1 wt % aqueous micelle dispersion formed by NP from polymers: a) PT (3.6-21.1-0.05) and b) PT (3.6-24.5-0.11). Arrows indicate the shell structure around the dark core (presence of grey halos around the micelles due to the electron dense MAT moieties). Images were recorded on a FEI Tecnai G2 Spirit BioTWIN transmission electron microscope (TEM) at -178 °C, and an accelerating voltage of 120 kV was applied onto a LaB_6 emitter. No external staining was used for TEM samples.

2.2.5 Stability of Micelles in Biological Media

The stability of polymeric nanocarriers in biological media is critical to their use in biological applications such as drug delivery. Therefore, to gain more insight into micelle stability in biologically-relevant environments, the polytrehalose-functionalized micelles were examined by nanoprecipitation in four different biological media types (PBS, serum-free Opti-MEM, DMEM containing 10% fetal bovine serum (FBS), and 100% FBS). The stability of the PT (3.6-21.5-0.05) micelle dispersions in PBS and Opti-MEM were first examined by diluting the micellar dispersion 1:5 (v/v) with media. The micellar stability from aggregation was then observed using DLS over a period of 14 hours.

As previously mentioned, REPES analysis of the micelles formed in water by NP revealed monodisperse dispersions with radii of approximately 15 nm, while the DD technique revealed micelle aggregation (Figure 2.3). Micelles were subsequently formed via NP in water, diluted with different biological media, and observed over time via DLS. Figure 2.5 shows the REPES distribution curves of PT (3.6-21.5-0.05) micelles at 0 and 14 hours after dilution. The micelles were found to be stable in PBS and Opti-MEM solutions over the 14 hour time period where only a slight size increase was noted (3 nm) upon micelle dilution in PBS when compared to the water solutions. A cumulant expansion function was used to verify the observed data (water, PBS and Opti-MEM), which determined that the hydrodynamic radii do not generally change (and a monomodal distribution was observed). However, when the micellar dispersion was diluted in either DMEM containing 10% FBS or 100% FBS, a bimodal size distribution was noticed in the REPES analysis, as shown in Figure 2.5. Yin et al. previously found that micelles containing glucose that are diluted in media containing serum also produce a bimodal distribution when analyzed using DLS.[32] That study also showed that micelles created from PDMA-PEP block copolymers also formed stable structures in biological media.[32] REPES analysis showed that the micelle peak overlapped with the FBS protein peaks (Figure 2.5). A double exponential analysis was performed to obtain the hydrodynamic radii as reported in Table 2.3. No other peaks evolved in the DLS over the period of 14 hours (at higher sizes) nor did the peaks shift to higher sizes, which signifies that the micelles are very stable in serum-containing media and do not aggregate with serum proteins. Overall, the DLS results revealed that micelles formed by NP with the PT block copolymers show excellent stability in all of the biological media including 100% serum for up to 14 hours.

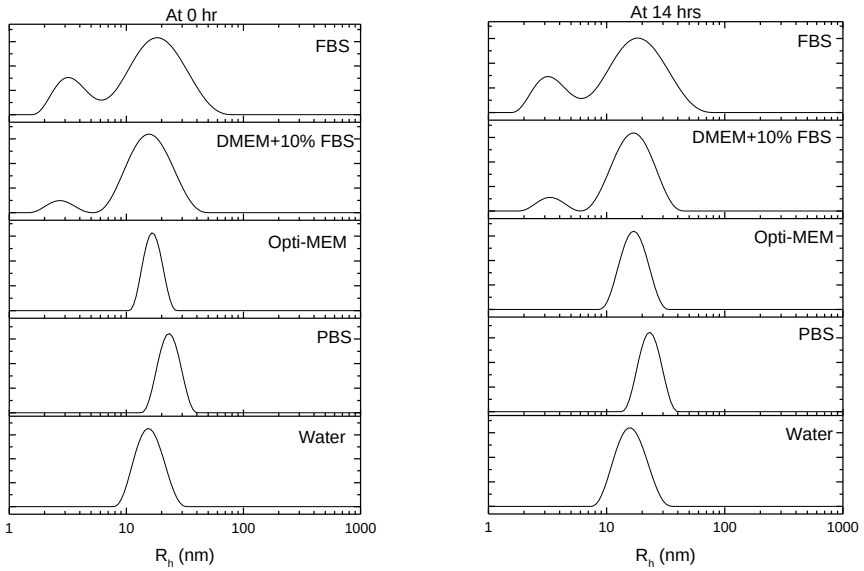

Figure 2.5 REPES distribution curves of PT (3.6-21.5-0.05) micelles formed by NP in water and subsequently diluted in the indicated biological media. Data were taken at time points of 0 and 14 hours following dilution. The scattering angle for the analysis was 90º.

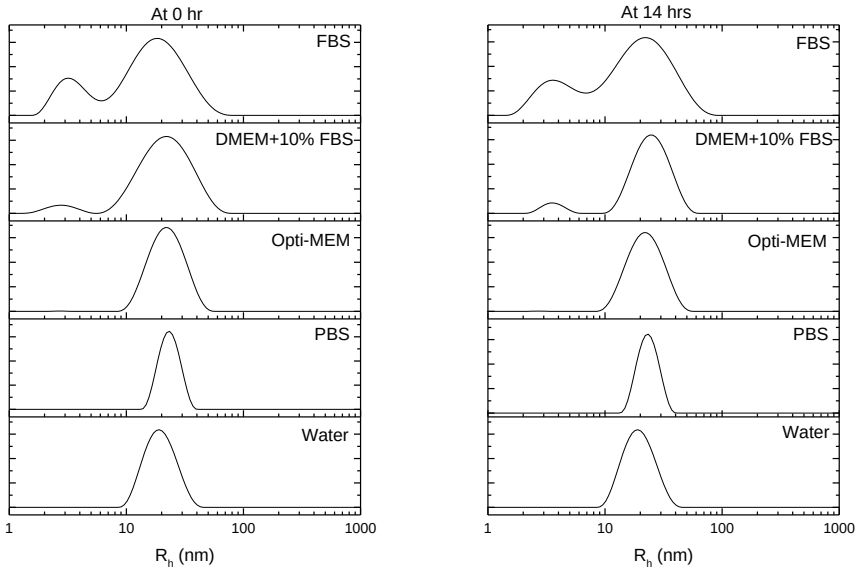

Figure 2.6 REPES distribution curves of PT (3.6-24.5-0.11) micelles formed by NP in water and subsequently diluted in the indicated biological media. Data were taken at time points of 0 and 14 hours following dilution. The scattering angle for the analysis was 90º.

Table 2.3 Hydrodynamic radii and dispersities for PT micelles calculated after performing cumulant or double exponential expansion functions.

Samples	Time (hr)	Water[b]	PBS[b]	Opti-MEM[b]	DMEM+10% FBS[c]	100% FBS[c]
PT(3.6-21.1-0.05)	0	16.3 ± 0.1 (0.141)[d]	19.4 ± 0.1 (0.082)[d]	16.6 ± 0.7 (0.134)[d]	17.9 ± 0.3 4 ± 0.2	23.3 ± 0.2 4.1 ± 0.1
	14	15.9 ± 0.1 (0.152)[d]	17.9 ± 0.1 (0.072)[d]	16.2 ± 0.1 (0.145)[d]	17.7 ± 0.2 4 ± 0.2	21.7 ± 0.1 3.8 ± 0.1
PT(3.6-24.5-0.11)	0	19.5 ± 0.1 (0.136)[d]	22 ± 0.1 (0.068)[d]	21.2 ± 0.1 (0.147)[d]	24.2 ± 0.2 4.8 ± 0.1	23.7 ± 0.3 4.1 ± 0.1
	14	18.5 ± 0.1 (0.124)[d]	24.1 ± 0.1 (0.082)[d]	20.7 ± 0.1 (0.101)[d]	24.8 ± 0.1 5.2 ± 0.2	23.9 ± 0.1 5.7 ± 0.8

[a]Dispersions (1 wt%) of two samples prepared by NP in water. [b]Hydrodynamic radii were calculated using a cumulant expansion function. [c]Hydrodynamic radius was calculated using a double exponential function. [d]μ/Γ^2 values at 90° scattering angle. The scattering angle was 90° for the reported Rh. Literature reported values for viscosity and refractive index for the calculation of Rh (in respective medium) were used.[32]

2.3 Conclusions

In summary, we have synthesized well-defined architectures of trehalose-functionalized, amphiphilic diblock terpolymers using a combination of RAFT and anionic polymerizations. The purpose of introducing trehalose in the polymer was to increase the difference in polarity between the hydrophilic and hydrophobic blocks, which leads to self-assembly of the micelle structures in water. The reactivity ratios determined for the MAT and DMA monomers (obtained via free radical polymerization) indicated that the hydrophilic blocks are gradient in nature, resulting in a higher DMA content near the PEP block and a higher trehalose content near the terpolymer end. The T_g of the PT diblock terpolymers increased as the mole percent of trehalose in the polymer backbone increased. Micelles were readily formed via NP for samples containing up to 11 mole percent of trehalose in the hydrophilic block. DLS and Cryo-TEM characterization data suggested that spherical micelles with monomodal hydrodynamic radii ca. 15 nm were observed. Micelles were also formed via DD for the sample containing the higher percentage of trehalose, PT (3.6-26.4-0.14), as micelles with this polymer were unable to be formed via NP. We also employed DD as a micelle formation method to determine the size difference between polymeric micelles formed using both techniques. The DD micelle formation technique generally revealed the formation of large aggregates. Cryo-TEM images revealed that the presence of trehalose was found to increase the shell contrast (grey halos around dark micelle cores) due to the electron rich MAT moieties in the diblock terpolymers. DLS analysis of the micelles indicated that these structures are stable from aggregation when incubated with a variety of salt and serum-containing media, thus supporting further optimization of these structures for systemic drug delivery applications.

2.4 Experimental Section

Materials: All chemicals were purchased from Sigma-Aldrich and used as acquired with the exception of: anhydrous D-trehalose (99%, Acros Organics), acetic anhydride (99.6%, Fisher), dry pyridine (99.8%, Sigma-Aldrich), sodium chloride (Fisher Scientific), silica gel (Sorbent Technologies, porosity: 60Å, size: 40-60μm), chlorotrimethylsilane (TMSCl; Fisher Scientific, 98%), triethylamine (TEA; Acros Organics, 99.7%), and HCl (1.25M) in methanol (Fluka). All solvents were obtained from Fisher Scientific excluding hexanes (Macron Chemical, ACS grade) and used as received unless otherwise specified. Tetrahydrofuran (THF, HPLC grade) and N,N-dimethylformamide (DMF, HPLC grade) were dried using a solvent purification system purchased from MBRAUN. N,N-dimethylacrylamide (DMA) and methyl acrylate (MA) were purified by passing through basic alumina to remove trace amounts of monoethyl ether hydroquinone stabilizer. All polymers were characterized using a Varian Inova 500 NMR Spectrometer.

Synthesis of poly(ethyelene-alt-polypropylene)-chain transfer agent (PEP-CTA)

Synthesis of PEP-OH was achieved by anionic polymerization, following a published procedure.[29] Next the PEP-CTA was also created by an established procedure. Briefly, the carboxy terminated CTA *S*-1-dodecyl-*S*'-(α,α'-dimethyl-α"-acetic acid) trithiocarbonate was reacted with oxalyl chloride to yield more a reactive acyl chloride derivative. The PEP-OH was then dissolved in DCM (dichloromethane) and treated with the acyl chloride derivative of the trithiocarbonate CTA yielding the PEP-CTA. The final PEP-CTA structure was purified by precipitation into ice cold and dry methanol five times from DCM.

M_n =3 .6 kg/mol by ^{1}H NMR in $CDCl_3$ and $Đ$ = 1.08 (Figure 2.10).

Reactivity ratio study of DMA and TMS-MAT

The reactivity ratios of DMA and TMS-MAT were determined by completing a free radical polymerization study with both monomers using azobisisobutyronitrile (AIBN) as the initiator at 70 °C in toluene. The feed composition of DMA (mole fraction) was varied from 0.10 to 0.90. The conditions were the same as used for the synthesis of the PT diblock terpolymers (described below) with the exception that the total concentration of the monomers (DMA and TMS-MAT) was 0.5 M. Solutions (1200 µL of a 0.5 M solution) of DMA and TMS-MAT were prepared in deuterated toluene.

Example: In an NMR tube, 300 µL (1.5×10^{-4} mol) of DMA and 50 µL (2.5×10^{-5} mol) of TMS-MAT were added. AIBN initiator was then added (3.5×10^{-7} to 1.75×10^{-5} mol) to the solutions. Nitrogen was bubbled through the solution in the NMR tube using a long syringe for 20 min before the NMR tube was placed into the preheated variable temperature NMR at 70 °C. ^{1}H NMR spectra were recorded at room temperature prior to varying the temperature. ^{1}H NMR was recorded at various time points (60 s for the first 15 min and 600s for next 1 hour). The spectra were analyzed using MestReNova (Version 6.2.1) to determine the feed ratio and mole fraction of monomers in the copolymers. The F_1 value, which is the mole fraction of TMS-MAT in copolymer, was calculated based on integration of the vinyl protons of TMS-MAT. Linear (Fineman and Ross, Figure 2.7) and non-linear least squares (Figure 2.1) fitting of the data was performed to calculate reactivity ratios.

Table 2.4 Details of the conversion of TMS-MAT and DMA used to determine the reactivity ratios for the copolymerization of TMS-MAT and DMA via free radical polymerization in toluene at 70 °C.

Run	f_1[a]	Conv. of TMS-MAT[b]	Conv. of DMA[b]	F_1[c]
1	0.11	7.5	12.5	0.07
2	0.21	9.5	15.6	0.14
3	0.33	7.0	18.0	0.17
4	0.47	8.7	21.0	0.27
5	0.64	5.4	14.3	0.40
6	0.79	5.3	20.5	0.49
7	0.91	1.9	12.0	0.62

[a]TMS-MAT mole fraction in the feed as determined by ^{1}H NMR spectroscopy, [b]Conversion of each monomer as determined ^{1}H NMR spectroscopy, [c]Mole fraction of TMS-MAT in the copolymer calculated from the feed mole fraction of TMS-MAT and the conversion. *Note:* The conversion of each monomer was restricted below 20 mol % to keep the instantaneous feed composition consistent during the time course of the polymerization.

Table 2.5 Analysis of the reactivity ratios by the Fineman-Ross method for TMS-MAT (monomer 1) and DMA (monomer 2). The mole fractions of TMS-MAT and DMA, f_1 and f_2 respectively, in the feed were calculated by ^{1}H NMR. F_1 and F_2 are the mole fractions of TMS-MAT and DMA in the copolymer.

	Fineman-Ross			
Run	f_1	f_2	F_1	F_2
1	0.111	0.889	0.067	0.933
2	0.209	0.791	0.138	0.862
3	0.333	0.667	0.171	0.829
4	0.467	0.533	0.270	0.730
5	0.638	0.362	0.400	0.600
6	0.787	0.213	0.491	0.509
7	0.909	0.091	0.620	0.380

Table 2.6 Calculations for determining the reactivity ratios (r_1 and r_2) using the Fineman and Ross linear fitting model.

TMS-MAT (Monomer 1)

f_{12}	F_{12}	f^2_{12}/F_{12}	$f_{12}(1-F_{12})/F_{12}$
0.12	0.07	0.22	1.62
0.26	0.16	0.44	1.39
0.50	0.21	1.21	1.92
0.88	0.37	2.08	1.49
1.76	0.67	4.66	0.88
3.69	0.96	14.2	0.14
9.99	1.63	61.2	-3.87

Where $f_{12} = f_{TMAT}/f_{DMA}$ (ratio of monomer TMAT to DMA)

$F_{12} = F_{TMAT}/F_{DMA}$ (ratio of monomer TMAT to DMA in the copolymer)

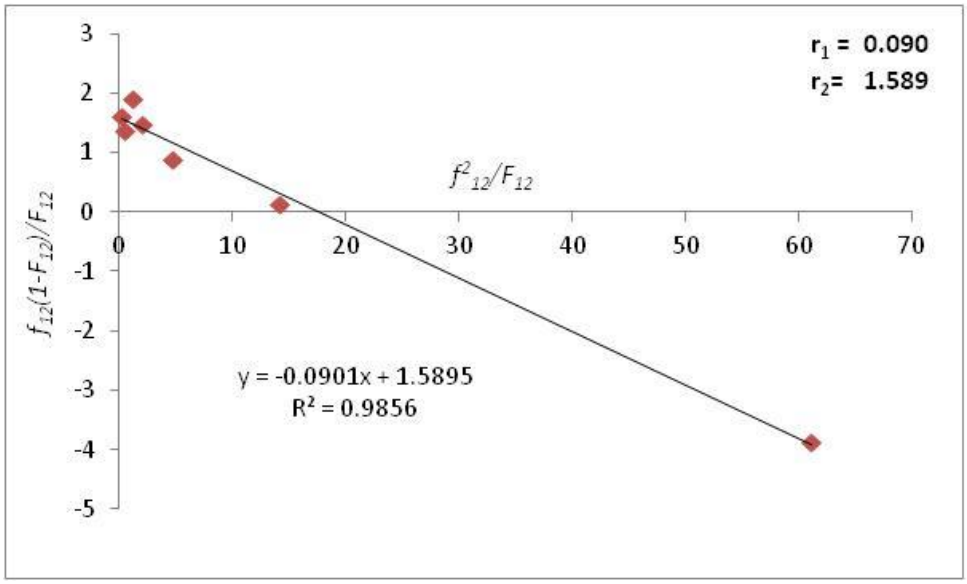

Figure 2.7 Linear fitting data using the Fineman-Ross method yielding reactivity ratios of TMS-MAT and DMA in free radical polymerization.
Where, $r_1 = k_{11}/k_{12}$
$r_2 = k_{22}/k_{21}$
k_{11} = Reaction rate of monomer TMS-MAT with monomer TMS-MAT
k_{12} = Reaction rate of monomer TMS-MAT with monomer DMA
k_{22} = Reaction rate of monomer DMA with monomer DMA
k_{21} = Reaction rate of monomer DMA with monomer TMS-MAT

Synthesis of poly(ethyelene-alt-polypropylene)-poly(DMA-grad-MAT) diblock (PT) terpolymers

Synthesis of the PT diblock terpolymers were achieved by copolymerization of DMA and TMS-MAT using RAFT polymerization (at 70 °C, AIBN initiator) in toluene with the PEP-CTA as the macromolecular chain transfer agent (MacroCTA). The feed composition for DMA and TMS-MAT is listed in Table 2.1. After polymerization, the TMS groups were deprotected in a 1.25 M HCl solution in methanol. A representative procedure is described in detail below.

PT (3.6-24.5-0.11) Example: To a single neck reaction flask charged with 0.3 g of PEP-CTA (8.3×10^{-3} mol), AIBN (0.68 mg, 4.41×10^{-6} mol), DMA (that was filtered through basic alumina) (1.48 gm, 1.49×10^{-2} mol), and TMS-MAT (1.52 gm, 1.66×10^{-3} mol) were added along with 8.3 mL of toluene. The reaction mixture was degassed for 45 min ($N_{2(g)}$) before placing in an oil bath preheated to 70 °C and the mixture was stirred at 700 rpm for 10 hours. The polymerization was quenched by cooling the mixture to 0 °C in an ice bath and opening it to air. Conversion by ^{1}H NMR: DMA = 99.5% and TMS-MAT = 91.5%, M_n by ^{1}H NMR = 38.1 kg/mol, $Đ$ = 1.23 by SEC (Figure 2.10, chloroform).
Conversion by ^{1}H NMR for PT (3.6-21.1-0.05): DMA = 92% and TMS-MAT = 92%, M_n by ^{1}H NMR = 29.3 kg/mol, $Đ$ = 1.19 by SEC (Figure 2.10, chloroform).
Conversion by ^{1}H NMR for PT (3.6-26.4-0.14): DMA = 93% and TMS-MAT = 87%, M_n by ^{1}H NMR = 43.2 kg/mol, $Đ$ = 1.28 by SEC (Figure 2.10, chloroform).

Next, the solvent was removed under vacuum and the reaction mixture was redissolved in THF (20 mL), which was then sonicated. To this mixture, 0.5 mL of 1.25 M HCl in methanol was added (mixture turned cloudy) and 3 mL of methanol was added

(resulting in a clear solution) to remove the TMS moieties from the trehalose groups. The solvent was then removed and the solid was redissolved in THF : MeOH (20:3) and precipitated into pentanes (2X) yielding a yellowish powder, 2.3g, 0.082 mmol, 93 % yield. ^{1}H NMR ≥ 99%. M_n = 28.1 kg/mol by ^{1}H NMR (Figure 2.9). PT (3.6-21.1-0.05): 1.8 g, 0.073 mmol, 67 % yield, M_n = 24.7 kg/mol. PT (3.6-26.4-0.14): 1.6g, 0.053 mmol, 89 % yield, M_n = 30 kg/mol. Removal of the trithiocarbonate chain portion from the PT diblock was attained through subsequent aminolysis followed by Michael addition as described below.

PT (3.6-24.5-0.11)[4]: 2.3 g (8.2×10^{-5} mol) of PT (3.6-24.5-0.11) was dissolved in 20 mL (4:1 v/v) THF : MeOH. The reaction mixture was degassed by bubbling nitrogen through the reaction mixture for 45 min. After bubbling, *n*-butyl amine (178 µL, 1.81×10^{-3} mol) and tris(2-carboxyethyl)phosphine hydrochloride (TCEP, 8.214×10^{-5} mol, 21 mg) were added and stirred for 24 hours at 25 °C (it was noticed that the bright yellow color of the reaction mixture disappeared). Next, methyl acrylate (MA, 2.87×10^{-3} mol, 260 µL) was added and stirred for another 24 hours at 25 °C. The solvent was removed and the final product (1.8 g) was precipitated into pentane (3X) (UV-Vis curve is shown in Figure 2.11) yield = 78%, 0.06 mmol, 1.8 g.

PT (3.6-21.1-0.05) = 1.5 g, 0.061 mmol, 83 % yield, M_n = 24.7 kg/mol.

PT (3.6-26.4-0.14) = 1.2 g, 0.04 mmol, 75 % yield, M_n = 30 kg/mol.

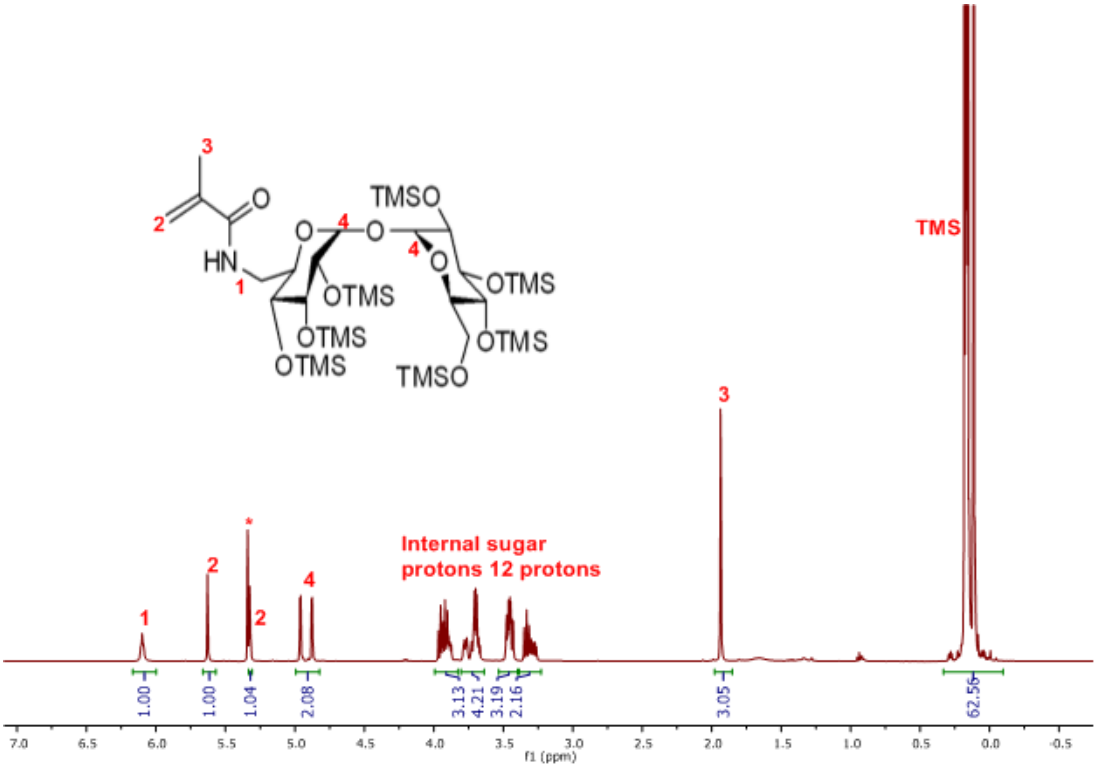

Figure 2.8 ^{1}H NMR spectrum of TMS-MAT monomer in CD_2Cl_2 at 21°C at 500 MHz. The integration values below the peak are relative to proton 2. "*" indicates the residual solvent peak.

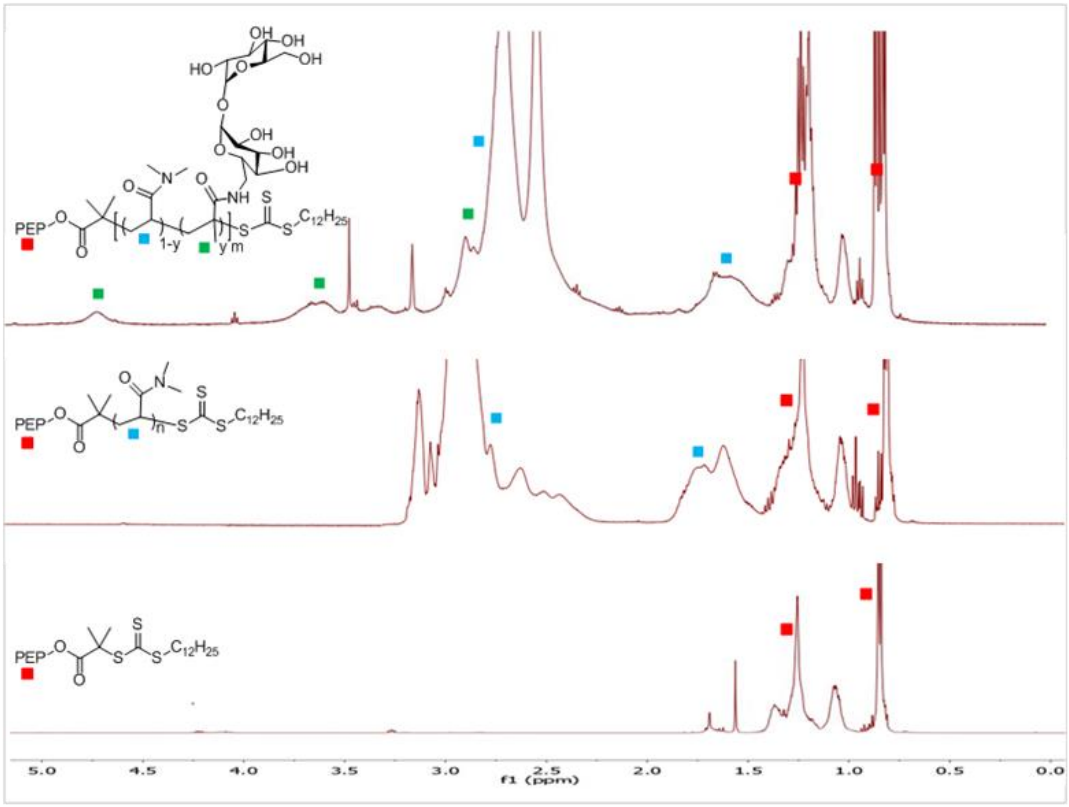

Figure 2.9 ^{1}H NMR spectrum of the PEP-CTA, PD (3.6-23.5) and PT (3.6-24.5-0.11). ^{1}H NMR spectra were recorded in $CDCl_3$ with the exception of the spectrum for PT (3.6-24.5-0.11) (two drops of deuterated methanol were added to help dissolve the sample).

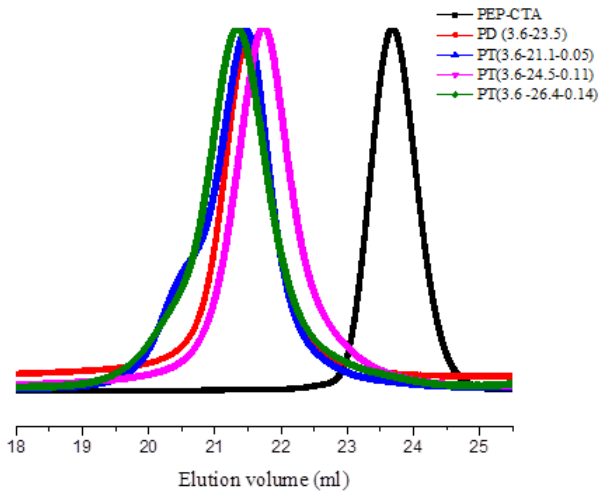

Figure 2.10 SEC chromatograms of the PEP-CTA, PD (3.6-23.5) and the TMS protected PT polymers: PT (3.6-21.1-0.05), PT (3.6-24.5-0.11), and PT (3.6-26.4-0.14) immediately following polymerization.

Chromatograms were recorded on a chloroform SEC equipped with three Jordi polydivinylbenzene columns with pore sizes of 10,000, 1,000, and 500 Å, respectively, and a Hewlett-Packard 1047A refractive index detector. The flow rate was set at 1.0 mL/min and the chromatography was run at 35 °C. The calibration curve was based on PS standards. $Đ$ = 1.07 for PEP-CTA, 1.12 for PEP-DMA and 1.23 for TMS protected PT (3.6-24.5-0.11).

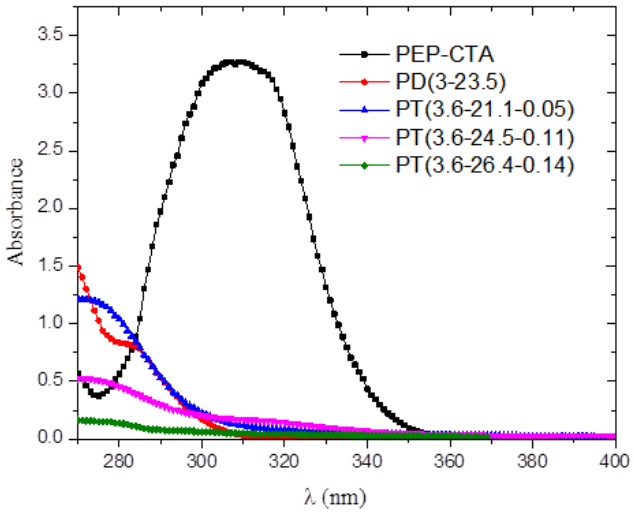

Figure 2.11 UV-Vis curve of PEP-CTA shows absorption at 309 nm. This characteristic peak of the trithiocarbonate moiety is absent in PD(3.6 – 23.5), PT(3.6-21.1-0.05), PT(3.6-24.5-0.11) and PT (3.6-26.4-0.14), suggesting successful aminolysis reactions and removal of the end groups.

THF was used as the solvent for the PEP-CTA and PD (3.6-23.5). For the polymers PT(3.6-21.1-0.05), PT(3.6-24.5-0.11) and PT (3.6-26.4-0.14), a mixture of THF:methanol (20:3 v/v) was used as the solvent.

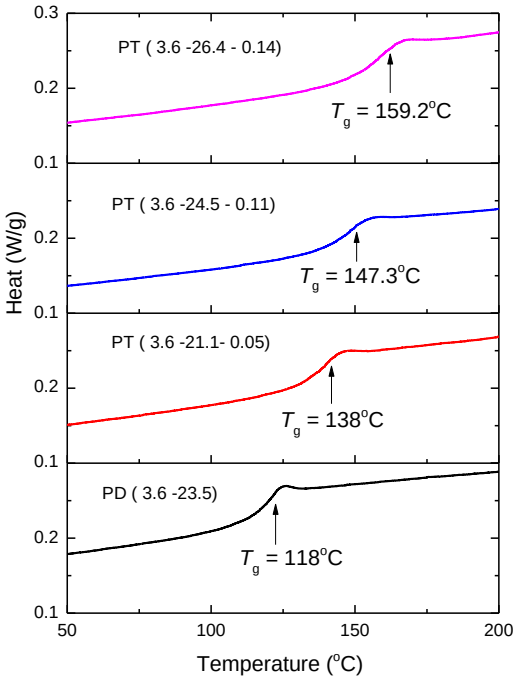

Figure 2.12 DSC thermograms of PD (3.6-23.5), PT (3.6-21.1-0.05), PT (3.6-24.5-0.11) and PT (3.6-26.4-0.14). *Conditions:* for each sample, between 5-8 milligrams of each polymer sample was placed in hermetically-sealed Tzero aluminum pans and analyzed on a Discovery DSC. The heating rate was 10 °C /min starting at 20 °C and heated to 200 °C. The second cycle of heating is shown above. TRIOS software is used to calculate glass transition temperature. The DSC thermograms showed increase in T_g with an increase in MAT content.

Dynamic light scattering (DLS)

All micellar dispersions were filtered through a 0.2 µm filter to remove large scatters before loading into dust free glass tubes, which were then sealed with several layers of Parafilm. Measurements were recorded over 5 different angles ranging from 60° to 150° at increments of 15°. For studies examining the serum stability of the micelles, 0.1 mL of each micellar dispersion (formed by nanoprecipitation) was diluted with 0.5 mL of biological media and filtered through a 0.2 µm filter into dust free tubes. The data were recorded at time 0 and 14 hours to determine micelle stability in different media at 90°. Scattering measurements were performed on a Mini L-30 Laser (Brookhaven Instruments) equipped with a red laser source (λ = 637 nm), BI-APD avalanche photo diode detector to determine scattering intensity, and a Brookhaven BI-9000 correlator. The samples were placed in a decalin oil bath at 25.0 ± 0.5 °C. The intensity correlation functions ($g_2(t)$) were measured over five different scattering angles between 60° and 120°, and converted into field correlation, ($g_1(t)$) using the Siegert relation $g_2(t) = 1 + g_1(t)^2$. Later, we used the cumulant (Equation 1) function for micellar dispersions with monomodal expansion and the double exponential function (Equation 2) for dispersion with multimodal expansion to extract information about the decay rate (Γ).

$$g_1(t) = A\, exp(-\Gamma t)\left(1 + \frac{\mu_2}{2!}\, t^2 - \frac{\mu_3}{3!}\, t^3\right) + bkgd \qquad \text{(Equation 1)}$$

$$g_1(t) = A_1\, exp(-\Gamma_1 t) + A_2\, exp(-\Gamma_2 t) + bkgd \qquad \text{(Equation 2)}$$

In Equation 1, μ_2 and μ_3 are the second and third cumulant values, respectively. In Equation 2, Γ_1 and Γ_2 are the fast and slow decay modes, respectively. Furthermore, the

particle size distribution was determined by the second cumulant (μ_2/Γ^2), a measure of the width of the decay rate distribution. The translational diffusion coefficient (D) can be obtained by the relation $\Gamma = q^2 D$ by performing linear regression using Origin software, where q is the scattering vector. Lastly, the apparent hydrodynamic radii (R_h) were calculated using the Stokes-Einstein equation (Equation 3).

$$R_h = (k_B T) / 6\pi\eta D \quad \text{(Equation 3)}$$

In this equation, k_B: Boltzmann constant, T: temperature, and η: viscosity of the medium. We used literature values of refractive indices (n) and viscosities of the specific media at 25 °C when analyzing samples prepared in the five different media formulations.[4]

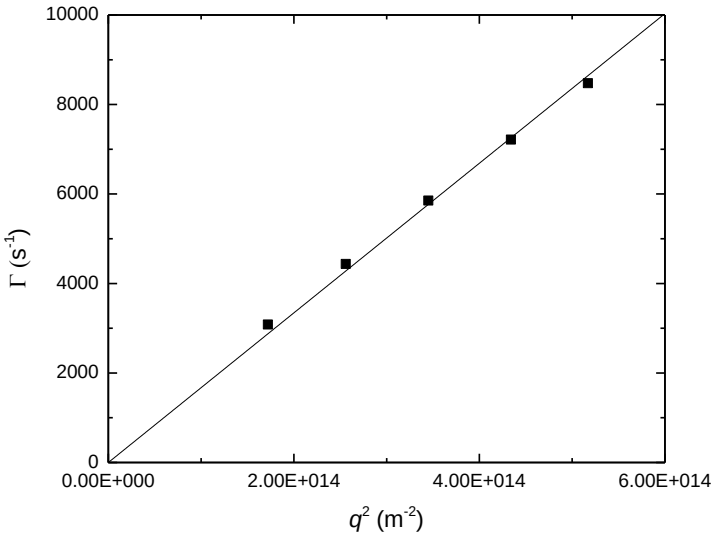

Figure 2.13 Linear regression of Γ vs. q^2 over 5 different angles varying from 60° to 120° of the two decay modes in water with PD (3.6-23.5) (micelles formed via nanoprecipitation). The correlation function $g_1(t)$ was fit using the cumulant expansion function. Micelles with radii of 14.7 ± 0.2 nm were determined and μ/Γ^2 value at 90° scattering angle was 0.07.

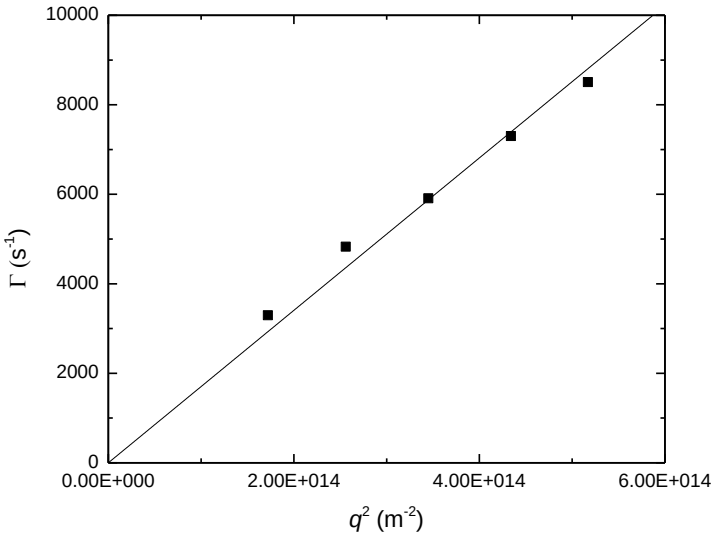

Figure 2.14 Linear regression of Γ vs. q^2 over five different angles varying from 60° to 120° of the two decay modes in water with PT (3.6-21.1-0.05) (micelles formed via nanoprecipitation). The correlation function $g_1(t)$ was fit using cumulant expansion function. Micelles with radii of 14.4 ± 0.4 nm were determined μ/Γ^2 value at 90° scattering angle is 0.152.

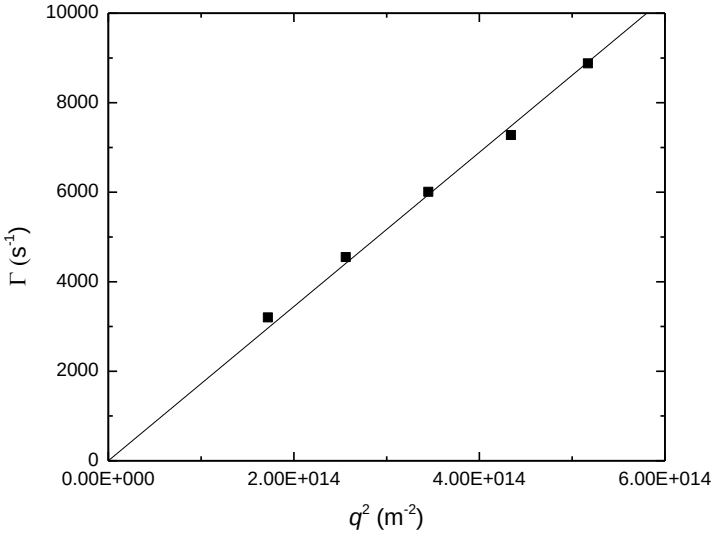

Figure 2.15 Linear regression of Γ vs. q^2 over 5 different angles varying from 60° to 120° of the two decay modes in water with PT (3.6-24.5-0.11) (micelles formed via nanoprecipitation). The correlation function $g_1(t)$ was fit using cumulant expansion

function. Micelles with radii of 14.3 ± 0.2 nm were determined μ/Γ^2 value at 90° scattering angle is 0.124.

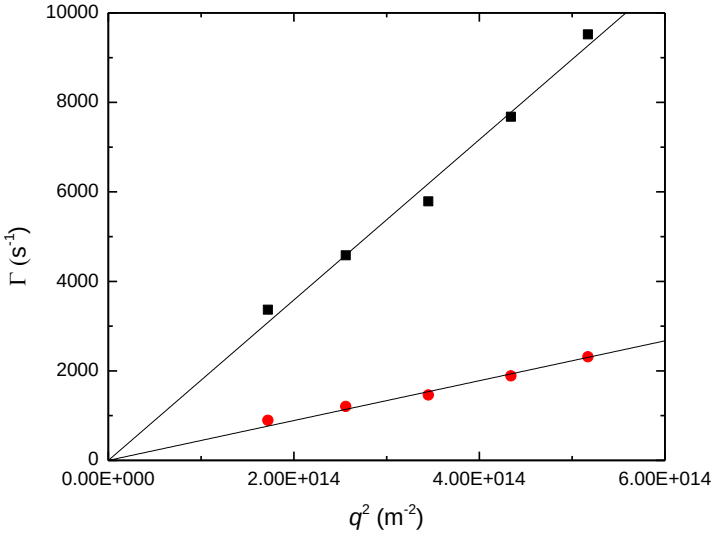

Figure 2.16 Linear regression of Γ vs. q^2 over 5 different angles varying from 60° to 120° of the two decay modes in water with PT (3.6-21.1-0.05) (micelles formed by direct dissolution). The correlation function $g_1(t)$ was fit using a double exponential function. Micelles with radii of 13.6 ± 0.3 nm and 55.0 ± 1.3 nm were determined.

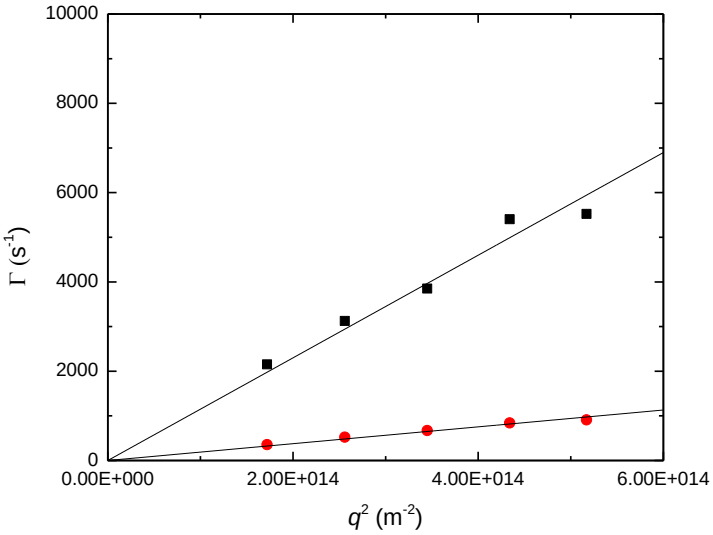

Figure 2.17 Linear regression of Γ vs. q^2 over 5 different angles varying from 60° to 120° of the two decay modes in water with PT (3.6-24.5-0.11) (micelles formed by direct

dissolution). The correlation function $g_1(t)$ was fit using double exponential function. Micelles with radii of 21.3 ± 0.7 nm and 129.7 ± 3.7 nm were determined.

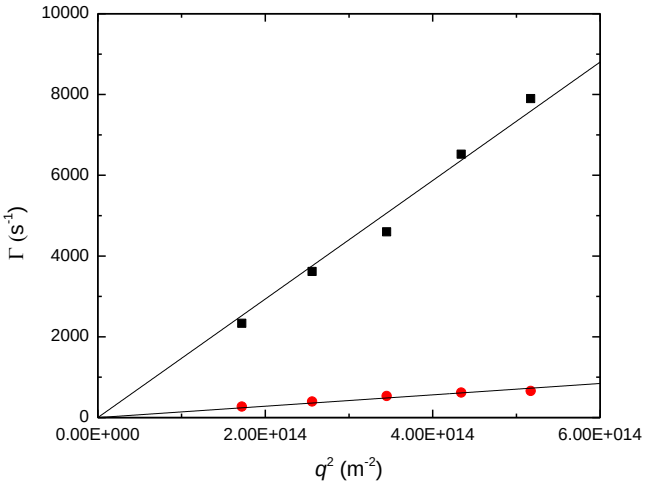

Figure 2.18 Linear regression of Γ vs. q^2 over 5 different angles varying from 60° to 120° of the two decay modes in water with PT (3.6-26.4-0.14) (micelles formed by direct dissolution). The correlation function $g_1(t)$ was fit using double exponential function. Micelles with radii of 16.7 ± 0.4 nm and 173.9 ± 7.2 nm were determined.

2.5 References

(1) Duncan, R. *Nat. Rev. Drug Discov.* **2003**, *2*, 347-360.

(2) van Vlerken, L. E.; Vyas, T. K.; Amiji, M. M. *Pharm. Res.* **2007**, *24*, 1405-1414.

(3) Maeda, H.; Wu, J.; Sawa, T.; Matsumura, Y.; Hori, K. *J. Control. Release* **2000**, *65*, 271-284.

(4) Owens, D. E.; Peppas, N. A. *Int. J. Pharm.* **2006**, *307*, 93-102.

(5) Gaucher, G.; Marchessault, R. H.; Leroux, J. C. *J. Control. Release* **2010**, *143*, 2-12.

(6) Miller, T.; Rachel, R.; Besheer, A.; Uezguen, S.; Weigandt, M.; Goepferich, A. *Pharm. Res.* **2012**, *29*, 448-459.

(7) K. Osada; Christie, R. J.; Kataoka, K. *J. R. Soc. Interface* **2009**, *6* S325-S339.

(8) N. Zhang; P. R. Wardwell; Bader, R. A. *Pharmaceutics* **2013**, *5*, 329-352.

(9) Knop, K.; Hoogenboom, R.; Fischer, D.; Schubert, U. S. *Angew. Chem. Int. Ed.* **2010**, *49*, 6288-6308.

(10) Mancini, R. J.; Lee, J.; Maynard, H. D. *J. Am. Chem. Soc.* **2012**, *134*, 8474–8479.

(11) A. Sizovs; L. Xue; Z. P. Tolstyka; N. P. Ingle; Y. Wu; M. Cortez; Reineke, T. M. *J. Am. Chem. Soc.* **2013**, *135*, 15417−15424.

(12) Yasugi, K.; Nakamura, T.; Nagasaki, Y.; Kato, M.; Kataoka, K. *Macromolecules* **1999**, *32*, 8024-8032.

(13) Elbein, A. D.; Pan, Y. T.; Pastuszak, I.; Carroll, D. *Glycobiology* **2003**, *13*, 17R-27R.

(14) Green, J. L.; Angell, C. A. *J. Phys. Chem.* **1989**, *93*, 2880-2882.

(15) Crowe, J. H.; Crowe, L. M.; Carpenter, J. F.; Wistrom, C. A. *Biochem. J.* **1987**, *242*, 1-10.

(16) Roser, B. *Trends Food Sci. Technol.* **1991**, *2*, 66-69.

(17) Teramoto, N.; Sachinvala, N. D.; Shibata, M. *Molecules* **2008**, *13*, 1773-1816.

(18) Crowe, J. H.; Crowe, L. M. *Nat. Biotechnol.* **2000**, *18*, 145-146.

(19) Clegg, J. S.; Seitz, P.; Seitz, W.; Hazlewood, C. F. *Cryobiology* **1982**, *19*, 306-316.

(20) Clegg, J. S. *Methods Enzymol.* **1986**, *127*, 230-239.

(21) Crowe, J. H.; Crowe, L. M.; Chapman, D. *Science* **1984**, *223*, 701-703.

(22) Kurita, K.; Hirakawa, N.; Morinaga, H.; Iwakura, Y. *Makromol. Chem.* **1979**, *180*, 2769-2773.

(23) Kurita, K.; Masuda, N.; Aibe, S.; Murakami, K.; Ishii, S.; Nishimura, S. I. *Macromolecules* **1994**, *27*, 7544-7549.

(24) Teramoto, N.; Arai, Y.; Shibasaki, Y.; Shibata, M. *Carbohydr. Polym.* **2004**, *56*, 1-6.

(25) Teramoto, N.; Niwa, M.; Shibata, M. *Materials* **2010**, *3*, 369-385.

(26) Srinivasachari, S.; Liu, Y. M.; Zhang, G. D.; Prevette, L. E.; Reineke, T. M. *J. Am. Chem. Soc.* **2006**, *128*, 8176-8184.

(27) Srinivasachari, S.; Liu, Y. M.; Prevette, L. E.; Reineke, T. M. *Biomaterials* **2007**, *28*, 2885-2898.

(28) Snyder, L. R.; Kirkland, J. J. In *Introduction to Modern Liquid Chromatography, second edition*; John Wiley & Sons: New York, 1979, p 246-268.

(29) Yin, L.; Hillmyer, M. A. *Macromolecules* **2011**, *44*, 3021-3028.

(30) Al-Deyab, S. S.; El-Newehy, M. H.; Al-Hazmi, A. M. *Molecules* **2010**, *15*, 4750-4756.

(31) Brown, A. M. *Comput. Methods Programs Biomed.* **2001**, *65*, 191-200.

(32) L. Yin; M. C. Dalsin; A. Sizovs; T. M. Reineke; M. A. Hillmyer *Macromolecules* **2012**, *45*, 4322-4332.

(33) Reineke, T. M.; Davis, M. E. *Bioconjug. Chem.* **2003**, *14*, 247-254.

(34) Wada, M.; Miyazawa, Y.; Miura, Y. *Polym. Chem.* **2011**, *2*, 1822-1829.

(35) Odian, G. *Principles of polymerization, 4th ed.*; John Wiley & Sons, Inc.: Hoboken, NJ, 2004.

(36) Lai, J. T.; Filla, D.; Shea, R. *Macromolecules* **2002**, *35*, 6754-6756.

(37) Jain, S.; Bates, F. S. *Science* **2003**, *300*, 460-464.

(38) S. Jain; Bates, F. S. *Macromolecules* **2004**, *37*, 1511-1523.

(39) Pearson, S.; Allen, N.; Stenzel, M. H. *J. Polym. Sci., Part A: Polym. Chem.* **2009**, *47*, 1706−1723.

(40) Smith, A. E.; Sizovs, A.; Grandinetti, G.; Xue, L.; Reineke, T. M. *Biomacromolecules* **2011**, *12*, 3015−3022.

(41) Ting, S. R. S.; Min, E. H.; Escale, P.; Save, M.; Billon, L.; Stenzel, M. H. *Macromolecules* **2009**, *42*, 9422−9434.

3 CHAPTER THREE

Solution-State Polymer Assmblies Influence BCS Class II Drug Dissolution and Supersaturation Maintenance

Adapted from:

Dalsin M.C.; Tale S. R.; Theresa T.M., Solution-State Polymer Assmblies Influence BCS Class II Drug Dissolution and Supersaturation Maintenance, *Biomacromolecules.* **2014**, 15(2), 500-511.

This work was a joint venture by this author who is responsible for synthesis and characterization of all amphiphilic and hydrophilic copolymers. Molly C. Dalsin who played a major role in spray drying, characterization of SDDs, data analysis, and dissolution studies of micelles.

3.1 Introduction

A large portion of new drug candidates are poorly water soluble, decreasing their bioavailability and effectiveness as therapeutics.[1-3] Amorphous solid dispersions (ASD) have arisen as a platform to increase drug apparent solubility and bioavailability, particularly to promote stability and bioavailability for oral drug delivery. ASDs typically consist of at least one drug dispersed in one polymer excipient, both of which are in the amorphous state. The high-energy, amorphous state of the drug increases its dissolution into aqueous media, and therefore increases the bioavailability and therapeutic effect. However, this high-energy state is only kinetically stable, and the drug may recrystallize, reverting to the more thermodynamically stable state, which negates any solubility increase and significantly decreases bioavailability. Stabilizing the amorphous state of the drug during the manufacturing process and long-term storage is a critical issue in improving oral therapeutic efficacy. This is typically achieved by reducing molecular mobility by utilizing a polymer exhibiting a high glass transition temperature (T_g), optimizing drug-polymer interactions (hydrogen bonding, van der Waals, etc.), and creating a homogenous mixture of drug and polymer.[4] Further, it is of equal importance to utilize an excipient that will solubilize the drug upon dissolution into aqueous media and maintain drug supersaturation by inhibiting crystal nucleation and growth,[4] which is of particular importance for enhancing *in vivo* pharmaceutical performance.

Spray drying has been extensively studied as a method to obtain ASDs.[5,6] This technique is scalable, used industrially, and amenable to a wide variety of polymers. The process involves dissolving polymer and drug into a volatile solvent, atomizing the solution into a drying chamber pumped with a hot and dry gas stream, and collecting the dry powder form using a filter. Both molecularly dissolved mixtures[7-9] and drug-polymer aggregates or emulsions[7,8,10] can be spray dried successfully. The drug-polymer interactions in the feed solvent are "frozen" in the resulting solid dispersion due to rapid solvent evaporation.[11] Since the drug-polymer interactions in the volatile solvent influence the resulting spray-dried dispersion (SDD), the spraying solvent can have a large impact on drug-polymer miscibility, shelf stability, and subsequent aqueous dissolution. The polymer conformation or polymer assemblies in solution especially have an effect on the resultant SDD due to the difference between an extended and swollen polymer chain and a compact and shrunken chain and their available interactions with drug molecules.

Excipients that form nanoaggregates or micelle-like structures in aqueous media have been shown to improve the dissolution of poorly water-soluble drugs.[12-15] One of the better performing polymer excipients, hydroxypropyl methylcellulose acetate succinate (HPMCAS), tends to form nanoaggregates during the dissolution process, which are hypothesized to aid in the supersaturation maintenance of the drug. Friesen and coworkers believe that hydrophobic drug molecules interact with the hydrophobic portions of the polymer, inducing the formation of nanoaggregates.[13] The hydrophilic portions are then likely exposed on the surface yielding a pseudo micelle-like structure, allowing the aggregates to remain stable in aqueous media.[13,14] To this end, investigating the role of polymer structure and solution assembly on drug-polymer miscibility and supersaturation

maintenance of ASDs will enhance our understanding of known excipients, and aid in the formulation of novel pharmaceutically relevant polymers to develop candidates for oral drug formulations.

The primary goal of this study was to examine how solution-state assemblies of polymers and drugs may lead to enhanced drug dissolution and supersaturation maintenance. The role of polymer micelle assembly on drug dissolution and supersaturation maintenance was examined with a variety of polymer structures that exhibit different solution properties. For example, *N,N*-dimethylacrylamide (DMA) is a hydrophilic and biocompatible[16] monomer that has received considerable attention in recent years due to its numerous applications in the medical and pharmaceutical fields.[17,18] A block copolymer of DMA containing poly(ethylene-*alt*-propylene) (PEP), PEP-PDMA, induces formation of solution state assemblies prior to spray drying, while polymers lacking a PEP block do not form distinct micelle assemblies. A third component, 2-methacrylamido glucopyranose (MAG), was introduced to a model polymer excipient system to increase the glass transition temperature of copolymer analogs. To this end, two physically-distinct Biopharmaceutical Classification System (BCS) class II drugs (phenytoin and probucol) were spray dried with four different model polymer excipients consisting of PEP, DMA, or MAG: 1) an amphiphilic diblock terpolymer, PEP-P(DMA-*grad*-MAG), 2) an amphiphilic diblock copolymer, PEP-PDMA, and the respective hydrophilic analogs to these polymers, 3) P(DMA-*grad*-MAG), and 4) PDMA. Selective (methanol, MeOH) and non-selective (tetrahydrofuran:methanol mixture, THF:MeOH) solvents for the hydrophilic block of the amphiphilic diblock polymers were used to induce or repress solution-state assemblies prior to spray drying. Drug-polymer assemblies were

studied with the different structures in both the feed solution (prior to spray drying) and in the dissolution media (post spray drying) by varying the polymer, drug, spray drying solvent, and drug loading. Further, the solid spray dried dispersions (SDDs) were characterized for drug crystallinity, amorphous drug stability, particle size and morphology, and the dissolution behavior of the drug was probed through non-sink, *in vitro* dissolution tests to determine drug release and supersaturation maintenance for the examined structures. Finally, four drug loadings were studied: 0, 10, 25, and 50 wt% of the total solids in the spray drying feed solution and the importance of nanostructure formation on enhancing dissolution performance in simulated intestinal conditions has been revealed.

3.2 Results and Discussion

3.2.1 Synthesis and Characterization of Polymers

The PEP-P(DMA-*grad*-MAG) diblock terpolymer and PEP-PDMA diblock copolymer were synthesized using a combination of anionic and reversible addition fragmentation chain transfer (RAFT) copolymerizations as described by Yin et al.[19] The copolymer P(DMA-*grad*-MAG) and homopolymer PDMA were RAFT polymerized in the same way as the hydrophilic block of their corresponding diblock analogs except that the chain transfer agent (CTA) was not a macromolecular PEP-CTA, but a small molecule trithiocarbonate CTA, namely 2-(Dodecylthiocarbonothioylthio)-2-methylpropionic acid. For P(DMA-*grad*-MAG), the TMS-MAG needed deprotection to yield the final, hydrophilic copolymer.

Four polymers were synthesized for this study, which are shown in Figure 3.1, including two amphiphilic diblock polymers, PEP-P(DMA-*grad*-MAG) and PEP-PDMA, and their corresponding hydrophilic analogs, P(DMA-*grad*-MAG) and PDMA. The hydrophobic PEP block is a macromolecular hydrocarbon chain. In contrast, the blocks and polymers containing DMA and MAG are water soluble and contain hydrogen bonding groups. All the polymers were synthesized for this study using similar methods described by Yin et al.[4,19], and details of polymer characteristics are shown in Table 3.1.

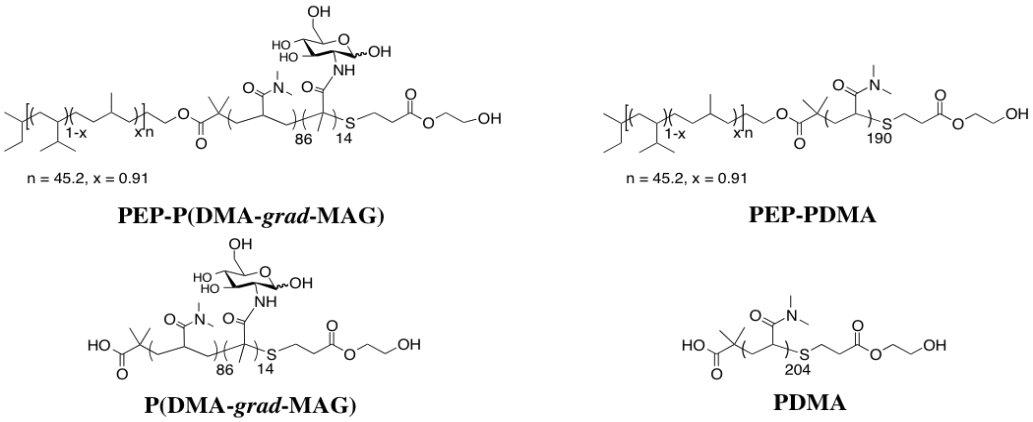

Figure 3.1 Structures of the polymers synthesized and examined in this study.

Table 3.1 Polymer characterization data.

Polymer	N_{EP}[a]	N_{DMA}[a]	MAG (mol %)[b]	MAG (wt %)	PEP (wt %)[c]	M_n (kg/mol)[d]	$Đ$[e]	T_g (°C)[f]
PEP-P(DMA-*grad*-MAG)	45	164	14	25	14	26	1.25	-65, 152.8
PEP-PDMA	45	190	0	0	16	23	1.21	-65, 106.6
PDMA	0	204	0	0	0	20	1.20	118.7
P(DMA-*grad*-MAG)	0	167	14	21	0	24	1.25	157.9

[a]Degree of polymerization. [b]Mole fraction of MAG in the hydrophilic block [c]Weight fraction of the hydrophobic PEP block [d]Total number-averaged molecular weight [e]Dispersity as measured on a SEC using $CHCl_3$ as the eluent at 35 °C relative to polystyrene standards. Values of the MAG-containing polymers are reported before hydrolysis. [f]Reported as the second heating with a 5 °C/min heating rate.

3.2.2 BCS Class II Model drugs

Probucol and phenytoin were chosen as model drugs to probe polymer-drug interactions, the polymer-drug assemblies, and the structure-property relationships for SDD dissolution performance. Both structures are Biopharmaceutical Classification System (BCS) Class II drugs (low aqueous solubility, high permeability through the gastrointestinal membrane) with highly different melting temperatures (T_m) and octanol/water partition coefficients (log P). These two drugs fall close to diagonally opposite ends of a log P vs melting point (T_m) chart (Figure 3.16) and thus are useful Class II drug models to examine SDD formulations. Melting temperature is an indication of the propensity for the drug to crystallize or the crystal lattice strength, and log P is an indication of the relative hydrophobicity. Studying both drug models allows the interpretation of differing polymer-drug interactions, potential for hydrophobic interactions, and crystallization propensity that may arise for various different drug formulations. Phenytoin is more hydrophilic, but has very high crystallization energy, whereas probucol is more hydrophobic, but does not crystallize as fast. Details of each drug are given in Figure 3.2 and Table 3.2.

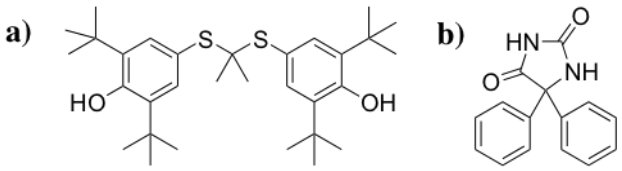

Figure 3.2 Structures of BCS class II drug molecules used in this study: a) probucol and b) phenytoin.

Table 3.2 Molecular characteristics of BCS class II drugs probucol and phenytoin**.**

	Probucol	Phenytoin
T_m (°C)	125, 116	286
Log P	8.9	2.2
water solubility (mg/mL)	4.18×10^{-5}	0.032
molecular weight (g/mol)	517	252
pka	10.29	8.33

It has been shown that the solvent of the feed solution in spray drying can greatly affect the properties of the SDD due to its influence on polymer conformation and polymer/drug interactions.[10,11,22-25] In particular, the solvent can promote or suppress polymer chain folding and polymer-polymer interactions, thereby influencing conformation and the ability of the polymer to interact with the drug. Furthermore, to prevent crystallization, a solvent should promote drug-polymer interactions in the solution state and drug-polymer miscibility in the solid state. For this study, two solvent systems were chosen to study how the polymer/drug solution assembly would influence the resulting SDD properties prior to spray drying. For the two hydrophilic polymers, the spray drying solvent employed was methanol (MeOH). For the amphiphilic diblock copolymer PEP-PDMA, a THF:MeOH (15:2, v/v) mixture was used as a non-selective solvent, and MeOH served as a selective solvent for the hydrophilic block to form the SDDs. When spray drying from the non-selective solvent, both polymer blocks could be effectively dissolved, and the drug was free to interact with either the PEP or the hydrophilic block. Alternatively, when spray drying from a selective solvent, the polymers self-assembled into micelles with a PEP core and PDMA corona. Given that the drugs are soluble in methanol and the micelles form quickly via the direct dissolution method, the drugs would not likely be encapsulated within the hydrophobic core of the micelles;

rather, they would likely remain dissolved in the methanol alongside the micelles. In this case, only the hydrophilic block is likely available to interact with drug. The amphiphilic diblock terpolymer PEP-P(DMA-*grad*-MAG) was only studied in THF:MeOH because the addition of MAG inhibits the ability of the polymer to be directly dissolved into micelles using MeOH.

3.2.3 Organic Solution Properties

To examine the assembly of polymers and drugs in the spray drying feed solutions, quantitative analysis of size and distribution was conducted using DLS. All solutions studied were prepared as 1 wt% polymer/drug dispersions in organic solvent. Four different compositions were used for the polymer/drug dispersions: 0, 10, 25, and 50 wt% probucol relative to polymer. It should be noted that dissolution results of SDDs containing phenytoin showed little solubility enhancement in aqueous media when compared to HPMC-AS (*vide infra*). Thus, the solution assembly prior to spray drying was not analyzed rigorously for these samples. Further, the SDDs of PEP-P(DMA-*grad*-MAG) and PEP-PDMA from the solvent system THF:MeOH showed very little drug dissolution enhancement (*vide infra*) and were not analyzed by DLS. The results for polymer/probucol samples are summarized in Figure 3.3, and detailed analysis is shown in Table 3.3. Figure 3.3 shows that the size of all the samples stays relatively constant even if the drug loading (in the spray dry solvent) is increased from 0 wt% to 50 wt%. This suggests that the drug is molecularly dissolved in the methanol. However, there is a large variance in hydrodynamic radius when comparing different polymers and solvents.

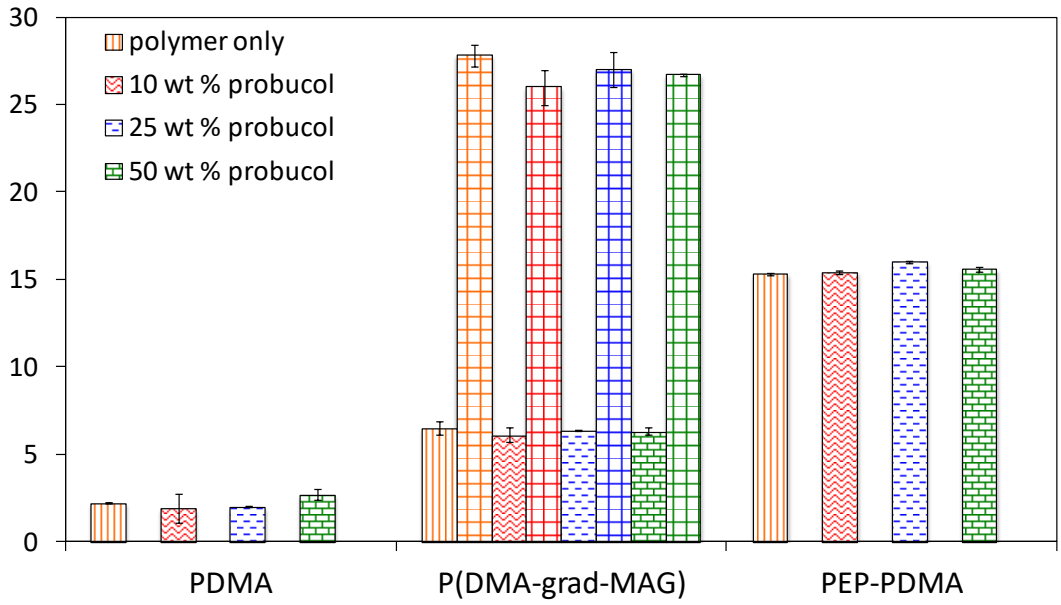

Figure 3.3 Hydrodynamic radii of PDMA, P(DMA-*grad*-MAG), and PEP-PDMA polymers in methanol with 0, 10, 25, or 50 wt% loadings of probucol. All dispersions were a total of 1 wt% solids in methanol. Hydrodynamic radii were calculated by fitting the correlation functions using either cumulant or double exponential expansions. Linear regressions of Γ vs q^2 were performed for five angles (60°, 75°, 90°, 105°, 120°). Large vertical, zig zag, dashed horizontal, and horizontal bricks represent the major contributing hydrodynamic radius in the sample, large grid bars represent the second mode, contributing to 3% or less of the weight fraction of the analyzed sample.

The hydrodynamic radii for PDMA in methanol as evaluated by REPES analysis yielded a bimodal distribution for samples with 0 wt% and 10 wt% probucol. A double-exponential fitting of the data yielded an R_h of 2.22 ± 0.05 nm and 24 ± 2 nm for 1 wt% PDMA in methanol, as an example. Shibayama's bimodal scattering analysis was used to elucidate the weight fractions of the fast and slow decay modes. For PDMA in methanol, the weight fraction of the mode corresponding to 2.22 nm was estimated to be 99.7% while that of 24 nm mode was 0.3%. The weight fraction of the mode corresponding to 24 nm was not observed after the weight fraction of PDMA in methanol was reduced to 90% with the introduction of 10% probucol. This data suggests that the PDMA polymer in solution is not aggregated and is likely in a morphology consisting of solvated free polymer chains. The higher size seen with the 1 wt% dispersion of PDMA in methanol is likely

due to a small fraction of polymer aggregates, which dissociate when the weight fraction of polymer is decreased from 1 wt % to 0.9 wt %.

Samples of P(DMA-*grad*-MAG) with probucol in methanol were evaluated by REPES analysis and also showed a bimodal distribution. Cumulant analysis confirmed a broad distribution of scattering by yielding an average R_h = 26 nm with high average dispersity (μ_2/Γ^2 = ~0.7). Fitting the data with a double-exponential expansion gave R_h = 6.1 ± 0.4 and 26 ± 1 nm for the sample containing P(DMA-*grad*-MAG) plus 10 wt % probucol, which matched the peaks given by REPES analysis. The particles of 6.1 nm radius were indicative of solvated polymer chains for the P(DMA-*grad*-MAG) sample, and the 26 nm radius suggests the formation of a loose aggregate solution structure. This aggregate does not disperse into free chains as more drug is introduced, which decreases the weight fraction of polymer in solution. Due to its high hydrophilicity, PMAG does not dissolve well in methanol, thus, it is hypothesized that the polymer aggregates are loose micelles with the MAG portion of the polymer in the core. Using Shibayama's bimodal scattering analysis, the weight fractions for the polymer aggregates in a methanol solution containing 10 wt % probucol had radii of 6.1 nm and 26 nm (corresponding to 97.5 % and 2.5 % of the sample, respectively). This indicates that a majority of the polymer is free chains dispersed in the methanol solution. Shibayama analysis for polymer P(DMA-*grad*-MAG) only with 25 wt % and 50 wt % loadings of probucol, yielded very similar results.

Finally, samples of PEP-PDMA diblock copolymer containing probucol in methanol were analyzed via DLS. Optically, the solutions of PEP-PDMA with probucol in methanol were clear with a slight bluish tinge, indicative of micelle formation. Further, REPES analysis yielded sharp, monomodal peaks. The correlation data for 1 wt % PEP-PDMA in methanol, as an example, was fit with a cumulant analysis, resulting in R_h = 15.3 ± 0.9 nm with a very low dispersity (μ_2/Γ^2 = 0.06). This data indicates a micellar dispersion with PEP as the core and PDMA as the corona in methanol. The low dispersity is characteristic of micelles with a tight interaction between polymers

and low chain equilibration due to the high disfavor of PEP in methanol. Further, the very low hydrophobic content (PEP = 16 wt %) and the low T_g of the PEP block (-65°C) make the polymers amenable to micellization via direct dissolution into an organic solvent (i.e. methanol). The size of the micelles is comparable to previous work by our group showing that PEP-PDMA diblock copolymer (same molecular weight) forms micelles of ~14 nm radius in water (via a nanoprecipitation procedure).[5,6,19] The slightly larger hydrodynamic radius of the PEP-PDMA in methanol is hypothesized to be primarily due to two factors: 1) The micellization method, in which direct dissolution would yield a larger radius (higher aggregation number) than nanoprecipitation due to the differences in PEP and methanol interfacial energy at the onset of micellization, and 2) The difference in solvent since PEP would be hypothesized to favor methanol as an anti-solvent over water.

Table 3.3 DLS characterization of 1 wt % polymer dispersions in methanol with or without probucol.

Polymer	wt % probucol	R_h (nm)[a]	μ_2/Γ^2 [b]	R_h (nm)[c]
PDMA	50	1.6 ± 0.1	0.59	0.4 ± 0.3, 2.7 ± 0.4
	25	5.3 ± 0.3	0.18	2 ± 0.04, 30 ± 8
	10	5.4 ± 0.2	0.77	1.9 ± 0.8, 20 ± 7
	0	6.3 ± 0.2	0.11	2.2 ± 0.05, 24 ± 2
P(DMA-*grad*-MAG)	50	26 ± 3	0.75	6.3 ± 0.2, 26.7 ± 0.1
	25	25.8 ± 0.1	0.77	6.3 ± 0.05, 27 ± 1
	10	26.1 ± 0.5	0.77	6.1 ± 0.4, 26 ± 1
	0	28.2 ± 0.1	0.74	6.5 ± 0.4, 27.8 ± 0.6
PEP-PDMA micelles	50	15.6 ± 0.1	0.12	NA
	25	16.0 ± 0.4	0.05	NA
	10	15.4 ± 0.1	0.12	NA
	0	15.3 ± 0.9	0.06	NA

All DLS analysis performed at 1 wt % concentration.

[a]Hydrodynamic radii determined by fitting the correlation functions with the cumulant expansion, then performing linear regression of Γ vs q^2 over five angles (60° to 120°).

[b]Average of μ^2/Γ^2 from scattering angles of 60°, 75°, 90°, 105°, and 120°.

[c]Hydrodynamic radii determined by fitting the correlation function with the double exponential expansion, then performing liner regressions of Γ vs q^2 for two separate decay modes over angles 60° to 120°.

3.2.4 Solid-State Properties

In general, the physical stability of a homogeneously mixed SDD is due to the thermodynamic stability of the drug molecule. This can include configurational entropy, fragility index, molecular mobility,[7-9,26-29] and drug-polymer interactions and miscibility[4,7,8,10,30-32]. Selection of appropriate spray-drying solvent and conditions can lead to a homogeneous mixture of amorphous drug and polymer.[11,33] A physically stable ASD allows the opportunity to enhance aqueous dissolution of the drug and increase bioavailability. To study the physical stability, homogeneity, and size/morphology of the SDDs produced, a combination of powder X-ray diffraction (PXRD), modulated differential scanning calorimetry (MDSC), and scanning electron microscopy (SEM) techniques were used.

PXRD is a common tool used to identify and characterize crystalline material present in SDDs.[12-15,34-37] For all SDDs of polymer with phenytoin (up to 50 wt% loading of drug), a broad, diffuse diffractogram with no Bragg peaks was observed, indicating that at least 95% of the drug in the SDD is amorphous (Figure 3.10). For all SDDs of polymer with probucol, the scattering patterns (Figure 3.4) look amorphous except for those of PEP-P(DMA-*grad*-MAG) with 25 and 50 wt% probucol sprayed from a non-selective solvent of THF:MeOH (15:2, v/v). These dispersions show Bragg peaks characteristic of probucol form II crystals – the less dense and lower melting temperature form.[13,38] On the contrary, PXRD of the unprocessed probucol shows a scattering pattern consistent with form I crystals – the more densely packed and higher melting temperature form. This suggests that the probucol crystal growth from the PEP-P(DMA-*grad*-MAG) matrix begins as the lower energy crystal form. However, others have noted that given time and humidity, probucol can transform to the higher energy crystal form I.[13,14,34]

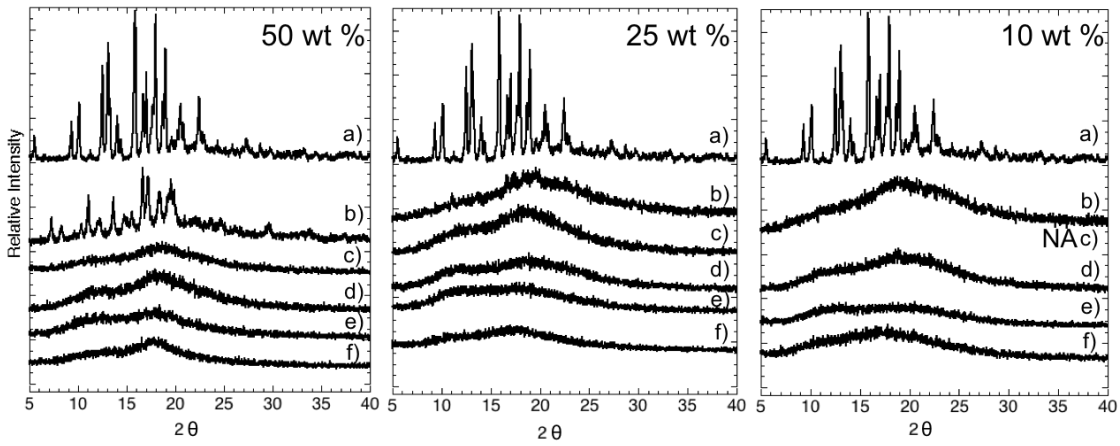

Figure 3.4 PXRD patterns for SDDs with probucol loadings of 50 wt%, 25 wt%, and 10 wt%, from left to right, comparing: a) crystalline probucol, b) PEP-P(DMA-*grad*-MAG) sprayed from THF:MeOH (15:2, v/v), c) PEP-PDMA sprayed from THF:MeOH (15:2, v/v) d) PEP-PDMA sprayed from MeOH e) PDMA sprayed from MeOH f) P(DMA-*grad*-MAG) sprayed from MeOH.

Depending on the crystal characteristics, PXRD can quantify crystalline material to about 5% or less.[16,39,40] However, DSC can quantitate crystallinity with higher sensitivity than PXRD in addition to providing information regarding the homogeneity of the SDD.[17,18,33] Therefore, DSC was used in tandem with PXRD to study the solid-state properties of the SDDs. To eliminate any potential overlap of enthalpic components with the glass transition, modulated DSC (MDSC) was used. This technique allows for the deconvolution of the total heat flow into a linear combination of reversing (heat capacity) and non-reversing (enthalpic recovery, solvent evaporation, crystallization) components.[19,33,41,42] From MDSC, the glass transition temperature (T_g) was studied to yield information such as the amorphous/homogeneous state of the drug/polymer[20,43-45] and the miscibility of the drug/polymer blend[46-48] in addition to indicating drug-polymer interactions such as hydrogen bonding.[49-51] Typically, the SDD will exhibit a single T_g that is in between the T_g of the pure amorphous drug and the pure polymer if the drug is molecularly dispersed in the polymer matrix. Furthermore, a shift in T_g (and the amount of the shift) can indicate drug-polymer interactions due to the incorporation of drug molecules between polymer chains. All MDSC

analyses and representative MDSC traces are shown in Figure 3.11, Figure 3.12, Table 3.6, and Table 3.7.

A glass transition comparison of all polymers and feed solution solvents revealed that there is a single T_g value for each SDD, which is indicative of a homogenous mixture of miscible amorphous drug and polymer. Further, the single T_g value decreases toward that of the amorphous drug as the drug wt% in the SDD increases. The polymers containing only hydrophilic groups consistently exhibited a higher T_g value than the diblock amphiphilic polymers. The lowering in the T_g value of the hydrophilic block (in the diblock polymers) could be caused by either the low T_g of the PEP block or possibly that the hydrophilic block interacts stronger with probucol (T_g = 28 °C) than what was observed with the polymer models containing only hydrophilic groups. P(DMA-*grad*-MAG) MeOH has a much higher T_g value (T_g = 141 °C) than the diblock analog (PEP-P(DMA-*grad*-MAG) THF:MeOH, T_g = 116 °C), suggesting that P(DMA-*grad*-MAG) may have higher inter- and intra-molecular interaction than PEP-P(DMA-*grad*-MAG) polymers. Interestingly, spray-dried P(DMA-*grad*-MAG) would not dissolve readily in PBS + FaSSIF media, however, when 10 wt% probucol was introduced, the SDD dissolved readily, indicating strong hydrogen bonding between polymer chains, yet these hydrogen bonds are disrupted when drug is introduced. For SDDs containing phenytoin, the T_g values are lower than that observed with probucol even though the T_g value for amorphous phenytoin is higher than for probucol (71 °C vs 28 °C).[14] This could be indicative of more polymer-drug interactions with phenytoin than with probucol, which could be justified by a detailed look at the polymer and drug structures and non-covalent bonding potential. For example, phenytoin has strong hydrogen bond donors and acceptors (thus a "strong crystallizer"), whereas in probucol, the benzylic position of the H-bond donor and acceptor groups may weaken H-bonding (thus, this structure is a "weaker crystallizer").

MDSC also gives information regarding crystallization during heating, an indication of drug-polymer interactions and the ability of the polymer to repress crystallization. It also shows if

a melting endotherm is already present, which suggests that crystalline material is innate to the solid dispersion. However, there are many caveats related to the value of the melt endotherm of the drug since it can be affected by polymer type,[52,53] large T_m changes,[33] and mixing of drug/polymer during heating[54]. A higher crystallization temperature means more polymer stabilization and crystallization inhibition (it takes more energy to crystallize the drug). To determine the amount of crystalline material before MDSC analysis for probucol-containing SDDs, the melt endotherm is subtracted from the crystallization enthalpy, and then normalized to the loading of drug. For phenytoin, calculating a percent crystallinity was not possible, and we can assume (to 5% error) that all phenytoin SDDs are amorphous from PXRD data. This implies that the crystallization seen in MDSC is due to heating.

The prepared SDDs all revealed crystallization transitions above the single T_g where extra mobility and energy from the heating process leads to enhanced crystallization rates. The higher the difference between the SDD T_g and the crystallization event, the better the polymer is able to prevent drug crystallization. Therefore, spray dry solvent played a role in drug stability where PEP-PDMA sprayed from MeOH was the most effective formulation at inhibiting phenytoin crystallization during heating, followed by P(DMA-*grad*-MAG) from MeOH, PDMA from MeOH, PEP-PDMA from THF:MeOH, and finally PEP-P(DMA-*grad*-MAG) from THF:MeOH. The same analysis of 50 wt % probucol in polymer yielded PEP-PDMA sprayed from MeOH and PDMA sprayed from MeOH as top performers followed by P(DMA-*grad*-MAG) from MeOH, PEP-PDMA from THF:MeOH, and PEP-P(DMA-*grad*-MAG) from THF:MeOH. These findings suggest that the proportion of DMA in the excipient is very important for drug-polymer interactions and drug polymer miscibility. Results of this analysis for 50 wt % probucol are shown in Table 3.4. These results show that although the SDDs created with PDMA from MeOH consistently had a higher T_g value than the SDDs created from PEP-PDMA from MeOH, PEP-PDMA micelles were more effective at inhibiting crystallization than PDMA free chains.

Table 3.4 Comparison of the weight fractions of monomers and drug in SDDs with 50 wt% loadings of probucol. The percent crystallinity of probucol was calculated from MDSC.

Sample	Solvent	Proposed morphology	SDD weight fraction				Ratio PDMA/PBC	% PBC crystallinity
			PEP	PDMA	PMAG	Probucol		
PEP-P(DMA-*grad*-MAG)	THF:MeOH	free chains	0.06	0.38	0.06	0.5	0.76	16.8
P(DMA-*grad*-MAG)	MeOH	aggregates	0	0.43	0.07	0.5	0.86	6.8
PEP-PDMA	THF:MeOH	free chains	0.07	0.43	0	0.5	0.86	6.3
PEP-PDMA	MeOH	micelles	0.07	0.43	0	0.5	0.86	0
PDMA	MeOH	free chains	0	0.50	0	0.5	1.00	0

It is important to note that the drug molecules are not loaded into the PEP core of the micelles of PEP-PDMA made from direct dissolution into MeOH, but rather likely interact with the corona of the micelles during the spray drying process. Evidence for this comes first from the fact that the drugs are soluble in methanol and have no driving force to be incorporated into the core of the micelles. Second, the micelles are formed kinetically through a direct dissolution process where the micelles form fast. Thus, unless some drug molecules were near the core of the micelle when formed, the micelles would not load drug into the core. Third, the micelle size does not change in methanol as the drug portion increases. Further, MDSC analysis suggests that the drug interacts with DMA-rich areas. If drug were incorporated into the PEP cores of the micelles, it would be expected to crystallize quickly due to the low T_g of the PEP block (promoting high molecular mobility). Finally, the size of the nanoaggregates increases with increasing drug concentration when the SDDs are dissolved in aqueous media (discussed below). Micelle size does not change when in MeOH since the drug is soluble and potentially not interacting with the corona of the micelles, but upon spray drying, the bulk state should consist of micelles with drug interspersed in the coronas and between micelles. Upon dissolution into aqueous media, the drugs prefer to interact with the corona of the micelles over the aqueous media, thus swelling the size of the micellar coronas (Figure 3.5).

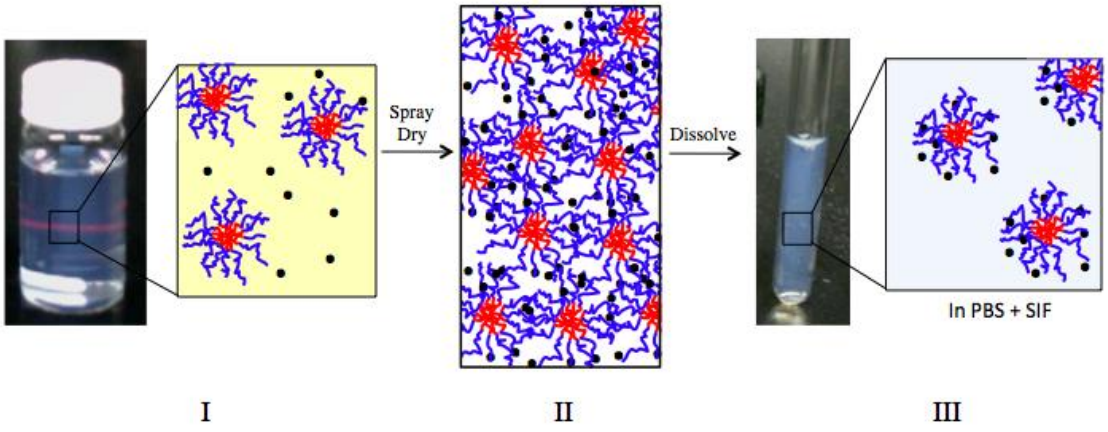

Figure 3.5 (I) Image of a 1 wt% dispersion of PEP-PDMA micelles with 10 wt% probucol showing the Tyndall effect, with cartoon showing PEP-PDMA micelles (blue = PDMA corona, red = PEP core) with dissolved drug (black dots) in methanol. (II) Cartoon of proposed morphology of the solid-state of the SDD in which drug is in the corona of the micelles as opposed to loaded into the core. (III) Image of PEP-PDMA from MeOH SDD with 10 wt% probucol dissolved in PBS + FaSSIF yielding a final drug concentration of 1000 μg/mL. Cartoon showing the possible dissolution mechanism in which drug stays associated with the PDMA corona of the micelles as the solid SDD particles break apart into micelles.

Scanning Electron Microscopy (SEM) of the spray-dried particles allows visualization of the particle morphology and size. Particle size is of particular importance for SDD performance since increased surface area is directly related to increased drug dissolution.[34,55] As seen in Figure 3.6, particle morphology and size of the SDD particles of the various polymer structures sprayed with probucol stays relatively consistent except for those with PEP-P(DMA-*grad*-MAG) and PEP-PDMA sprayed from THF:MeOH, which show coalescing particles. These particles also exhibited a lower yield due to the increased stickiness of the particles, and thus deposition on the drying chamber wall. This is consistent with the observation of Bhandari et al. when spray drying polymers above their T_g.[56] The buckling morphology observed in particles formed from PEP-PDMA sprayed from MeOH, P(DMA-*grad*-MAG) from MeOH, and PEP-P(DMA-*grad*-MAG) from THF:MeOH is likely due to the larger hydrodynamic radius of the aggregates in the feed solution. We hypothesize that the larger radius reduces the diffusion coefficient of the polymer within the atomized droplets, which may increase the concentration of the polymer at the particle surface,

forming a shell-like structure upon drying (remaining solvent trapped in the droplet rapidly diffused out of the particle, leading to buckling).[10] With the PDMA from MeOH samples, the majority of the polymer is in a free chain conformation leading to the formation of spherical particles with slight shell folding. The slight shell folding is likely due to the formation of a non-rigid shell during PDMA spray dry processing. Slight differences in morphology can be seen when increasing the drug content in the SDD from 0 wt% to 50 wt%, however, the particle size stays relatively the same (Figure 3.13, Figure 3.14). It should be noted that no significant differences in particle size and morphology was noticed when comparing SDDs of phenytoin versus probucol.

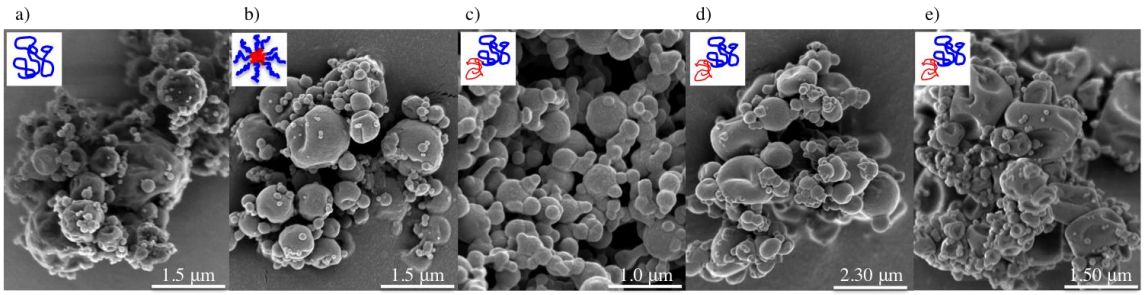

Figure 3.6 SEM images for 50 wt% probucol sprayed with (a) PDMA sprayed from MeOH, (b) PEP-PDMA sprayed from MeOH, (c) PEP-PDMA sprayed from THF:MeOH (15:2, v/v) at 0.1 total wt%, (d) PEP-P(DMA-*grad*-MAG) sprayed from THF:MeOH (15:2, v/v), and (e) P(DMA-*grad*-MAG) sprayed from MeOH. Cartoon inset illustrates the proposed morphology of the polymers in organic solution before spray drying.

3.2.5 Aqueous Solution State Properties Post-Spray Drying

Ultimately, the goal of a SDD is to increase the absorption of poorly water-soluble drugs when administered orally. To this end, a SDD should enhance drug solubility and maintain supersaturation by decreasing crystal nucleation and growth in the intestinal lumen. Therefore, non-sink, *in vitro* dissolution testing in aqueous media, simulating conditions in the intestinal lumen, was performed on all SDDs to elucidate the drug concentration enhancement relative to the bulk crystalline material for both phenytoin and probucol. In the dissolution experiments, "dissolved drug" includes any species that are not removed by centrifugation at 13,000 rpm for one minute,

which includes free drug, drug in bile salt micelles, drug-polymer colloids and aggregates, or drug-polymer micelles.

Figure 3.7 shows an example dissolution plot of all tested polymers with 10 wt% probucol loading. Polymers showing the highest enhanced drug solubility and supersaturation maintenance exhibit a burst release profile to create a supersaturated drug solution that is maintained over the 6 hour incubation period (ex. PEP-PDMA from MeOH). Poor performing polymers exhibit lower drug release as compared to the crystalline form [ex. PEP-P(DMA-*grad*-MAG) from THF:MeOH]. Figure 3.8 displays the area under the curve (AUC) from the dissolution profiles (Figure 3.15) of all SDDs with probucol and phenytoin at drug loadings of 10, 25, and 50 wt%. HPMC-AS was included as a positive control for comparison since it is known to be a high-performing excipient that forms nanoaggregates upon exposure to dissolution media.

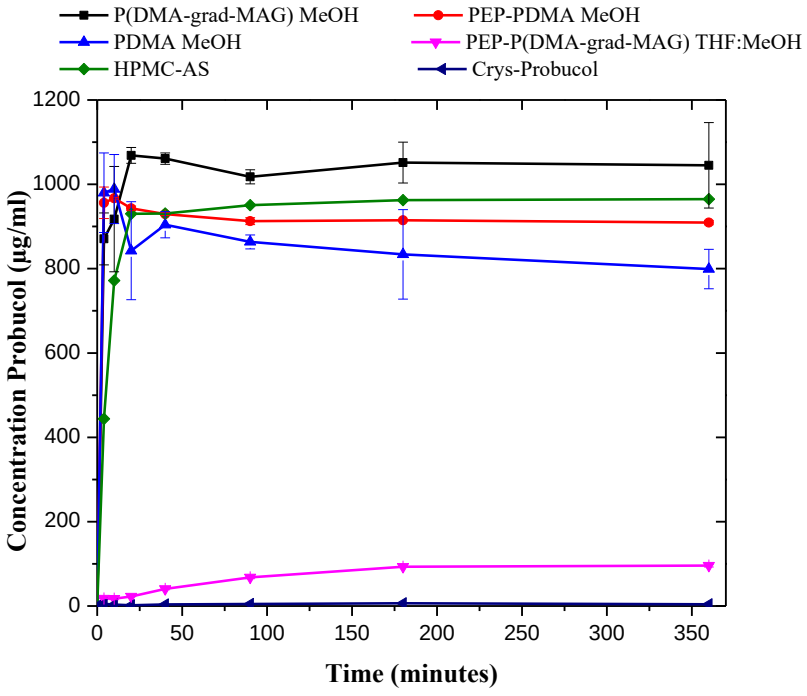

Figure 3.7 Dissolution data of SDDs with 10 wt% probucol showing excellent burst release and supersaturation maintenance for P(DMA-*grad*-MAG) sprayed from MeOH, PEP-PDMA sprayed from MeOH, and PDMA sprayed from MeOH, yet minimal release for insoluble PEP-P(DMA-*grad*-MAG) sprayed from THF:MeOH (15:2, v/v). Error bars represent the standard deviation of duplicate samples.

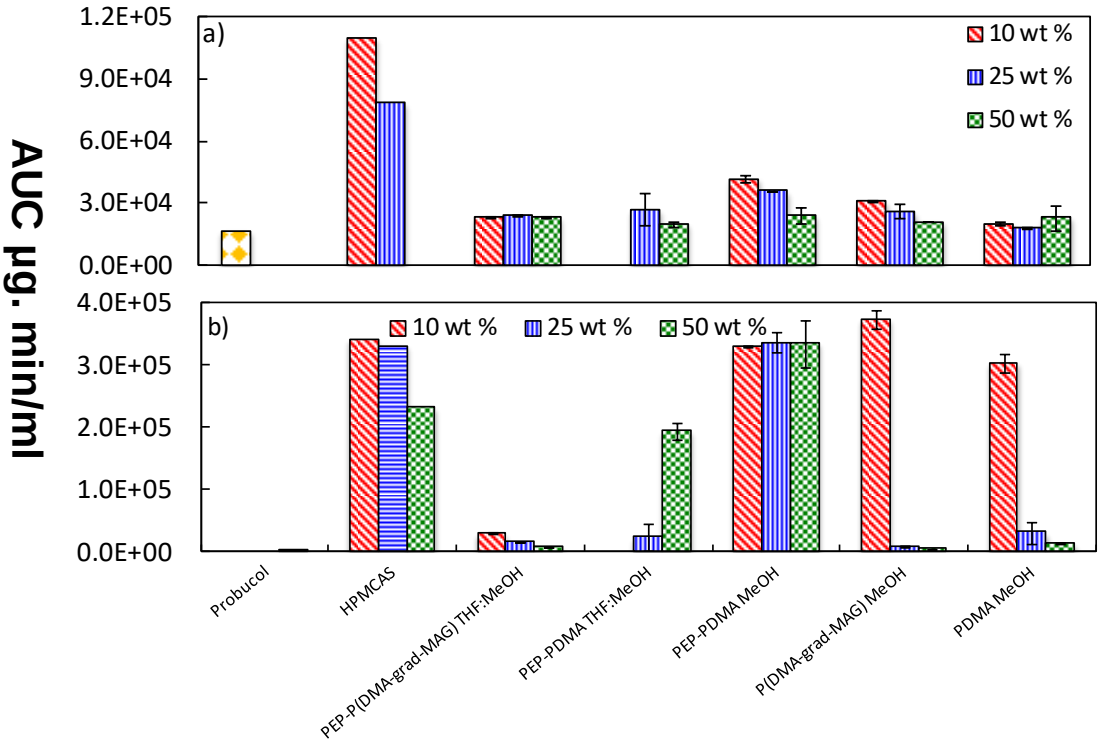

Figure 3.8 Area under the curve (AUC) as calculated at 360 min from the dissolution data of SDDs with loadings of a) phenytoin or b) probucol. Yellow diamonds represent crystalline drugs, phenytoin in a) and probucol in b) and horizontal blue lines in b) represent HPMCAS spray dried at 33 wt% with probucol.

For phenytoin-loaded SDDs, none of the polymers exhibited a significant increase in soluble drug over the crystalline material, and HPMC-AS was still the highest performing excipient. The low increase in phenytoin solubility is hypothesized to be due to the extremely fast nucleation and growth of phenytoin crystals when introduced to aqueous media.[57] During dissolution testing, when the PBS + FaSSIF solution was added to the SDD, precipitation occurred immediately, suggesting that the drug-polymer interactions are not strong enough to inhibit nucleation and growth of phenytoin crystals.

For probucol-loaded SDDs, each of the polymers showed an increase in drug solubility over crystalline probucol. The amphiphilic diblock polymers, PEP-P(DMA-*grad*-MAG) and PEP-PDMA sprayed from the non-selective solvent (THF:MeOH, 15:2 v/v), were not soluble in the

dissolution media due to the lack of solubility of the hydrophobic PEP block in water. Subsequently, there was very little drug dissolution, suggesting carrier-controlled dissolution.[58] Further, SEM analysis showed coalesced particles due to the low T_g of the PEP block, thus decreasing the surface area available for drug dissolution. SDDs of the hydrophilic-only polymers, PDMA and P(DMA-*grad*-MAG) sprayed from methanol, showed burst releases of almost 100% of the drug and maintained supersaturation over the 6 hours at loadings of 10 wt%, but show very little release at both 25 and 50 wt% probucol loadings. It is hypothesized that the polymer to drug ratio may be too low at drug loadings of 25 and 50 wt% to inhibit immediate drug crystal nucleation, thus completely inhibiting solubilization. SDDs of PEP-PDMA sprayed from methanol were the best performers, releasing almost 100% of the drug immediately and sustaining supersaturation over 6 hours of incubation at 37 °C. It is theorized that this effect is due to the forced aggregation of PDMA chains (by the PEP blocks) forming the corona in the micelle structures.

To elucidate how aggregate versus non-aggregate polymer structures contribute to the drug dissolution profiles, DLS experiments were performed at the first and last time points of the dissolution testing (corresponding to time 0 and 360 minutes). Samples were made in duplicate (one sample was for the first time point of dissolution and the other was incubated for the 6 hours at 37 °C). SDDs of three of the polymers with probucol were tested: PDMA sprayed from MeOH, P(DMA-*grad*-MAG) from MeOH, and PEP-PDMA from MeOH (all were formed with 0, 10, 25, and 50 wt% loading of probucol). PEP-PDMA and PEP-P(DMA-*grad*-MAG) sprayed from THF:MeOH were not studied via DLS since the polymers were not soluble in the dissolution medium. Figure 3.9 shows the major contributing hydrodynamic radii versus the polymer type at the first and last time point during dissolution testing. Detailed analysis of the DLS data is shown in Table 3.5, including cumulant and double exponential analyses.

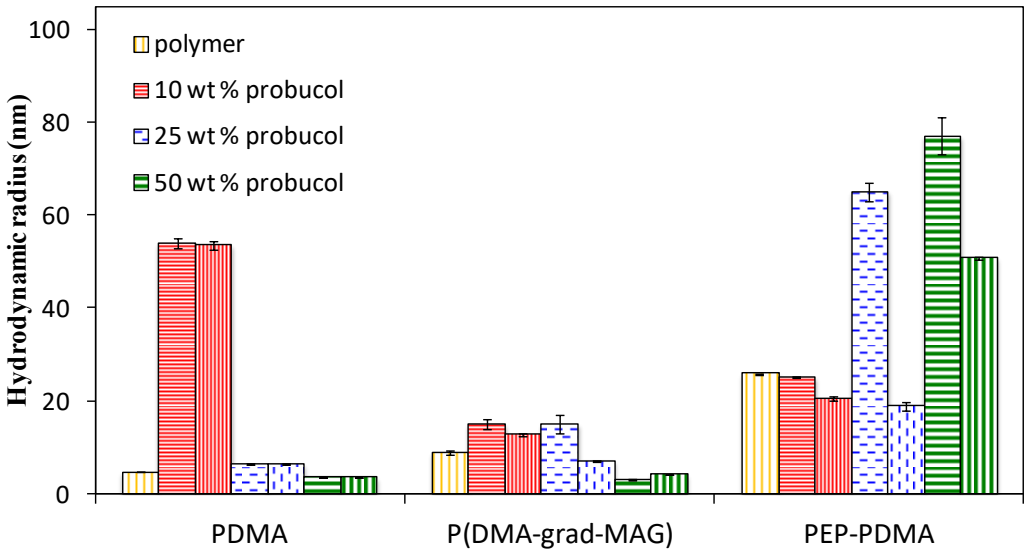

Figure 3.9 Hydrodynamic radii (R_h) of SDDs of PDMA sprayed from MeOH, P(DMA-*grad*-MAG) sprayed from MeOH, and PEP-PDMA sprayed from MeOH with 0, 10, 25, and 50 wt% probucol when exposed to PBS + FaSSIF and filtered through a 0.45 μm filter. The narrow horizontal lines (red, blue, and green) corresponds to the first time point during dissolution (t = 0 minutes) and the narrow vertical lines (red, blue, and green) corresponds to the last time point during dissolution (t = 360 minutes). The broad vertical lines (yellow) represent the R_h of spray-dried polymer only (no drug). The hydrodynamic radii shown are the major contributing weight fraction of scattering.

Table 3.5 DLS characterization of aggregates from SDDs of PDMA sprayed from MeOH, P(DMA-*grad*-MAG) from MeOH, and PEP-PDMA from MeOH with 0, 10, 25, and 50 wt% loadings of probucol when exposed to PBS + FaSSIF at the first (t = 0 minutes) and last (t = 360 minutes) time points during aqueous dissolution.

Polymer	wt % probucol	Time (min)	R_h (nm)[a]	μ_2/Γ^2 [b]	R_h (nm)[c]
PDMA	50	0	13.1 ± 0.4	0.72	3.40 ± 0.06, 24.6 ± 0.4
		360	16.8 ± 0.7	0.88	3.44 ± 0.04, 38.7 ± 0.7
	25	0	6.3 ± 0.2	0.08	2.77 ± 0.09, 17 ± 1
		360	6.4 ± 0.2	0.12	2.8 ± 0.2, 9 ± 2
	10	0	54 ± 1	0.51	31.9 ± 0.8, 33.0 ± 0.4
		360	53.5 ± 0.9	0.47	30 ± 1, 33.5 ± 0.8
	0	0	14.5 ± 0.4	0.48	4.59 ± 0.04, 33.1 ± 0.9
P(DMA-*grad*-MAG)	50	0	8 ± 2	0.26	2.98 ± 0.02, 14 ± 1
		360	15.0 ± 0.3	0.69	4.17 ± 0.05, 25.5 ± 0.7
	25	0	61 ± 6	0.52	15 ± 2, 100 ± 22
		360	26.1 ± 0.5	0.71	7.06 ± 0.08, 29.4 ± 0.5
	10	0	48 ± 2	0.68	15 ± 1, 47 ± 4
		360	46 ± 2	0.71	12.7 ± 0.4, 54 ± 1
	0	0	35 ± 1	0.79	8.9 ± 0.4, 46 ± 4
PEP-PDMA micelles	50	0	77 ± 4	0.173	NA
		360	50.8 ± 0.3	0.309	41 ± 2, 41 ± 2
	25	0	65 ± 2	0.299	35 ± 1, 36.8 ± 0.8
		360	36.9 ± 0.3	0.415	18.8 ± 0.9, 26 ± 3
	10	0	25.1 ± 0.2	0.212	13.3 ± 0.3, 14.5 ± 0.3
		360	20.5 ± 0.4	0.15	NA
	0	0	25.8 ± 0.2	0.24	13.7 ± 0.1, 15.1 ± 0.2

All DLS analysis performed at 1 wt % concentration. [a]Hydrodynamic radii determined by fitting the correlation functions with the cumulant expansion, then performing linear regressions of Γ vs q^2 over 5 angles from 60° to 120°. [b]Average of μ_2/Γ^2 from scattering angles of 60°, 75°, 90°, 105°, and 120°. [c]Hydrodynamic radii determined by fitting the correlation function with the double exponential expansion, then performing linear regressions of Γ vs q^2 for the two separate decay modes over 5 angles from 60° to 120°.

The light scattering analysis of the dissolved SDDs with probucol for PDMA, P(DMA-*grad*-MAG) and PEP-PDMA presented interesting insight into the relationship between solution-state assembly, drug dissolution, and supersaturation maintenance. Firstly, SDDs of PDMA with 0 and 10 wt% probucol dissolved readily into PBS + FaSSIF, yielding a clear solution for 0 wt% probucol and a clear solution with a slight blueish tinge for 10 wt% probucol. SDDs at higher drug loadings did not dissolve into PBS + FaSSIF and subsequently much of the solids were filtered out

through the 0.45 μm filter before DLS analysis. Samples of spray-dried PDMA with 0, 25, and 50 wt% loadings of probucol exhibited two distinct modes as seen in the REPES distribution curves. When analyzed through double exponential analysis, the hydrodynamic radii corresponding to the fast decay mode were under 5 nm and that of the slow decay mode was between 17 and 34 nm for all three samples. It was found that over 97% of the population of scatterers were under 5 nm, and less than 3% were the aggregates between 17 and 34 nm. This would suggest that the majority of scatterers were dissolved polymer instead of polymer/drug aggregates. Further, dissolution data shows very little drug release for these two systems. However, when the SDD of PDMA with 10 wt% probucol was dissolved in PBS + FaSSIF, a colloidal solution was produced and the REPES distribution curve showed three modes in which R_h = 6, 21, and 85 nm. This suggests that some dissolved polymer, as well as two distinctly sized drug/polymer aggregates exist for this SDD formulation. Dissolution data for this system shows full, burst release and sustained supersaturation. After incubation at 37 °C for 360 minutes, SDDs with 25 and 50 wt% showed little change, and the weight fraction of the smaller R_h increased to 99%. The colloidal dispersion of SDD with 10 wt% probucol also showed no significant change.

For SDDs of P(DMA-*grad*-MAG), 10 wt% probucol was the only sample which immediately dissolved upon introduction to PBS + FaSSIF. The dissolution produced a milky, colloidal solution, which remained unchanged after passage through a 0.45 μm filter. The calculated hydrodynamic radii revealed two populations, R_h = 15 nm and 47 nm, with corresponding weight fractions of 98.9% and 1.1%. This suggests a small and a large drug/polymer aggregate dispersion, and dissolution data for this sample shows excellent release and supersaturation maintenance. Interestingly, P(DMA-*grad*-MAG) does not dissolve in PBS + FaSSIF as a 1 wt%, polymer-only solution. This is believed to be due to strong hydrogen bonding between polymer chains. When 10 wt% drug is introduced, the resulting SDD is soluble in PBS + FaSSIF, implying that the drug is plasticizing the polymer and is breaking up the hydrogen bonding between chains to some degree.

Following this reasoning, it can be assumed that the insolubilities for higher probucol loadings when dissolved in PBS + FaSSIF are due to drug precipitating out of solution, and likely not insoluble polymer aggregates. SDDs with 0, 25, and 50 wt% probucol had much of the insolubilities filtered out of the sample before DLS analysis. The hydrodynamic radii of P(DMA-*grad*-MAG) spray dried polymer, as calculated by double exponential analysis, was 8.9 nm and 46 nm with weight percents of 99.0% and 1.0%, respectively. The hydrodynamic radii as calculated by double exponential for 25 and 50 wt% loadings and was found to each yield a bimodal distribution: for 25% loading, R_h = 15 nm and 100 nm (weight percent of 99.8% and 0.2%) and for 50% loading, R_h = 2.98 nm and 14 nm (weight percent of 96.8% and 3.2%). Samples with 25 and 50 wt% probucol showed very little drug release during dissolution. After 6 hours of incubation at 37 °C, the duplicate samples were removed and analyzed by DLS for size and dispersity. Samples of the SDDs all decreased in size and the weight percent of the smaller radius increased. In summary, probucol acts as a plasticizer to break hydrogen bonding between chains at 10 wt% of drug loading for SDDs of P(DMA-*grad*-MAG), and aid the release of the drug in PBS + FaSSIF solution. Higher drug loadings led to drug precipitating out of solution, and resulted in poor dissolution profiles.

All samples of PEP-PDMA micelles from methanol dissolved readily into PBS + FaSSIF to yield colloidal solutions that appeared clear with a blue tinge. For spray dried PEP-PDMA micelles, cumulant analysis revealed an R_h = 25.8 nm with μ_2/Γ^2 = 0.24, a radius larger than that of the micelles in methanol, which could suggest that the SDD particles are not completely broken apart or dissolved into the micelles at the first dissolution time point. DLS data for the remaining systems were analyzed by cumulant analysis as the REPES curves demonstrated monomodal distributions. For 10, 25, and 50 wt% probucol loadings, the size of the aggregates increased with increasing drug, but the dispersity stayed relatively low ($\mu_2/\Gamma^2 \leq 0.30$). As with the polymer-only sample, this could indicate that the micelles are not completely dissolved at this early time point,

or could be an indication of the effect of increased drug loading on the size of the micelle corona. The samples analyzed at the 6 hour time point during dissolution all decreased in size from the initial dissolution and the dispersities were variable for each sample. For PEP-PDMA micelles, increasing the amount of hydrophobic drug in the SDD could decrease the wettability and lead to aggregates of micelles that are not completely broken apart. This could account for the initial size increase of the PEP-PDMA aggregates in the dissolution medium with increasing drug. At the 6 hour point, the aggregate sizes decreased, indicating dissolution of the drug or breaking apart of the micelles. Polymers that show increased wetting or surface-active properties have been hypothesized to reduce agglomeration, therefore increasing the surface area and dissolution of poorly water soluble drugs.[55]

Because PDMA does not show the same release and supersaturation maintenance as PEP-PDMA micelles, the forced aggregation of multiple PDMA chains (with a PEP core) held together as a micelle likely imparts favorable interactions on the polymer/drugs. It bears repeating that the drug is interacting with the corona or DMA portion of the micelles; the drug was not loaded into the core. This could relate to what Ilevbare and coworkers[59] observed in studying ritonavir SDDs with many different polymers. They found that more flexible polymers were not as effective at inhibiting crystal growth as those with a more rigid structure. The aggregation of polymers to form micelles forces the DMA into a more rigid conformation than a free solvated chain, which in turn, could impart more monomer-drug interactions.

For the hydrophilic polymers, PDMA and P(DMA-*grad*-MAG), there seems to be sufficient polymer in the SDD with 10 wt% probucol to inhibit crystal nucleation and growth when exposed to the dissolution medium. However, for 25 and 50 wt% probucol, the polymer does not inhibit nucleation and the amorphous drug seems to crystallize upon contact with the dissolution medium (not through crystallization from a supersaturated solution). The hydrophilic polymers of PDMA and P(DMA-*grad*-MAG) could be released from the SDD into the aqueous media much

faster that the hydrophobic drug. To study this, polymer release kinetics could be studied along with the drug release kinetics. Further, these polymers could simply be interacting more strongly with the dissolution medium than with the drug. This depletion of polymer could cause drug crystallization as the polymer is no longer available to sterically protect the drug, therefore allowing the drug to kinetically move more freely.[59] At 10 wt% drug, there is a low ratio of drug such that the dissolved polymer was able to inhibit crystal nucleation and growth. To test this hypothesis, future studies are in progress to compare the undissolved solid crystallinity of SDDs of PDMA and P(DMA-*grad*-MAG) sprayed from MeOH and PEP-PDMA and PEP-P(DMA-*grad*-MAG) sprayed from THF:MeOH to determine if the drug is crystalline or amorphous.

Overall, this study shows that when PEP-PDMA micelles are used as the excipient in SDDs with probucol, dissolution of the drug is enhanced, even over HPMC-AS (Figure 3.8). HPMC-AS is hypothesized to be an excellent-performing excipient due to its tendency to form nanoaggregates between hydrophobic portions of the polymer and hydrophobic drugs. Drug/polymer colloids are thought to increase drug dissolution because they are readily formed upon introduction into aqueous media, show stability in aqueous media, and tend to sustain supersaturation over a biologically-relevant time frame.[13] However, the formation of such nanoaggregates is poorly understood and difficult to predict and control for oral drug delivery purposes. The results of this study reveal that a more controlled system of aggregates, PEP-PDMA micelles, clearly leads to enhanced drug dissolution and supersaturation maintenance.

3.3 Conclusions

We synthesized four polymers (PEP-P(DMA-*grad*-MAG), PEP-PDMA, PDMA, and P(DMA-*grad*-MAG)) and spray dried them with two different drugs (probucol and phenytoin) to examine the role of drug/polymer assemblies in assisting drug dissolution and supersaturation maintenance. Polymers that were insoluble in aqueous media, PEP-P(DMA-grad-MAG) and PEP-PDMA, sprayed from the non-selective solvent THF:MeOH, showed little to no drug release during

dissolution. Hydrophilic polymers, P(DMA-*grad*-MAG) and PDMA, showed good dissolution profiles for 10 wt% loadings of probucol, but little to no drug release for 25 and 50 wt% probucol loadings. It is hypothesized that there is an insufficient polymer to drug ratio at higher drug loadings to inhibit drug crystal nucleation and growth. However, when PEP-PDMA micelles are formed prior to spray drying and used as an excipient in the SDDs, there is a significant increase in dissolution performance; an almost complete burst release of the drug was found to occur, and supersaturation was sustained over the 6 hour incubation period for up to 50 wt% drug loading. The forced aggregation of the PDMA chains through the micellization of PEP-PDMA is thought to sustain drug-polymer interactions even when exposed to the aqueous dissolution medium. This is supported by the studies of the high performing excipient, HPMC-AS, which show nanoaggregates are formed during the dissolution process. This study reveals that nanoaggregates have a particular importance for drug dissolution and supersaturation maintenance, and that using micelle structures in excipient formulations results in a simple and controlled platform to further explore SDDs for oral drug delivery applications.

3.4 Experimental Section

Materials and Methods

Materials. All chemicals were reagent grade and used as received unless otherwise noted. All solvents were HPLC or analytical grade. *Sec*-butyllithium (1.4 M in cyclohexane, Aldrich), oxalyl chloride (Aldrich, 99+%), *D*-glucosamine hydrochloride (Acros, 98+%), *N*,*O*-bis(trimethylsilyl)acetamide (BSA, Acros, 95%), methacryloyl chloride (Acros, 95%), triethylamine (TEA, Acros, 99.7%), *n*-butyl amine (Sigma-Aldrich, 99.5%), tris(2-carboxyethyl)phosphine hydrochloride (TCEP, Aldrich, powder), methanol (Sigma-Aldrich, anhydrous, 99.8%). 2,2'-Azobis(2-methylpropionitrile) (AIBN, Aldrich, 98%) was recrystallized from methanol once and stored in a dark, –20 °C refrigerator. *N*,*N*-Dimethylacrylamide (DMA) (Aldrich, 99+%), 2-hydroxyethyl acrylate (HEA, Aldrich, 96%), and methyl acrylate (MA, Aldrich,

99%) were purified by passage through activated basic alumina columns to remove trace amounts of inhibitors. Hydrochloric acid (Sigma-Aldrich, 37%) was diluted with DI water to prepare a 1.3 M solution before use. 1,3-isoprene (Aldrich,99%) and ethylene oxide (Aldrich, 99.5+%) were degassed with three freeze-pump-thaw cycles followed by removal of trace amounts of acidic impurities by multiple treatments with *n*-butyllithium (2.5 M in hexanes, Aldrich) for 1 hour each and *n*-butylmagnesium chloride (2.0 M in diethyl ether, Aldrich) for 4 hours each, respectively. Toluene (Sigma-Aldrich, HPLC grade, 99.9+%), dichloromethane (Sigma-Aldrich, anhydrous, 99.8+%), and tetrahydrofuran (THF, Sigma-Aldrich, HPLC grade, 99.9+%, inhibitor free) were purified via a solvent purification system. Probucol (PBC) and phenytoin (PTN) were purchased from Sigma-Aldrich (Milwaukee, WI) and used without further purification. HPMC-AS (AFFINISOL™ 912G, The Dow Chemical Company) were used as received. Fasted-state simulated intestinal fluid powder (FaSSIF) was purchased from Biorelevant (Surrey, UK). Phosphate buffered saline (PBS) consisted of 82 mM sodium chloride (Fisher, ≥99.0%), 20 mM sodium phosphate dibasic heptahydrate (Fisher, 98%), and 47 mM potassium phosphate monobasic (J.T. Baker, ≥99.0%).

Methods.

Spray Drying. Spray drying was performed on a Bend Research Mini Spray Drier under the following conditions: inlet temperature of 68 °C, nitrogen flow rate of 28.6 SLPM, a 1.3 mL/min syringe flow rate, and samples were collected on a 4" Whatman filter. Unless otherwise noted, the total solute content spray dried was always 1 wt%. Solutions were either sprayed from MeOH or THF:MeOH mixture (15:2, v/v). SDD composition is reported as the weight percent (wt%) drug in the dispersion. For example, an SDD of 10 wt% probucol/PEP-PDMA consists of 1 part probucol drug and 9 parts PEP-PDMA polymer by weight.

The abbreviations for the spray-dried dispersions (SDDs) in this publication consist of the polymer acronym followed by the solvent, polymer, and drug were spray dried from. For example, poly(N,N,-dimethylacrylamide) spray dried from methanol would be reported as PDMA MeOH.

Dynamic Light Scattering (DLS). The aggregation state of drug/polymer mixtures in organic solvent and in the dissolution medium (PBS + FaSSIF) were studied using DLS. DLS experiments were performed using a Brookhaven Instrument system consisting of a Mini L-30 red laser source (λ = 637 nm), a BI-APD avalanche photodiode detector, and a BI-9000AT digital correlator, all aligned on a BI-200SM goniometer. The temperature was controlled at 25.0 ± 0.3°C, and a decalin bath was used as the RI-matching medium.

All samples were passed through 0.45 μm syringe filters, then loaded into dust-free glass tubes for analysis. The pre-spray drying samples, in organic solvent, consisted of 1 wt% dispersions of polymer or polymer and drug. However, the post-spray drying samples, in PBS + FaSSIF, varied in the total wt% since they mimicked the dissolution testing concentration (total drug concentration if fully dissolved is 1,000 μg/mL). The second-order scattering intensity correlation function ($g_2(t)$) for each sample was measured at five angles (60°, 75°, 90°, 105°, and 120°) and was subsequently converted to the first-order correlation function ($g_1(t)$) by applying the Siegert relation of $g_2(t) = 1 + |g_1(t)|^2$. The first-order correlation functions were then fit by the cumulant expansion, which describes a monomodal distribution of aggregates with a dispersity ($\mu_2/\Gamma^2 < 0.3$)[20], and with the double exponential expansion that assumes two distinct decay modes with no dispersity. The translational diffusion coefficient was determined from a linear fitting of Γ and q^2, from which the hydrodynamic radius (R_h) was calculated using the Stokes-Einstein relationship. Shibayama's bimodal scattering analysis was used to elucidate the weight fractions of the two decay modes for double exponential analysis.[1-3,21]

Powder X-Ray Diffraction (PXRD) Analysis. PXRD experiments were carried out on a Bruker-AXS (Siemens) D5005 diffractometer. Samples were packed into standard glass holders with zero background. Data for each sample was collected from 5° to 40° on the 2θ scale over approximately 30 minutes at a scan step of 0.5 seconds and a step size of 0.02°/s. The x-ray source (KCuα, λ = 1.54 Å) was operated at a voltage of 45 kV and a current of 40 mA.

Thermal Analysis. Modulated differential scanning calorimetry (MDSC) to determine thermal characteristics of the SDDs was conducted using a TA Instruments Discovery DSC equipped with an autosampler. Samples (2–10 mg) were placed in T-zero aluminum pans. MDSC analysis was performed with a nitrogen flow rate of 50.00 mL/min and a heating rate of 5 °C/min from -80 °C to 180 °C. Temperature was modulated ± 2 °C with a period of 40 s. The first heating scans are reported. For polymer only samples (not spray dried), the temperature was not modulated, but was ramped between -80 °C and 180 °C at a rate of 5 °C/min. The second heating scans are reported for those samples. For all samples, TA TRIOS software version 2.2 was used to analyze T_g values and enthalpic components. Phenytoin MDSC runs were only analyzed to 180 °C and not up to the melting point of phenytoin due to polymer degradation above 200 °C.

Scanning Electron Microscopy (SEM). SEM was used to obtain particle size and morphology data from the SDDs. A Hitachi S-900 microscope was used and samples were sputtered with gold/palladium for 30 seconds at 40 kV on a Denton DV-502A High Vacuum Deposition System to provide a conductive coating for analysis.

In Vitro Dissolution Testing. Dissolution testing was performed on SDDs and crystalline drug to determine the amount of soluble drug and supersaturation maintenance. Dissolution testing medium consisted of phosphate buffered saline (as described in *Materials*) supplemented with 0.5 wt% fasted-state simulated intestinal fluid (FaSSIF) containing 3 mM sodium taurocholate, 0.2 mM

lecithin, 34.8 mM sodium hydroxide (NaOH), 68.62 mM sodium chloride (NaCl), 19.12 mM maleic acid. The medium was adjusted to pH 6.5 with NaOH.

Each SDD or crystalline drug sample was accurately weighed into 2.0 mL microcentrifuge tubes to give an ultimate total drug concentration of 1,000 mg/mL if fully dissolved (n=2). To begin the testing, 1.8 mL of PBS + FaSSIF medium (pH 6.5, 37 °C) was added to the tubes, which were then vortexed for one minute and placed into an aluminum heating block held at 37 °C. At 4, 10, 20, 40, 90, 180, and 360 minutes the tubes were centrifuged at 13,000 rpm, 37 °C for 1 minute and then 50 µL of supernatant was aliquoted into HPLC vials. The samples were then vortexed for 30 seconds and placed back into the 37 °C block until the next time point. The supernatant in the HPLC vials was then diluted with 250 µL of methanol and analyzed for drug via HPLC.

The HPLC consisted of a reversed-phase EC-C18 column (Poroshell 120, 4.6 x 50 mm, 2.7 µm, Agilent, USA). For probucol detection, a mobile phase of 96:4 (v/v) acetonitrile:water was pumped at a flow rate of 1.0 mL/min at 30 °C. A 10 µL aliquot of sample was injected, and the column effluent was detected at 241 nm with a UV detector (1260 Infinity Multiple Wavelength Detector, Agilent). The probucol concentration in the samples was determined using a calibration curve of 0.1–500 µg/mL concentrations. Phenytoin was detected using a mobile phase of 40:60 (v/v) acetonitrile:water under the same conditions as probucol detection. Phenytoin was detected at 215 nm and the sample concentration was determined using a calibration curve of 0.1–500 µg/mL concentrations.

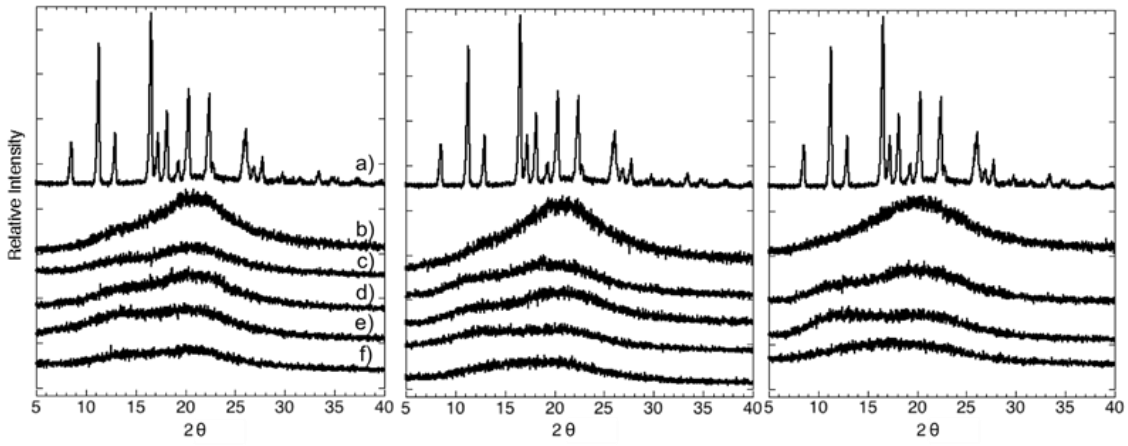

Figure 3.10 PXRD patterns for SDDs with phenytoin loadings of 50 wt%, 25 wt%, and 10 wt%, from left to right, comparing: a) crystalline phenytoin, b) PEP-P(DMA-*grad*-MAG) THF:MeOH (15:2, v/v), c) PEP-PDMA THF:MeOH (15:2, v/v) d) PEP-PDMA MeOH e) PDMA MeOH f) P(DMA-*grad*-MAG) MeOH.

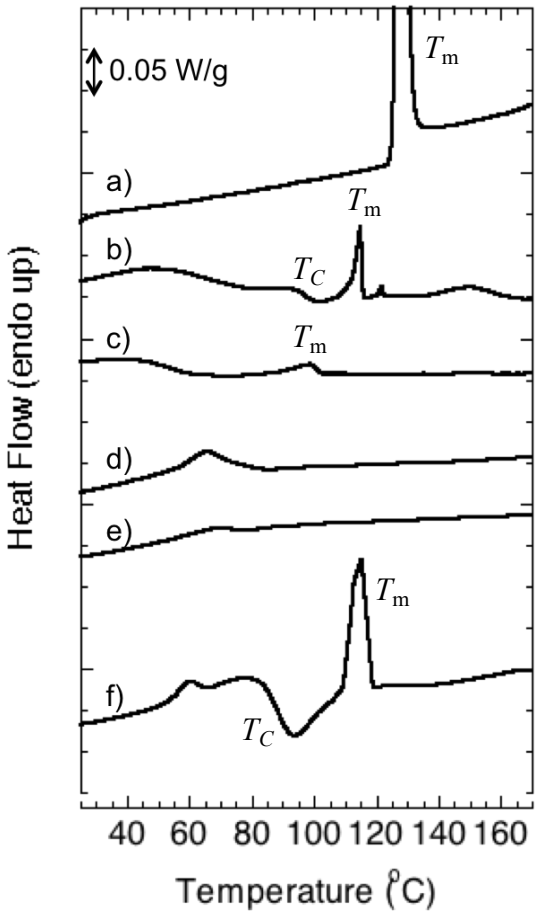

Figure 3.11 MDSC traces of total heat flow from a) crystalline probucol, and SDDs (b-f) containing 50 wt% probucol and the following polymers and feed solvents: b) PEP-P(DMA-*grad*-MAG) THF:MeOH (15:2, v/v), c) PEP-PDMA THF:MeOH (15:2, v/v), d) PEP-PDMA MeOH, e) PDMA MeOH, and f) P(DMA-*grad*-MAG) MeOH. Samples were analyzed between 20 °C and 180 °C with a ramp of 5 °C/min, temperature modulation of ± 2 °C, and a period of 40 s. First heating scans are shown.

Table 3.6 MDSC analysis of SDDs with probucol.

Probucol loading	SDD	T_g (°C)	T_c (°C)	Enthalpy (J/g)	T_m (°C)	Enthalpy (J/g)	T_c (°C)	Enthalpy (J/g)	T_m (°C)	Enthalpy (J/g)
50 wt %	PEP-P(DMA-*grad*-MAG) THF:MeOH	87.8	101.4	9.8	114.8	15.6	120.9	0.52	121.8	0.5
	PEP-PDMA THF:MeOH	54.8	–	–	104.4	2.2	–	–	–	–
	PEP-PDMA MeOH	71.3	–	–	–	–	–	–	–	–
	PDMA MeOH	83.0	–	–	–	–	–	–	–	–
	P(DMA-*grad*-MAG) MeOH	62.5	93.7	8.1	115.2	10.2	–	–	125.3	0.2
25 wt %	PEP-P(DMA-*grad*-MAG) THF:MeOH	118.4	–	–	110.8	1.3	–	–	–	–
	PEP-PDMA THF:MeOH	75.3	–	–	103.8	0.3	–	–	–	–
	PEP-PDMA MeOH	102.6	–	–	–	–	–	–	–	–
	PDMA MeOH	101.0	–	–	–	–	–	–	–	–
	P(DMA-*grad*-MAG) MeOH	149.4	–	–	–	–	–	–	–	–
10 wt %	PEP-P(DMA-*grad*-MAG) THF:MeOH	115.8	–	–	–	–	–	–	–	–
	PEP-PDMA THF:MeOH	NA	–	–	–	–	–	–	–	–
	PEP-PDMA MeOH	102.7	–	–	–	–	–	–	–	–
	PDMA MeOH	113.5	–	–	–	–	–	–	–	–
	P(DMA-*grad*-MAG) MeOH	141.2	–	–	–	–	–	–	–	–

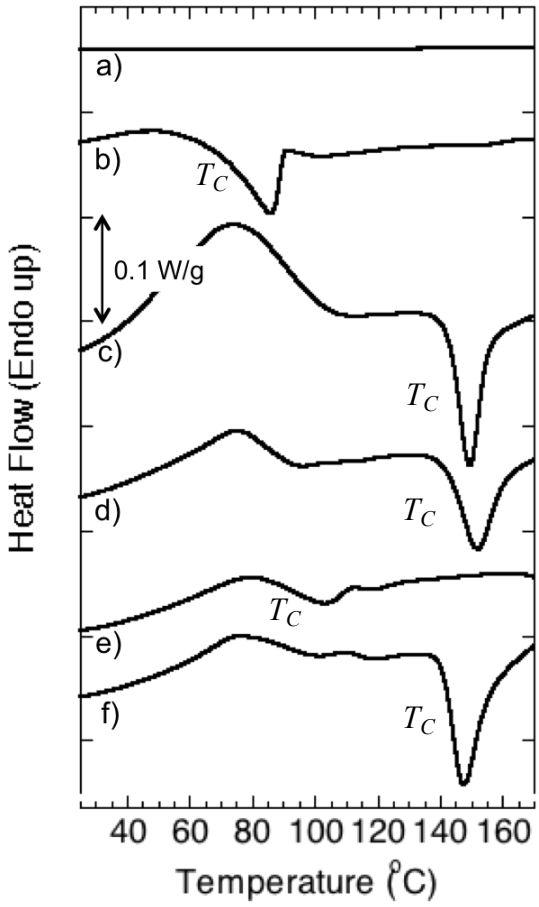

Figure 3.12 MDSC traces of total heat flow from a) crystalline phenytoin, and SDDs (b-f) containing 50 wt% phenytoin and the following polymers and feed solvents: b) PEP-P(DMA-*grad*-MAG) THF:MeOH (15:2, v/v), c) PEP-PDMA THF:MeOH (15:2, v/v), d) PEP-PDMA MeOH, e) PDMA MeOH, and f) P(DMA-*grad*-MAG) MeOH. Samples analyzed between 20 °C and 180 °C with a ramp of 5 °C/min, temperature modulation of ± 2 °C, and a period of 40 s. First heating scans are shown.

Table 3.7 MDSC analysis of SDDs with phenytoin.

Phenytoin loading	SDD	T_g (°C)	T_c (°C)	Enthalpy (J/g)
50 wt %	PEP-P(DMA-*grad*-MAG) THF:MeOH	75.2	86.1	51.5
	PEP-PDMA THF:MeOH	73.4	149.7	15.4
	PEP-PDMA MeOH	98.8	152.1	14.8
	PDMA MeOH	111.3	119.9	1.4
	P(DMA-*grad*-MAG) MeOH	105.2	147.6	17.3
25 wt %	PEP-P(DMA-*grad*-MAG) THF:MeOH	91.5	–	–
	PEP-PDMA THF:MeOH	64.6	–	–
	PEP-PDMA MeOH	114.1	–	–
	PDMA MeOH	116.5	125.7	0.8
	P(DMA-*grad*-MAG) MeOH	127.3	–	–
10 wt %	PEP-P(DMA-*grad*-MAG) THF:MeOH	101.9	–	–
	PEP-PDMA THF:MeOH	NA	–	–
	PEP-PDMA MeOH	105.2	–	–
	PDMA MeOH	117.9	–	–
	P(DMA-*grad*-MAG) MeOH	140.2	–	–

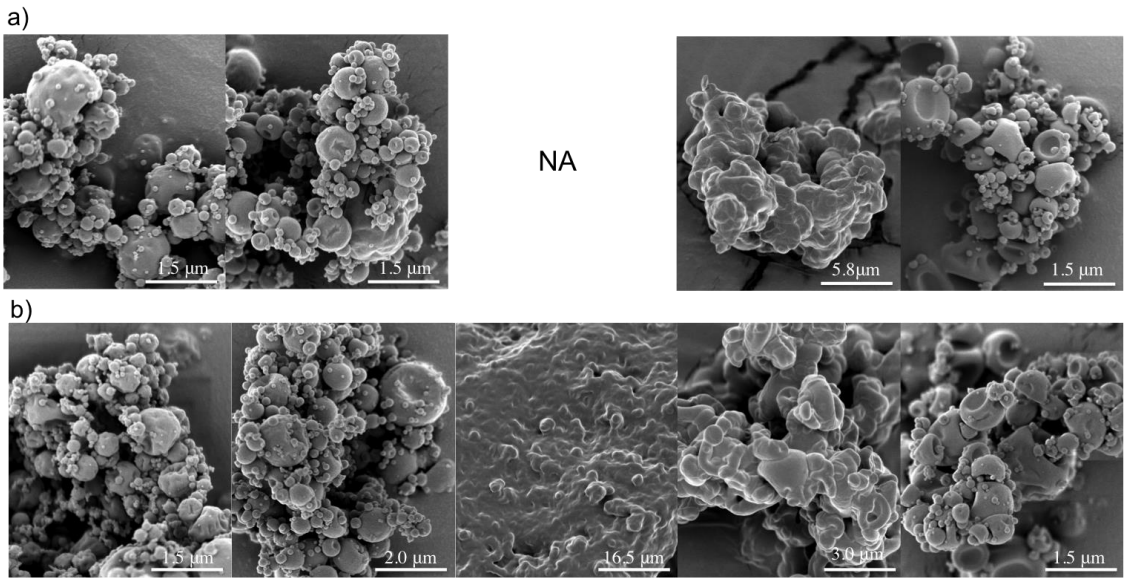

Figure 3.13 SEM images for polymers sprayed with a) 10 wt% probucol and b) 25 wt% probucol. Polymers and solvent from left to right: PDMA MeOH, PEP-PDMA MeOH, PEP-PDMA THF:MeOH (15:2, v/v), PEP-P(DMA-*grad*-MAG) THF:MeOH (15:2, v/v), P(DMA-*grad*-MAG) MeOH.

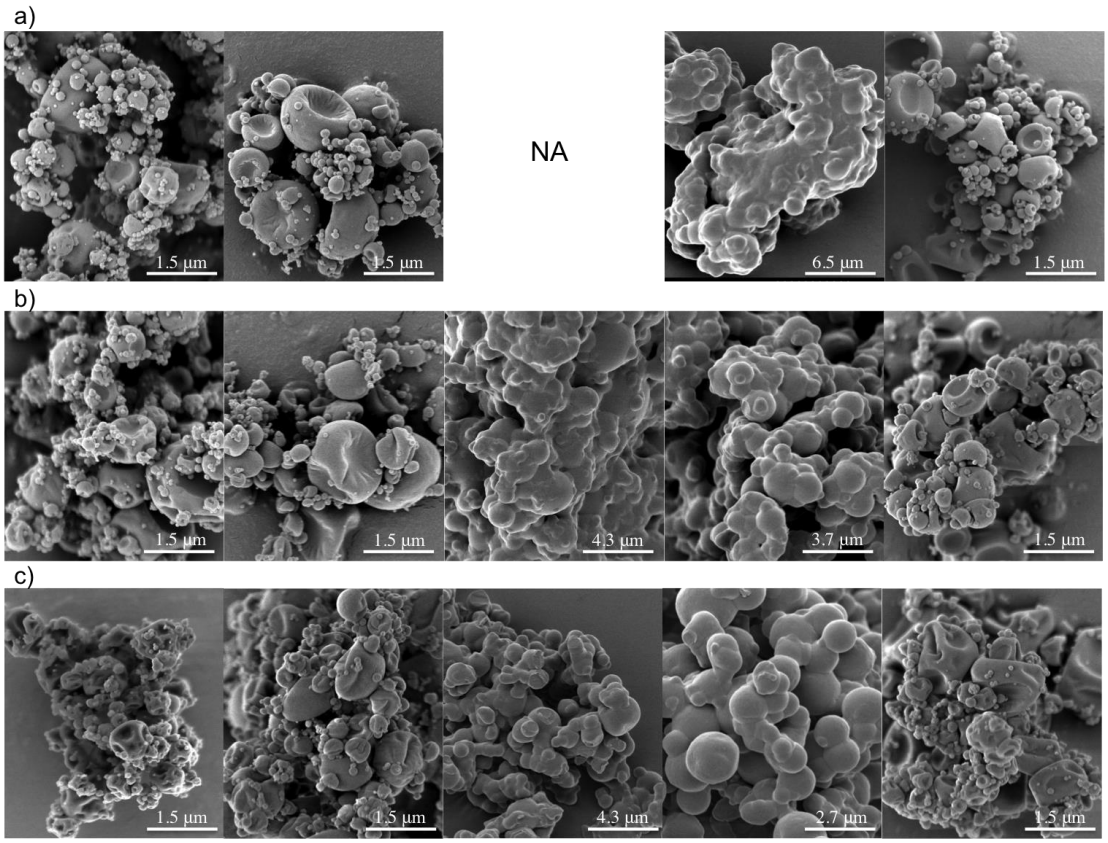

Figure 3.14 SEM images for polymers sprayed with a) 10 wt% phenytoin, b) 25 wt% phenytoin, and c) 50 wt% phenytoin. Polymers and solvent from left to right: PDMA MeOH, PEP-PDMA MeOH, PEP-PDMA THF:MeOH (15:2, v/v), PEP-P(DMA-*grad*-MAG) THF:MeOH (15:2, v/v), P(DMA-*grad*-MAG) MeOH.

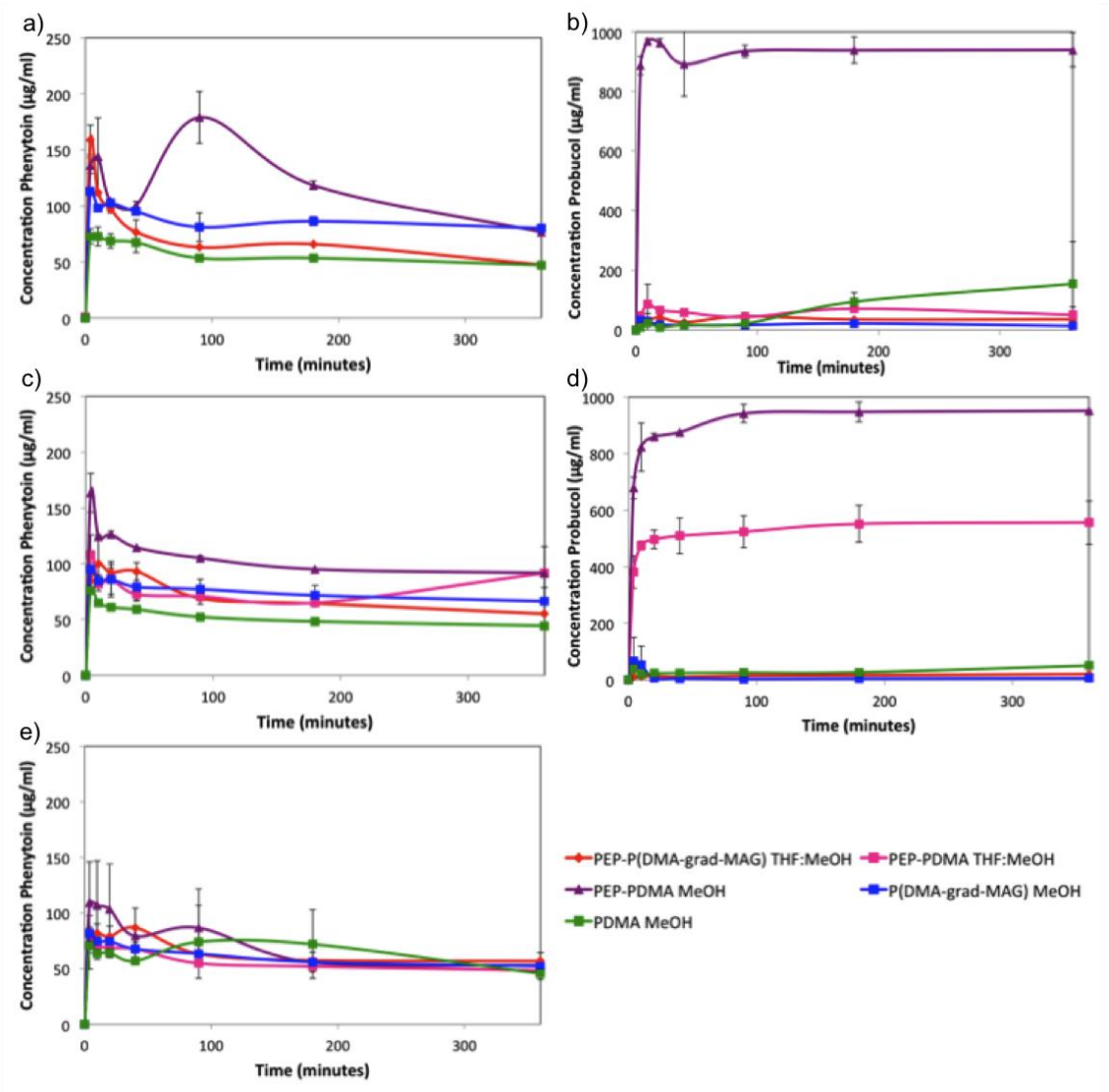

Figure 3.15 Dissolution data comparing polymers and spray drying solvents (see legend) with various drug loadings: a) 10 wt% phenytoin, b) 25 wt% probucol, c) 25 wt% phenytoin, d) 50 wt% probucol, and e) 50 wt% phenytoin.

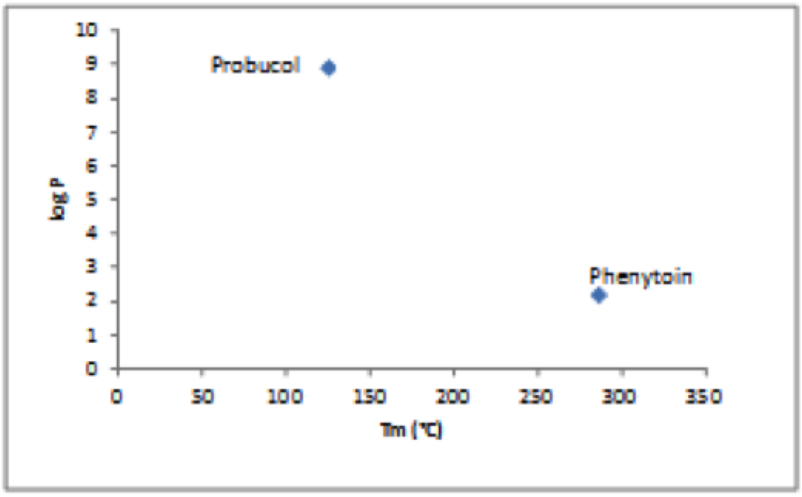

Figure 3.16 Log P vs T_m (melting point) chart indicating physiochemical properties of common model APIs. This highlights that probucol and phenytoin have disparate properties, which is the rationale for choosing them as model APIs.

3.5 References

(1) Serajuddin, A. T. M. *J. Pharm. Sci.* **1999**, *88*, 1058–1066.

(2) Leuner, C.; Dressman, J. *Eur. J. Pharm. Biopharm.* **2000**, *50*, 47–60.

(3) Lipinski, C. A. *J. Pharmacol. Toxicol. Methods* **2000**, *44*, 235–249.

(4) Qian, F.; Huang, J.; Hussain, M. A. *J. Pharm. Sci.* **2010**, *99*, 2941–2947.

(5) Ormes, J. D.; Zhang, D.; Chen, A. M.; Hou, S.; Krueger, D.; Nelson, T.; Templeton, A. *Pharm. Dev. Technol.* **2013**, *18*, 121–129.

(6) Vasconcelos, T.; Sarmento, B.; Costa, P. *Drug Discov. Today* **2007**, *12*, 1068–1075.

(7) Van den Mooter, G.; Weuts, I.; De Ridder, T.; Blaton, N. *Int. J. Pharm.* **2006**, *316*, 1–6.

(8) Chauhan, B.; Shimpi, S.; Paradkar, A. *Eur. J. Pharm. Sci.* **2005**, *26*, 219–230.

(9) Mizuno, M.; Hirakura, Y.; Yamane, I.; Miyanishi, H.; Yokota, S.; Hattori, M.; Kajiyama, A. *Int. J. Pharm.* **2005**, *305*, 37–51.

(10) Rizi, K.; Green, R. J.; Donaldson, M.; Williams, A. C. *J. Pharm. Sci.* **2010**, *100*, 566–579.

(11) Al-Obaidi, H.; Brocchini, S.; Buckton, G. *J. Pharm. Sci.* **2009**, *98*, 4724–4737.

(12) Uchiyama, H.; Tozuka, Y.; Imono, M.; Takeuchi, H. *Eur. J. Pharm. Biopharm.* **2010**, *76*, 238–244.

(13) Friesen, D. T.; Shanker, R.; Crew, M.; Smithey, D. T.; Curatolo, W. J.; Nightingale, J. A. S. *Mol. Pharm.* **2008**, *5*, 1003–1019.

(14) Miller, J. M.; Beig, A.; Carr, R. A.; Spence, J. K.; Dahan, A. *Mol. Pharm.* **2012**, *9*, 2009–

2016.

(15) Qi, S.; Roser, S.; Edler, K. J.; Pigliacelli, C.; Rogerson, M.; Weuts, I.; Dycke, F.; Stokbroekx, S. *Pharm. Res*. **2012**, *30*, 290–302.

(16) Peppas, N. A. *Hydrogels in Medicine and Pharmacy: Polymers*; CRC, 1987; Vol. 2.

(17) Bergbreiter, D. E.; Zhang, L.; Mariagnanam, V. M. *J. Am. Chem. Soc.* **1993**, *115*, 9295–9296.

(18) Liu, S.; Tong, Y.; Yang, Y. *Biomaterials* **2005**, *26*, 5064–5074.

(19) Yin, L.; Dalsin, M. C.; Sizovs, A.; Reineke, T. M.; Hillmyer, M. A. *Macromolecules* **2012**, *45*, 4322–4332.

(20) Chu, B. *Laser Light Scattering: Basic Principles and Practice*; 2nd ed. Academic Press: Boston, 1991.

(21) Shibayama, M.; Karino, T.; Okabe, S. *Polymer* **2006**, *47*, 6446–6456.

(22) Trasi, N. S.; Taylor, L. S. *Cryst. Eng. Comm.* **2012**, *14*, 5188–5197.

(23) Paudel, A.; Mooter, G. *Pharm. Res.* **2011**, *29*, 251–270.

(24) Guns, S.; Dereymaker, A.; Kayaert, P.; Mathot, V.; Martens, J. A.; Mooter, G. *Pharm. Res.* **2010**, *28*, 673–682.

(25) Janssens, S.; De Zeure, A.; Paudel, A.; Van Humbeeck, J.; Rombaut, P.; Van den Mooter, G. *Pharm. Res.* **2010**, *27*, 775–785.

(26) Zhou, D.; Zhang, G. G. Z.; Law, D.; Grant, D. J. W.; Schmitt, E. A. *J. Pharm. Sci.* **2002**, *91*, 1863–1872.

(27) Angell, C. A. *Science* **1995**, *267*, 1924–1935.

(28) Graeser, K. A.; Patterson, J. E.; Zeitler, J. A.; Gordon, K. C.; Rades, T. *Eur. J. Pharm. Sci.* **2009**, *37*, 492–498.

(29) Hancock, B. C.; Shamblin, S. L.; Zografi, G. *Pharm. Res.* **1995**, *12*, 799–806.

(30) Taylor, L. S.; Zografi, G. *Pharm. Res.* **1997**, *14*, 1691–1698.

(31) Ivanisevic, I.; Bates, S.; Chen, P. *J. Pharm. Sci.* **2009**, *98*, 3373–3386.

(32) Newman, A.; Engers, D.; Bates, S.; Ivanisevic, I.; Kelly, R. C.; Zografi, G. *J. Pharm. Sci.* **2008**, *97*, 4840–4856.

(33) Baird, J. A.; Taylor, L. S. *Adv. Drug Deliv. Rev.* **2012**, *64*, 396–421.

(34) Thybo, P.; Pedersen, B. L.; Hovgaard, L.; Holm, R.; Müllertz, A. *Pharm. Dev. Technol.* **2008**, *13*, 375–386.

(35) Wegiel, L. A.; Mauer, L. J.; Edgar, K. J.; Taylor, L. S. *J. Pharm. Sci.* **2012**, *102*, 171–184.

(36) Willart, J. F.; Descamps, M. *Mol. Pharm.* **2008**, *5*, 905–920.

(37) Caron, V.; Tajber, L.; Corrigan, O. I.; Healy, A. M. *Mol. Pharm.* **2011**, *8*, 532–542.

(38) Gerber, J. J.; Caira, M. R.; Lotter, A. P. *J. Crystallogr. Spectrosc. Res.* **1993**, *23*, 863–869.

(39) Clas, S.-D.; Faizer, R.; O'Connor, R. E.; Vadas, E. B. *Int. J. Pharm.* **1995**, *121*, 73–79.

(40) de Villiers, M. M.; Wurster, D. E.; Van der Watt, J. G.; Ketkar, A. *Int. J. Pharm.* **1998**, *163*, 219–224.

(41) Sauer, B. B.; Kampert, W. G.; Neal Blanchard, E.; Threefoot, S. A.; Hsiao, B. S. *Polymer* **2000**, *41*, 1099–1108.

(42) McPhillips, H.; Craig, D. Q.; Royall, P. G.; Hill, V. L. *Int. J. Pharm.* **1999**, *180*, 83–90.

(43) Gupta, P.; Kakumanu, V. K.; Bansal, A. K. *Pharm. Res.* **2004**, *21*, 1762–1769.

(44) Ambike, A. A.; Mahadik, K. R.; Paradkar, A. *Pharm. Res.* **2005**, *22*, 990–998.

(45) Bhattacharya, S.; Suryanarayanan, R. *J. Pharm. Sci.* **2009**, *98*, 2935–2953.

(46) Vasanthavada, M.; Tong, W.-Q.; Joshi, Y.; Kislalioglu, M. S. *Pharm. Res.* **2004**, *21*, 1598–1606.

(47) Khougaz, K.; Clas, S.-D. *J. Pharm. Sci.* **2000**, *89*, 1325–1334.

(48) Marsac, P. J.; Rumondor, A. C. F.; Nivens, D. E.; Kestur, U. S.; Stanciu, L.; Taylor, L. S. *J. Pharm. Sci.* **2010**, *99*, 169–185.

(49) Gupta, P.; Bansal, A. K. *J. Pharm. Pharmacol.* **2005**, *57*, 303–310.

(50) Kalaiselvan, R.; Mohanta, G. P.; Manna, P. K.; Manavalan, R. *Pharmazie* **2006**, *61*, 618–624.

(51) Albers, J.; Alles, R.; Matthée, K.; Knop, K.; Nahrup, J. S.; Kleinebudde, P. *Eur. J. Pharm. Biopharm.* **2009**, *71*, 387–394.

(52) Marsac, P. J.; Shamblin, S. L.; Taylor, L. S. *Pharm. Res.* **2006**, *23*, 2417–2426.

(53) Forster, A.; Hempenstall, J.; Tucker, I.; Rades, T. *Int. J. Pharm.* **2001**, *226*, 147–161.

(54) Sun, Y.; Tao, J.; Zhang, G. G. Z.; Yu, L. *J. Pharm. Sci.* **2010**, *99*, 4023–4031.

(55) Craig, D. Q. M. *Int. J. Pharm.* **2002**, *231*, 131–144.

(56) Bhandari, B. R.; Howes, T. *J. Food Eng.* **1999**, *40*, 71–79.

(57) Zipp, G. L.; Rodriguez-Hornedo, N. *Int. J. Pharm.* **1993**, *98*, 189–201.

(58) Dubois, J.-L.; Ford, J. L. *J. Pharm. Pharmacol.* **2011**, *37*, 494–495.

(59) Ilevbare, G. A.; Liu, H.; Edgar, K. J.; Taylor, L. S. *Cryst. Growth Des.* **2012**, *12*, 3133–3143.

4 CHAPTER FOUR

Trehalose-based diblock terpolymers increase hydrophobic drug solubility and offer new excipient design parameters

In part from:

[†]Tale S. R.; [†]Purchel A.A.; Theresa T.M., Diblock Terpolymers Are Tunable and pH Responsive Vehicles To Increase Hydrophobic Drug Solubility for Oral Administration, *Mol. Pharmaceutics.* **2017**, 14, 4121-4127. ([†]equal contribution)

This work was a joint venture by this author who is responsible for synthesis and characterization of Trehalose-based diblock terpolymers, spray drying, characterization of SDDs, and dissolution studies of all polymers at different pH. Anatoli P. played a major role in DLS characterizations, MDSC analysis, cloud point measurements, and addressing reviewers comments.

4.1 Introduction

Oral delivery routes are the most convenient method for routine administration of pharmaceuticals in the solid dose form.[1-3] This preferred administration route promotes increased patient compliance and lower costs as systemic injection routes are avoided. Approximately 40-60% of new drug candidates in the pharmaceutical pipeline suffer from poor aqueous solubility in gastrointestinal track, resulting in reduced bioavailability and low therapeutic effect.[4,5] About 70% of pipeline drug candidates belong to the Biopharmaceutics Classification System (BCS) Class II compounds, which denote compounds with low aqueous solubility and high permeability across the GI tract.[6] Synthetic and natural polymers have shown great potential to improve bioavailability, shelf life, and therapeutic efficacy of BCS class II drugs for oral administration.[7] Various methods exist to disperse a drug in a polymer matrix to form drug-polymer solid dispersions (*i.e.*, spray drying, hot melt extrusion).[8-12] Spray drying has emerged as a convenient technology for the formulation of amorphous solid dispersions, which are then tableted for ease in packaging and dosing.[9] This formulation technology is readily scalable and has been utilized commercially in developing new formulations with various drugs, such as with Ivacaftor, a drug with a high tendency to crystallize (melting point 291°C), but can be dispersed in hydroxypropyl methyl cellulose acetate succinate (HPMCAS).[13] Indeed, polymer-drug interactions play a critical role in dictating dissolution performance of spray dried dispersions. Therefore, to fully employ the promise of polymer excipients, it is vital to understand the fundamental structure-property relationships of drug dissolution with polymer excipients to fine-tune design parameters for optimizing SDD performance.[14]

To date, hydroxypropyl methylcellulose acetate succinate (HPMCAS) is one of the top performing polymer excipients on the market that effectively inhibits drug nucleation, crystal growth, and maintains high levels of drug supersaturation, leading to an increase in drug absorption in the GI tract.[15,16] HPMCAS solid dispersion formulations are currently part of FDA-approved formulations on the market, for example for Telaprevir (Hepatitis C), Vemurafenib (last stage of melanoma), and Ivacaftor (cystic fibrosis).[13] For these formulations, HPMCAS has led to enhanced aqueous drug solubility, improved bioavailability, and increased therapeutic effect for these drugs. However, understanding the structure property relationship of drugs with HPMCAS has been challenging due to the high dispersity of industrially manufactured HPMCAS and challenges to fully characterize its physiochemical properties.[7]

Our work on amphiphilic block copolymers that can self-assemble into micelles prior to spray drying has shown success in improving aqueous solubility of poorly water soluble drugs.[11] Previously, we demonstrated that micelle structures in excipient formulations improve drug dissolution and supersaturation maintenance when compared to polymer formulations with the same composition that were not preassembled into micelles.[11] Mundargi et al. showed that a diblock copolymer, PLA-PEG, composed of polylactic acid (PLA) and polyethylene glycol (PEG) can be utilized as an excipient to control the release of zidovudine.[17] Ting et al. revealed that sugar-deprotected polymers outperformed their protected analogs by demonstrating superior drug release and supersaturation maintenance.[7] In that study, it was also demonstrated that hydrogen bonding played an important role in their SDD systems, which served to increase drug-polymer interactions, enhancing solubility and stability of their systems, and inhibiting

molecular mobility of the drug. Therefore, the effect of intermolecular hydrogen bonding between drug and polymer on drug release and supersaturation maintenance is clearly evident.[7]

Herein, we report the synthesis of three well-defined block copolymers and evaluate their efficiency as excipients in SDDs with a model drug system. We sought to understand the effect of hydrophobic (PEP, lacks hydrogen bonding sites), hydrophilic (PNIPAm, 1 H-bond donor and 1 H-bond acceptor), and pH responsive (PDEAEMA, 3 hydrogen bonding acceptor sites) blocks on drug release and super saturation maintenance through systematic variance of the block structure in these new excipient models. In this study, three diblock polymers displaying these compositions were synthesized using reversible addition−fragmentation chain-transfer (RAFT) polymerization, which are shown in Scheme 1, including PEP-b-P(DMA-*grad*-MAT), PNIPAm-b-P(DMA-*grad*-MAT), and PDEAEMA-b-P(DMA-*grad*-MAT). We maintained consistent molecular weight of the second block containing DMA and MAT to assess the effect of the differing chemical parameters arising by altering the second block containing either PEP, PNIPAm, or PDEAEMA blocks on the drug dissolution profiles. We chose DMA due to its aqueous solubility, biocompatibility, and numerous applications in pharmaceutical field.[18,19] The primary purpose of incorporating the third component MAT to these excipient models, was to increase the glass transition temperature of the diblock polymers. The hydroxyl groups of MAT can also provide additional sites for hydrogen bonding and has been used previously in its molecular form as an excipient, thus potentially aiding to increase the shelf life of the SDDs.[20] The PEP-b-P(DMA-*grad*-MAT) diblock terpolymer was synthesized by the combination of anionic and reversible addition–fragmentation chain transfer

(RAFT) polymerizations as reported in the literature.[11] The other two polymers PNIPAm-b-P(DMA-*grad*-MAT) and PDEAEMA-b-P(DMA-*grad*-MAT were synthesized exclusively by RAFT polymerization. Table 4.1 and the Experimental section include details of the polymer synthesis, conditions, and characterization. Probucol was selected as the model drug to study polymer-drug interactions and structure-property relationships with these new polymer excipients. Probucol is classified as a BCS class II drug and has a very low aqueous solubility of 0.042 μg/mL.[21] Herein, we demonstrate that these new polymer matrices can be tuned to release, solubilize, and maintain supersaturation of probucol (up to 100% of drug at a concentration of 1000 mg/mL).

4.2 Results and Discussion

4.2.1 Synthesis of the diblock terpolymers

Synthesis of TMS-MAT (2) was achieved in six steps according to our previously published procedure.[22] The macromolecular chain transfer agent (CTA), PEP-CTA (1a), was synthesized according to a published procedure by Yin et al.[14] The M_n of the PEP-CTA (^{1}H NMR spectroscopy, end group analysis) was determined to be 3.6 kg mol^{-1}, and had dispersity ($Đ$) of 1.06 using chloroform as the eluent (relative to PS standards). The two other macromolecular CTAs, PNIPAm-CTA (1b) and PDEAEMA-CTA (1c), were synthesized by reversible addition-fragmentation chain transfer (RAFT) polymerization using 4-Cyano-4-(propylsulfanylthiocarbonyl) sulfanylpentanoic Acid (CPP) [23] as the CTA. The M_n of PNIPAm-CTA and PDEAEMA-CTA (^{1}H NMR spectroscopy) was determined to be 5.6 kg mol^{-1} and 8.0 kg mol^{-1} respectively. Details of synthesis and characterization are detailed in the Table 4.2, Figure 4.5, Figure 4.6.

Three diblock terpolymers PEP-b-P(DMA-*grad*-MAT), PNIPAm-b-P(DMA-*grad*-MAT), and PDEAEMA-b-P(DMA-*grad*-MAT) were prepared by copolymerizing the macromolecular-CTA (1a, 1b, 1c) with DMA and TMS-MAT in toluene at 70 °C using AIBN as the initiator. The reported literature values for the reactivity ratios of TMS-MAT and DMA were $r_1 = 0.09$ and $r_2 = 1.62$.[24] According to these reactivity ratios, the copolymer was gradient in nature and consisted of an initial higher DMA ratio (close to PEP block) and terminated with a higher content of MAT. The TMS groups were then deprotected by using HCl in methanol to yield the diblock terpolymers. All polymers were purified by precipitation in ether and vacuum dried 40°C for 10 h. Table 4.1 contains characterization details of diblock terpolymers and Figure 4.7 and Figure 4.8 includes ^{1}H NMRs of

purified PNIPAm-b-P(DMA-*grad*-MAT)and PDEAEMA-b-P(DMA-*grad*-MAT) polymers.

Scheme 1 Synthesis of the diblock terpolymers

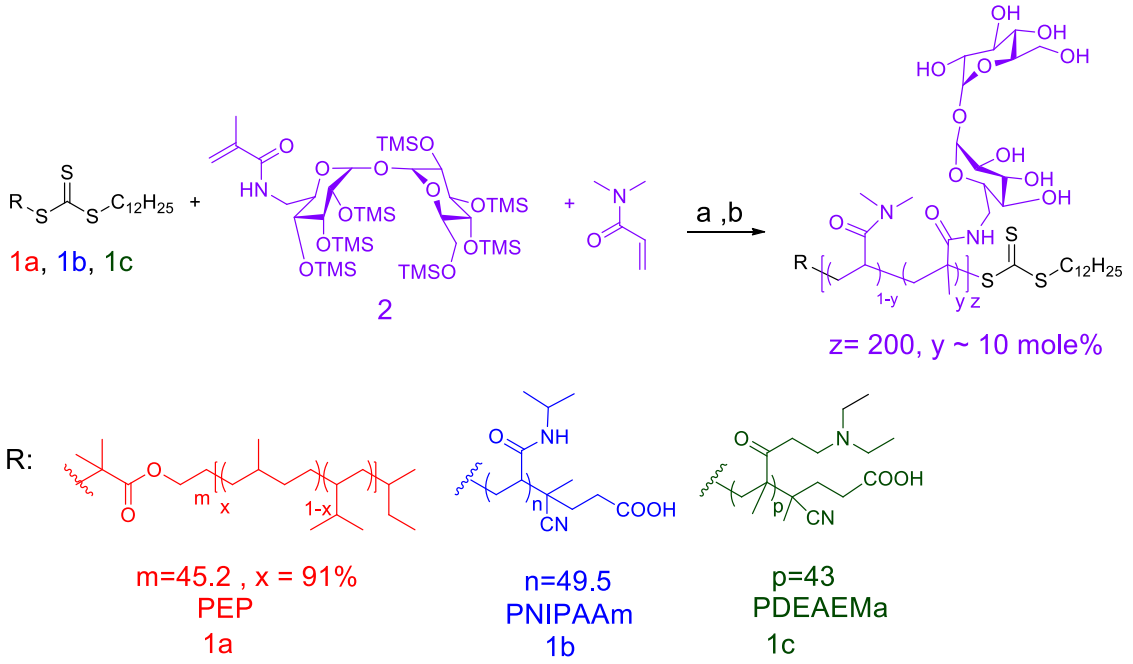

Reagents and Conditions: a) AIBN, 70 °C, Toluene b) 1.25M HCl in methanol

Table 4.1 Molecular and thermal characterization of the and diblock terpolymers

Sample[a]	[AIBN] : [Poly-CTA]: [DMA] : [TMS-TMAT][b]	$[M_0]$	Time (h)	Conv. of DMA[c]	Conv. of TMS-TMAT[c]	M_n kg/mole[d]	$Đ$[e]	T_g[f], °C
PEP-b-P(DMA-*grad*-MAT) (3.6-24.5-0.1)	0.05 : 1: 180 : 20	1.69	10	99%	92%	28.1	1.23	147
PNIPAAm-b-P(DMA-grad-MAT) (5.6-26.4-0.1)	0.05 : 1: 180 : 20	1.69	12	99%	99%	32	1.21	157
PDEAEMa-b-P(DMA-grad-MAT) (8-23-0.1)	0.05 : 1: 180 : 20	1.69	19	89%	85%	31	1.33	122

[a]The first value in parentheses indicates the number average molecular weight of either PEP, PNIPAAm, or PDEAEMa in kg/mole and the second number indicates the number average molecular weight of the PDMA/PMAT block in kg/mole. The third number indicates the mole fractions of MAT (trehalose) repeat units in the block of the terpolymers. [b]Initial composition of the AIBN (initiator), poly(CTA), and monomers in the feed. [c]Conversion of DMA and TMS-MAT as monitored by ^{1}H NMR spectroscopy. [d]Number average molecular weight of the diblock terpolymers after deprotection of the TMS groups.

[e]Polydispersity of the diblock terpolymers before the removal of the trimethylsilyl protecting groups. [f]Glass transition temperature of polymers reported as the second heating with a 5 °C/min heating rate.

All samples were spray dried using a Bend Research lab scale Mini Spray Drier. For example, 270 mg of PEP-b-P(DMA-*grad*-MAT) and 30 mg of probucol were dissolved in THF:MeOH mixture (15:2, v/v) and spray dried to obtain SDDs at 10 wt% of drug loading. In general, the physical stability of the SDDs is a critical component for thermodynamic stability of the drug molecules.[25] The drug should be molecularly dispersed in the polymer matrix yielding an amorphous mixture. A physically stable and amorphous SDD formulation leads to increased aqueous solubility of the drug, improved bioavailability (potentially leading to decreased costs and side effects).[25] A combination of scanning electron microscopy (SEM), powder X-ray diffraction (powder XRD), and differential scanning calorimetry (DSC) were used to study the bulk properties (homogeneity, morphology, and crystallinity) of the SDDs.

4.2.2 Solid State Characterization of SDDs

SEM is an important tool to investigate information about morphology and particle size distribution of the SDDs. As shown in Figure 4.1, all spray dried dispersions with probucol revealed wrinkled, collapsed sphere morphologies, which is indicative of increased surface area of the SDD powders. The increased surface area is directly related to aiding increased drug dissolution.

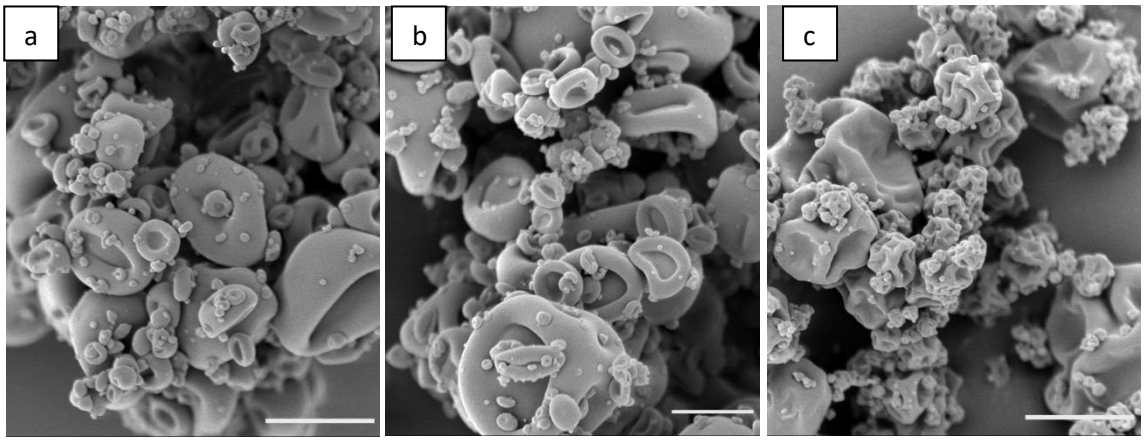

Figure 4.1 SEM images of the SDDs created by spraying a THF:MeOH (15:2) solution of Probucol with (a) PEP-b-P(DMA-*grad*-MAT), (b) PNIPAAm-b-P(DMA-*grad*-MAT), and (c) PDEAEMa-b-P(DMA-*grad*-MAT) as the polymer excipients at 25 wt % of drug loading. The scale bars indicate 1 μm.

PXRD is a non-destructive technique to determine the presence of crystalline material in SDDs.[15,26] The X-ray diffraction pattern of pure probucol showed distinctive sharp peaks in the diffraction pattern indicating a highly crystalline material. All SDDs with probucol revealed broad, diffused powder XRD patterns at 50 wt% of drug loading, except PEP-b-P(DMA-*grad*-MAT) (Figure 4.2). The sharp peaks in this dispersion belongs to probucol form II crystals as compared to pure probucol, which exhibits a scattering pattern of form I probucol crystals. SDDs with PNIPAm-b-P(DMA-*grad*-MAT) and PDEAEMA-b-P(DMA-*grad*-MAT) exhibited a broad and featureless diffractogram indicating that at least 95% of the probucol in the polymer matrices is amorphous in nature.

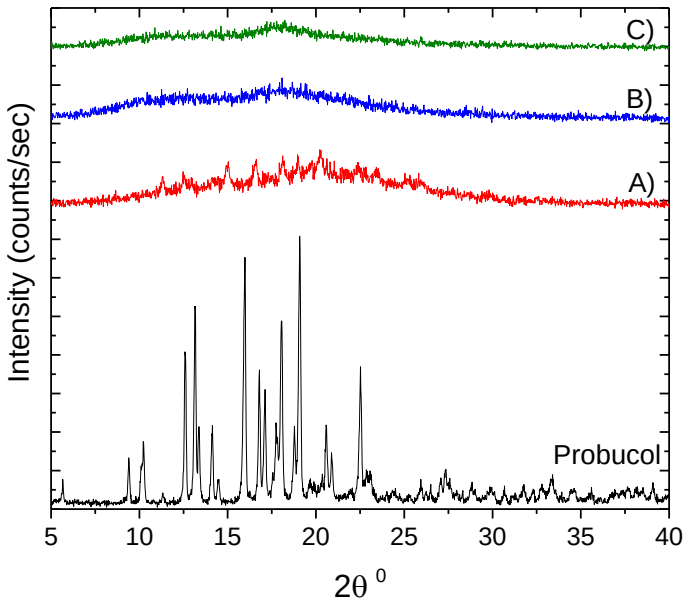

Figure 4.2 Powder XRD patterns of crystalline probucol comparing SDDs with A) PEP-b-P(DMA-*grad*-MAT), B) PNIPAm-b-P(DMA-*grad*-MAT), and C) PDEAEMA-b-P(DMA-*grad*-MAT) as the matrices at 50 wt % probucol.

Differential scanning calorimetry (DSC) is a powerful method to determine the presence of crystalline material in SDDs with higher sensitivity compared to PXRD.[27] In addition, DSC thermograms yield information about how the drug is molecularly dispersed in the polymer matrix.[27,28] To study these properties, we utilized modulated DSC (MDSC), which measures reversible (heat capacity) and non-reversible (crystallization, solvent evaporation) transitions and has significant advantages over DSC.[29,30] MDSC offers information about drug crystallization upon heating, which in turn, provides information about polymer-drug interactions and the ability of the polymer to inhibit crystallization (keep the drug in the amorphous state). Moreover, MDSC thermograms show a single glass transition temperature if the drug is homogenously mixed with polymer matrix. Also, a change in the T_g values indicate how strongly the drug is associated with the polymer matrix.[31-35] All MDSC analysis and traces are shown in (Table 4.3, Table 4.4, and Figure 4.10).

A single glass transition temperature (T_g) was observed for all SDDs (Table 4.4), indicating that the drug is homgenously dispersed in the polymer matrix. The T_g of the SDDs decreases towards that of the amorphous drug with increased drug loading, when comparing 10, 25 and 50 wt% of probucol loading. Furthermore, the data in Table 4.3 indicate that the increase in the number of hydrogen bonding sites in the polymer backbone (PDEAEMA > PNIPAm > PEP), increases the amorphous nature of probucol (decresases the percentage of crystalline Probucol, assuming 100% crystallization). To calculate the percent of probucol crystallinity, the melt endotherm was substracted from the crystallization enthalpy of the drug, which is normalized to the drug loading. At 10, 25, and 50 wt% of drug loading, SDDs formulated from PDEAEMA-b-P(DMA-*grad*-MAT) did not reveal any crystallization events or melt enotherms in the MDSC (Table 4.4 and Figure 4.10). This implies that Probucol strongly interacts with the PDEAEMA-b-P(DMA-*grad*--MAT) polymer matrix as compared to PEP-b-P(DMA-*grad*-MAT) and PNIPAm-b-P(DMA-*grad*-MAT). PDEAEMA chains have more hydrogen bonding sites per repeat unit (3 sites/repeat) as compared to that present in PEP (0 sites) and PNIPAm (2 sites), which could contribute to interaction of the polymer with the drug. At 50 wt% of drug of loading, the SDD created with the PEP-b-P(DMA-*grad*-MAT) matrix showed crystallization at 56.8 °C, whereas the SDD created with PNIPAm-b-P(DMA-*grad*-MAT) revealed a first crystallization event at 74.9 °C (Table 4.4 and Figure 4.10). This indicates that the PNIPAm-b-P(DMA-*grad*-MAT) polymer matrix may be better to supress crystallization of the Probucol than PEP-b-P(DMA-*grad*-MAT) polymer matrix at higher temperature.

4.2.3 In Vitro Dissolution Performance

Next, we studied how well the SDDs achieve and maintain the *in vitro* dissolution performance of probucol. Ideally, a dispersion of the drug and polymer should be able to maintain supersaturation levels of drug and inhibit crystal nucleation in the GI tract. Simulated intestinal fluid power (SIF powder) was added to the dissolution media to test the *in vitro* performance of all the SDDs. Addition of SIF powder gives a better indication of how the drug will dissolve and release in the buffered conditions. In the dissolution tests, undissolved probucol was removed by centrifugation at 13,000 rpm for 1 min, and the concentration of probucol was monitored by HPLC by taking aliquots at different time intervals.

Figure 4.3 shows the dissolution profiles of all the SDD formulations at 10 and 25 wt% of probucol loading. We compared the dissolution performance of all SDDs with commerically available HPMCAS-M grade (positive control). As shown in Figure 4.3, the SDD of PNIPAm-b-P(DMA-*grad*-MAT) showed an excellent burst release profile with probucol in aqueous solution and maintained drug supersaturation for 6 hours. We attributed the excellent performance of PNIPAm-b-P(DMA-*grad*-MAT) to its ability to dissolve rapidly in aqueous solution, release probucol in the dissolution media, and inhibit crystal nucleation. The PEP-b-P(DMA-*grad*-MAT) did not dissolve fully in the dissolution media and resulted in a poor solubilization/release profile with probucol. Due to the insolubility of the polymer matrix, the drug may be trapped in the polymer matrix and may precipitate out with the polymer in the dissolution media. The PDEAEMA-b-P(DMA-*grad*-MAT) polymer also did not dissolve in dissolution at pH 6.5 and revealed a poor drug solubilization/release profile.

The DEAEMA is a pH responsive component of this system and it is well documented in the literature that DEAMEMA becomes protonated in aqueous solution upon lowering of the pH. Therefore, we conducted dissolution tests of this SDD at a lower pH of 5.1 and 3.1, respectively. At pH 5.1, the SDD is still insoluble and there is no significant change in the dissolution profile of the SDD formulation containing PDEAEMa-b-P(DMA-*grad*-MAT). However, PDEAEMa-b-P(DMA-*grad*-MAT) exhibited controlled release of Probucol at pH 3.1. At pH 3.1, the PDEAEMa portion of the polymer matrix gets protonated and the polymer dissolves slowly in the dissolution media. As a result, Probucol is released from the polymer matrix in the dissolution media and polymer maintained drug supersaturation for 6 h.

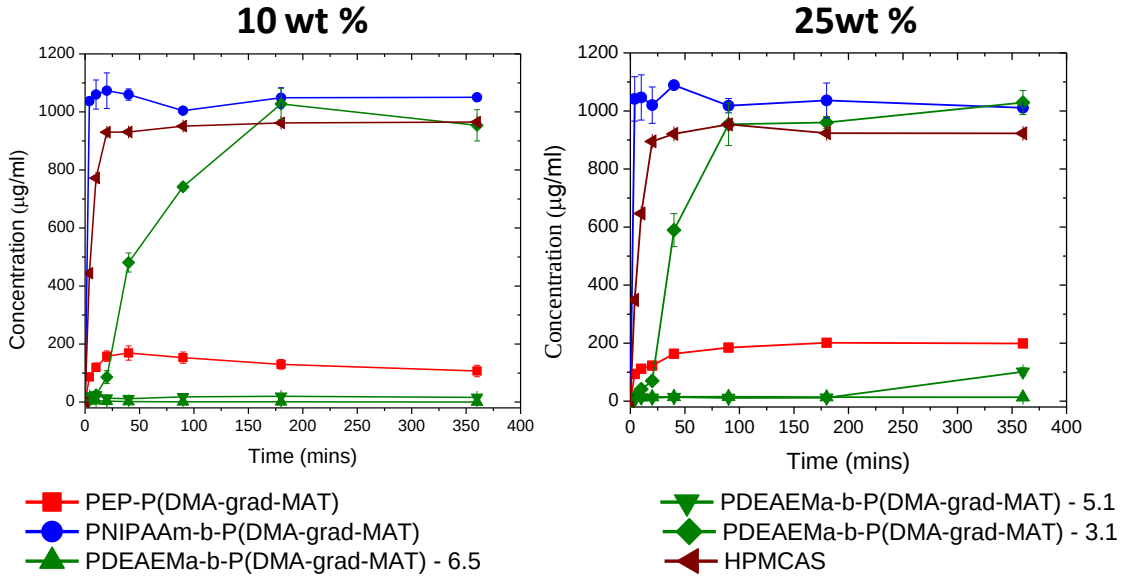

Figure 4.3 Dissolution data of the SDDs with 10 and 25 wt% of probucol. PNIPAm-b-P(DMA-*grad*-MAT) showing an excellent burst release and super saturation maintenance profile for probucol at pH 6.5. On the other hand, PDEAEMA-b-P(DMA-*grad*-MAT) showed controlled release profile for probucol at pH 3.1. The target concentration of probucol was 1000 µg/mL (denoting 100% drug solubility).

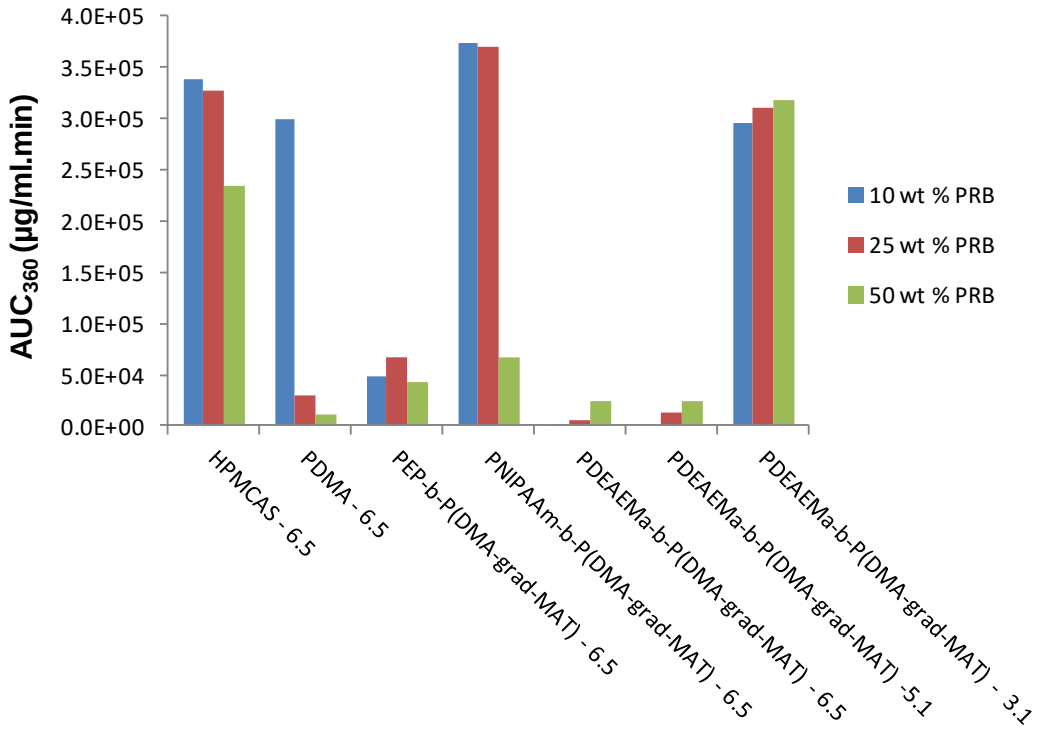

Figure 4.4 Area under the curve (AUC) as calculated at 360 min from the dissolution data of SDDs with 10, 25, and 50 wt % probucol loading. The calculated AUC is the average of two trials. The data for homopolymer of PDMA with probucol SDD was obtained from previously published work.[11]

The area under the curve ($AUC_{360_{min}}$) is the area under the drug concentration – time profile curves over the period of a 6 h dissolution test and represents the solubility maintenance of the excipient system for a particular drug. The $AUC_{360_{max}}$ is the theoretical maximum area under the drug concentration time profile over period of a 6 h dissolution test. For ideal excipient, our $AUC_{360_{max}}$ is = 3.6×10^5 ug.min/mL (which denote 100% burst release and supersaturation maintenance of a drug). Therefore, the theoretical engineering target maximum is unity ($AUC_{360_{min}}/AUC_{360_{max}} = 1$). Incorporating a higher drug loading percentage in a SDD formulation is desirable; however, there is a fine interplay between higher drug loading, and the increased tendency of the drug to crystallize. With HPMCAS,

the targeted probucol solubility concentration was achieved (up to 25 wt% of drug loading; see Figure 4.4 and Table 4.5). At 50 wt% of drug loading, only 64% of the targeted drug concentration was soluble, which was likely due to the lower amount of polymer excipient to aid solubility of the hydrophobic drug molecules. The SDD of PEP-b-P(DMA-MAT) exhibited poor solubility enhancement at all drug loading percents. Similar to HPMCAS, the SDD of PNIPAm-b-P(DMA-*grad*-MAT) was able to achieve the targeted drug solubility concentration (100% soluble) up to 25 wt% of drug loading. However, this polymer matrix only achieved 18% of targeted drug concentration at 50 weight percent of drug loading. The SDD of the homopolymer PDMA control achieved 83% of targeted drug concentration at 10 weight percent of loading but failed to perform at 25 and 50 weight percent of drug loading. This result indicated that the PNIPAm component of PNIPAm-b-P(DMA-*grad*-MAT) is essential to achieve targeted drug concentrations at 25 wt % of drug loading. The SDD of PDEAEMA-b-P(DMA-grad-MAT) failed to show any significant increase in $AUC_{360_{min}}$ at pH 6.5 and 5.1. Interestingly, at a lower pH of 3.1, the SDD formulation was able to achieve almost 90% of the targeted probucol concentration at all drug loadings (10, 25, and 50 wt%). The $AUC_{360_{min}}$ value gradually increased by increasing the pH of the dissolution media with 10, 25 and 50 weight percent of drug loading. Therefore, this particular SDD, at a lower pH, outperformed HPMCAS by demonstrating 1.5 times increase in $AUC_{360_{min}}$ value at the highest drug loading percent tested (50 wt %).

4.3 Conclusions

In conclusion, we have synthesized three well-defined architectures of diblock polymers : PEP-b-P(DMA-*grad*-MAT), PNIPAAm-b-P(DMA-*grad*-MAT), and PDEAEMa-b-P(DMA-*grad*-MAT) and formulated spray dried dispersions with Probucol. The role of these polymer matrices in assisting drug dissolution and super saturation maintenance was examined. MAT was introduced to increase the T_g of these polymers so they are able to be formulated with drugs via spray drying. The SDD formulations were characterized using PXRD, SEM, and MDSC. PXRD data revealed broad, diffuse diffractograms with the SDDs containing PNIPAAm-b-P(DMA-*grad*-MAT) and PDEAEMa-b-P(DMA-*grad*-MAT) polymer matrices that were formulated up to 50% of probucol loading. This indicates that at least 95% of the drug is in the amorphous form. SEM images showed no significant difference in the bulk appearance of SDD powder dispersions when comparing the different polymers and loading concentrations. MDSC data indicated that the PDEAEMA-b-P(DMA-*grad*-MAT) polymer matrix was better at suppressing probucol crystallization upon heating (with the formulations up to 50 wt% of probucol loading) when compared to P(DMA-*grad*-MAT) and PNIPAAm-b-P(DMA-*grad*-MAT). The individual polymer matrices showed a very distinctive dissolution performance in enhancing probucol supersaturation at different drug loadings. The SDD of PNIPAAm-b-P(DMA-*grad*-MAT) was completely soluble in the dissolution media at pH 6.5 and able to achieve burst release of probucol in solution and maintained supersaturation concentration at 10 and 25 wt% of probucol loading. This particular SDD showed similar drug dissolution profiles as HPMCAS at 10 and 25 wt% of probucol loading. The SDD of PNIPAAm-b-P(DMA-*grad*-MAT) and HPMCAS failed to achieve targeted drug

concentration at 50 wt% of drug loading since less polymer matrix is incorporated. The SDD of PDEAEMA-b-P(DMA-*grad*-MAT) also failed to release loaded probucol at pH 6.5 and 5.1 due to insolubility of the polymer matrix in the dissolution media. Upon decreasing the pH to 3.1, this particular SDD readily dissolved in the dissolution media and demonstrated burst release and maintained drug supersaturation concentration over 6 h up to 50 weight percent of probucol loading. This particular SDD outperformed HPMCAS by demonstrating 1.5 times increase in the $AUC_{360_{min}}$ value. Our results clearly indicate that the solubility of polymer matrices in dissolution media and increase in hydrogen bonding sites in polymer matrices are critical to decrease probucol crystallinity, increase $AUC_{360_{min}}$ value, and achieve supersaturation concentration of probucol in the dissolution media. Our study gives new insight into the field of excipient design by demonstrating the importance of monomer selection to tune drug release at different pH. The development of high performance excipients and efforts to understand the structure-activity relationships may help decrease the currently high attrition rate of drugs in the pharmaceutical development pipeline.

4.4 Experimental Section

Materials. All chemicals were used as received (reagent grade) unless otherwise noted. All solvents utilized were HPLC or analytical grade. Anhydrous D-trehalose (99%, Acros Organics), iodine (Aldrich, >99.8%), triphenylphosphine (Aldrich, 99%), acetic anhydride (99.6%, Fisher), dry pyridine (99.8%, Sigma Aldrich), sodium azide (Aldrich, >99.5%), Pd/C (Aldrich), sodium methoxide (Aldrich, 95%), sodium chloride (Fisher), silica gel (Sorbent technologies, porosity 60Å size 40-60μm), chlorotrimethylsilane (TMSCl; Fisher, 98%), triethylamine (TEA; Acros Organics, 99.7%), and HCl (1.25M) in methanol (Fluka), 2,2'-Azobis(2-methylpropionitrile) (AIBN, Aldrich, 98%) were used as received. Freshly distilled methacryloyl chloride (Acros, 95%) was used for synthesis. *N*,*N*-Dimethylacrylamide (DMA) (Aldrich, 99+%) was purified by passage through activated basic alumina columns to remove trace amounts of inhibitors. The monomers N-isopropylacrylamide (NIPAm) (Aldrich, >99%), 2-(Diethylamino)ethylmethacrylate (DEAEMA) (Aldrich, 99%), 2-(dodecylthiocarbonothioylthio)-2-methylpropionic acid (Aldrich, 98%) were used as received. *Sec*-butyllithium (1.4 M in cyclohexane, Aldrich), 1,3-isoprene (Aldrich, 99%) and ethylene oxide (Aldrich, 99.5+%) were degassed with three freeze-pump-thaw cycles followed by removing trace amounts of acidic impurities by multiple treatments with *n*-butyllithium (2.5 M in hexanes, Aldrich) for 1 hour each and *n*-butylmagnesium chloride (2.0 M in diethyl ether, Aldrich) for 4 hours each, respectively. Toluene (Sigma-Aldrich, HPLC grade, 99.9+%), and dichloromethane (Sigma-Aldrich, anhydrous, 99.8+%), and tetrahydrofuran (THF, Sigma-Aldrich, HPLC grade, 99.9+%, inhibitor free) were purified via a MBRAUN solvent purification system. Probucol (PBC) and phenytoin (PTN) were purchased from Sigma-Aldrich (Milwaukee, WI) and used

without further purification. HPMCAS (AFFINISOL™ 912G, The Dow Chemical Company) was used as received. Fasted simulated intestinal fluid powder (FaSSIF) was purchased from Biorelevant (Surrey, UK). Phosphate buffered saline (PBS) was prepared in lab consisted of 82 mM sodium chloride (Fisher, ≥99.0%), 20 mM sodium phosphate dibasic heptahydrate (Fisher, 98%), 47 mM potassium phosphate monobasic (J.T. Baker, ≥99.0%).

The synthesis of TMS-MAT was achieved as described in the literature. The ^{1}H NMR was in agreement with previously published spectral data.[22,36] The diblock terpolymer PEP-P(DMA-*grad*-MAT) was synthesized using a combination of anionic and reversible addition fragmentation chain transfer (RAFT) copolymerizations. The PEP-b-P(DMA-*grad*-MAT) was characterized by ^{1}H NMR and size exclusion chromatography (SEC). The analysis data was in agreement with previously published data.[36] The synthesis of the diblock terpolymers PNIPAAm-b-P(DMA-*grad*-MAT) (Figure 4.7, ^{1}H NMR) and PDEAEMA-b-P(DMA-*grad*-MAT) (Figure 4.8, ^{1}H NMR) was achieved from macromolecular chain transfer agents (CTA), PNIPAm-CTA and PDEAEMA-CTA respectively. For example, a 25 mL round conical flask was charged with PNIPAm-CTA (0.6 g, 0.1 mmol), DMA(1.8 g, 18 mmol), TMS-MAT (1.8 g, 2 mmol) AIBN (0.8 mg, 0.0005 mmol), and 1,4-dioxane (10 ml). The reaction mixture degassed for 1 h by bubbling nitrogen and subjected to preheated oil bath at 70 °C for 12 h. Both polymers were purified by precipitation in diethyl ether twice and dried in a vacuum oven for 24 h at 45 °C. Detailed characterization information is reported in Table 4.1 and Figure 4.9 shows SEC chromatograms for PNIPAm-b-P(DMA-*grad*-MAT) and PDEAEMA-b-P(DMA-*grad*-MAT). The PNIPAm-CTA (Figure 4.5, ^{1}H NMR) and PDEAEMA-CTA (Figure 4.6, ^{1}H

NMR) were obtained by RAFT polymerization using a small molecule trithiocarbonate based CTA, 2-(dodecylthiocarbonothioylthio)-2-methylpropionic acid in 1,4 dioxane using AIBN as an initiator at 70 °C. For example, a 50 mL round conical flask was charged with NIPAm (5 g, 44.9 mmol), 357 mg of CTA (357 mg, 0.88 mmol), AIBN (7.2 mg, 0.044 mmol), and 1,4-dioxane (22 mL, 1.69 M). The reaction mixture was degassed for 45 min by bubbling nitrogen. The reaction flask was subjected to preheated oil bath at 70 °C for 6 h. PNIPAm-CTA was isolated by precipitation into pentane and followed by dialysis against water to remove trace amounts of impurities such as of monomers and solvent. PDEAEMA-CTA was purified by precipitation into diethyl ether twice. Detailed characterization information is reported in Table 4.2. The yield for PNIPAm-CTA and PDEAEMA-CTA were 87% and 72%, respectively. Macromolecular-CTA were dried in vacuum oven for 48 h at 40 °C before utilizing to synthesize diblock terpolymers.

Methods.

SEC Method. SEC measurements were carried out on a Agilent 1260 Infinity liquid chromatograph equipped with a Waters Styragel guard column and three Waters Styragel columns (HR6, HR4, and HR1) provide effective separation for an effective molecular weight 100-10,000,000 g/mol housed to an Agilent 1260 VWD UV-vis detector, a Wyatt Dawn Heleos II light-scattering detector, and a Wyatt Optilab T-rEX refractive-index detector. Tetrahydrofuran was used a mobile phase at 1.0 mL/min at 25 °C.

Spray drying. Spray drying was performed on a Bend Research Mini Spray Drier under the following conditions: inlet temperature of 68 °C, nitrogen flow rate of 12.8 SLPM, and a 0.65 mL/min syringe flow rate. The SDDs were collected on a 4“ Whatman filter. Unless

otherwise noted, the total solute content spray dried was always 1 wt%. Solutions were sprayed from a THF:MeOH mixture (15:2, v/v). All diblock terpolymers were completely soluble in a THF:MeOH mixture prior to spray drying. The SDD composition is reported as the weight percent (wt%) drug in the dispersion. For example, 30 mg of probucol and 270 mg of polymer were dissolved in 29.7 gm of THF:MeOH mixture to make 10 wt% probucol with (PEP-b-P(DMA-*grad*-MAT)). Three different compositions were used for the polymer/drug dispersions: 10, 25, and 50 wt% probucol/phenytoin relative to polymer.

Powder X-ray Diffraction (Powder XRD). PXRD experiments were carried out on a Bruker- AXS (Siemens) D5005 diffractometer. Samples (50 mg) were packed into standard 0.5 mm deep glass holders with zero background. The X-ray source (KCuα, λ = 1.54 A) was operated at a voltage of 45 kV and a current of 40 mA. Data for each sample was collected from 5° to 40° on the 2θ scale over approximately 30 minutes at a scan step of 1 seconds and a step size of 0.02°/s.

Differential Scanning Calorimetry (DSC). Modulated differential scanning calorimetry (MDSC) was used to determine the thermal features of the SDDs and was conducted on a TA-Instruments Discovery DSC equipped with an autosampler. Samples from 5−10 mg were placed in T-zero aluminum pans and sealed with a hermetic lid. MDSC analysis was performed with a nitrogen flow rate of 50.00 mL/min and a heating rate of 1 °C/min from 0 to 180 °C. The temperature was modulated at ±2 °C with a period of 40 s. The first heating scans are reported. For polymer only samples (not spray dried), the temperature was not modulated, but was ramped between -50 °C and 180 °C at a rate of 10 °C/min. The second heating scans are reported for those samples. For all samples, TA TRIOS software version 2.2 was used to analyze *T*g values and enthalpic components.

Scanning Electron Microscopy (SEM). A Hitachi S-900 microscope was used, and samples were sputtered with gold/palladium for 30 s at 40 kV on a Denton DV-502A High Vacuum Deposition System to provide a conductive coating for analysis. SEM was used to obtain particle size and information about morphology data from the SDDs.

In Vitro Dissolution Test. Dissolution testing was performed on either each SDD formulation or the crystalline drug to determine the concentration of drug in the dissolution media and maintenance of supersaturation. The dissolution medium consisted of phosphate buffer saline (82 mM sodium chloride, 20 mM sodium phosphate dibasic, 47 mM potassium phosphate monobasic) supplemented with 0.5 wt% simulated intestinal fluid powder. The medium was adjusted to pH 6.5 with NaOH. An appropriate amount of SDD or crystalline drug was weighed and added into 2.0 mL microcentrifuge tubes to yield a final total drug concentration of 1000 mg/mL if all material is fully dissolved. For example: At 10 wt% of drug loading, we took 18.0 mg of SDD consisting of 1.8 mg of drug and 16.2 mg of polymer was diluted with 1.8 mL of PBS buffer solution for dissolution testing. All samples were analyzed in duplicate (n=2). The first step in dissolution testing involve vortexing samples for 1 min in 1.8 mL of PBS + FaSSIF medium and then placing the sample into an aluminum heating block that was isothermal held at 37°C. At each time point 4,10, 20, 40, 90, 180, and 250 min, tubes were removed from the heating blocks and centrifuged at 13000 rpm, 37 °C for 1 min to remove undissolved drug from dissolved drug, then 50 μL of the supernatant was aliquoted into an HPLC vial. The samples were again vortexed 30 s and held at 37 °C until the next time point. The supernatant in the HPLC vials was then diluted with 250 μL of methanol and analyzed for drug via HPLC. The mobile phase consisting of acetonitrile-water (96:4, v/v) was used for detecting drug

concentration in all SDDs. Drug concentration in each aliquot was determined by reverse phase HPLC. The HPLC consisted of a reversed-phase EC-C18 column (Poroshell 120, 4.6 × 50 mm, 2.7 μm, Agilent, USA). A mobile phase of 96:4 (v/v) acetonitrile:water was used for probucol detection with a flow rate of 1.0 mL/min at 30 °C. A 10 μL aliquot of sample was injected, and the column effluent was detected at 241 nm with a UV detector (1260 Infinity Multiple Wavelength Detector, Agilent). The probucol concentration in the samples was determined using a calibration curve of 0.1−500 μg/mL concentrations.

Table 4.2 Molecular characterization of homopolymers.

Sample	[AIBN] : [CTA]: [Monomer]	$[M_0]$	Time (h)	Conv. of monomer	M_n kg/mole[a]	$Đ$[b]
PNIPAAm-CTA	0.05 : 1: 50	1.69	6	99%	5.6	1.07
PDEAEMa-CTA	0.05 : 1: 50	1.69	8	87%	8	1.15

[a]The number average molecular weight of the poly (CTA) as determined by ^{1}H NMR spectroscopy. [b]The dispersities of poly (CTA) as determined by SEC using THF as a mobile phase. *Note:* The CTA used was 2-(dodecylthiocarbonothioylthio)-2-methylpropionic acid.

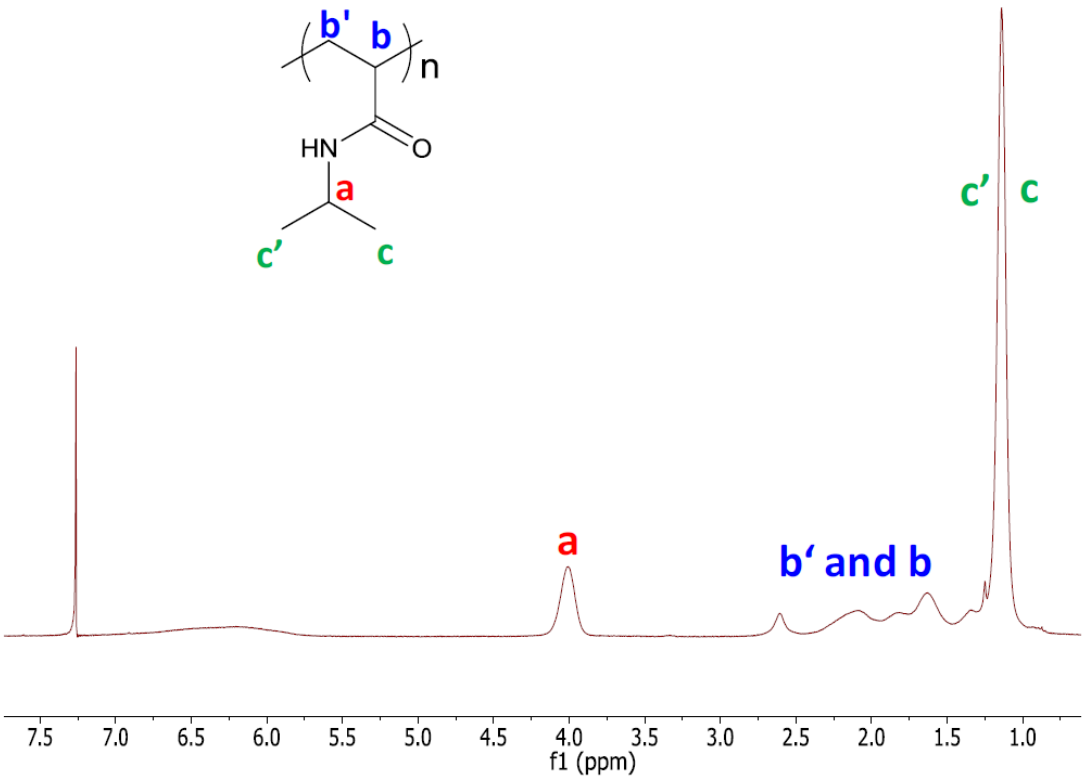

Figure 4.5 ^{1}H NMR spectrum recorded for PNIPAm-CTA in $CDCl_3$.

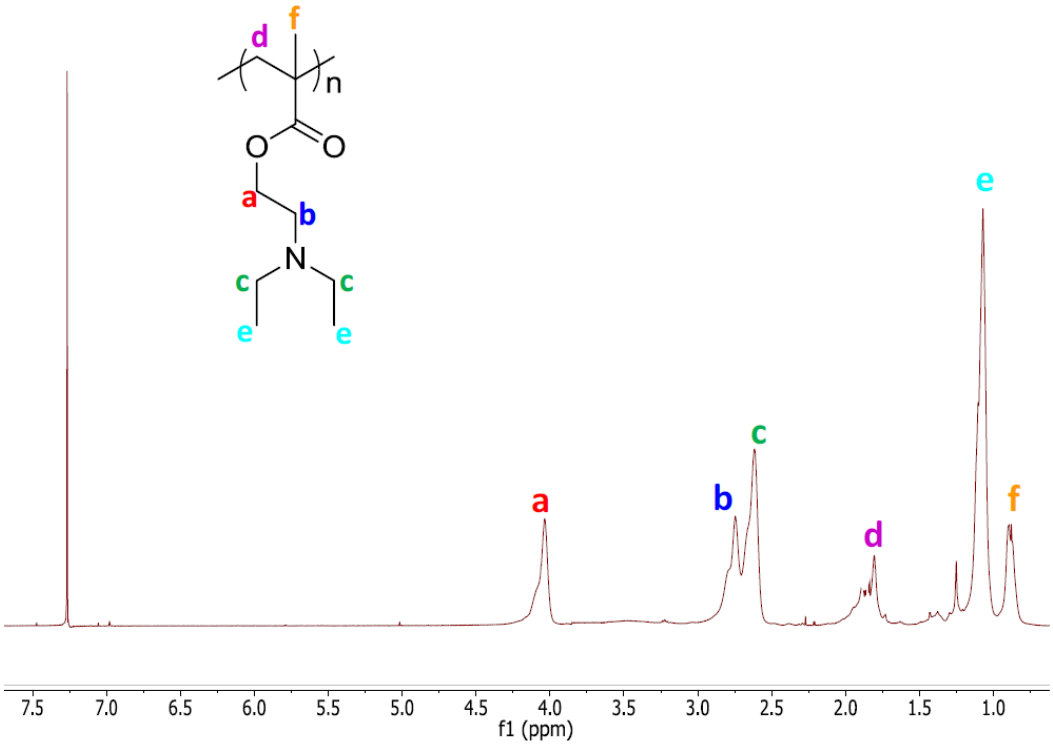
f
d
n
O
O
a
b
N
c
c
e
e
a
b
c
d
e
f
7.5
7.0
6.5
6.0
5.5
5.0
4.5
4.0
3.5
3.0
2.5
2.0
1.5
1.0
f1 (ppm)

Figure 4.6 ^{1}H NMR spectrum recorded for PDEAEMA-CTA in $CDCl_3$.

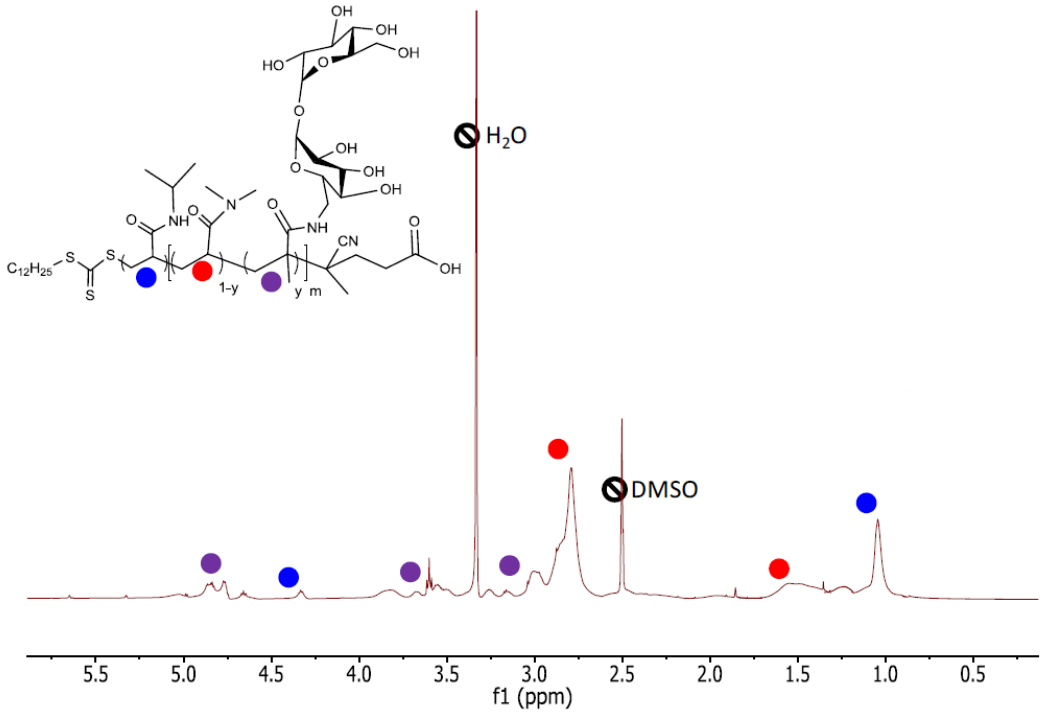

Figure 4.7 ^{1}H NMR spectrum recorded for PNIPAm-b-P(DMA-*grad*-MAT) in d6-DMSO.

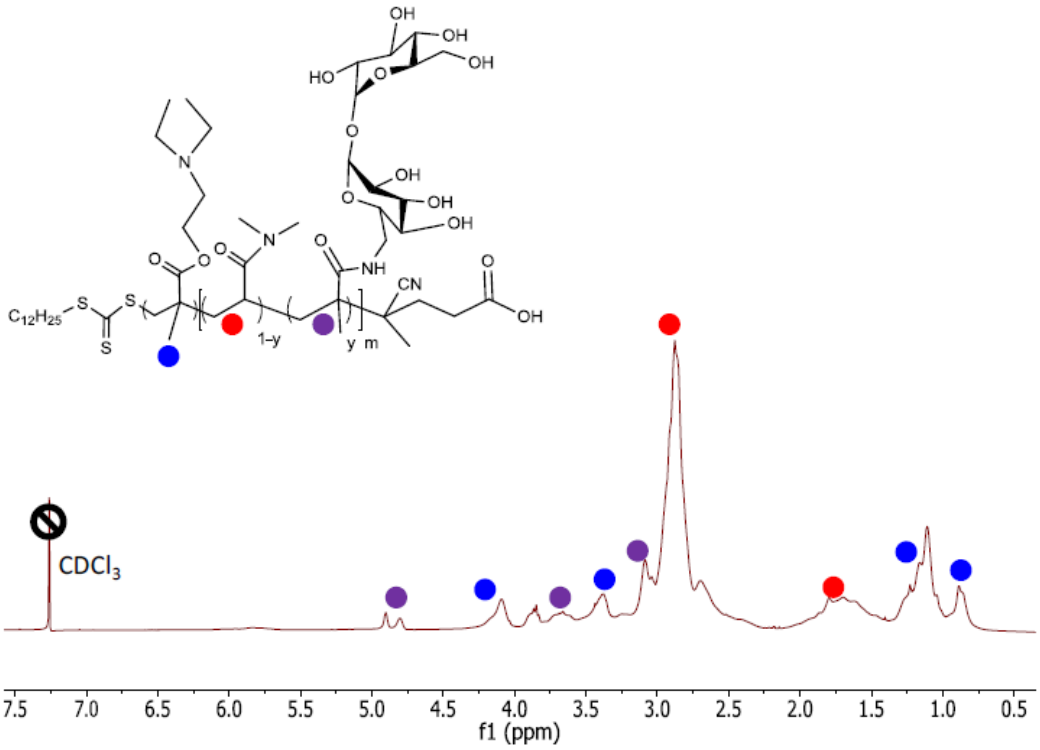

Figure 4.8 ^{1}H NMR spectra recorded for PDEAEMA-b-P(DMA-*grad*-MAT) in $CDCl_3$.

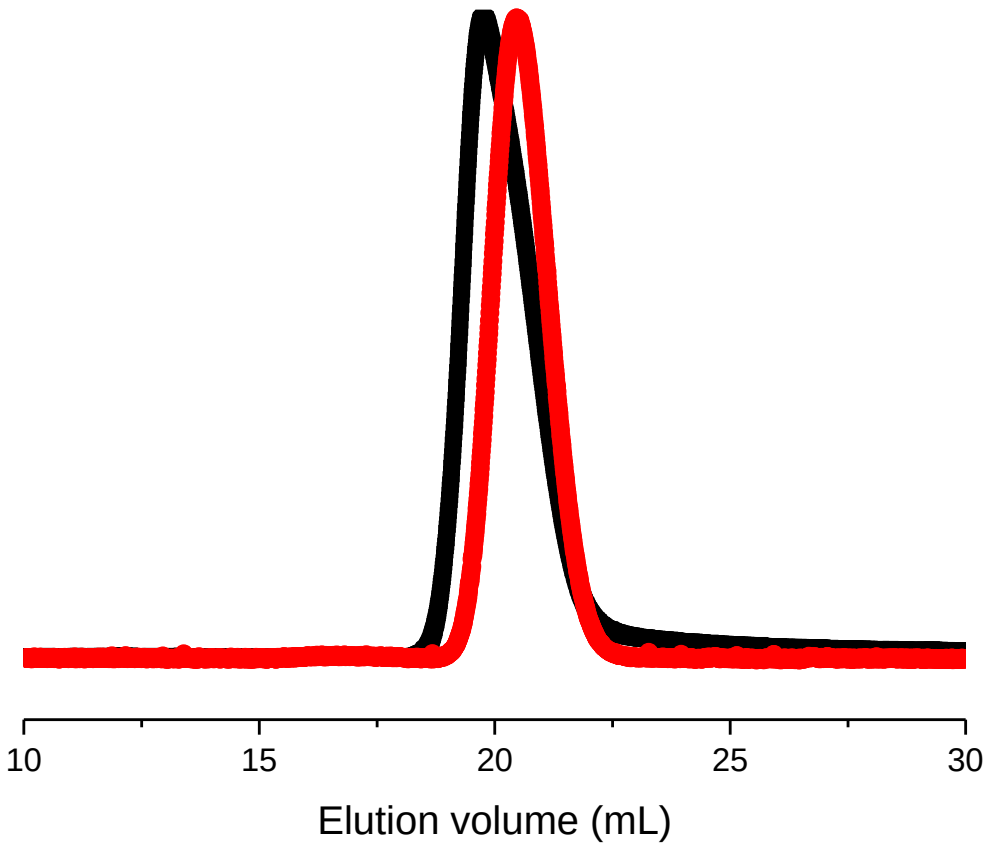

Figure 4.9 SEC chromatograms of the TMS protected PNIPAm-b-P(DMA-*grad*-MAT) and PDEAEMA-b-P(DMA-*grad*-MAT) immediately after polymerization. Chromatograms were recorded on a THF SEC with a flow rate of 1.0 mL/min and a run temperature of 25 °C. The calibration curve was based on PS standards. The SEC chromatogram for PEP-b-P(DMA-grad-MAT) was published previously.[11]

Table 4.3 Comparison of the weight fraction of monomers and drugs in the SDDs and the percent of Probucol crystalinity.

Sample	SDD Weight fraction					Probucol loading	% PBC Crystallinity
	PEP	PNIPAAm	PDEAEMa	PDMA	PMAT		
PEP-b-P(DMA-*grad* -MAT)	0.06	0	0	0.31	0.13	0.5	42.1
PNIPAAm-b-P(DMA-*grad* -MAT)	0	0.09	0	0.29	0.12	0.5	35.8
PDEAEMa-b-P(DMA-grad-MAT)	0	0	0.13	0.26	0.11	0.5	-

Table 4.4 MDSC analysis of SDDs with probucol.

Probucol loading	SDDs	T_g (°C)	T_{c1} (°C)	Enthalpy (J/g)	T_{c2} (°C)	Enthalpy (J/g)	T_{m1} (°C)	Enthalpy (J/g)	T_{m2} (°C)	Enthalpy (J/g)	% PBC Crystallinity
10 wt%	PEP-b-P(DMA-*grad*-MAT)	106.4	-	-	-	-	-	-	-	-	-
	PNIPAAm-b-P(DMA-*grad*-MAT)	127.6	-	-	-	-	-	-	-	-	-
	PDEAEMa-b-P(DMA-grad-MAT)	150.2	-	-	-	-	-	-	-	-	-
25 wt%	PEP-b-P(DMA-*grad*-MAT)	NA	NA	NA	NA	NA	NA	NA	NA	NA	NA
	PNIPAAm-b-P(DMA-*grad*-MAT)	116.6	80.2	2.6	-	-	107.6	4.8	-	-	12.9%
	PDEAEMa-b-P(DMA-grad-MAT)	126.9	-	-	-	-	-	-		-	-
50 wt%	PEP-b-P(DMA-*grad*-MAT)	104.3	56.8	15.95	-	-	107.9	28.9	120.3	1.46	42.1%
	PNIPAAm-b-P(DMA-*grad*-MAT)	105.9	74.9	5.3	98.2	2.05	112.4	18.4	121.1	1.2	35.8%
	PDEAEMa-b-P(DMA-grad-MAT)	111.1	-	-	-	-	-	-	-	-	-

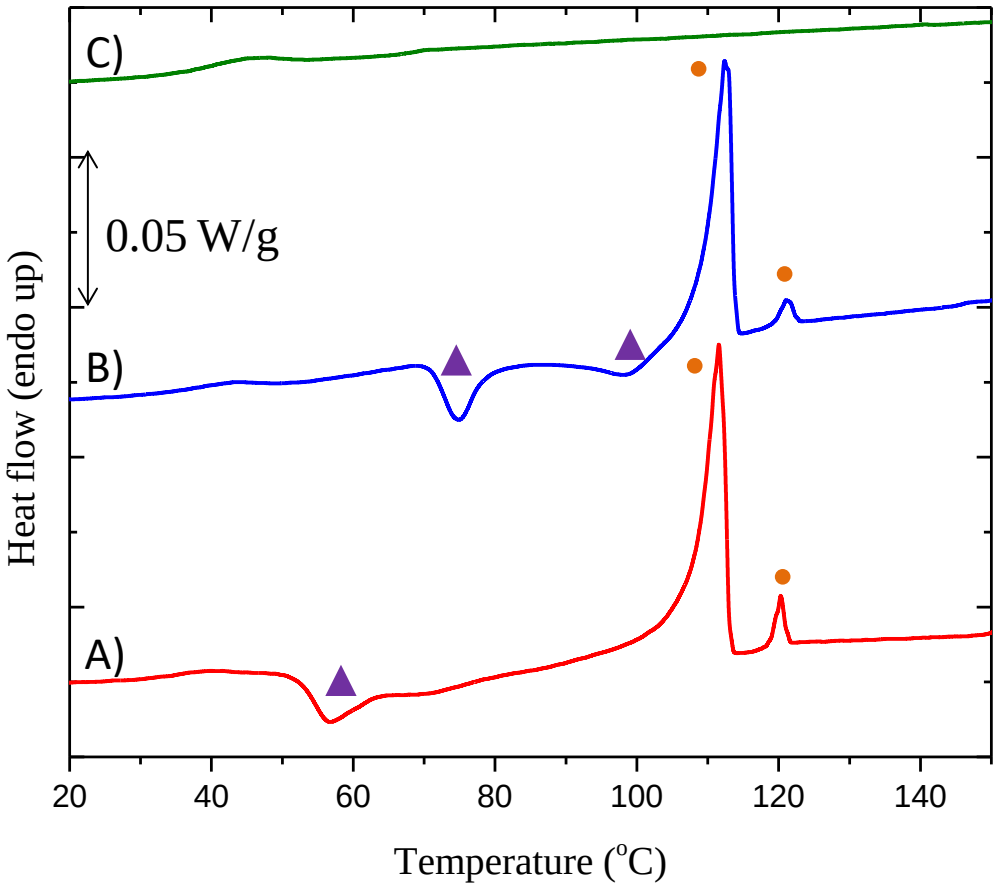

Figure 4.10 MDSC thermograms of total heat flow from SDDs containing 50 wt% of probucol: A) PEP-b-P(DMA-*grad*-MAT), B) PNIPAm-b-P(DMA-*grad*-MAT), and C) PDEAEMA–b-P(DMA-*grad*-MAT).

Table 4.5 Calculated area under the curve (AUC) for solubilization of probucol and all polymer excipient SDD formulations at 10, 25, and 50 wt% drug loading.

Polymer	10 wt %		25 wt %		50 wt %	
	AUC_{360}min (µg/mL)	AUC_{360}min/ AUC_{360}max (min µg/mL)	AUC_{360}min (µg/mL)	AUC_{360}min/ AUC_{360}max (min µg/mL)	AUC_{360}min (µg/mL)	AUC_{360}min/ AUC_{360}max (min µg/mL)
HPMCAS - 6.5	3.4×10^5	0.97	3.3×10^5	0.92	2.3×10^5	0.64
PEP-P(DMA-MAT) - 6.5	4.8×10^4	0.13	6.7×10^4	0.19	4.2×10^4	0.12
PNIPAAm-P(DMA-MAT) - 6.5	3.7×10^5	~1.0	3.7×10^5	~1.0	6.6×10^4	0.18
PDEAEMa-P(DMA-grad-MAT) - 6.5	3.9×10^2	0	5.1×10^3	0.01	2.3×10^4	0.06
PDEAEMa-P(DMA-grad-MAT) - 5.1	4.2×10^2	0	1.2×10^4	0.03	2.4×10^4	0.07
PDEAEMa-P(DMA-grad-MAT) - 3.1	2.9×10^5	0.81	3.1×10^5	0.86	3.2×10^5	0.89
PDMA - 6.5	3.0×10^6	0.83	2.9×10^4	0.08	1.1×10^4	0.03

The $AUC_{360_{min}}$ values for PDMA at pH 6.5 were obtained from previously published work.[11]

4.5 References

(1) Gaucher, G.; Satturwar, P.; Jones, M. C.; Furtos, A.; Leroux, J. C. *Eur. J. Pharm. Biopharm.* **2010**, *76*, 147-158.

(2) Delie, F.; Blanco-Prieto, M. J. *Molecules* **2005**, *10*, 65-80.

(3) Shaji, J.; Patole, V. *Indian J Pharm Sci* **2008**, *70*, 269-277.

(4) Hauss, D. J. *Adv. Drug Del. Rev.* **2007**, *59*, 667-676.

(5) Lipinski, C. A. *J. Pharmacol. Toxicol. Methods* **2000**, *44*, 235-249.

(6) Lipp, R. *The Innovator Pipeline: Bioavailability Challenges and Advanced Oral Drug Delivery Opportunities*, 2013.

(7) Ting, J. M.; Navale, T. S.; Bates, F. S.; Reineke, T. M. *Macromolecules* **2014**, *47*, 6554-6565.

(8) Wilson, M.; Williams, M. A.; Jones, D. S.; Andrews, G. P. *Ther. Deliv.* **2012**, *3*, 787-797.

(9) Paudel, A.; Worku, Z. A.; Meeus, J.; Guns, S.; Van den Mooter, G. *Int. J. Pharm.* **2013**, *453*, 253-284.

(10) Loftsson, T.; Brewster, M.; Másson, M. *Am. J. Drug Deliv.* **2004**, *2*, 261-275.

(11) Dalsin, M. C.; Tale, S.; Reineke, T. M. *Biomacromolecules* **2013**, *15*, 500-511.

(12) Ormes, J. D.; Zhang, D.; Chen, A. M.; Hou, S.; Krueger, D.; Nelson, T.; Templeton, A. *Pharm. Dev. Technol.* **2013**, *18*, 121-129.

(13) Huang, Y.; Dai, W. G. *Acta Pharm. Sin. B* **2014**, *4*, 18-25.

(14) Yin, L. G.; Hillmyer, M. A. *Mol. Pharm.* **2014**, *11*, 175-185.

(15) Friesen, D. T.; Shanker, R.; Crew, M.; Smithey, D. T.; Curatolo, W. J.; Nightingale, J. A. *Mol. Pharm.* **2008**, *5*, 1003-1019.

(16) Tanno, F.; Nishiyama, Y.; Kokubo, H.; Obara, S. *Drug Dev. Ind. Pharm.* **2004**, *30*, 9-17.

(17) Mundargi, R. C.; Rangaswamy, V.; Aminabhavi, T. M. *J. Appl. Polym. Sci.* **2011**, *122*, 2244-2251.

(18) Liu, S. Q.; Tong, Y. W.; Yang, Y. Y. *Biomaterials* **2005**, *26*, 5064-5074.

(19) Yeh, J. C.; Hsu, Y. T.; Su, C. M.; Wang, M. C.; Lee, T. H.; Lou, S. L. *J. Biomater. Appl.* **2014**, *29*, 442-453.

(20) Ohtake, S.; Wang, Y. J. *J. Pharm. Sci.* **2011**, *100*, 2020-2053.

(21) Yamashita, S.; Matsuzawa, Y. *Atherosclerosis* **2009**, *207*, 16-23.

(22) Sizovs, A.; Xue, L.; Tolstyka, Z. P.; Ingle, N. P.; Wu, Y.; Cortez, M.; Reineke, T. M. *J. Am. Chem. Soc.* **2013**, *135*, 15417-15424.

(23) Xu, X.; Smith, A. E.; Kirkland, S. E.; McCormick, C. L. *Macromolecules* **2008**, *41*, 8429-8435.

(24) Tale, S. R.; Yin, L.; Reineke, T. M. *Polym. Chem.* **2014**, *5*, 5160-5167.

(25) Qian, F.; Huang, J.; Hussain, M. A. *J. Pharm. Sci.* **2010**, *99*, 2941-2947.

(26) Uchiyama, H.; Tozuka, Y.; Imono, M.; Takeuchi, H. *Eur. J. Pharm. Biopharm.* **2010**, *76*, 238-244.

(27) Baird, J. A.; Taylor, L. S. *Adv. Drug Del. Rev.* **2012**, *64*, 396-421.

(28) Yin, L.; Dalsin, M. C.; Sizovs, A.; Reineke, T. M.; Hillmyer, M. A. *Macromolecules* **2012**, *45*, 4322-4332.

(29) Sauer, B. B.; Kampert, W. G.; Neal Blanchard, E.; Threefoot, S. A.; Hsiao, B. S. *Polymer* **2000**, *41*, 1099-1108.

(30) McPhillips, H.; Craig, D. Q.; Royall, P. G.; Hill, V. L. *Int. J. Pharm.* **1999**, *180*, 83-90.

(31) Gupta, P.; Bansal, A. K. *J. Pharm. Pharmacol.* **2005**, *57*, 303-310.

(32) Kalaiselvan, R.; Mohanta, G. P.; Manna, P. K.; Manavalan, R. *Die Pharmazie* **2006**, *61*, 618-624.

(33) Albers, J.; Alles, R.; Matthee, K.; Knop, K.; Nahrup, J. S.; Kleinebudde, P. *Eur. J. Pharm. Biopharm.* **2009**, *71*, 387-394.

(34) Gupta, P.; Kakumanu, V. K.; Bansal, A. K. *Pharm. Res.* **2004**, *21*, 1762-1769.

(35) Vasanthavada, M.; Tong, W. Q.; Joshi, Y.; Kislalioglu, M. S. *Pharm. Res.* **2004**, *21*, 1598-1606.

(36) Tale, S. R.; Yin, L.; Reineke, T. M. *Poly Chem* **2014**, *5*, 5160-5167.

5 CHAPTER FIVE

Dissolution and solubility enhancement of highly lipophilic drug Phenytoin via interaction with poly(*N*-isopropylacrylamide-*co*-vinylpyrrolidone) excipients

Adapted from:

Widanapathirana L.; Tale S. R.; Theresa T.M., Dissolution and Solubility Enhancement of the Highly Lipophilic Drug Phenytoin via Interaction with Poly(*N*-isopropylacrylamide-*co*-vinylpyrrolidone) Excipients, *Mol. Pharmaceutics*. **2015**, 12(7), 2537-2543.

This work was a joint venture by this author who is responsible for characterization of SDDs, LCST measurements, spray drying of all random copolymers to obtain ASDs. Lakmini W. who played a major role in synthesis, characterizations of polymers, and dissolution studies of ASDs.

5.1 Introduction

It has been estimated that Biopharmaceutics Classification System (BCS) class II drugs make up approximately 60% of active pharmaceutical ingredients (API) under current development as new pharmaceuticals.[1] Formation of amorphous solid dispersions (ASDs) of poorly aqueous soluble active ingredients with excipients has emerged as a promising modality to increase the solubility and bioavailability of drug candidates with challenging physical properties towards solubilization.[2,3] Excipients are pharmacologically inert materials that can be of natural product or synthetic origin and may make up a substantial portion of a pharmaceutical product. For example, many polysaccharide derivatives have been examined for drug solubility enhancement properties such as cyclodextrin[4,5] and various cellulose derivatives, including hydroxypropylmethylcellulose (HPMC),[6-8] hydroxypropylmethylcellulose acetate succinate (HPMCAS),[6,9] and ethylcellulose.[8,10] In addition, synthetic excipient models, such as polyethylene glycol,[11] polymethacrylates,[12] and soluplus,[13] have been examined. Among the synthetic excipient compound class, polyvinylpyrrolidone (PVP) is a useful material in the pharmaceutical industry due to its solubility in aqueous and polar organic solvents in addition to its biocompatibility. A wide range of vinylpyrrolidone homopolymers with varying molecular weights are available from BASF under the name Kollidon®. Copolymer-based excipients have been prepared by copolymerization of vinyl acetate (VAc) with VP [poly(VAc–*co*–VP)] and are available from BASF as Kollidon® VA64 (copovidone). Incorporation of the VAc monomer in VP chain results in excipients that are less hygroscopic and have a longer shelf-life stability.

ASDs containing PVP have been repeatedly shown to inhibit the crystallization of a variety of drugs such as ketoprofen,[14] piroxicam,[15] lansoprazole,[16] curcumin,[17] and probucol,[18] resulting in improved solubility, dissolution rates, and bioavailability. While PVP is known to improve drug performance, the solubility enhancement is still not optimal for certain drugs such as carbamazepine,[19] itraconazole,[20] griseofulvin,[21] and phenytoin.[22] It was reported that HPMC, which contains numerous hydrogen bond donor sites (*i.e.*, free hydroxyl groups) along the backbone is a better stabilizer for itraconazole (with multiple hydrogen bond acceptor sites) in solution compared to PVP, which has hydrogen bond acceptors in the form of carbonyl groups along the backbone.[20] Therefore, this drug-dependent performance of PVP may be attributed to the specific intermolecular interactions of the polymer with the functional groups of the API in solution, which results in variations in nucleation and crystal growth inhibition at supersaturated conditions.

To this end, we sought to understand the role of PVP-containing materials to solubilize phenytoin, a BCS class II drug used primarily in the management of complex partial seizures (see Figure 5.1 for phenytoin properties). Due to the drug's poor aqueous solubility (32 μg/mL), the high lipophilicity (2.2 indicated by the log P value or octanol/water partition coefficient), and the strong intermolecular interactions indicated by the high melting temperature (286 °C), the oral absorption of phenytoin is severely limited by its dissolution rate and high crystallization propensity, thus requiring significant enhancement in solubility in order to increase its oral bioavailability.

Improvement of the dissolution rate and bioavailability of phenytoin by ASDs prepared by coprecipitation with PVP have been investigated previously. Sekikawa et al. reported that a phenytoin-PVP co-precipitate (1:3) improved the dissolution of the drug.

However the maximum concentration reached was about 63 μg/mL.[23] The co-precipitation of phenytoin with a carrier combination of sodium deoxycholate and PVP (DC-Na-PVP) at the ratio of 1:1:1 was found to improve the dissolution by 9 fold at 5 mins (up to 278 μg/mL). However, the high drug-to-excipient ratio used resulted in a gradual concentration decrease over time due to phenytoin crystallization from the solution.[24] Furthermore, the use of DC-Na, which is a surface active carrier, resulted in poor *in vivo* safety profiles for the above excipient. Given that the drug dissolution rate increases as the excipient level increases in solid dispersions, Jachowich et al. reported a 30-40% drug dissolution and a solubility enhancement of phenytoin when it was incorporated in a solid dispersions with PVP (10 wt%) with varying molecular weights.[25] The best dissolution profile reported so far for phenytoin was achieved by Franco et al. when employing a solid dispersion of phenytoin with PVP K-30 at a 5 wt% drug loading.[26] The poor dissolution enhancement of phenytoin in the presence of PVP excipients is likely due to the lack of sufficient hydrogen bonding sites in the polymer. With only hydrogen bond acceptor carbonyl groups along the backbone, PVP can interact only with the two amide -NH protons of the phenytoin molecule. Therefore, the introduction of structurally similar hydrogen bond donor sites to the polymer backbone would be an interesting strategy to enhance the polymer excipient interactions with drugs containing both hydrogen bond donor and acceptor functional groups.

Herein, the role of a polymer excipient as a solubility enhancer and an antinucleating agent was examined to promote the solubilization and superstaturation maintenance of the model drug phenytoin. NIPAm comonomers, which have hydrogen bond donor (-NH) and acceptor (-C=O) functionalities, were introduced to a VP polymer

chain at various ratios in order to modify the hydrogen bonding capacity of the excipient. The introduction of NIPAm allowed us to create a polymer that is temperature-sensitive. ASD formulations of each copolymer with phenytoin at different drug loadings were prepared by spray drying. Very similar bulk properties were displayed by all the ASDs prepared as revealed by powder X-ray diffraction (PXRD). However, their dissolution performance exhibited significant dependence on the copolymer composition. We reveal that copolymerization of these monomers can be used to modify the chemical composition of a polymer excipient and thereby tune its physiochemical and pharmacological properties. Thus, understanding the structure-activity relationships of new excipient designs and drug formulations will aid with the rational design of new structures to promote drug solubility for challenging pharmaceutical candidates.

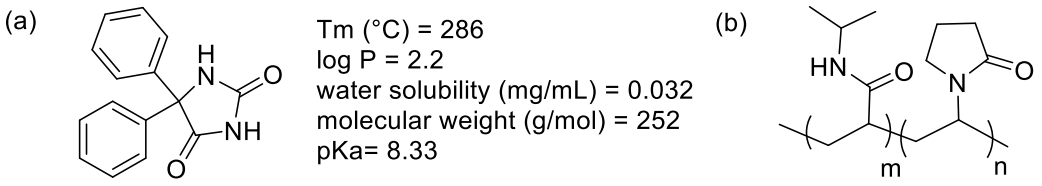

Figure 5. 1 Chemical structure of (a) phenytoin (with physical properties) and (b) poly(NIPAAm-*co*-VP)

5.2 Results and Discussion

5.2.1 Synthesis and Characterization of P(NIPAAm-*co*-VP)

Copolymerization of NIPAm with VP using various monomer feed ratios were carried out by a free radical polymerization technique in DMF at 70 °C using AIBN as the free radical initiator at various monomer feed ratios (Table 5.1) (the detailed procedure is available in the Experimental section). The polymers were isolated by precipitation with diethyl ether, dried under vacuum and the final copolymer compositions were obtained by ^{1}H NMR spectroscopy using peak integration for the monomer functional groups. The number averaged molecular weight and dispersity were determined by size exclusion chromatography (SEC), and the glass transition temperatures (T_g) were reported using differential scanning calorimetry (DSC) (Table 5.1).

Table 5.1 Polymer characterization data

Feed mol%		Actual mol% [a]		$M_{n,SEC}$ [b] (g/mol)	$Đ$ [c]	$T_{g,DSC}$ [d] (°C)
NIPAAm	VP	NIPAAm	VP			
100	0	100	0	42800	1.76	96
75	25	74	26	108000	1.44	100
60	40	59	41	158000	1.34	94
50	50	49	51	326000	1.37	96
40	60	42	58	220000	1.22	92
25	75	26	74	370000	2.44	96
0	100	0	100	341000	2.32	104

[a]mol % of NIPAm and VP in the polymer backbone determined by ^{1}H NMR spectroscopy in $CDCl_3$. [b]Total number averaged molecular weight and [c]dispersity as measured on a SEC based on dn/dc in THF. [d]Reported as the second heating cycle with a 10 °C/min heating rate.

5.2.2 LCST determination

The incorporation of NIPAm into the VP model polymer excipients offered hydrogen bonding donating sites to the system (for optimizing polymer-drug interactions) and also offered the added advantage of thermoresponsiveness to the excipient. The lower critical solution temperature (LCST) of NIPAm can be modulated around the physiological temperature (37 °C) by copolymerization with a suitable hydrophilic monomer such as VP.[27,28] Below the LCST of NIPAm, this polymer displays extensive hydrogen bonding interactions with the surrounding water molecules (and potential drug molecules), which allows NIPAm containing polymers to be soluble in aqueous media. However, the polymer becomes insoluble upon heating above its LCST due to the disruption of the hydrogen bonds with water and formation of inter- and intramolecular hydrogen bonding and hydrophobic interactions among polymer chains.[29] Thus, it is hypothesized that the hydrogen bonding of phenytoin with poly(NIPAm-*co*-VP) is optimal at solution temperatures below the phase transition temperature where extended polymer chains are present. Above this temperature, the NIPAm moieties are buried in the collapsed polymer structure and cannot interfere with the surroundings to a great extent. Herein, we sought to examine the role of hydrogen bonding capacity of the polymer excipient on the dissolution enhancement of phenytoin, a drug that contains both hydrogen bond donating and accepting sites and that is a challenging candidate for solubilization due to its high crystallization tendency.

The LCST of each polymer composition was measured in PBS buffer containing 0.5 wt % fasted-state simulated intestinal fluid (FaSSIF) as a function of % transmittance at 450 nm. At low temperatures, the polymer solution was clear, thus the transmittance of

light was high. With an increase in the temperature, the polymers phase separated (due to aggregation), which caused the solution to become turbid, and the transmittance decreased rapidly. The solubility of the polymers at physiological temperature were then studied by dissolving the polymer in a known amount of the PBS buffer. According to Figure 5.2, the LCST profiles of the thermoresponsive, water soluble copolymers were elevated from 28 °C to 51 °C with the increasing amount of VP in the polymer composition. With LCST values above 37 °C, the NIPAm segments of all the copolymers exist in its free form in aqueous dissolution media, exposing most of the hydrogen bond donor and acceptor sites to its surroundings. Furthermore, due to the hydrophilicity imparted by the 2-pyrrolidone ring, water solubility of the copolymer at physiological temperature also increased from 0 to 72 mg/mL with increasing amount of VP from 0 to 100%.

(a)

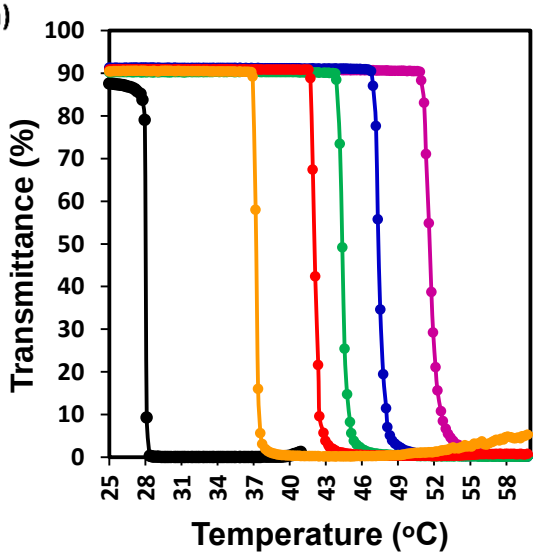

(b)

NIPAAm-*co* -VP Polymer composition	Solubility (mg/mL)
100:0	negligible
75:25	33
60:40	39
50:50	54
40:60	68
25:75	69
0:100	72
Marketed Product	66

Figure 5.2 (a) Copolymer composition-LCST behavior relationship for poly(NIPAm-*co*-VP) 100:0 (●), 75:25 (●), 60:40 (●), 50:50 (●), 40:60 (●), and 25:75 (●). The LCST values were found to be 28, 37, 42, 44, 46, and 51 °C respectively. (b) Solubility of the polymers at 37 °C in PBS/FaSSIF at pH 6.5. Solubility of a marketed PVP product (Kollidon® 25) was used as a control.

5.2.3 Preparation and Characterization of Amorphous Solid dispersions

ASDs are typically obtained by solvent evaporations methods, such as spray drying, which is an extensively studied technique to obtain solid dispersions.[3,17,18,30] The relatively short processing time, versatility for a wide range of polymers, and scalability from milligram to kilogram quantities make this technique unique and advantageous over other solvent methods. A typical spray drying process involves dissolving the excipient and drug into a volatile solvent, atomizing the solution into a spray of droplets of micron size in a drying chamber pumped with a hot and dry gas stream, and collecting the dried particles using a filter.[30] Formulations of polymer excipients and phenytoin were prepared by spray drying a mixture of each polymer with 10 and 25 wt % drug loadings in tetrahydrofuran at an inlet temperature of 68 °C. To characterize the physical state and stability of the ASDs, PXRD patterns of the spray dried phenytoin-polymer mixtures were obtained and compared to that of the crystalline drug (Figure 5.8). The characteristic crystalline peaks of phenytoin were absent in all spray dried dispersions (SDD) and a broad, diffuse diffractogram was observed indicating that at least 95% of the drug in the SDD is transformed to the amorphous state.

5.2.4 Dissolution Performance of SDDs

The main goal of these excipient model formulations was to understand the role of copolymer composition in facilitating solubility and supersaturation maintenance of BCS II drugs, specifically phenytoin. To determine the extent of drug solubility and supersaturation maintenance, *in vitro* dissolution testing was performed on all SDDs in phosphate buffered saline (pH 6.5) containing 0.5% FaSSIF at physiological temperature (37 °C). Crystalline phenytoin only and a physical mixture of 10 wt% crystalline phenytoin

and poly(NIPAm-*co*-VP) 60:40 were used as negative controls. To estimate the total amount of phenytoin dissolved in the dissolution media over the course of 6 hours, the area under the curve (AUC_{360}) for the dissolved concentration versus time curve was calculated (Table 5.2).

The dissolution performance of SDDs in solution reveals their potential to improve the bioavailability of phenytoin *in vivo*. During the assay, crystalline phenytoin that was formulated via a physical mixture of the drug with the polymer excipient showed a negligible dissolution profile (less than 10%) compared to the SDD formulations (see Figure 5.3a inset). This observation can be ascribed to the conversion of the drug from its crystalline state to the high energy amorphous state during the solid dispersion preparation.

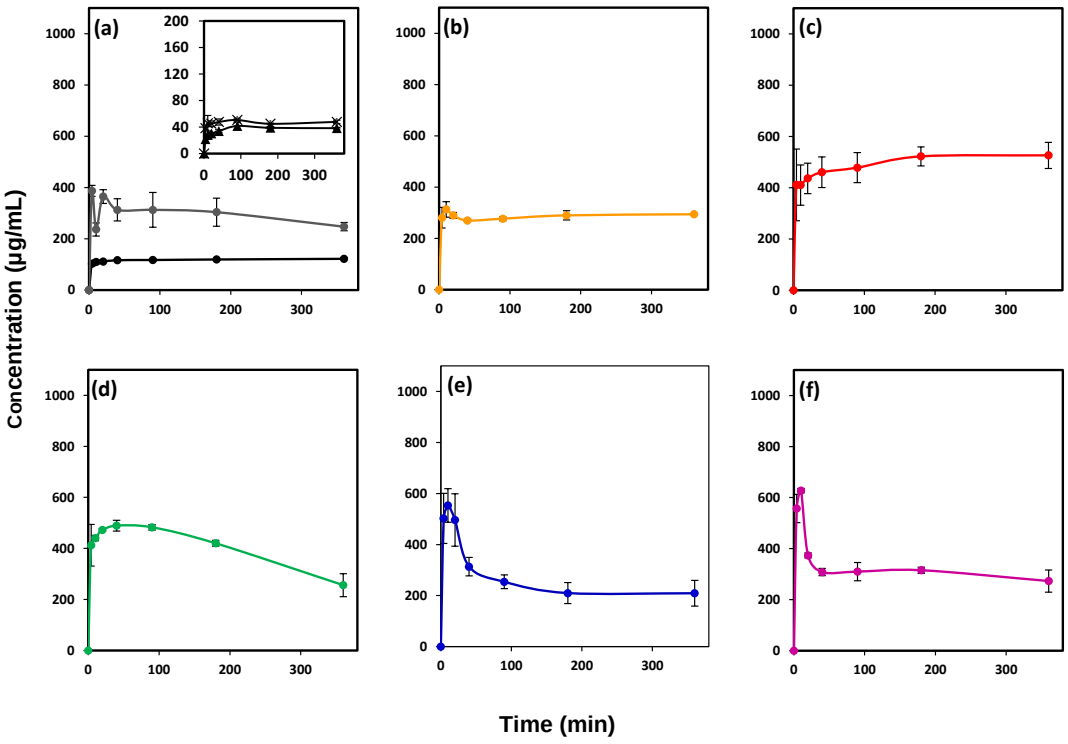

Figure 5.3 Dissolution data of SDDs with 10 wt% phenytoin loading at 37 °C. Polymer compositions that were tested include poly(NIPAm-co-VP) 100:0 (●), 75:25 (●), 60:40 (●), 50:50 (●), 40:60 (●), 25:75 (●) and 0:100 (●). The inset represent the dissolution data for crystalline phenytoin (×) and poly(NIPAm-*co*-VP) 60:40 physically mixed with

10 wt% phenytoin (▲) used as a negative control. The target concentration of phenytoin was 1000 μg/mL. Error bars represent the standard deviation where n=2.

Table 5.2 Dissolution results of SDDs with poly(NIPAm-*co*-VP) excipients at 10 and 25 wt% phenytoin loadings.

	10 wt%				25 wt%			
Poly(NIPAM-*co*-VP) composition	c_{max} (μg/mL)[a]	c_{360} (μg/mL)[b]	AUC_{360} (μg.min/mL)[c]	EF[d]	c_{max} (μg/mL)[a]	c_{360} (μg/mL)[b]	AUC_{360} (μg.min/mL)[c]	EF[d]
100:0	122	122	4.2 E+04	2.5	241	116	4.2 E+04	2.5
75:25	313	294	1.0 E+05	6.1	309	275	9.9 E+04	5.9
60:40	526	526	1.8 E+05	10.6	469	247	1.4 E+05	8.1
50:50	489	256	1.4 E+05	8.5	504	251	1.5 E+05	8.6
40:60	600	245	8.9 E+04	5.3	612	162	8.6 E+04	5.1
25:75	627	273	1.1 E+05	6.7	516	255	8.8 E+04	5.2
0:100	384	236	1.1 E+05	6.2	383	235	9.9 E+04	5.9
Marketed Product	175	87	4.0 E+04	2.4	134	63	2.5 E+04	1.5

[a]Maximum concentration of phenytoin. [b]Concentration of phenytoin at 360 min. [c]Total area under the curve during the 6 hour dissolution test. [d]Enhancement factor defined as the ratio of AUC_{360} of a SDD to that of crystalline phenytoin. The c_{max}, c_{360}, and AUC_{360} of crystalline phenytoin was 38 μg/mL, 48 μg/mL, and 1.7×10^4 min μg/mL, respectively.

The concentration-time profiles showed several types of behaviors for the SDDs prepared with 10% drug loading. For poly(NIPAm-*co*-VP) 100:0, the homopolymer of NIPAm, the concentration of phenytoin gradually increased over the course of 6 h, but the c_{max} achieved was only 122 μg/mL, which is a 3-fold increase in solubility compared to that of crystalline drug (38 μg/mL) in the dissolution media (Figure 5.3a). The corresponding area under the curve for the concentration-time profile (AUC_{360}) is 4.2×10^4 μg min/mL, which is a 2.5 times increase compared to the crystalline drug. The AUC_{360} of the NIPAm homopolymer is comparable to that of the marketed PVP product as well.

With an LCST (28 °C) lower than physiological temperature (37 °C), PNIPAm is poorly soluble in the dissolution media at the condition tested for solubility. Consequently,

PNIPAm offered only a slight improvement in phenytoin dissolution. This result suggests that the interactions between the drug, NIPAm homopolymer chains, and the aqueous buffer at 37 °C are not strong enough to inhibit nucleation and growth of phenytoin crystals.

The homopolymer of VP [Poly(NIPAm-*co*-VP) 0:100] and poly(NIPAm-*co*-VP) 75:25 showed similar dissolution profiles with slightly higher c_{max} values of 384 and 313 µg/mL, respectively, which provided approximately 10-fold solubility enhancement to the crystalline drug (Figure 5.3a, Figure 5.3b). The AUC_{360} shows a six-fold improvement compared to the crystalline drug for both compositions. Although the dissolution performance of PVP was lower than most of the (NIPAm-*co*-VP) copolymer formulations, the PVP homopolymer revealed a considerable amount of phenytoin dissolution. This observation is likely due to two reasons: 1) interactions between phenytoin and the hydrogen bond accepting 2-pyrrolidone rings in PVP may inhibit the association of drug molecules to form the crystal nucleus and 2) increased viscosity of the aqueous dissolution medium provided by the PVP polymer slow down the diffusion and nucleation of drug molecules required for crystal growth.[15,31] Also, significant differences in the dissolution profiles for the synthesized PVP and marketed PVP product where found (AUC_{360} 1.1×10^5 µg.min/mL vs 4.0×10^4 µg.min/mL) and could be due to the differences in dispersity, molecular weight and aqueous solubility among the two samples. The number averaged molecular weight of the marketed product (Kollidon® 25) is reported to be 28000 – 34000 g/mol thus fairly small compared to the PVP polymer synthesized. The aqueous solubility of the synthesized PVP is 72 mg/mL while it is 66 mg/mL for the marketed product. Miller *et al.* reported that a high molecular weight PVP grade enhances the supersaturation of Itraconazole for a greater extent compared to a smaller analogue.[20] The observation is

attributed to the stronger interaction of the high molecular weight polymer with the API due to the increased number of functional groups (hydrogen bonding sites in this case) present in the polymer. Furthermore, the increased viscosity provided by the high molecular weight polymer could reduce the molecular mobility of the drug, hence higher crystal growth inhibition leading to the above observation.

Most of the poly(NIPAAm-*co*-VP) SDDs display improved drug dissolution profiles compared to the VP and NIPAAm homopolymer analogs as well as the marketed product. The best dissolution performance for Phenytoin was observed with the poly(NIPAAm-*co*-VP) 60:40 composition in aqueous media (Figure 5.3c). A high level of supersaturation was achieved at early time points (411 μg/mL at 4 mins) and the concentration increased over 6 hours to obtain a c_{max} of 526 μg/mL, which is a 14-fold solubility enhancement compared to crystalline Phenytoin. The AUC_{360} for this composition is 1.8×10^5 μg.min/mL and outperforms crystalline Phenytoin by 11 times and the marketed PVP product by 4.5 times. For poly(NIPAAm-*co*-VP) 50:50 model, the concentration of Phenytoin also achieved rather high levels of supersaturation at early time points, but it stayed constant for a significant amount of time (90 mins) before slowly decreasing to a c_{360} of 256 μg/mL (Figure 5.3d). The phenytoin solubility showed a 13-fold enhancement however the AUC_{360} started to decrease at this composition compared to the best performer. For copolymers poly(NIPAAm-*co*-VP) 40:60 and 25:75, the concentration of dissolved Phenytoin achieved maximum values at the beginning of the experiment but was not very effective at maintaining the concentration, the high level of dissolution quickly decreased after the initial period, and plateaued over the rest of the time of the experiment (Figure 5.3e, Figure 5.3f).

In summary, the dissolution rate decreased for SDDs with both higher (100:0, 75:25) and lower (50:50, 25:75, 0:100) NIPAAm compositions along the polymer backbone at 10% drug loading (Figure 5.3). Similar trends were observed for the SDDs prepared with 25% drug loading (Figure 5.9). Overall, poly(NIPAAm-*co*-VP) 60:40 and 50:50 models were found to significantly increase Phenytoin dissolution and supersaturation maintenance compared to the other polymer models. It should be noted that the LCST of these copolymers did not change upon SDD preparation (Figure 5.7) and that the observed LCST values for all of the copolymer compositions were at or above the physiological temperature (Figure 5.2), therefore all of the polymers were soluble in the dissolution media. In addition, the solubility of the copolymer formulations were found to increase with an increase in VP content (Figure 5.2b). The polymer solubility for all the copolymers except the homopolymer of NIPAAm were more than the administrated polymer concentration (9 mg/mL for 10 wt% drug loading and 3 mg/mL for 25 wt% drug loading), and thus are completely soluble in the aqueous dissolution media. To this end, it is hypothesized that both the 50:50 and the 60:40 copolymer compositions perform best due to a synergistic combination of including both VP monomers (hydrogen bond accepting and promotes solubility) and NIPAAm monomers (hydrogen bond donating and accepting and thermoresponsivness). It is reported that Phenytoin molecules adsorb onto the crystal surface and interacts with other Phenytoin molecules in the crystal lattice during crystal growth via π- π interactions between the phenyl rings as well as a 'ribbon-like' hydrogen bonding chains between amide and carbonyl groups. Phenytoin crystal growth at supersaturation conditions occur mainly along the direction of this hydrogen-bond chain.[32] Thus it is reasonable that a disturbance to these uniaxial Phenytoin-Phenytoin hydrogen

bonding chains by competitive hydrogen bonding with a structurally similar moiety would inhibit the nucleation and crystal growth at supersaturation conditions. Therefore, it can be hypothesized that the copolymers containing NIPAAm (with hydrogen bond donor –NH and acceptor –C=O) moieties in the copolymer inhibits Phenytoin crystal growth (due to the structural similarity) aiding supersaturation maintenance. Therefore, altering the NIPAAm content in the copolymer has a direct impact on the solubility and supersaturation maintenance of Phenytoin in aqueous dissolution media. Increasing the NIPAAm content can result in polymers with poor solubility in solution at physiological temperature due to the reduction of the LCST below physiological temperature as well as the reduction of VP content. On the other hand, the reduction of NIPAAm content reduces the number of hydrogen bond donor sites along the polymer backbone, which are essential for increasing the interaction of Phenytoin with the excipient (influences crystallization inhibition). The dissolution results indicate that the balance between these two factors govern the performance of poly(NIPAAm-*co*-VP) as an excipient for improving the drug solubility and bioavailability. Consequently, these chemical moieties are very promising for incorporation into excipient candidates for Phenytoin, which possesses substandard solubility due to its high crystallization ability.

5.3 Conclusions

In conclusion, copolymerization was used as a strategy to alter inter- and intramolecular interactions of a polymer with its surroundings (drug and solvent) and thereby tune the physical properties towards better excipient design. Herein, we sought to examine the role of excipient hydrogen bonding capacity, and solubility on the dissolution and supersaturation maintenance of the highly lipophilic drug phenytoin. The LCST and the solubility of poly(NIPAAm-*co*-VP) increased with increasing amount of VP in the copolymer. Two copolymer compositions poly(NIPAAm-*co*-VP) 50:50 and 60:40 were found to significantly increase drug dissolution. This was attributed to the transformation of crystalline Phenytoin into its high energy amorphous form upon spray drying. We propose that it is essential to incorporate similar chemical groups in the polymer backbone that are also present in the drug molecular structure, which can interfere with the drug crystallization mechanism and inhibit crystal nucleation. The specific drug-polymer interactions provided by NIPAAm and VP moieties, along with the enhanced solubility of VP in aqueous conditions collectively assist in inhibiting nucleation and crystal growth of Phenytoin, which is essential for the supersaturation maintenance. The balance between the VP and NIPAAm content is the key to improve the solubility and prevent the drug crystallization at the same time. This improvement in dissolution and supersaturation maintenance may aid in improving bioavailability and dose reduction of various drug species and can be used as a general design parameter in excipient design.

5.4 Experimental Section

Materials: All chemicals were reagent grade and used as received unless otherwise noted. All solvents were HPLC or analytical grade. *N*-isopropylacrylamide (NIPAAm, Aldrich,

≥99.9%), 5,5-Diphenylhydantoin (Phenytoin, Aldrich, ≥99.9%), dimethylformamide (DMF, Aldrich, 99.8%), methanol (fisher), diethyl ether (anhydrous, Fisher), and tetrahydrofuran (THF, Fisher). Fasted simulated intestinal fluid powder (FaSSIF, consisting of 3 mM sodium taurocholate, 0.2 mM lecithin, 34.8 mM sodium hydroxide, 68.62 mM sodium chloride, and 19.12 mM maleic acid)was purchased from Biorelevant (Surrey, UK). 1-vinyl-2-pyrrolidone (VP, Aldrich, ≥99.9%) was purified by distillation under vacuum and stored at –20 °C refrigerator under nitrogen. *2,2'*-Azobis(2-methylpropionitrile) (AIBN, Aldrich, 98%) was recrystallized from methanol and stored in a dark, –20 °C refrigerator. Phosphate buffered saline (PBS, pH = 6.5) was prepared from 82 mM sodium chloride (Fisher, ≥99.0%), 20 mM sodium phosphate dibasic heptahydrate (Fisher, 98%), and 47 mM potassium phosphate monobasic (J.T. Baker, ≥99.0%).

Copolymerization procedure

The monomer reactivity ratios evaluated by ^{1}H NMR experiments for NIPAAm (M_1) and VP (M_2) pair under similar reaction conditions are reported in literature to be r_1- = 0.47 and r_2= 0.5.[28] The method for the synthesis of Poly (NIPAAm-*co*-VP) 60:40 is as follows. NIPAAm (2.04 g, 0.018 mol), VP (1.28 mL, 0.012 mol), AIBN (10 mg, 3×10^{-5} mol) and DMF (15 mL) were placed in a round bottom flask. The reaction mixture was flushed with nitrogen gas for at least 30 min and stirred in a thermostated oil bath at 70 °C. The polymerizations were quenched after approximately five hours by cooling to 0 °C and opening the flask to air. The resultant poly (NIPAAm-*co*-VP) was isolated from the reaction mixture by precipitation with diethyl ether followed by filtration under vacuum. The copolymer obtained was re-dissolved in methanol, precipitated and filtered under

vacuum, and washed several times with diethyl ether to remove residual monomer and DMF. The solid was dried under vacuum at 40 °C overnight to yield 2.92g (87%) of the copolymer. A similar procedure was used to synthesize all the polymer compositions.

Copolymer Characterization

Copolymer composition. The chemical compositions of the polymers synthesized were analyzed by proton nuclear magnetic resonance (^{1}H NMR) spectroscopy carried out in a Bruker Avance III HD 500 spectrometer at 22 °C. The percentage of each monomer in the polymer was calculated by comparing the characteristic monomer proton integrations of C-(**CH$_3$**)$_2$ (1.1 ppm, 6H) for NIPAAm with C-**CH$_2$** (3.2 ppm, 2H) for VP.

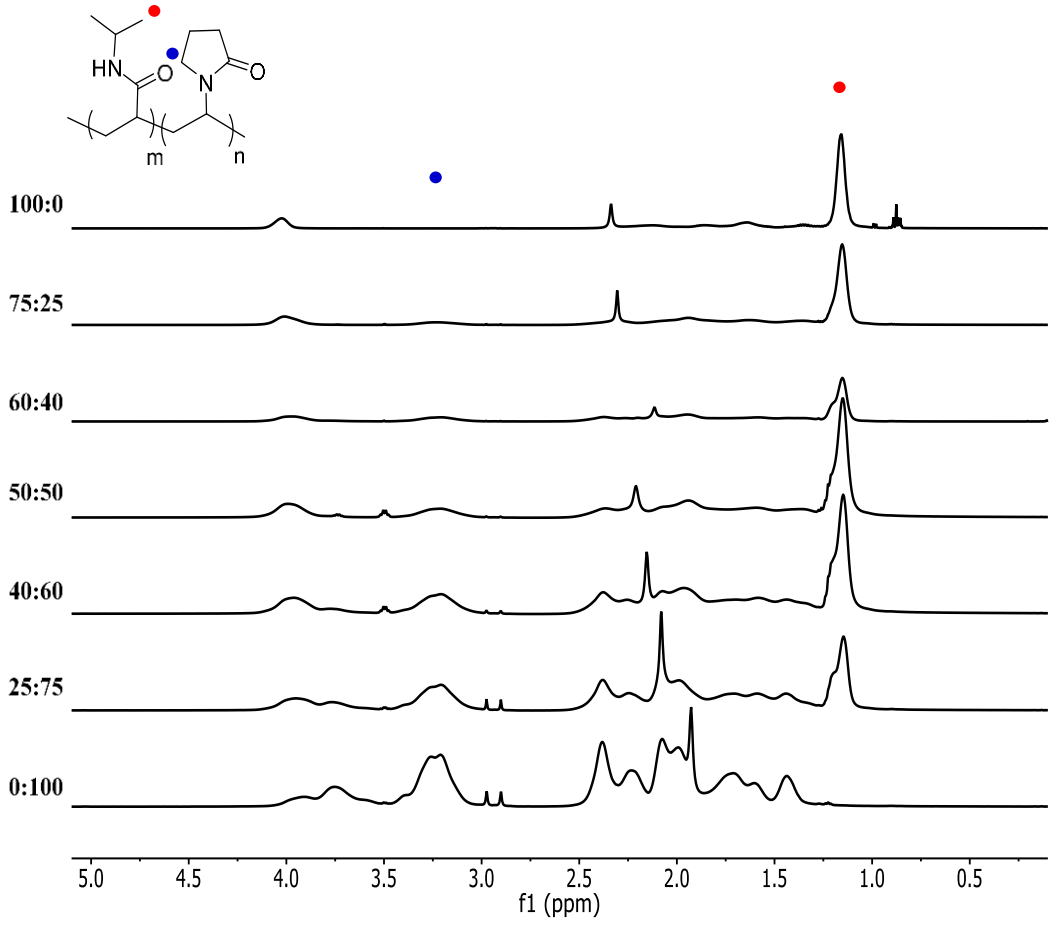

Figure 5.4 (top to bottom) 1H NMR spectra of poly(NIPAAm-co-VP) 100:0, 75:25, 60:40, 50:50, 40:60, 25:75, and 0:100 in CDCl3. The percentage of each monomer in the polymer

chain was calculated by comparing the characteristic monomer proton integrations of C-$(CH_3)_2$ (1.1 ppm, 6H,●) for NIPAAm with C-CH_2 (3.2 ppm, 2H,●) for VP.

The molecular weights and dispersity values were determined by size exclusion chromatography (SEC) conducted on an Agilent 1260 Infinity liquid chromatogram equipped with an Agilent 1260 Infinity Variable Wavelength Detector monitoring at 254 nm (80 Hz data collection frequency), a Wyatt Dawn Heleos II multiangle laser light scattering (MALS) detector at a laser wavelength of 663.6 nm (18 angles from 10° to 160°), and a Wyatt Optilab T-rEX refractive index detector operating at 658 nm. Tetrahydrofuran (THF) was run as the mobile phase at 1.0 mL/min at 25 °C. The dn/dc values were measured in THF assuming 100% mass recovery. Figure 5.5 contains a representative SEC chromatogram of Poly (NIPAAm-*co*-VP) 50:50 composition.

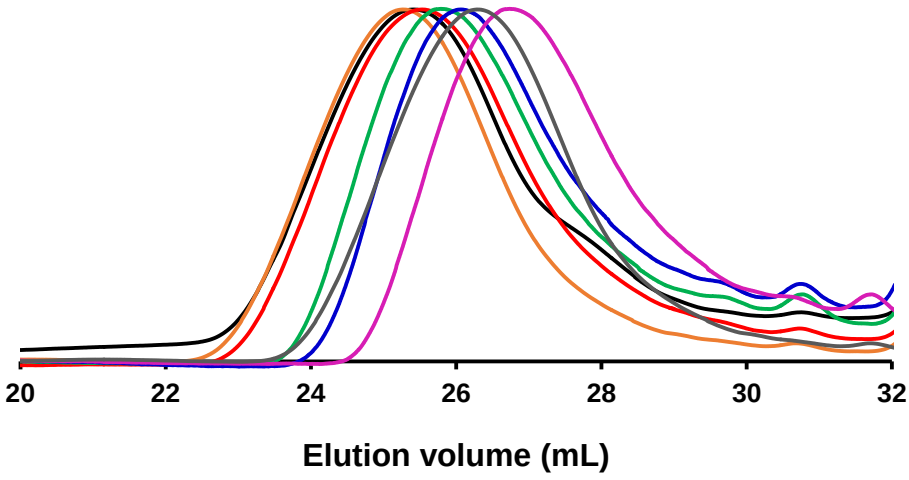

Figure 5.5 SEC chromatogram of poly(NIPAAm-*co*-VP) 100:0 (●), 75:25 (●), 60:40 (●), 50:50 (●), 40:60 (●), 25:75 (●) and 0:100 (●).

Thermal behavior. The glass transition temperature of the polymers was determined using Differential Scanning Calorimetry (DSC) using a TA Instruments Discovery DSC. All samples (~4−6 mg) were placed in T-zero aluminum pans. The

temperature was ramped between 0 °C and 180 °C at a rate of 10 °C/min and the T_g values were analyzed using TA TRIOS software version 2.2. The second heating scans are reported.

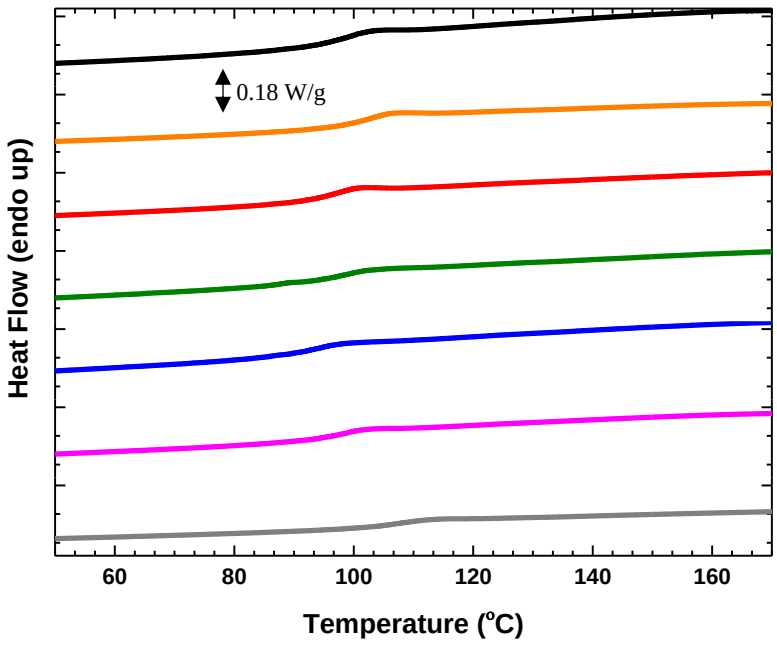

Figure 5.6 DSC traces of total heat flow for poly(NIPAAm-*co*-VP) 100:0 (●), 75:25 (●), 60:40 (●), 50:50 (●), 40:60 (●), 25:75 (●) and 0:100 (●) polymers. Samples were analyzed between 0 °C and 180 °C with a ramp of 10 °C/min. Second heating scans are shown.

Lower critical solution temperature (LCST) measurements. LCST measurements were performed in a UV spectrophotometer equipped with a heating system and temperature control unit. The temperature of the polymer solutions (1.0 wt.%) in phosphate buffered saline (as described in *Materials*) supplemented with 0.5 wt % simulated fasted duodenal solution (FaSSIF) at pH 6.5 was increased at a rate of 0.2 °C/min starting from 25 °C to 70 °C. The % transmittance of the solutions at a wavelength of 450 nm was recorded at 0.2 °C intervals. The LCST was taken as the midpoint between the onset and end set of the transmittance (%) decay.

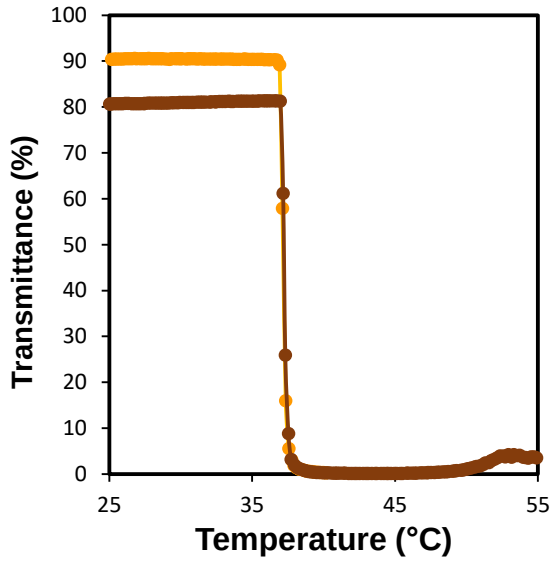

Figure 5.7 Copolymer composition-LCST behavior relationship for poly(NIPAm-co-VP) 75:25 free polymer (●), and spray dried polymer (●) dissolved in PBS + FaSSIF to make a final concentration of 1 wt% of polymer. The LCST of the free polymer is 37 °C and does not change upon spray drying.

Polymer Solubility measurements. For each polymer, approximately 20 mg was weighed in to a glass vial and the weight was recorded. Aliquots of phosphate buffered saline (as described in *Materials*) supplemented with 0.5 wt% fasted-state simulated intestinal fluid (FaSSIF) at pH 6.5 was added to each vial followed by vortexing for 1-2 minutes until the polymer is completely dissolved. Solubility was calculated using the amount of polymer and the volume of dissolution media used.

SDD preparation by spray drying

Samples of phenytoin in combination with different polymer excipients at 10 and 25 wt% were dissolved in a suitable amount of THF. The solvent was subsequently removed by spray drying to obtain the amorphous material. The spray drying was carried out using Bend Research Mini Spray Drier under the following conditions: inlet temperature of 68 °C, nitrogen flow rate of 28.6 SLPM, a 1.3 mL/min syringe flow rate,

and collected on a 4" Whatman filter. Unless otherwise noted, the total solute content spray dried was always 1 wt%.

Solid-state Characterization of SDDs

Powder X-Ray Diffraction (PXRD) Analysis. PXRD experiments were carried out on a Bruker-AXS (Siemens) D5005 diffractometer. Samples were packed into standard glass holders with zero background. Data for each sample was collected from 5° to 40° on the 2θ scale over approximately 30 minutes at a scan step of 0.5 seconds and a step size of 0.02°/s. The X-ray source (KCuα, λ = 1.54 Å) was operated at a voltage of 45 kV and a current of 40 mA.

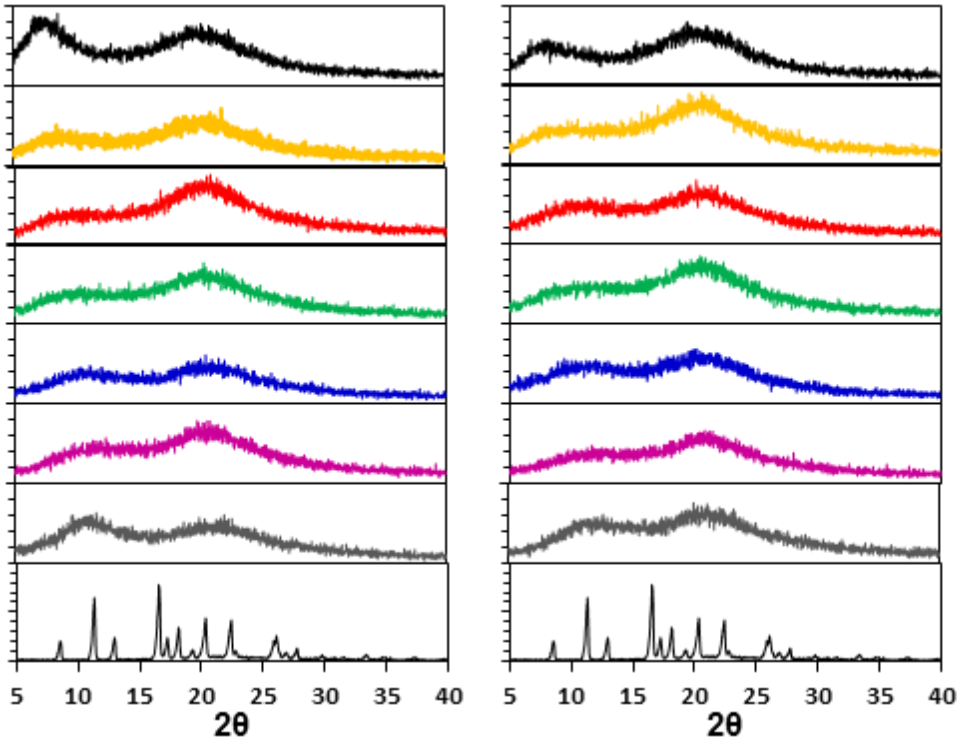

Figure 5.8 PXRD patterns for SDDs with Phenytoin loadings of 10 wt% (a) and 25 wt% (b) comparing poly(NIPAm-*co*-VP) 100:0 (●), 75:25 (●), 60:40 (●), 50:50 (●), 40:60 (●), 25:75 (●) and 0:100 (●). PXRD pattern for crystalline phenytoin is shown for comparison. All SDDs were found to be amorphous.

In Vitro Dissolution Testing. Dissolution testing was performed on the SDDs, a drug-polymer physical mixture, and crystalline drug to determine the amount of soluble drug and supersaturation maintenance. Dissolution testing medium consisted of phosphate buffered saline (as described in *Materials*) supplemented with 0.5 wt% FaSSIF adjusted to pH 6.5.

Each sample was accurately weighed into 2.0 mL microcentrifuge tubes to give an ultimate total drug concentration of 1,000 mg/mL if fully dissolved. To begin the testing, 1.8 mL of PBS + FaSSIF medium (pH 6.5, 37 °C) was added to the tubes which were then vortexed for one minute and placed into an aluminum heating block held at 37 °C. At 4, 10, 20, 40, 90, 180, and 360 minutes the tubes were centrifuged at 13,000 rpm, 37 °C for 1 minute, then 50 µL of supernatant was aliquoted into HPLC vials. The samples were then vortexed for 30 seconds and placed back into the 37 °C block until the next time point. The supernatant in the HPLC vials was then diluted with 250 µL of methanol and analyzed for drug via HPLC.

The HPLC consisted of a reversed-phase EC-C18 column (Poroshell 120, 4.6 x 50 mm, 2.7 µm, Agilent, USA). For phenytoin detection, a mobile phase of 40:60 (v/v) acetonitrile:water was pumped at a flow rate of 1.0 mL/min at 30 °C. A 10 µL aliquot of sample was injected, and the column effluent was detected at 241 nm with a UV detector (1260 Infinity Multiple Wavelength Detector, Agilent). Phenytoin was detected at 215 nm and the sample concentration was determined using a calibration curve of 0.1 – 500 µg/mL concentrations.

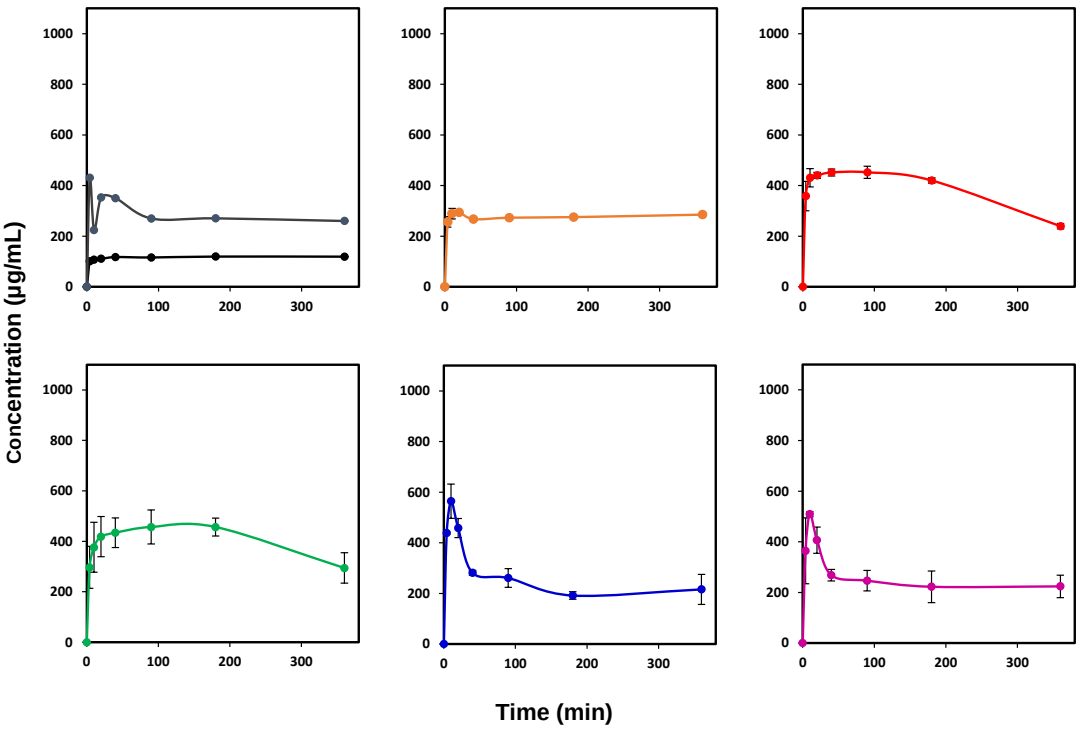

Figure 5.9 Dissolution data of SDDs with 25 wt% phenytoin loading at 37 °C. Polymer compositions used are, poly(NIPAm-co-VP) 100:0 (●), 75:25 (●), 60:40 (●), 50:50 (●), 40:60 (●), 25:75 (●) and 0:100 (●). The target concentration of phenytoin was 1000 µg/mL. Error bars represent the standard deviation where n=2.

5.5 References

(1) Lindenberg, M.; Kopp, S.; Dressman, J. *Eur. J. Pharm. Biopharm.* **2004**, *58*, 265-278.

(2) Leuner, C.; Dressman, J. *Eur. J. Pharm. Biopharm.* **2000**, *50*, 47-60.

(3) Vasconcelos, T.; Sarmento, B.; Costa, P. *Drug Discovery Today* **2007**, *12*, 1068-1075.

(4) Rodier, E.; Lochard, H.; Sauceau, M.; Letourneau, J.; Freiss, B.; Fages, J. *Eur. J. Pharm. Sci.* **2005**, *26*, 184-193.

(5) Loftsson, T.; Brewster, M. *J. Pharm. Sci.* **2012**, *101*, 3019-3032.

(6) Konno, H.; Taylor, L. *J. Pharm. Sci.* **2006**, *95*, 2692-2705.

(7) Won, D.; Kim, M.; Lee, S.; Park, J.; Hwang, S. *Int. J. Pharm.* **2005**, *301*, 199-208.

(8) Ohara, T.; Kitamura, S.; Kitagawa, T.; Terada, K. *Int. J. Pharm.* **2005**, *302*, 95-102.

(9) Friesen, D.; Shanker, R.; Crew, M.; Smithey, D.; Curatolo, W.; Nightingale, J. *Mol. Pharm.* **2008**, *5*, 1003-1019.

(10) Desai, J.; Alexander, K.; Riga, A. *Int. J. Pharm.* **2006**, *308*, 115-123.

(11) Urbanetz, N. *Eur. J. Pharm. Sci.* **2006**, *28*, 67-76.

(12) Huang, J.; Wigent, R.; Bentzley, C.; Schwartz, J. *Int. J. Pharm.* **2006**, *319*, 44-54.

(13) Shamma, R.; Basha, M. *Powder Technol.* **2013**, *237*, 406-414.

(14) Di Martino, P.; Joiris, E.; Gobetto, R.; Masic, A.; Palmieri, G.; Martelli, S. *J. Cryst. Growth* **2004**, *265*, 302-308.

(15) Tantishaiyakul, V.; Kaewnopparat, N.; Ingkatawornwong, S. *Int. J. Pharm.* **1999**, *181*, 143-151.

(16) Zhang, X.; Sun, N.; Wu, B.; Lu, Y.; Guan, T.; Wu, W. *Powder Technol.* **2008**, *182*, 480-485.

(17) Paradkar, A.; Ambike, A.; Jadhav, B.; Mahadik, K. *Int. J. Pharm.* **2004**, *271*, 281-286.

(18) Thybo, P.; Pedersen, B.; Hovgaard, L.; Holm, R.; Mullertz, A. *Pharm. Dev. Technol.* **2008**, *13*, 375-386.

(19) Nair, R.; Gonen, S.; Hoag, S. *Int. J. Pharm.* **2002**, *240*, 11-22.

(20) Miller, D.; DiNunzio, J.; Yang, W.; McGinity, J.; Williams, R. *Drug Dev. Ind. Pharm.* **2008**, *34*, 890-902.

(21) Vasanthavada, M.; Tong, W.; Joshi, Y.; Kislalioglu, M. *Pharm. Res.* **2005**, *22*, 440-448.

(22) Bühler, V.; SpringerLink (Online service); Springer-Verlag Berlin Heidelberg: Berlin, Heidelberg, 2005.

(23) Sekikawa, H.; Fujiwara, J.; Naganuma, T.; Nakano, M.; Arita, T. *Chem. Pharm. Bull.* **1978**, *26*, 3033-3039.

(24) Yakou, S.; Yamazaki, S.; Sonobe, T.; Nagai, T.; Sugihara, M. *Chem. Pharm. Bull.* **1986**, *34*, 3408-3414.

(25) Jachowicz, R. *Int. J. Pharm.* **1987**, *35*, 7-12.

(26) Franco, M.; Trapani, G.; Latrofa, A.; Tullio, C.; Provenzano, M.; Serra, M.; Muggironi, M.; Biggio, G.; Liso, G. *Int. J. Pharm.* **2001**, *225*, 63-73.

(27) Nam, I.; Bae, J.; Jee, K.; Lee, J.; Park, K.; Yuk, S. *Mol. Res.* **2002**, *10*, 115-121.

(28) Dincer, S.; Rzaev, Z.; Piskin, E. *J. Polym. Res.* **2006**, *13*, 121-131.

(29) Roy, D.; Brooks, W.; Sumerlin, B. *Chem. Soc. Rev.* **2013**, *42*, 7214-7243.

(30) Ormes, J.; Zhang, D.; Chen, A.; Hou, S.; Krueger, D.; Nelson, T.; Templeton, A. *Pharm. Dev. Technol.* **2013**, *18*, 121-129.

(31) Van den Mooter, G.; Wuyts, M.; Blaton, N.; Busson, R.; Grobet, P.; Augustijns, P.; Kinget, R. *Eur. J. Pharm. Sci.* **2001**, *12*, 261-269.

(32) Zipp, G.; Rodriguezhornedo, N. *J. Phys. D: Appl. Phys* **1993**, *26*, B48-B55.

6 CHPATER SIX

Systematic study to investigate, understand, and enhance aqueous solubility of model BCS class II drugs using High-Throughput Synthesis

In part from:

Tale, S. R.; Theresa, T. M.; Bates, F. S.; Ting, J. M.; Widanapathirana, L.; Guillaudeu, S. J.; Guo, L., Copolymers as excipients for effective solubilization of poorly water-soluble substances from solid mixtures, *US Patent Application* 20180066091A1.

This work was a joint venture of University of Minnesota with Dow chemical company. The author is responsible for novel concept of using NIPAAm as an excipient for poorly water-soluble drugs, synthesis and characterization of random copolymers of NIPAAm and DMA, spray drying, characterization of SDDs and dissolution studies. Jeff T., Lakmini W. and Li G. assisted in High-Throughput synthesis, characterization, screening of polymers to determine lead candidates for spray drying, characterization and establishing structure-property relationship.

6.1 Introduction

Drug discovery is the first and foremost step to transform a molecule into a new drug. Recent advances in computer modeling, biotechnology, high throughput screening, and genomics have revolutionized the ability of scientists to predict lead molecules.[1] Computer modeling helps to predict the lead molecules[2] and biotechnology has enabled scientists to genetically engineer living cells to produce biological molecules of medicinal value.[3] The latest developments in robotics (high throughput screening) allows a researcher to assay thousands of molecules against a target, and identify active molecules.[4] Despite the progress in drug discovery and development, the attrition rates of new molecules in preclinical trials is still extremely high.[5,6] Further, the exorbitant costs and enormous time required to develop and deliver one successful drug to patients are decelerating the process of drug discovery.[6]

Oral drug delivery is one of the most efficient, attractive, and widely used methods to administer drugs into the human body.[7] Approximately 40–60% of potential drug candidates in the pharmaceutical pipeline suffer from poor aqueous solubility.[8] Large amounts of drugs in the pharmaceutical development pipeline fall under the BCS Class II category, which represents drugs with poor aqueous solubility and high permeability through the gastrointestinal (GI) tract.[9] If a drug remains insoluble in the GI tract, then it cannot reach the desired target site in the body. Drugs that do not dissolve are eventually excreted and are rendered useless for the patients.[10] Therefore, the ability to enhance the aqueous solubility of poorly water soluble drugs is of paramount importance to the pharmaceutical industry.

To overcome this issue and improve bioavailability of poorly water soluble drugs, researchers are evaluating different approaches, which include the use of surfactants,[11] complexation with cyclodextrin,[12,13] salt formation,[14] and the use of amorphous solid dispersions.[15,16] Tachibana et al. in 1965, first reported the use of amorphous polymers in solid dispersions to improve solubility of drugs.[17] Amorphous solid dispersions typically consist of two components: an amorphous drug substance dispersed in a polymer matrix.[18] The most common techniques to manufacture amorphous solid dispersions include spray drying[19] and hot melt extrusion.[20] Hot melt extrusion processes are carried out at temperatures above the melting point of the drug substance in order to obtain solid dispersions. Therefore, this method is less applicable for thermally-sensitive active pharmaceutical ingredients (APIs) or APIs with higher melting points. In addition, the hot melt extrusion method consumes relatively large quantities of APIs for early formulation screening process, resulting in high development costs.[21] However, spray drying methods protect APIs from experiencing excessive heat during the formulation process and requires smaller quantities of APIs to obtain solid dispersions.[22] The first step of spray drying involves dissolving the drug and polymer in an organic solvent. In the second step, an atomizer is used to disperse the solution in controlled size droplets into a drying chamber, which is pumped with a stream of hot gas. The last step involves collecting the resulting solid powder on filter paper.

The polymer matrix plays a crucial role in determining the dissolution performance of solid dispersions. Hydroxypropyl methylcellulose acetate succinate (HPMCAS) is one of the leading excipients in the pharmaceutical industry.[23] HPMCAS is very effective at achieving initial burst release and maintaining supersaturation of drugs by inhibiting

recrystallization of dissolved drugs.[24] HPMCAS outperforms other homopolymers such as poly(ethylene glycol) (PEG), poly(vinylpyrrolidone) (PVP), and other cellulosic derivatives such as hydroxypropyl methylcellulose (HPMC) and hydroxylpropyl methylcellulose phthalate (HPMCP).[25-28] However, efforts to understand and establish structure property relationships between drugs and polymer is difficult due to its complex substitution patterns.[29]

Poly(N-isopropyl acrylamide) (PNIPAm) is the most frequently used thermoresponsive polymer in the areas of microgels, membranes, tissue engineering, biomedical engineering, biosensors, and controlled drug delivery research.[30,31] However, to date, there are no reports of use of PNIPAm as an excipient in solid dispersions. PNIPAm possesses a unique phase transition around 32 °C in aqueous solutions, also known as the lower solution critical temperature (LCST). Below LCST, the polymer is hydrated due to formation of hydrogen bonds between the pendant amide groups of PNIPAm and surrounding water molecules. However, above the LCST, the hydrogen bonding network is unstable due to dominant hydrophobic interactions between the isopropyl groups of PNIPAm. As a result, the polymer is no longer soluble in aqueous media and it precipitates out.[32] Since the LCST of PNIPAm is lower than body temperature (37 °C), it is extremely important to increase the LCST of PNIPAm to allow its use in biological applications.

The LCST of PNIPAm can be increased by copolymerizing with hydrophilic monomers.[31] N,N-dimethylacrylamide (DMA) is a hydrophilic monomer that is also known to be biocompatible.[33] This monomer has received substantial interest in recent years in the field of pharmaceuticals. The primary goal of this study is to generate a reliable

database that allows us to deduce structure-property relationships between polymer matrices and drugs chosen for this study.

Originally, probucol and phenytoin (BCS Class II) were chosen as model drugs to study and understand drug-polymer interaction and establish structure-property relationship between drug molecules and polymer groups. Probucol is an anti-hyperlipidemic drug, which has a very low aqueous solubility of 0.042 µg/mL. The log P of probucol is 8.9, which is an indication of liphophilicity of the compound. Probucol also has a low melting temperature (T_m) of 125 °C, an indication of strong intermolecular interactions within crystals.[34] On the other hand, phenytoin has a higher melting temperature (T_m) of 296 °C that indicate phenytoin's higher tendency to crystallize than probucol. Phenytoin has a moderately high log P of 1.9 and a low aqueous solubility of 27.1 µg/mL.[24] Therefore, these two drugs exhibit distinctive melting temperatures (T_m) and octanol/water partition coefficients (log P). Phenytoin is more hydrophilic than probucol. However, due to its high T_m, phenytoin crystallizes more easily than probucol.

To the best of our knowledge, modified HPMCAS with substituted cyclohexylthiol synthesized by Ligeng et al. is the most effective excipient for phenytoin reported in the literature.[24] The formulation with HPMCAS-CyS-0.57 (the number indicates the degree of cyclohexylthiol substituents), at 10wt% drug loading, exhibits initial supersaturation levels lower than reported with HPMCAS. However, the calculated AUC_{360min} for the cyclohexylthiol variant amounts to 2.1 × 105 min µg/mL, two times greater compared to HPMCAS. The targeted AUC_{360max} was 3.6×10^5 min µg/mL. Therefore, the best excipient was able to achieve only 58% of its engineering target at 10 wt% of drug loading.[24] This demonstrates that it is very difficult to maintain supersaturation concentration of phenytoin

in dissolution media due to its high tendency to crystallize out. Zippi et al. proved that phenytoin crystallizes out by the virtue of intermolecular hydrogen bonding between its amide functionalities (Figure 6.8).[35,36] We hypothesized that when phenytoin is formulated with a NIPAm based polymer, the intermolecular hydrogen bonding between their respective amide functions would inhibit crystallization of the drug. NIPAm serves a dual purpose as it has tunable lower solution critical temperature (LCST) and essential amide moieties to inhibit crystal nucleation. DMA is a hydrophilic monomer, and is incorporated to increase the LCST of the system.[37]

To prove our hypothesis, initially we synthesized six different random copolymers of P(NIPAm-co-DMA) and spray dried with probucol and phenytoin to obtain amorphous solid dispersions. Initial screening of six polymers helped us to narrow down the compositional window of the P(NIPAm-co-DMA) system. To better understand the effect of molecular weight and composition on PNIPAm in the polymer backbone, we synthesized libraries of random copolymers of P(NIPAm-co-DMA) system using high-throughput synthesis (HTS) capabilities at The Dow Chemical Company. The use of HTS is highly reproducible and allowed us to generate a large database to establish structure-property relationships between polymer matrices and drugs. [37-39]

6.2 Results and Discussion

6.2.1 Synthesis of P(NIPAAm-*co*-DMA) Statistical Polymers

Initially, six polymers were synthesized for this study, homopolymers PNIPAm and PDMA, and random copolymers of NIPAm and DMA, or CND-0.23, CND-0.46, CND-0.70 and CND-0.84 (Table 6.1). The random copolymers are named as CND followed by mole fraction of NIPAm in the copolymer system. For example, CND-0.23 stands for copolymer of NIPAm and DMA with a 0.23 NIPAm mole fraction in the polymer backbone. The LCST of NIPAm is slightly lower than the physiological temperature and thus limits its use in biological applications. To overcome this limitation, we copolymerized NIPAm with a hydrophilic monomer, DMA to increase the LCST, and synthesized four different random copolymers by changing the monomer feed ratio using controlled reversible addition-fragmentation chain-transfer polymerization (RAFT).

We synthesized four different random copolymers of NIPAm and DMA with a targeted degree of polymerization (DP = total monomer concentration/chain transfer agent concentration) of 200. Monomers were dissolved in 1,4-dioxane followed by addition of AIBN initiator and 4-cyano-4-(propylsulfanylthiocarbonyl)sulfanylpentanoic acid (CPP) chain transfer agent.[40] The reaction flask was then heated to 70 °C to initiate polymerization. All random copolymers were purified by precipitation (twice) into diethyl ether (Scheme 1). The homopolymers of NIPAm and DMA were synthesized using the same protocol. PDMA was purified by precipitation into diethyl ether and PNIPAm was purified by precipitation into diethyl ether followed by dialysis against water to remove trace amount of monomer (Figure 6.9). According to the literature, the reactivity ratios of NIPAm and DMA are r_{NIPAM} = 0.838 and r_{DMA} = 1.105, respectively, which suggests

random placement of monomers along the backbone of polymer.[41] All polymers were fully characterized by ^{1}H NMR spectroscopy, SEC, and DSC (Table 1). Differential scanning calorimetry (DSC) revealed an increase in the glass transition temperature with increasing NIPAm content.

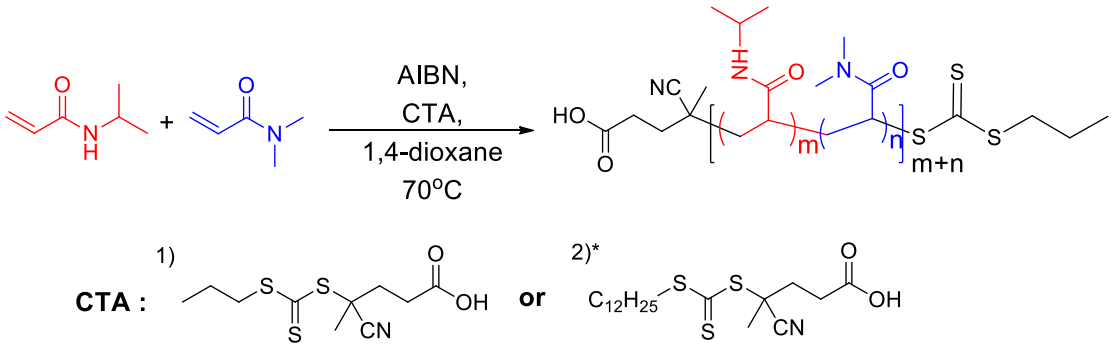

Scheme 1. Synthesis of random copolymers of P(NIPAm-*co*-DMA) using reversible addition chain transfer polymerization (RAFT). *Note:* The 2)* CTA was used to synthesize three different libraries of random copolymers of P(NIPAm-*co*-DMA).

Table 6.1 Characterization of random copolymers of P(NIPAm-*co*-DMA)

Polymer	NIPAAm/DMA[a] (DP)	dn/dc	$M_{n,\,SEC}$[b] (g/mol)	$M_{n,\,theo}$[c] (g/mol)	$Đ$[d]	$T_{g,\,DSC}$[e] (°C)
PDMA	0/204	NA	23,000	20,200	1.18	118
CND-0.23	46.2/153.8	0.0982	26,000	20,600	1.28	110
CND-0.46	87.6/103.4	0.1012	24,000	20,700	1.10	125
CND-0.70	132.8/55.8	0.0915	25,000	20,900	1.04	136
CND-0.84	156.4/30.0	0.0912	25000	23,900	1.20	146
PNIPAAm	200/0	NA	27,000	25,600	1.23	135

[a]NIPAm/DMA degree of polymerization in polymer backbone determined by ^{1}H NMR in $CDCl_3$. [b]Number average molecular weight determined by SEC using THF as an eluent. The flow rate was set at 1.0 mL/min and the chromatography was run at 35 °C. [c]Number average molecular weight determined using formula: [(monomer/CTA)* conversion* mole. wt. of monomer] + 277.43 (mole. wt. of CTA). [d]Dispersity of polymers determined by SEC using THF as an eluent. [e]The glass transition temperature as determined by DSC.

6.2.2 Influence of DMA on LCST of Copolymers

The lower critical solution temperature (LCST) was determined by measuring the transmittance of the polymer solution with 450 nm light using a UV-Vis spectrometer while controlling the temperature of the sample. It is well documented in the literature that NIPAm is hydrated (soluble) below the LCST due to the formation of a hydrogen bonding network between amide groups of NIPAm and water molecules.[31] However, above the LCST, this hydrogen bonding network collapses due to strong hydrophobic interaction between isopropyl groups of NIPAm chains and the polymer precipitates out. The LCST of NIPAm can be tuned by copolymerizing it with another hydrophilic monomer. Copolymerization with a hydrophilic monomer can improve the ability of NIPAm to retain water molecules and, as a result, raise the LCST of the system.

The LCST was determined in water and PBS + FaSSIF solution at 1 wt% of polymer concentration (Figure 6.1, Table 6.2). The measurements in water indicate an increase in the LCST with increasing DMA concentration in the copolymer. This trend is in agreement with the literature; addition of DMA increases the hydrophilicity of the copolymers, and increases the LCST. We observed lower LCST value in PBS + FaSSIF solution compared to that of water. Addition of salt ions in the solution attracts some water molecules, and therefore there is less number of water molecules to interact with the copolymer. Due to the overall decrease in available water molecules, hydrophobic interaction between polymer chains becomes stronger which results in a reduced LCST value. This result is in good agreement with the literature.[42]

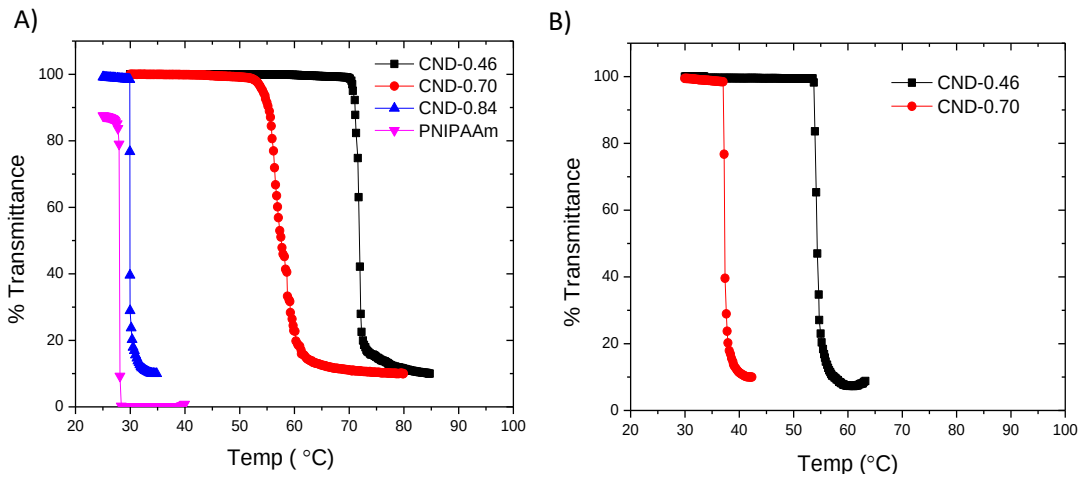

Figure 6.1 LCST profiles of copolymers of P(NIPAm-*co*-DMA), measured transmittance at 500 nm by using a heating rate of 0.2 °C/min. A) in water, B) in PBS + FaSSIF solution.

Table 6.1 Effect of increasing PNIPAm concentration on the LCST of copolymers. The numbers are extrapolated from Figure 6.1.

Sample	LCST in Water (° C)	LCST in PBS+SIF (° C)
PDMA	NA	NA
CND-0.23	> 90	> 90
CND-0.46	71	53.5
CND-0.70	55	37
CND-0.84	30	NA
PNIPAAm	28	NA

6.2.3 Formulation of Probucol and Phenytoin with Polymers

Recently, spray drying has evolved as a feasible industrial method to formulate dispersions of active pharmaceutical ingredients (APIs) with excipients. It is a preferred industrial method due to its ability to produce both a consistent particle size distribution and continuous dry solid powders from a liquid feedstock. Specifically, this method involves use of an atomizer to disperse a solvent containing mixture of APIs and excipients (one or more) into fine droplets by rapid evaporation of solvent due to a hot and dry gas stream. It is well documented in the literature that spray drying a mixture of drugs and excipients from a solution converts a thermodynamically stable (crystalline) form of drug molecules to a thermodynamically unstable (amorphous) form by kinetically trapping drug molecules in a polymer matrix.[15,23,43] The amorphous form of the drugs leads to a substantial increase in aqueous solubility.[44,45] The polymer matrix plays a vital role in stabilizing the high energy state of the drug molecules, preventing them from reverting back to its more stable state and dictates the dissolution performance of SDDs.

Each excipient (polymer) was spray dried with probucol and phenytoin at 10 and 25 wt% of drug loading. For example, 270 mg of CND-0.23 and 30 mg of drug was dissolved in THF and spray dried to obtain 10 wt% of SDD (total 24 SDDs). Initially we studied the effect of increasing NIPAm content in the SDDs using powder X-ray diffraction (PXRD).

6.2.4 SDDs with Phenytoin and Probucol

PXRD is a common analytical tool to determine the presence of crystalline material in SDDs. A representative PXRD pattern of an amorphous material should appear as a broadened, featureless diffractogram with no Bragg peaks. However, sharp peaks in a

PXRD pattern are indicative of the presence of crystalline material in the prepared SDDs.[33] We recorded PXRD patterns at 25 wt% of drug (phenytoin/probucol) loadings and compared these patterns with the unprocessed drugs (Figure 6.2). The pure drugs revealed sharp peaks in PXRD pattern, which indicates a definite arrangement of atoms. All SDDs of probucol and phenytoin at 25 wt% of drug loading featured diffuse diffractogram patterns indicative of amorphous SDDs within the PXRD detection limit (Figure 6.2). This result also indicates that the spray drying method effectively break up the ordered molecular arrangements of the drug.

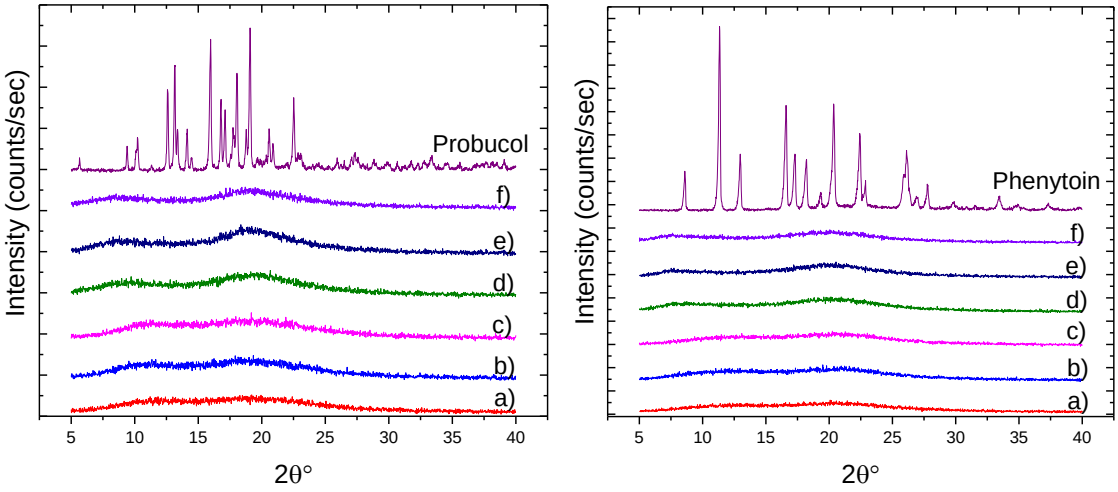

Figure 6.2 PXRD patterns for SDDs with probucol (left) and phenytoin (right) at 25 wt% of drug loading, comparing a) PDMA, b) CND-0.23, c) CND-0.46, d) CND-0.70, e) CND-0.84, f) PNIPAm with crystalline probucol (left) and phenytoin (right).

6.2.5 Effect of Copolymer Compositions on Dissolution Profiles

Microcentrifuge dissolution testing (MCT) is a powerful method to determine the *in vitro* concentration of released drugs and can be used to analyze SDDs for their ability to achieve and maintain supersaturation levels. This method is routinely employed in the pharmaceutical industry to anticipate the *in vivo* bioavailability of drugs. The intended final drug concentration for all MCTs was 1000 µg/mL assuming all materials were fully dissolved in the phosphate-buffered saline (PBS, pH 6.5), supplied with 0.5 wt% FaSSIF

(to mimic conditions in the GI tract). All SDDs were incubated at 37 °C and analyzed by high performance liquid chromatography (HPLC) for concentration of the drug from 4 min to 6 h. Details of the MCT procedure are reported in the experimental section. The experimentally measured solubility of phenytoin and probucol in PBS/FaSSIF solution was 37 and 5 μg/mL over 360 min, respectively. We evaluated the *in vitro* performance of all polymers at 10 and 25 wt% of drug (phenytoin and probucol) loadings. According to PXRD data (Figure 6.2), all SDDs are expected to be amorphous in nature to the limit of its detection.

As shown in Figure 6.3, the dissolution profiles of SDDs formulated with PDMA, CND-0.23, CND-0.46, and CND-0.70 at 10 wt% of probucol loading revealed similar performance as that of HPMCAS. On the other hand, SDDs formulated with CND-0.84 and PNIPAm at 10 wt % of probucol loading exhibited a decrease in $AUC_{360(min)}$ compared to aforementioned copolymer systems. The poor dissolution rate of CND-0.84 and PNIPAm systems might be attributed to their poor solubility in the aqueous dissolution media at 37 °C. A system that can enhance dissolution rate at higher drug loading is always desirable to attain therapeutic effect. At 25 wt% of Probucol loading, all SDDs demonstrated poor dissolution profiles compared to those at 10 wt%. The SDDs formulated with 25 wt% of probucol loading were ineffective at achieving initial high levels of supersaturation. Ting et al. proved that the higher drug loading leads to crystalline and crystalline rich domains in the SDDs, which can create nucleation sites to provoke crystallizations and reduce the total achievable drug concentration.[34] All SDDs showed lower $AUC_{360(min)}$ at 25 wt% of probucol loading compared to 10 wt% (Table 6.2).

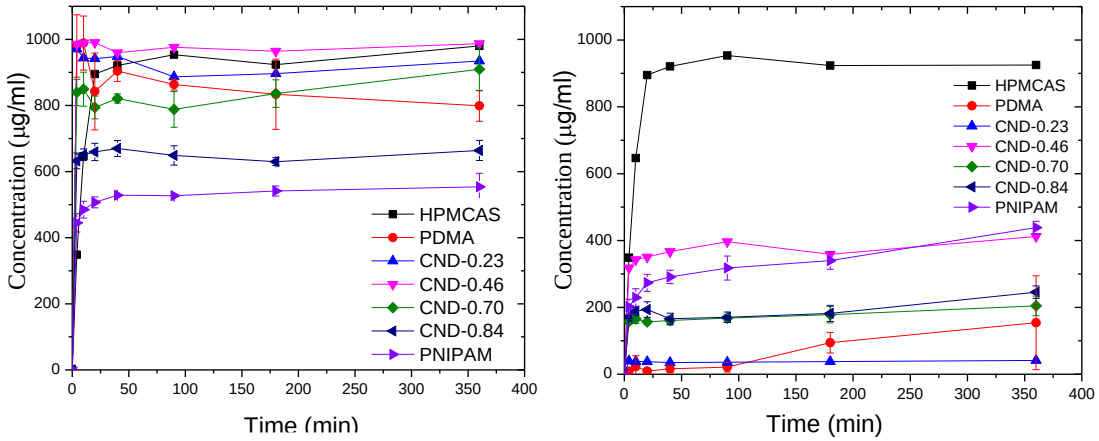

Figure 6.3 Dissolution profiles of SDDs at 10 (left) & 25 (right) wt% probucol loading. The polymeric matrices are HPMCAS, homopolymer of PDMA, four copolymers of P(NIPAm-*co*-DMA), and homopolymer of PNIPAm. The engineering targeted concentration of probucol was 1000 μg/mL.

Table 6.2 Calculated area under the curve (AUC) from dissolution profiles of SDDs with 10 and 25 wt% of probucol loadings.

Sample	10 wt%				25 wt%			
	C_{max} [a] (μg/mL)	C_{360min} [b] (μg/mL)	AUC_{360min} [c] (min μg/mL)	$AUC_{360min}/AUC_{360(max)}$	C_{max} [a] (μg/mL)	C_{360min} [b] (μg/mL)	AUC_{360min} [c] (min μg/mL)	$AUC_{360min}/AUC_{360(max)}$
HPMCAS	440	970	3.4×10^5	0.94	349	924	3.3×10^5	0.94
PDMA	980	799	3.0×10^5	0.83	9	154	2.9×10^4	0.08
CND-0.23	970	934	3.3×10^5	0.92	40	41	1.3×10^4	0.04
CND-0.46	985	987	3.5×10^5	0.97	318	412	1.3×10^5	0.36
CND-0.70	839	909	3.0×10^5	0.83	158	205	6.4×10^4	0.18
CND-0.84	632	664	2.3×10^5	0.64	172	246	6.7×10^4	0.19
PNIPAm	445	554	1.9×10^5	0.53	202	439	1.2×10^5	0.33

[a]Concentration of phenytoin at 4 min. [b]Concentration of phenytoin at 360 min. [c]The area under the dissolution profile over the period of a 6 h dissolution test. The targeted $AUC_{360(max)}$ is 3.6×10^5. Therefore, the targeted $AUC_{360min}/AUC_{360(max)}$ is 1.

Phenytoin has a strong tendency to crystallize out from aqueous solution than probucol. As shown in Figure 6.4, at 10 wt% of phenytoin, HPMCAS was effective at achieving initial high levels of supersaturation; however, the concentration of the drug drops significantly over 20

min due to rapid crystallization of phenytoin. PDMA and CND-0.23 (23 mol % of NIPAm in the polymer backbone) revealed poor dissolution rate for phenytoin. The dissolution profile of CND-0.46 was similar to HPMCAS. Conversely, CND-0.70 not only achieved initial levels of supersaturation but also maintained desirable high concentration (1000 µg/mL) for 6 h. However, further increase in the mole percentage of NIPAm in the polymer backbone (CND-0.80, PNIPAm) lead to poor dissolution profiles. We attribute the poor performance of CND-0.80 and PNIPAm to its decreased LSCT in the dissolution media. At higher NIPAm content, hydrophobic interactions between isopropyl groups of the polymer is dominant, which leads to insoluble polymer above the LCST. In this case, the experimentally measured LCST of CND-0.80 and PNIPAm are 30 and 28 °C (in water), which are below the temperature at which MCT is conducted (37 °C). These polymers precipitate out in the dissolution media at 37 °C, and there is no polymer in the solution to interact with phenytoin. At 25 wt% phenytoin loading, all polymers exhibited the same trend analogous to 10 wt% (Figure 6.4). The best performer, CND-0.70 outperformed HPMCAS by demonstrating 3-fold increase in AUC_{360min} at 10 wt% and 2-fold increase at 25 wt% of phenytoin loading (Table 6.3).

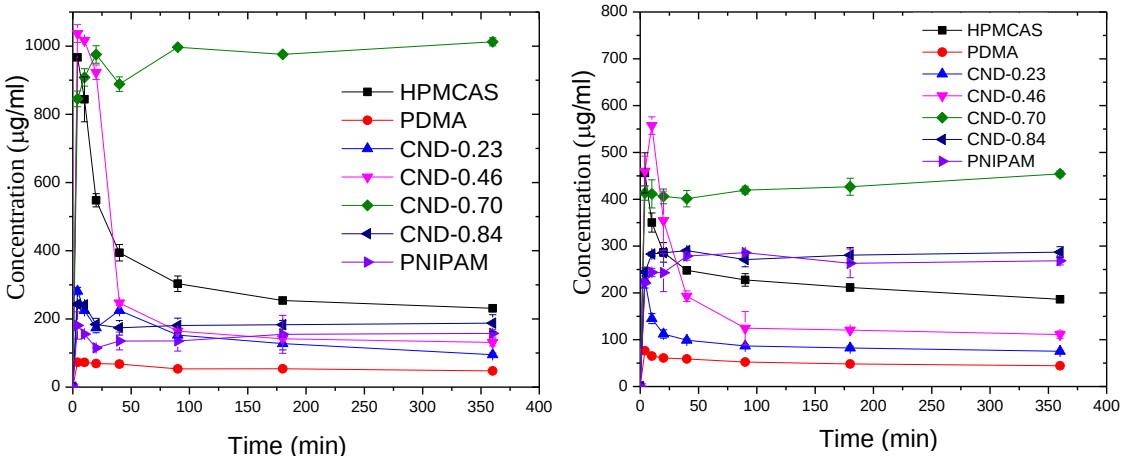

Figure 6.4 Dissolution profiles of SDDs at 10 (left) & 25 (right) wt% phenytoin loading. The polymeric matrices are HPMCAS, homopolymer of PDMA, four copolymers of P(NIPAm-*co*-DMA), and homopolymer of PNIPAm. The engineering targeted concentration of phenytoin was 1000 μg/mL.

Table 6.3 Calculated area under the curve (AUC) from dissolution profiles of SDDs with 10 and 25 wt% of phenytoin loadings.

Sample	10 wt %				25 wt %			
	C_{max} [a] (μg/mL)	C_{360min} [b] (μg/mL)	AUC_{360min} [c] (min μg/mL)	$AUC_{360min}/AUC_{360(max)}$	C_{max} [a] (μg/mL)	C_{360min} [b] (μg/mL)	AUC_{360min} [c] (min μg/mL)	$AUC_{360min}/AUC_{360(max)}$
HPMCAS	960	230	1.1×10^5	0.31	450	180	7.9×10^4	0.22
PDMA	73	47	1.9×10^4	0.05	76	44	1.8×10^4	0.05
CND-0.23	290	91	5.6×10^4	0.14	230	75	3.1×10^4	0.09
CND-0.46	1030	131	7.8×10^4	0.22	460	110	6.4×10^4	0.15
CND-0.70	845	1010	3.5×10^5	0.97	410	450	1.5×10^5	0.42
CND-0.84	243	187	6.6×10^4	0.18	244	287	1.0×10^5	0.33
PNIPAm	180	157	5.3×10^4	0.15	220	268	9.6×10^4	0.26

[a]The concentration of phenytoin at 4 min. [b]Concentration of phenytoin at 360 min. [c]The area under the dissolution profile over the period of a 6 h dissolution test. The targeted $AUC_{360(max)}$ is 3.6×10^5. Therefore, the targeted $AUC_{360min}/AUC_{360(max)}$ is 1.

We attribute the outstanding performance of CND-0.70 to its LCST value in PBS + FaSSIF solution (37 °C). We hypothesize that this particular copolymer composition sits

at the interface of phase separation, and prevents crystallization of dissolved phenytoin. To test our hypothesis, dissolution tests were conducted above (50 °C) and below (24 °C) the LCST of CND-0.70, and compared with dissolution profiles of CND-0.70 and HPMCAS at physiological temperature (Figure 6.10). The data revealed that above the LCST, the dissolution profile dropped dramatically due to precipitation of the polymer, decreasing the overall AUC_{360min}. Below the LCST, we noticed a parallel trend to the dissolution profile at 37 °C. The polymer is fully soluble below the LCST and retains supersaturation high levels of the phenytoin. This data indicates that the LCST might not be the critical component of these systems and have no influence on the dissolution profiles as long as the polymer is soluble in the dissolution media. Although, we think that the LCST of the polymer closer to 37 °C might aid the drug to adsorb on the surface of the polymer. This data also implies that the composition of the polymer plays a vital role in dictating the drug solubility and supersaturation maintenance.

To investigate and understand the effect of polymer composition on drug release, we synthesized three libraries (A1-A8, B1-B8, and C1-C8), each containing 8 random copolymers of NIPAm and DMA, using the high throughput capabilities at Dow. In library A, we retained 70% mole percentage of NIPAm in the polymer backbone, and varied the molecular weight from 10kDa to 60kDa to understand the effect of molecular weight on dissolution profile. In libraries B and C, the target molecular weights of polymers were 20 kDa and 60 kDa, respectively. The molar composition of NIPAm was varied from 10% to 80% to reveal the optimal composition, which would maintain the desired drug release profile.

6.2.6 High throughput synthesis and characterization of library A, B, and C

High throughput experimentation is as a powerful method to identify lead compounds, proteins, and antibodies.[4,38,39] In recent years, high throughput synthesis has gained attention among polymer researchers. This method facilitates the synthesis of a large library of polymers via parallel reactions. Polymerizations were carried out in assembly consisting of 8 small reactors equipped with overhead stirrers. Stock solutions of NIPAm, DMA, AIBN, and 4-Cyano-4-[(dodecylsulfanylthiocarbonyl)sulfanyl]pentanoic acid (CTA) were prepared in 1,4 dioxane. All solutions were degassed for an hour, and the required amounts were dispensed into each reactor. The temperature of the assembly was then raised to 70 °C to initiate polymerization. All polymers were purified by precipitation into diethyl ether and dried in a vacuum oven for 12 h. Three libraries (A, B, and C) consisting of a total of 24 polymers were synthesized with varying compositions and molecular weights. Details of the syntheses are reported in Table 6.6 in Experimental Section.

All polymers were fully characterized by ^{1}H NMR, SEC, and DSC. Details of characterization are reported in Table 6.4. We also checked the solubility of all polymers in 1 wt% of PBS + FaSSIF solution at 6.5 pH. All polymers were fully soluble in PBS + FaSSIF at room temperature (Table 6.7). For example, 10 mg of A1-CND-0.66 was dissolved in 1 mL of water and solution was stirred for an hour. Solubility was judged visually as completely, mostly soluble, hazy, and insoluble.

Table 6.4 Characterization details of libraries of P(NIPAm-co-DMA) copolymers with different compositions and molecular weights.

Samples	Polymers	NIPAM in the feed (mol %)[a]	NIPAM in the polymer (mol %) [b]	$M_{n,\ theo}$ (g/mol)[c]	$M_{n,\ SEC}$ (g/mol)[d]	$M_{w,\ SEC}$ (g/mol)[d]	*PDI*[d]	*Tg*[e] (°C)
A1	CND-0.66	70%	66%	10,000	10,950	11,300	1.04	127.2
A2	CND-0.66	70%	66%	20,000	20,000	21,000	1.06	127.6
A3	CND-0.67	70%	67%	30,000	30,000	33,000	1.09	126.8
A4	CND-0.65	70%	65%	40,000	42,000	48,000	1.14	128.2
A5	CND-0.66	70%	66%	50,000	69,000	81,000	1.17	126.5
A6	CND-0.68	70%	68%	60,000	54,500	65,800	1.21	129.8
A7	CND-0.63	65%	63%	20,000	18,900	20,000	1.06	129.2
A8	CND-0.73	75%	73%	20,000	17,700	20,500	1.07	133.7
B1	CND-0.08	10%	8%	20,000	20,600	21,800	1.05	102.6
B2	CND-0.19	20%	19%	20,000	17,900	18,900	1.05	118.2
B3	CND-0.30	30%	30%	20,000	n/a	n/a	n/a	125.5
B4	CND-0.42	40%	42%	20,000	19,600	23,600	1.20	132.2
B5	CND-0.54	50%	54%	20,000	14,300	16,200	1.13	130.5
B6	CND-0.63	60%	63%	20,000	17,800	18,800	1.06	138.5
B7	CND-0.76	80%	76%	20,000	11,300	12,300	1.08	135.6
B8	CND-0.90	90%	90%	20,000	n/a	n/a	n/a	138.3
C1	CND-0.09	10%	9%	50,000	47,700	54,400	1.14	105.3
C2	CND-0.18	20%	18%	50,000	44,600	50,400	1.13	115.9
C3	CND-0.31	30%	31%	50,000	51,600	57,000	1.11	122.7
C4	CND-0.43	40%	43%	50,000	49,900	54,300	1.09	125.1
C4	CND-0.50	50%	50%	50,000	36,500	40,400	1.11	136.5
C6	CND-0.63	60%	63%	50,000	31,900	35,400	1.11	134.3
C7	CND-0.78	80%	78%	50,000	40,400	45,700	1.13	135.8

C8	CND-0.89	90%	89%	50,000	44,100	50,200	1.14	138.6
D1	CND-0.66*	70%	66%	150000	-	-	-	-

[a]Targeted molar composition of NIPAm in the copolymer system. [b]Molar composition of NIPAm, determined from ^{1}H NMR spectroscopy. [c]Targeted number average molecular weight of the copolymer system. [d]Number average molecular weight, molecular weight distribution, and dispersity of the polymer system, determined from SEC using tetrahydrofuran (THF) as an eluent at 25 °C. [e]The glass transition temperature of the copolymer system, determined from DSC.

6.2.7 *In Vitro* High Throughput Supersaturation Evaluation

Investigation of supersaturation is employed to identify lead candidates for spray drying that maintain supersaturation levels of poorly water soluble drugs. Vandecruys et al. developed an efficient supersaturation assay, which consumes small amounts of compounds, and is based on solvent shift that identifies excipients affecting supersaturation.[46] Similarly, Yamashita et al. introduced a high throughput 96 well plate assay to estimate the ability of excipients to maintain itraconozole supersaturation.[47] This type of screening method helps eliminate sub-optimal excipients, and saves a lot of time and effort in formulating solid dispersions with potentially weak excipients. The details of the method are reported in the experimental section.

To evaluate the capacity of polymers to stabilize supersaturation, we selected two drugs: phenytoin and griseolfulvin. Griseolfulvin is structurally different than phenytoin, however, it possess low log P (2.71) and high melting point (220 °C) analogous to phenytoin. The purpose of introducing griseolfulvin (negative control) is to establish structure-property relationships between drugs and polymers. As shown in Figure 6.5A, the molecular weights of polymers with similar composition (A1-A6) have negligible influence on supersaturation maintenance of phenytoin. Figure 6.5B (A1, A7, A8, B1-B8) and Figure 6.5C (A6, C1-C8) indicate the effect of increasing molar composition of

NIPAm in the polymer backbone on supersaturation of phenytoin at fixed molecular weight. As shown in Figure 6.5B, A1 (CND-0.66, 11 kDa), A7 (CND-0.63, 19 kDa), A8 (CND-0.73, 18 kDa), and B6 (CND-0.63, 18 kDa) outperformed HPMCAS, M grade by demonstrating superior ability to stabilize supersaturation. All other polymers exhibited poor performance on supersaturation process. This data clearly indicates that there is a drastic increase in supersaturation levels of phenytoin when copolymer contains 63-73 mole percent of NIPAm. We believe that below 63 mole percent there is not enough NIPAm present in polymer backbone to inhibit crystallization of phenytoin, as a result, drug crystallizes out from dissolution medium. Above 73 mole percent of NIPAm, the LCST of the copolymer drops below the physiological temperature (37 °C), therefore, polymer precipitates out which in turn leads to drug crystallization. As per data in Figure 6.5C, A6 (CND-0.68, 55 kDa) and C6 (CND-0.63, 32 kDa) outperform the positive control, and also proves that molecular weight has minor influence on supersaturation of phenytoin. In Figure 6.5D, we show the effect of molecular weights of polymers (A1-A6, similar composition) on supersaturation of griseofulvin. All polymers failed to exhibit superior supersaturation performance than M grade HPMCAS. Figure 6.5E and F, show the effect on increasing molar composition of NIPAm on supersaturation of griseofulvin at fixed molecular weights. This data indicates that none of the CND systems with griseofulvin were able to outperform HPMCAS. We attribute superior performance of the CND systems (A1, A6, A7, A8, B6, and C6) with Phenytoin supersaturation to the process of phenytoin crystallization. According to Zipp et al., the phenytoin crystal growth occurs by formation of hydrogen bonds between amide groups of phenytoin (Figure 6.8). We believe that the CND systems with precise mole fraction of NIPAm inhibit this crystal growth process via

formation of hydrogen bond chains between amide groups of NIPAm and phenytoin (Figure 6.8). On the other hand, griseofulvin lacks an amide group and has a different crystal growth mechanism. Therefore, there is no driving force for CND systems to interact with griseofulvin due to structural dissimilarities between the polymer and the drug.

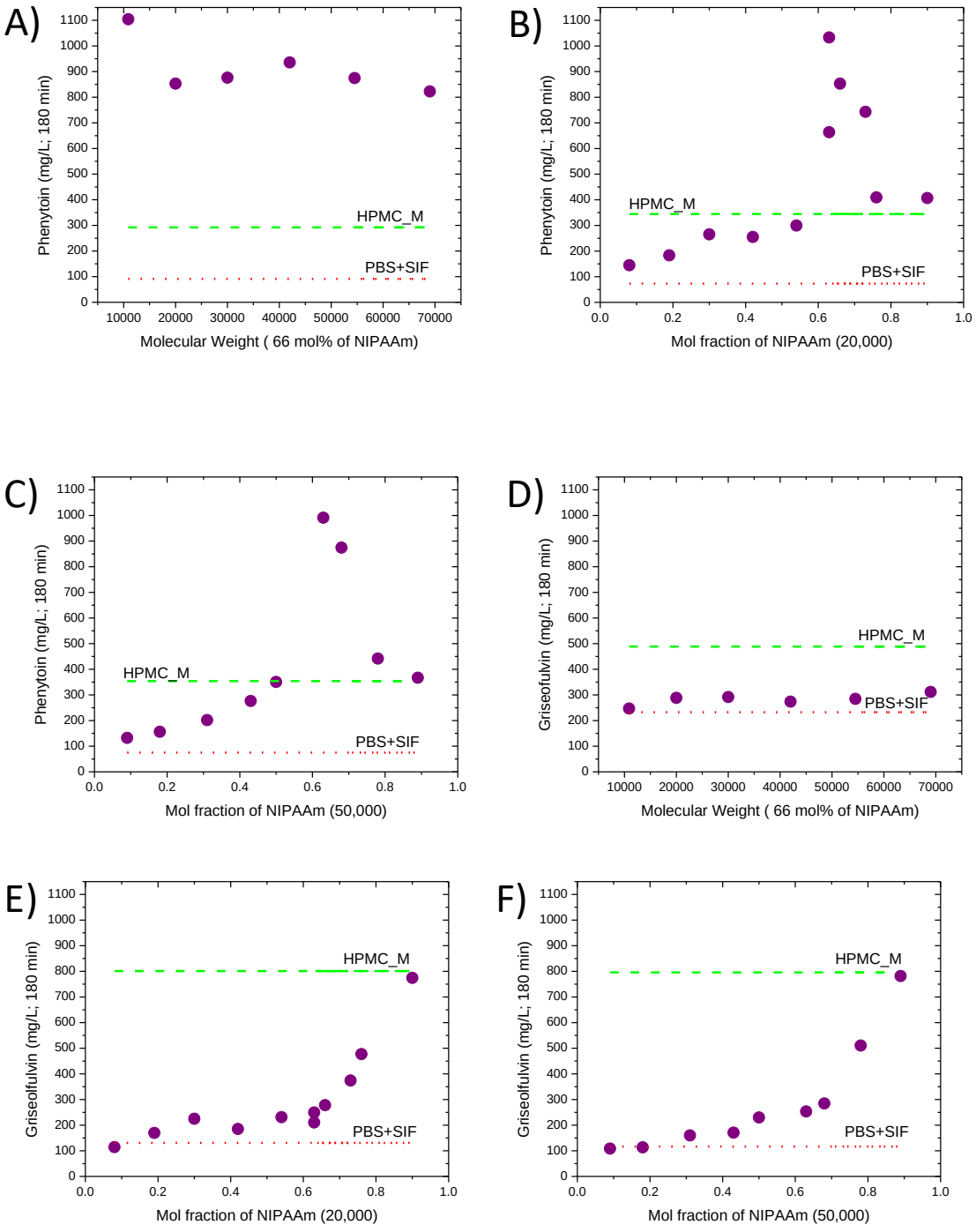

Figure 6.5 Supersaturation testing of libraries of P(NIPAm-*co*-DMA) copolymers with phenytoin and griseofulvin (180 min.). A) and D) shows effect of increasing molecular weight of P(NIPAm-*co*-DMA) copolymers on supersaturation performance, while holding the molar composition of the NIPAm constant in the polymer backbone. B) and E) shows effect of increasing molar composition of the NIPAm in the polymer backbone, while holding the molecular weight of the polymer constant at 20 kDa. C) and F) shows effect of increasing molar composition of the NIPAm in the polymer backbone, while holding the molecular weight of the polymer constant at 60 kDa. Note: HPMC_M stands for M grade HPMCAS. PBS + FaSSIF solution is used as negative control.

6.2.8 Evaluation of Dissolution Profiles of Spray Dried Dispersions

Based on our supersaturation results, we selected a few choice compositions of the CND systems to spray dry with phenytoin and griseofulvin. We decided to spray dry A1, A2, A5, A7, A8, B6, B7, C6, and D1 with 25 wt% of phenytoin loading. For example, with A1 (CND-0.66, 11 kDa), the concentration of phenytoin achieved levels of supersaturation up to (C_{max}) 410 μg/mL at early time points, and gradually increased during the 6 h dissolution test with a plateau value at 510 μg/mL. However, in the case of HPMCAS, high initial levels of supersaturation were achieved at (C_{max}) 726 μg/mL at initial time points, but the concentration of dissolved drug dropped significantly to 168 μg/mL during the dissolution test. The C_{max} obtained by A1 was smaller than that of HPMCAS, but the AUC_{360min} was 1.7×10^5 min μg/mL, which was two times larger than that with HPMCAS. Similar performance was observed with other selected CND compositions (Figure 6.6). The polymer D1 (CND-0.66, 150 kDa), which was synthesized by free radical polymerization techniques also exhibited similar trends. D1 was able to achieve up to (C_{max}) 300 μg/mL and maintained concentration during 6 h test. The calculated AUC_{360min} was 1.2×10^5, which is still 1.5 times larger than HPMCAS. This result suggests that the composition of the polymer is a key factor in dissolving phenytoin and maintaining supersaturation levels rather than the architecture of the polymer (Figure 6.6).

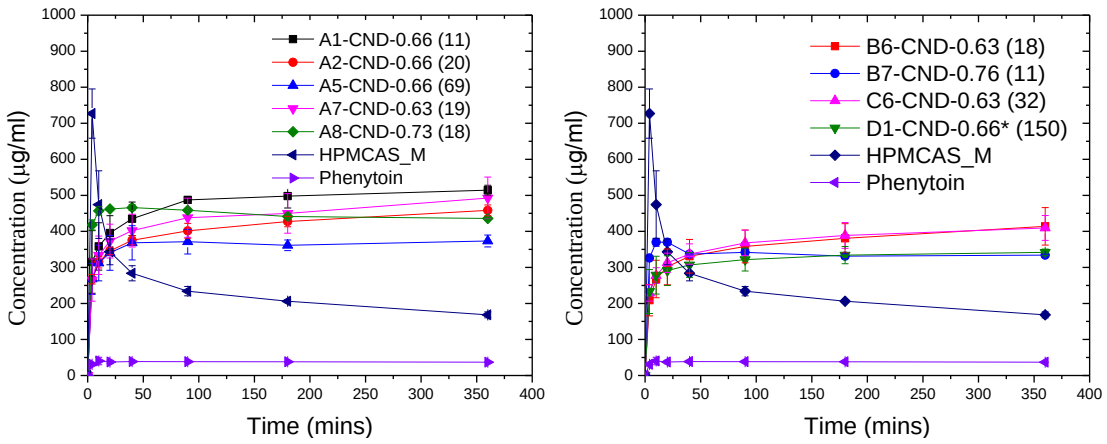

Figure 6.6 Dissolution data of selected SDDs with 25 wt% of phenytoin loading, compared with crystalline phenytoin (negative control) and HPMCAS_M (positive control). All SDDs outperformed HPMCAS_M by demonstrating better release profiles and supersaturation maintenance. The dissolution profile of phenytoin is added as a negative control.

However, all selected polymers A2, A7, B7, and D1 at 25 wt% of griseofulvin loading did not show superior performance to HPMCAS. A2 (CND-0.66, 20 kDa) and A7 (CND-0.63, 19 kDa) were able to achieve high levels of initial supersaturation up to 930 and 900 µg/mL respectively, but the concentration of drug drastically plummeted to 50 µg/mL after 10 min. Similar performance was observed in case of HPMCAS. B7 and D1 failed to achieve initial burst release and showed poorer dissolution profiles compared to HPMCAS, A2, and A7. These dissolution profiles clearly indicate that the CND systems failed to achieve and maintain supersaturation for griseolfulvin (Figure 6.7). This might be due to the difference in structure of griseofulvin compared to phenytoin. Phenytoin contains amide moieties and by the virtue of homo intermolecular hydrogen bonding, the drug crystallizes out. CND systems were able to interact and inhibit crystallization of phenytoin by forming hetero intermolecular hydrogen bonds. Griseolfulvin lacks amide moieties, and therefore it may not be possible for the CND system to interact and inhibit crystallization of griseolfulvin.

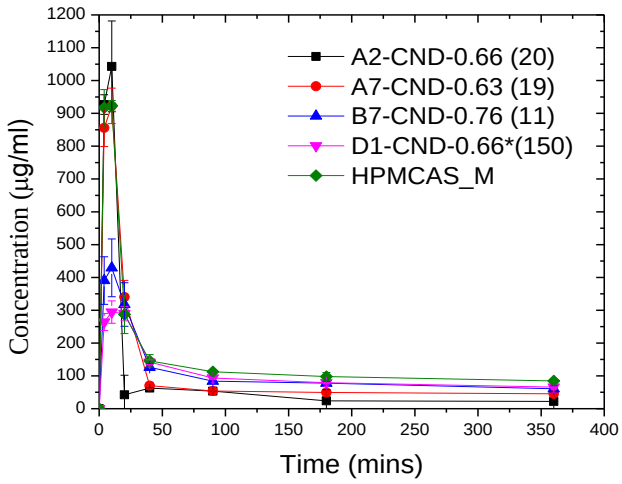

Figure 6.7 Dissolution data of selected SDDs with 25 wt% of griseofulvin loading, compared with HPMCAS_M (positive control). All SDDs failed to maintain supersaturation concentration**.**

Our study clearly indicates that NIPAm is a critical component of the CND system to achieve and maintain supersaturation of phenytoin. DMA increases the LCST of the NIPAm based polymers, and thus is accountable for aqueous solubility of the polymers in dissolution media. Our group is further investigating the superior performance of the CND system by synthesizing libraries of hydrophilic and thermo responsive polymers.

6.3 Conclusions

In summary, starting from homopolymer of NIPAm, we have synthesized four different random copolymers of NIPAm and DMA using RAFT polymerization technique. The rationale of utilizing NIPAm was to establish structure property relationship between polymers and drugs, and enhance the aqueous solubility of model hydrophobic drugs. The DMA component of the polymers increases the LCST of the system, which thus led to

polymers soluble in aqueous media. According to the reactivity ratios reported in the literature, NIPAm and DMA co-polymers are random in nature. LCST measurements in water and PBS + FaSSIF solution indicated a decrease in the LCST of polymers with increasing PNIPAm content. We formulated spray dried dispersions of all polymers with two BCS class II model drugs, probucol and phenytoin. The PXRD revealed no significant differences in solid state properties of all spray dried dispersions. However, in vitro dissolution test, polymers demonstrated vastly different dissolution profiles for both drugs at 10 and 25 wt% of drug loadings. At 10 wt% of probucol loading, PDMA, CND-0.23, CND-0.46, and CND-0.70 showed burst release and maintained supersaturation levels similar to that of HPMCAS for 6 h. CND-0.84 and PNIPAm failed to exhibit superior performance due to their LCST lower than the physiological temperature. However, at 25 wt% of probucol loading, all polymers failed to outperform HPMCAS, and resulted in poorer dissolution profiles. We attributed poor performance at higher drug loading to lack of excipient in solution to prevent precipitation of drug. Phenytoin crystallizes faster than probucol, and as per our knowledge there is no excipient present in the market to drastically improve the aqueous solubility of this drug. HPMCAS is effective at achieving initial levels of high concentration at 10 wt% of loading, however, the concentration of dissolved drug dropped considerably past 10 min into the dissolution test. Compared to other formulations, the CND-0.70 was not only able to achieve initial levels of supersaturation but also maintained high concentration for 6 h of dissolution test. At 25 wt% of phenytoin loading, this formulation outperforms HPMCAS by demonstrating a 2-fold increase in AUC_{360min}. We attributed excellent performance of CND-0.70 to its ability to interact and interfere with the phenytoin crystallization process. We believe that this formulation contains

sufficient concentration of NIPAm to interact and form hydrogen bonds in solution with phenytoin molecules and retard its crystallization.

To investigate the effect of molecular weight and understand precise composition window of CND system to prevent crystallization of phenytoin, we synthesized libraries of random copolymers by varying molecular weights at fixed NIPAm composition (10 kDa to 60 kDa) and by varying molar compositions of NIPAm at fixed molecular weight. Our supersaturation results indicated that molecular weights of system at fixed molar composition (66 mole percent of NIPAm) has a minor influence on the ability of polymers to stabilize supersaturation. However, the composition of the NIPAm in the polymer backbone is a vital factor to maintain supersaturation. Our data reveled that to inhibit crystallization of phenytoin in solution, the formulation required 63 to 73 mole percent of NIPAm in the polymer backbone. Ultimately, we verified supersaturation test results by formulating spray dried dispersions at 25 wt % phenytoin loading with selected CND systems. This study clearly indicates that it is necessary to incorporate groups in the excipient formulation that can interact and interfere with drug crystallization process to increase and maintain its aqueous solubility. We also propose that in designing excipients for drugs with lower lattice energy (lower melting point), hydrophilicity of the excipient is the prime factor to consider. However, for drugs with higher lattice energy (high melting point), it is necessary to design an excipient which exhibits specific interactions with the drug groups responsible for the crystallization mechanism.

6.4 Experimental Section

Materials.

All chemicals were used as received (reagent grade) unless otherwise noted. All solvents utilized were HPLC or analytical grade. N-isopropylacrylamide (NIPAm) (Aldrich, >99%), 4-Cyano-4-[(dodecylsulfanylthiocarbonyl)sulfanyl]pentanoic acid (RAFT-CTA, Aldrich, 97%), chloroform-d (Aldrich, 99.8 atom % D), methanol-d4 (MeOD, Aldrich, 99.96 atom % D), tetrahydrofuran (THF, anhydrous, Aldrich, ≥99.9%), 1,4-Dioxane (Aldrich, ≥99.0%), Diethyl ether (Aldrich, ≥99.0%), phenytoin (Aldrich, 99+%), probucol (Aldrich), griseolfulvin (Aldrich) were used as received. *N*,*N*-Dimethylacrylamide (DMA) (Aldrich, 99+%) was purified by passage through basic alumina columns to remove trace amounts of inhibitors. HPMC-AS (AFFINISOL™ 912G, The Dow Chemical Company) were used as received. Fasted-state simulated intestinal fluid powder (FaSSIF) was purchased from Biorelevant. Phosphate buffered saline (PBS) was prepared in lab consisted of 82 mM sodium chloride (Fisher, ≥99%), 20 mM sodium phosphate dibasic heptahydrate (Fisher, 98%), 47 mM potassium phosphate monobasic (J.T. Baker, ≥99.0%). RAFT agent 4-cyano-4-(propylsulfanylthiocarbonyl)-sulfanylpentanoic acid (CPP) was synthesized and purified as described.[40]

Polymer Characterization:

Size Exclusion Chromatography (SEC).

SEC measurements were carried out on a Agilent 1260 Infinity liquid chromatograph equipped with a Waters Styragel guard column and three Waters Styragel columns (HR6, HR4, and HR1). Waters columns are packed with 5 micrometer styrene divinylbenzene particles. Columns dimensions are 7.8*300 mm (guard column: 4.6*30

mm). Columns are housed to an Agilent 1260 VWD UV-Vis detector, a Wyatt Dawn Heleos II light-scattering detector (Laser wavelength at 663.6 nm), and a Wyatt Optilab T-rEX refractive-index detector. Tetrahydrofuran (THF) was used a mobile phase at 1.0 mL/min at 25°C. The run time for the method was 45 min.

Differential Scanning Calorimetry (DSC)

Samples of known mass (2−10 mg) were weighed in Tzero aluminum pans and analyzed on a Discovery DSC (TA Instruments). To determine the T_g of a polymer: The temperature was ramped from 20 and 120 °C at a rate of 10 °C min^{-1} and then cooled down to 22 °C. In second heating cycle, the temperature was ramped to 180 °C at a rate of 2.5 °C min^{-1}, and again cooled down to 22 °C at a rate of 10 °C min^{-1}. In third heating cycle the temperature was ramped to 180 °C at a rate of 2.5 °C min^{-1}. T_g was determined using the second heating scan. All analyses were carried out using TA TRIOS software version 2.2.

LCST Measurements.

LCST of polymers were determined using UV-Vis spectrophotometer coupled with temperature controller in water and PBS + SIF solution. LCST were measured from the transmittance at 450 nm. The polymer solutions were prepared by dissolving 18 mg of polymer in 1.8 mL of water or PBS + SIF solution. The heating rate was 0.2 °C/min.

Powder X-ray Diffraction (Powder XRD).

Powder samples (~70 mg) were filled in a 0.5 mm deep zerobackground glass frame and placed on a Bruker-AXS D5005 diffractometer. The X-ray source (Cu, $\lambda = 1.54$

Å) was run at a current of 40 mA and at a voltage of 45 kV. Data were collected from 5 to 40° (2θ) with a step size of 0.02° and a scan rate of 1 s/step.

Supersaturation Testing

Supersaturation testing was performed using a high-throughput method. Phosphate buffer solution (PBS, 82 mM sodium chloride, 20 mM sodium phosphate dibasic, 47 mM potassium phosphate monobasic, 0.5 wt% simulated intestinal fluid powder, adjusted to pH 6.5 with NaOH) and aqueous solutions of excipients (912 µL) were robotically delivered into designated 1 mL vials arranged on an aluminum 96 (8x12) well array using the Evo 2000 platform. Organic drug solutions (phenytoin and griseolfulvin were evaluated, 20 g/L drug in organic solvent, 48 uL) were dispersed onto the excipients solutions. Final concentration of drug is 1000 µg/mL. Samples were set in an isothermal aluminum sample holder at 37 °C. At each time point (30, 90, 180 min), samples were centrifuged at 13,000 g for 1 min, and a 30 µL aliquot was removed and diluted with 150 µL of methanol. The samples were again held at 37 °C until the next time point. The drug concentration in each aliquot was determined by reverse phase HPLC.

Spray Drying

Spray drying was performed on a laboratory scale using a Bend Research Mini Spray Dryer (Bend, OR). A 1 wt% of polymer and drug solution at 10 and 25 wt% of drug loading in THF (1:1, *v*/*v*) was prepared, with the following as an example: 30 mg phenytoin and 270 mg of polymer were combined with 29.7 g THF to prepare a spray-dried dispersion (SDD). The solution was transferred to a 20.0 mL syringe and injected at the following processing parameters: solution feed rate = 0.65 mL min^{-1}, inlet temperature = 68 °C, nitrogen feed rate = 12.8 standard liter per minute (SLPM). SDDs were collected from the

1.5" Whatman filter paper with assistance from an antistatic bar, dried *in vacuo* (10 mTorr) overnight for at least 12 h, and stored in a vacuum desiccator at 22 °C.

Dissolution of Solid Dispersions.

Dissolution tests were carried out using a microcentrifuge dissolution test method under non-sink conditions. Measured samples were weighed in duplicate into 2.0 mL plastic conical microcentrifuge tubes. Phosphate buffer saline (PBS, pH 6.5) with 0.5 wt% fasted simulated intestinal fluid powder (FaSSIF) at 37 °C was added (time = 0 min) to achieve a final drug concentration of 1000 µg/mL if all material were fully dissolved (e.g., 7.2 mg of a CND-0.70 SDD loaded with 25 wt% probucol, consisting of 1.8 mg drug and 5.4 mg polymer, was carefully measured into a conical tube and diluted with 1.8 mL PBS and FaSSIF solution). Samples were vortexed for 30 s and incubated in an isothermal aluminum heating block at 37 °C. At each time point (4, 10, 20, 40, 90, 180, and 360 min), samples were centrifuged for 1 min at 13,000 RPM, and a 50 µL aliquot was taken from the supernatant and diluted with 250 µL methanol. The samples were then vortexed again for an additional 30 s and held at 37 °C until the next time point.

Solubilized drug concentration in each aliquot sample was determined by reverse phase high-performance liquid chromatography (HPLC) analysis. The HPLC consisted of a reversed-phase EC-C18 column (Poroshell 120, 4.6 x 50 mm, 2.7 µm, Agilent, USA) and a mobile phase of acetonitrile/water (MeCN:Water) (96:4, %, *v/v*) pumped at a flow rate of 1.0 mL/min at 30 °C. A 10 µL aliquot of sample was injected, and the column effluent was detected at 241 nm with a UV detector (1260 Infinity Multiple Wavelength Detector, Agilent). A calibration curve for probucol was made by preparing samples in the range of 0.1 to 500 µg/mL. The concentration-time area under the curve (AUC_{360min}) from 0 to 360

min was determined using the trapezoidal rule. For phenytoin, the mobile phase was 40:60 (v/v) of MeCN/Water, and a calibration was made in the range of 10−1000 μg/mL.

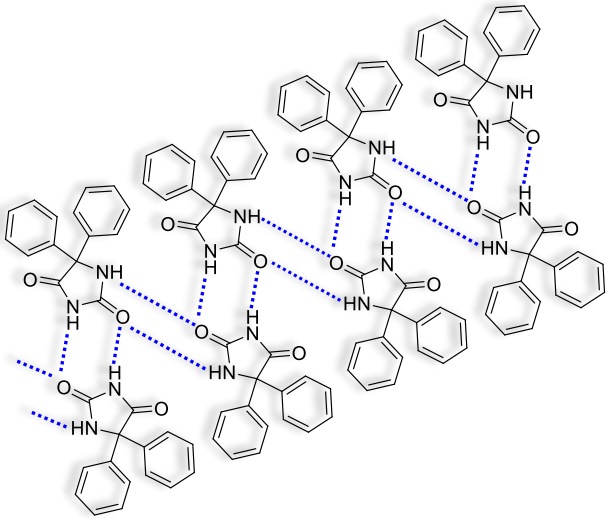

Figure 6.8 Crystallization mechanism of phenytoin.

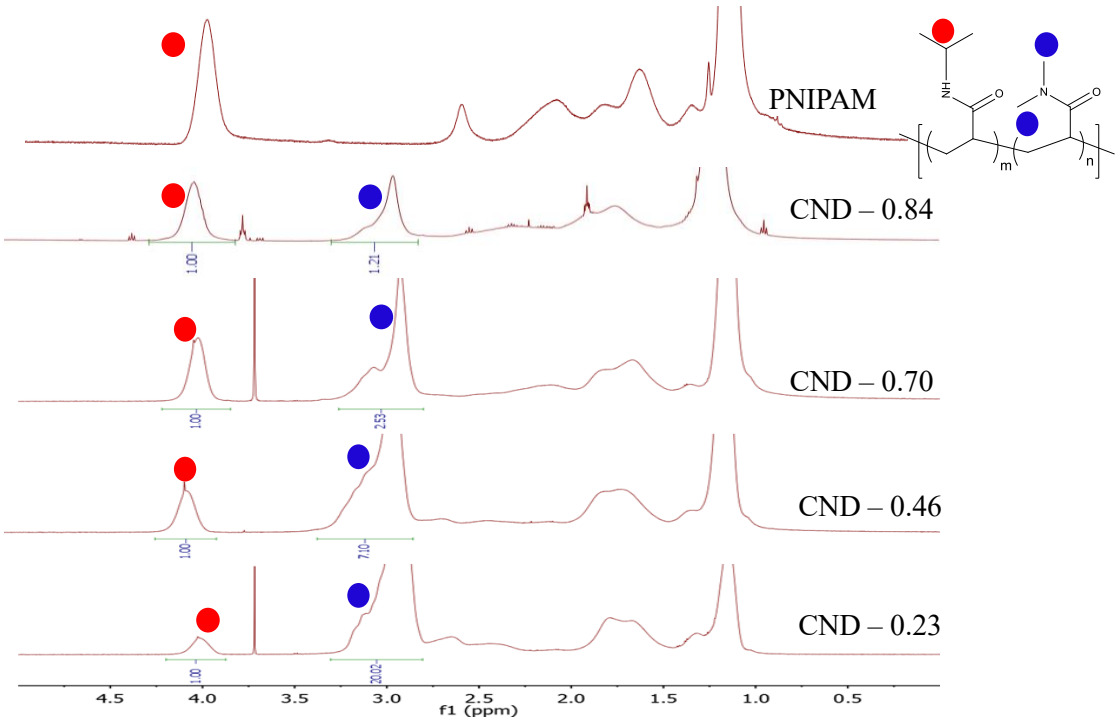

Figure 6.9 Representative 1H NMR spectra of P(NIPAm-co-DMA) copolymers recorded in MeOD at 500 MHz. The integration values below the peak are relative to methine proton of NIPAm. The mole ratio of NIPAm was calculated from the integration ratio between methine (1H) proton of NIPAm and methyl (6H) protons of DMA.

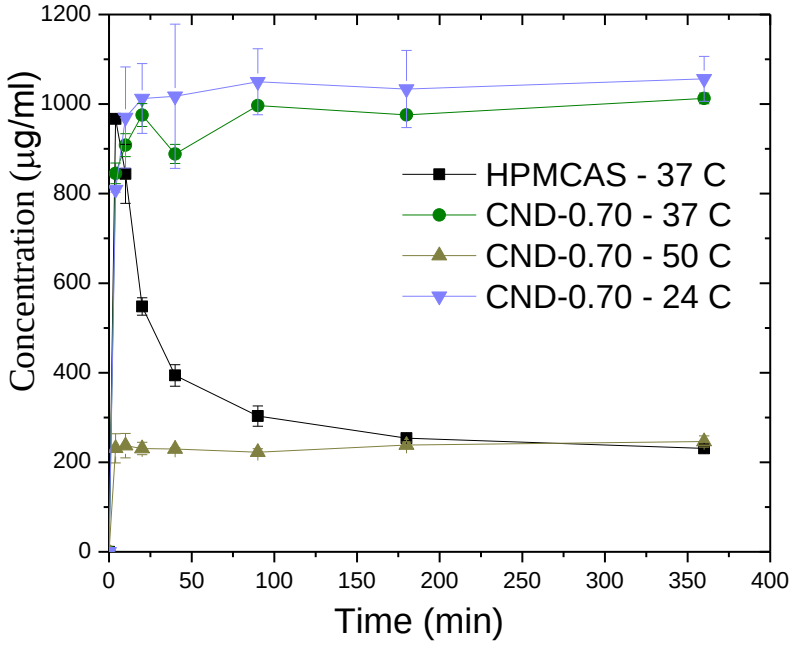

Figure 6.10 The dissolution profiles of SDD with polymer matrix CND-0.70 with 10 wt% phenytoin loading at 37 °C (i.e. the LCST of CND-0.70 in PBS + FaSSIF), 50 °C (above LCST), and 24 °C (below LCST).

Table 6.5 Reactions used to synthesize libraries of random copolymers NIPAM-co-DMA.

Sample	NIPAm (g)	DMA (g)	RAFT-CTA (g)*	AIBN (mg)	Dioxane (g)	M/CTA	NIPAm in the feed (mol %)	$M_{n,\ theo}$ (g/mol)
A1	1.11	0.42	0.056	5.0	6.3	101/1	70%	10,000
A2	1.11	0.42	0.028	2.5	6.3	202/1	70%	20,000
A3	1.11	0.42	0.0187	1.7	6.3	303/1	70%	30,000
A4	1.11	0.42	0.014	1.3	6.3	404/1	70%	40,000
A5	1.11	0.42	0.011	1.0	6.3	505/1	70%	50,000
A6	1.11	0.42	0.009	0.8	6.3	606/1	70%	60,000
A7	1.03	0.49	0.028	2.5	6.3	202/1	65%	20,000
A8	1.19	0.35	0.028	2.5	6.3	202/1	75%	20,000

B1	0.16	1.25	0.028	2.5	6.4	202/1	10%	20,000
B2	0.32	1.11	0.028	2.5	6.4	202/1	20%	20,000
B3	0.48	0.83	0.028	2.5	6.5	202/1	30%	20,000
B4	0.63	0.69	0.028	2.5	6.5	202/1	40%	20,000
B5	0.79	0.56	0.028	2.5	6.5	202/1	50%	20,000
B6	0.95	0.42	0.028	2.5	6.5	202/1	60%	20,000
B7	1.27	0.28	0.028	2.5	6.3	202/1	80%	20,000
B8	1.43	0.14	0.028	2.5	6.2	202/1	90%	20,000
C1	0.16	1.25	0.011	1.0	6.4	505/1	10%	50,000
C2	0.32	1.11	0.011	1.0	6.4	505/1	20%	50,000
C3	0.48	0.83	0.011	1.0	6.5	505/1	30%	50,000
C4	0.63	0.69	0.011	1.0	6.5	505/1	40%	50,000
C5	0.79	0.56	0.011	1.0	6.5	505/1	50%	50,000
C6	0.95	0.42	0.011	1.0	6.5	505/1	60%	50,000
C7	1.27	0.28	0.011	1.0	6.3	505/1	80%	50,000
C8	1.43	0.14	0.011	1.0	6.3	505/1	90%	50,000

*Commercially available RAFT-CTA was used in this synthesis. The structure of CTA is shown in Scheme 1 as (2).

Table 6.6 Summary of copolymer solubility in several solvents.

Samples	*NIPAM in the polymer (mol%) (NMR)*	$M_{n,theo}$ (g/mol)	$M_{n,SEC}$ (g/mol)	*PDI*	*Tg (°C)*	*10 wt% in THF*	*10 wt% in Acetone*	*1 wt% in PBS buffer (pH = 6.5)*
A1-CND-0.66(11)	66%	10,00	10,950	1.04	127.2	complete	complete	complete
A2-CND-0.66	66%	20,00	20,000	1.06	127.6	complete	complete	complete
A3-CND-0.67	67%	30,00	30,000	1.09	126.8	complete	complete	complete
A4-CND-0.65	65%	40,00	42,000	1.14	123.2	complete	complete	complete
A5-CND-0.66	66%	50,00	69,000	1.17	95.7	complete	complete	complete
A6-CND-0.68	68%	60,00	54,500	1.21	102.2	complete	complete	complete
A7-CND-0.63	63%	20,00	18,900	1.06	129.2	complete	complete	complete
A8-CND-0.73	73%	20,00	17,700	1.07	133.7	complete	complete	complete
B1-CND-0.08	8%	20,00	20,600	1.05	125.9	complete	complete	complete
B2-CND-0.19	19%	20,00	17,900	1.05	129.7	complete	complete	complete
B3-CND-0.30	30%	20,00	n/a	n/a	102.2	complete	complete	complete
B4-CND-0.42	42%	20,00	19,600	1.20	117.0	complete	complete	complete
B5-CND-0.54	54%	20,00	14,300	1.13	123.1	complete	complete	complete
B6-CND-0.63	63%	20,00	17,800	1.06	126.8	complete	complete	complete
B7-CND-0.76	76%	20,00	11,300	1.08	128.7	complete	complete	complete
B8-CND-0.90	90%	20,00	n/a	n/a	132.4	complete	complete	complete
C1-CND-0.09	9%	50,00	47,700	1.14	127.3	complete	complete	complete
C2-CND-0.18	18%	50,00	44,600	1.13	132.2	complete	complete	complete
C3-CND-0.31	31%	50,00	51,600	1.11	88.2	complete	complete	complete
C4-CND-0.43	43%	50,00	49,900	1.09	95.4	complete	complete	complete
C5-CND-0.50	50%	50,00	36,500	1.11	102.2	complete	complete	complete
C6-CND-0.63	63%	50,00	31,900	1.11	103.6	complete	complete	complete
C7-CND-0.78	78%	50,00	40,400	1.13	142.8	complete	complete	complete
C8-CND-0.89	89%	50,00	44,100	1.14	106.7	complete	complete	complete

Solubility was judged visually as complete, mostly soluble, hazy, and insoluble. The number in the parentheses indicates the molecular weight of the polymers (A1 to A8).

6.5 References

(1) Bull, A. T.; Ward, A. C.; Goodfellow, M. *Microbiol. Mol. Biol. Rev.* **2000**, *64*, 573-606.

(2) Grosdidier, S.; Totrov, M.; Fernandez-Recio, J. *Adv. Appl. Bioinform. Chem.* **2009**, *2*, 101-123.

(3) Baltes, N. J.; Voytas, D. F. *Trends in Biotechnology, ASAP*

(4) Szymanski, P.; Markowicz, M.; Mikiciuk-Olasik, E. *Int. J. Mol. Sci.* **2012**, *13*, 427-452.

(5) Basavaraj, S.; Betageri, G. V. *Acta Pharm. Sin. B* **2014**, *4*, 3-17.

(6) Hoelder, S.; Clarke, P. A.; Workman, P. *Mol. Oncol.* **2012**, *6*, 155-176.

(7) Rosen, H.; Abribat, T. *Nat. Rev. Drug. Discov.* **2005**, *4*, 381-385.

(8) Lipinski, C. A.; Lombardo, F.; Dominy, B. W.; Feeney, P. J. *Adv.Drug Deliv. Rev.* **2001**, *46*, 3-26.

(9) Prentis, R. A.; Lis, Y.; Walker, S. R. *Br. J. Clin. Pharmacol.* **1988**, *25*, 387-396.

(10) Stegemann, S.; Leveiller, F.; Franchi, D.; de Jong, H.; Linden, H. *Eur. J. Pharm. Sci.* **2007**, *31*, 249-261.

(11) Strickley, R. G. *Pharm. Res.* **2004**, *21*, 201-230.

(12) Loftsson, T.; Brewster, M.; Másson, M. *Am. J. Drug. Deliv.* **2004**, *2*, 261-275.

(13) Loftsson, T.; Brewster, M. E. *J. Pharm. Sci.* **2012**, *101*, 3019-3032.

(14) Serajuddin, A. T. *Adv.Drug Deliv. Rev.* **2007**, *59*, 603-616.

(15) Leuner, C.; Dressman, J. *Eur. J. Pharm. Biopharm.* **2000**, *50*, 47-60.

(16) Vasconcelos, T.; Sarmento, B.; Costa, P. *Drug Discov. Today* **2007**, *12*, 1068-1075.

(17) Sareen, S.; Mathew, G.; Joseph, L. *Int. J. Pharm. Investig.* **2012**, *2*, 12-17.

(18) Huang, Y.; Dai, W.-G. *Acta Pharm. Sin. B* **2014**, *4*, 18-25.

(19) Re, M. I. *Drying Technol.* **2006**, *24*, 433-446.

(20) Vehring, R. *Pharm. Res.* **2008**, *25*, 999-1022.

(21) Hughey, J. R.; Keen, J. M.; Brough, C.; Saeger, S.; McGinity, J. W. *Int. J. Pharm.* **2011**, *419*, 222-230.

(22) Ormes, J. D.; Zhang, D.; Chen, A. M.; Hou, S.; Krueger, D.; Nelson, T.; Templeton, A. *Pharm. Dev. Technol.* **2013**, *18*, 121-129.

(23) Friesen, D. T.; Shanker, R.; Crew, M.; Smithey, D. T.; Curatolo, W. J.; Nightingale, J. A. *Mol. Pharm.* **2008**, *5*, 1003-1019.

(24) Yin, L.; Hillmyer, M. A. *Mol. Pharm.* **2014**, *11*, 175-185.

(25) Tanno, F.; Nishiyama, Y.; Kokubo, H.; Obara, S. *Drug Dev. Ind. Pharm.* **2004**, *30*, 9-17.

(26) Rumondor, A. C.; Stanford, L. A.; Taylor, L. S. *Pharm. Res.* **2009**, *26*, 2599-2606.

(27) Tajarobi, F.; Larsson, A.; Matic, H.; Abrahmsen-Alami, S. *Eur. J. Pharm. Biopharm.* **2011**, *78*, 125-133.

(28) Qian, F.; Wang, J.; Hartley, R.; Tao, J.; Haddadin, R.; Mathias, N.; Hussain, M. *Pharm. Res.* **2012**, *29*, 2765-2776.

(29) Ting, J. M.; Navale, T. S.; Bates, F. S.; Reineke, T. M. *ACS Macro Letters* **2013**, *2*, 770-774.

(30) Islam, M. R.; Ahiabu, A.; Li, X.; Serpe, M. J. *Sensors* **2014**, *14*, 8984-8995.

(31) Ward, M. A.; Georgiou, T. K. *Polymers* **2011**, *3*, 1215-1242.

(32) Messing, R.; Schmidt, A. M. *Polym. Chem.* **2011**, *2*, 18-32.

(33) Dalsin, M. C.; Tale, S.; Reineke, T. M. *Biomacromolecules* **2014**, *15*, 500-511.

(34) Ting, J. M.; Navale, T. S.; Bates, F. S.; Reineke, T. M. *Macromolecules* **2014**, *47*, 6554-6565.

(35) Nokhodchi, A.; Bolourtchian, N.; Dinarvand, R. *Int. J. Pharm.* **2003**, *250*, 85-97.

(36) Zipp, G. L.; Rodriguezhornedo, N. *J. Phys. D: Appl. Phys.* **1993**, *26*, B48-B55.

(37) Warren, D. B.; Bergstrom, C. A. S.; Benameur, H.; Porter, C. J. H.; Pouton, C. W. *Mol. Pharm.* **2013**, *10*, 2823-2848.

(38) Schmatloch, S.; Meier, M. A. R.; Schubert, U. S. *Macromol. Rapid Commun.* **2003**, *24*, 33-46.

(39) Barillaro, V.; Pescarmona, P. P.; Van Speybroeck, M.; Do Thi, T.; Van Humbeeck, J.; Vermant, J.; Augustijns, P.; Martens, J. A.; Van Den Mooter, G. *J. Comb. Chem.* **2008**, *10*, 637-643.

(40) Xu, X. W.; Smith, A. E.; Kirkland, S. E.; McCormick, C. L. *Macromolecules* **2008**, *41*, 8429-8435.

(41) Bauri, K.; Roy, S. G.; Arora, S.; Dey, R. K.; Goswami, A.; Madras, G.; De, P. *J. Therm. Anal. Calorim.* **2013**, *111*, 753-761.

(42) Deng, K. L.; Tian, H.; Zhang, P. F.; Ren, X. B.; Zhong, H. B. *Express Polym. Lett.* **2009**, *3*, 97-104.

(43) Gupta, P.; Kakumanu, V. K.; Bansal, A. K. *Pharm. Res.* **2004**, *21*, 1762-1769.

(44) Miller, J. M.; Beig, A.; Carr, R. A.; Spence, J. K.; Dahan, A. *Mol. Pharm.* **2012**, *9*, 2009-2016.

(45) Hancock, B. C.; Parks, M. *Pharm. Res.* **2000**, *17*, 397-404.

(46) Vandecruys, R.; Peeters, J.; Verreck, G.; Brewster, M. E. *Int. J. Pharm.* **2007**, *342*, 168-175.

(47) Yamashita, T.; Ozaki, S.; Kushida, I. *Int. J. Pharm.* **2011**, *419*, 170-174.

Bibliography

Silverman, R. B. *The Organic Chemistry of Drug Design and Drug Action*; Second Edition ed.

Watt, A.; Morrison, D. *Drug Discov. Today* **2001**, *6*, 290-292.

Khanna, I. *Drug Discov. Today* **2012**, *17*, 1088-1102.

Jain, K. K. *Curr. Opin. Mol. Ther.* **2006**, *8*, 487-492.

Guido, R. V.; Oliva, G.; Andricopulo, A. D. *Comb. Chem. High Throughput Screen.* **2011**, *14*, 830-839.

Mudshinge, S. R.; Deore, A. B.; Patil, S.; Bhalgat, C. M. *Saudi Pharm. J.* **2011**, *19*, 129-141.

Gupta, S.; Kesarla, R.; Omri, A. *ISRN Pharm.* **2013**, *2013*, 848043.

Davis, S. S.; Illum, L. *Biomaterials* **1988**, *9*, 111-115.

Kim, S. W.; Bae, Y. H.; Okano, T. *Pharmaceut. Res.* **1992**, *9*, 283-290.

Uekama, K.; Otagiri, M. *Crit. Rev. Ther. Drug Carrier Syst.* **1987**, *3*, 1-40.

Kwon, G. S.; Okano, T. *Adv. Drug Deliv. Rev.* **1996**, *21*, 107-116.

Torchilin, V. P. *Nat. Rev. Drug Discov.* **2005**, *4*, 145-160.

Lee, T. W.; Boersen, N. A.; Hui, H. W.; Chow, S. F.; Wan, K. Y.; Chow, A. H. *Curr. Pharm. Des.* **2014**, *20*, 303-324.

Jitendra; Sharma, P. K.; Bansal, S.; Banik, A. *Indian J. Pharm. Sci.* **2011**, *73*, 367-375.

Siepmann, J.; Siepmann, F. *J. Control. Release* **2012**, *161*, 351-362.

Brewster, M. E.; Loftsson, T. *Adv. Drug Deliv. Rev.* **2007**, *59*, 645-666.

Williams, H. D.; Trevaskis, N. L.; Charman, S. A.; Shanker, R. M.; Charman, W. N.; Pouton, C. W.; Porter, C. J. *Pharmacol. Rev.* **2013**, *65*, 315-499.

Davis, M. E.; Brewster, M. E. *Nat. Rev. Drug Discov.* **2004**, *3*, 1023-1035.

Jones, M. C.; Leroux, J. C. *Eur. J. Pharm. Biopharm.* **1999**, *48*, 101-111.

Xu, W.; Ling, P.; Zhang, T. *J. Drug Deliv.* **2013**, *2013*, 15.

Jhaveri, A. M.; Torchilin, V. P. *Front. Pharmacol.* **2014**, *5*, 77.

Wu, Y. T.; Jiaang, W. T.; Lin, K. G.; Huang, C. M.; Chang, C. H.; Sun, Y. L.; Fan, K. H.; Hsu, W. C.; Wang, H. E.; Lin, S. B.; Chen, S. T. *Curr. Drug Deliv.* **2004**, *1*, 119-127.

Kim, S. H.; Goto, M.; Akaike, T. *J. Biol. Chem.* **2001**, *276*, 35312-35319.

Tiwari, G.; Tiwari, R.; Sriwastawa, B.; Bhati, L.; Pandey, S.; Pandey, P.; Bannerjee, S. K. *Int. J. Pharm. Investig.* **2012**, *2*, 2-11.

van Vlerken, L. E.; Vyas, T. K.; Amiji, M. M. *Pharmaceut. Res.* **2007**, *24*, 1405-1414.

Ahmad, Z.; Shah, A.; Siddiq, M.; Kraatz, H. B. *R. Soc. Chem. Adv.* **2014**, *4*, 17028-17038.

Lavasanifar, A.; Samuel, J.; Kwon, G. S. *Adv. Drug Deliv. Rev.* **2002**, *54*, 169-190.

Kadajji, V. G.; Betageri, G. V. *Polymers* **2011**, *3*, 1972-2009.

Osada, K.; Christie, R. J.; Kataoka, K. *J. R. Soc. Interface* **2009**, *6 Suppl 3*, S325-339.

Zhao, W.; Gody, G.; Dong, S. M.; Zetterlund, P. B.; Perrier, S. *Polym. Chem.* **2014**, *5*, 6990-7003.

Zhang, N.; Wardwell, P. R.; Bader, R. A. *Pharmaceutics* **2013**, *5*, 329-352.

Knop, K.; Hoogenboom, R.; Fischer, D.; Schubert, U. S. *Angew. Chem. Int. Ed.* **2010**, *49*, 6288-6308.

Hatakeyama, H.; Akita, H.; Harashima, H. *Biol. Pharm. Bull.* **2013**, *36*, 892-899.

Huang, Y.; Dai, W. G. *Acta Pharm. Sin. B* **2014**, *4*, 18-25.

Friesen, D. T.; Shanker, R.; Crew, M.; Smithey, D. T.; Curatolo, W. J.; Nightingale, J. A. *Mol. Pharm.* **2008**, *5*, 1003-1019.

Konno, H.; Handa, T.; Alonzo, D. E.; Taylor, L. S. *Eur. J. Pharm.Biopharm.* **2008**, *70*, 493-499.

Curatolo, W.; Nightingale, J. A.; Herbig, S. M. *Pharmaceut. Res.* **2009**, *26*, 1419-1431.

Tajarobi, F.; Larsson, A.; Matic, H.; Abrahmsen-Alami, S. *Eur J Pharm Biopharm* **2011**, *78*, 125-133.

Ilevbare, G. A.; Liu, H. Y.; Edgar, K. J.; Taylor, L. S. *Cryst. Growth Des.* **2012**, *12*, 3133-3143.

Duncan, R. *Nat. Rev. Drug Discov.* **2003**, *2*, 347-360.

van Vlerken, L. E.; Vyas, T. K.; Amiji, M. M. *Pharm. Res.* **2007**, *24*, 1405-1414.

Maeda, H.; Wu, J.; Sawa, T.; Matsumura, Y.; Hori, K. *J. Control. Release* **2000**, *65*, 271-284.

Owens, D. E.; Peppas, N. A. *Int. J. Pharm.* **2006**, *307*, 93-102.

Gaucher, G.; Marchessault, R. H.; Leroux, J. C. *J. Control. Release* **2010**, *143*, 2-12.

Miller, T.; Rachel, R.; Besheer, A.; Uezguen, S.; Weigandt, M.; Goepferich, A. *Pharm. Res.* **2012**, *29*, 448-459.

K. Osada; Christie, R. J.; Kataoka, K. *J. R. Soc. Interface* **2009**, *6* S325-S339.

N. Zhang; P. R. Wardwell; Bader, R. A. *Pharmaceutics* **2013**, *5*, 329-352.

Knop, K.; Hoogenboom, R.; Fischer, D.; Schubert, U. S. *Angew. Chem. Int. Ed.* **2010**, *49*, 6288-6308.

Mancini, R. J.; Lee, J.; Maynard, H. D. *J. Am. Chem. Soc.* **2012**, *134*, 8474–8479.

A. Sizovs; L. Xue; Z. P. Tolstyka; N. P. Ingle; Y. Wu; M. Cortez; Reineke, T. M. *J. Am. Chem. Soc.* **2013**, *135*, 15417−15424.

Yasugi, K.; Nakamura, T.; Nagasaki, Y.; Kato, M.; Kataoka, K. *Macromolecules* **1999**, *32*, 8024-8032.

Elbein, A. D.; Pan, Y. T.; Pastuszak, I.; Carroll, D. *Glycobiology* **2003**, *13*, 17R-27R.

Green, J. L.; Angell, C. A. *J. Phys. Chem.* **1989**, *93*, 2880-2882.

Crowe, J. H.; Crowe, L. M.; Carpenter, J. F.; Wistrom, C. A. *Biochem. J.* **1987**, *242*, 1-10.

Roser, B. *Trends Food Sci. Technol.* **1991**, *2*, 66-69.

Teramoto, N.; Sachinvala, N. D.; Shibata, M. *Molecules* **2008**, *13*, 1773-1816.

Crowe, J. H.; Crowe, L. M. *Nat. Biotechnol.* **2000**, *18*, 145-146.

Clegg, J. S.; Seitz, P.; Seitz, W.; Hazlewood, C. F. *Cryobiology* **1982**, *19*, 306-316.

Clegg, J. S. *Methods Enzymol.* **1986**, *127*, 230-239.

Crowe, J. H.; Crowe, L. M.; Chapman, D. *Science* **1984**, *223*, 701-703.

Kurita, K.; Hirakawa, N.; Morinaga, H.; Iwakura, Y. *Makromol. Chem.* **1979**, *180*, 2769-2773.

Kurita, K.; Masuda, N.; Aibe, S.; Murakami, K.; Ishii, S.; Nishimura, S. I. *Macromolecules* **1994**, *27*, 7544-7549.

Teramoto, N.; Arai, Y.; Shibasaki, Y.; Shibata, M. *Carbohydr. Polym.* **2004**, *56*, 1-6.

Teramoto, N.; Niwa, M.; Shibata, M. *Materials* **2010**, *3*, 369-385.

Srinivasachari, S.; Liu, Y. M.; Zhang, G. D.; Prevette, L. E.; Reineke, T. M. *J. Am. Chem. Soc.* **2006**, *128*, 8176-8184.

Srinivasachari, S.; Liu, Y. M.; Prevette, L. E.; Reineke, T. M. *Biomaterials* **2007**, *28*, 2885-2898.

Snyder, L. R.; Kirkland, J. J. In *Introduction to Modern Liquid Chromatography, second edition*; John Wiley & Sons: New York, 1979, p 246-268.

Yin, L.; Hillmyer, M. A. *Macromolecules* **2011**, *44*, 3021-3028.

Al-Deyab, S. S.; El-Newehy, M. H.; Al-Hazmi, A. M. *Molecules* **2010**, *15*, 4750-4756.

Brown, A. M. *Comput. Methods Programs Biomed.* **2001**, *65*, 191-200.

L. Yin; M. C. Dalsin; A. Sizovs; T. M. Reineke; M. A. Hillmyer *Macromolecules* **2012**, *45*, 4322-4332.

Reineke, T. M.; Davis, M. E. *Bioconjug. Chem.* **2003**, *14*, 247-254.

Wada, M.; Miyazawa, Y.; Miura, Y. *Polym. Chem.* **2011**, *2*, 1822-1829.

Odian, G. *Principles of polymerization, 4th ed.*; John Wiley & Sons, Inc.: Hoboken, NJ, 2004.

Lai, J. T.; Filla, D.; Shea, R. *Macromolecules* **2002**, *35*, 6754-6756.

Jain, S.; Bates, F. S. *Science* **2003**, *300*, 460-464.

S. Jain; Bates, F. S. *Macromolecules* **2004**, *37*, 1511-1523.

Pearson, S.; Allen, N.; Stenzel, M. H. *J. Polym. Sci., Part A: Polym. Chem.* **2009**, *47*, 1706−1723.

Smith, A. E.; Sizovs, A.; Grandinetti, G.; Xue, L.; Reineke, T. M. *Biomacromolecules* **2011**, *12*, 3015−3022.

Ting, S. R. S.; Min, E. H.; Escale, P.; Save, M.; Billon, L.; Stenzel, M. H. *Macromolecules* **2009**, *42*, 9422−9434.

Serajuddin, A. T. M. *J. Pharm. Sci.* **1999**, *88*, 1058–1066.

Leuner, C.; Dressman, J. *Eur. J. Pharm. Biopharm.* **2000**, *50*, 47–60.

Lipinski, C. A. *J. Pharmacol. Toxicol. Methods* **2000**, *44*, 235–249.

Qian, F.; Huang, J.; Hussain, M. A. *J. Pharm. Sci.* **2010**, *99*, 2941–2947.

Ormes, J. D.; Zhang, D.; Chen, A. M.; Hou, S.; Krueger, D.; Nelson, T.; Templeton, A.

Pharm. Dev. Technol. **2013**, *18*, 121–129.

Vasconcelos, T.; Sarmento, B.; Costa, P. *Drug Discov. Today* **2007**, *12*, 1068–1075.

Van den Mooter, G.; Weuts, I.; De Ridder, T.; Blaton, N. *Int. J. Pharm.* **2006**, *316*, 1–6.

Chauhan, B.; Shimpi, S.; Paradkar, A. *Eur. J. Pharm. Sci.* **2005**, *26*, 219–230.

Mizuno, M.; Hirakura, Y.; Yamane, I.; Miyanishi, H.; Yokota, S.; Hattori, M.; Kajiyama, A. *Int. J. Pharm.* **2005**, *305*, 37–51.

Rizi, K.; Green, R. J.; Donaldson, M.; Williams, A. C. *J. Pharm. Sci.* **2010**, *100*, 566–579.

Al-Obaidi, H.; Brocchini, S.; Buckton, G. *J. Pharm. Sci.* **2009**, *98*, 4724–4737.

Uchiyama, H.; Tozuka, Y.; Imono, M.; Takeuchi, H. *Eur. J. Pharm. Biopharm.* **2010**, *76*, 238–244.

Friesen, D. T.; Shanker, R.; Crew, M.; Smithey, D. T.; Curatolo, W. J.; Nightingale, J. A. S. *Mol. Pharm.* **2008**, *5*, 1003–1019.

Miller, J. M.; Beig, A.; Carr, R. A.; Spence, J. K.; Dahan, A. *Mol. Pharm.* **2012**, *9*, 2009–2016.

Qi, S.; Roser, S.; Edler, K. J.; Pigliacelli, C.; Rogerson, M.; Weuts, I.; Dycke, F.; Stokbroekx, S. *Pharm. Res*. **2012**, *30*, 290–302.

Peppas, N. A. *Hydrogels in Medicine and Pharmacy: Polymers*; CRC, 1987; Vol. 2.

Bergbreiter, D. E.; Zhang, L.; Mariagnanam, V. M. *J. Am. Chem. Soc.* **1993**, *115*, 9295–9296.

Liu, S.; Tong, Y.; Yang, Y. *Biomaterials* **2005**, *26*, 5064–5074.

Yin, L.; Dalsin, M. C.; Sizovs, A.; Reineke, T. M.; Hillmyer, M. A. *Macromolecules* **2012**, *45*, 4322–4332.

Chu, B. *Laser Light Scattering: Basic Principles and Practice*; 2nd ed. Academic Press:

Boston, 1991.

Shibayama, M.; Karino, T.; Okabe, S. *Polymer* **2006**, *47*, 6446–6456.

Trasi, N. S.; Taylor, L. S. *Cryst. Eng. Comm.* **2012**, *14*, 5188–5197.

Paudel, A.; Mooter, G. *Pharm. Res.* **2011**, *29*, 251–270.

Guns, S.; Dereymaker, A.; Kayaert, P.; Mathot, V.; Martens, J. A.; Mooter, G. *Pharm. Res.* **2010**, *28*, 673–682.

Janssens, S.; De Zeure, A.; Paudel, A.; Van Humbeeck, J.; Rombaut, P.; Van den Mooter, G. *Pharm. Res.* **2010**, *27*, 775–785.

Zhou, D.; Zhang, G. G. Z.; Law, D.; Grant, D. J. W.; Schmitt, E. A. *J. Pharm. Sci.* **2002**, *91*, 1863–1872.

Angell, C. A. *Science* **1995**, *267*, 1924–1935.

Graeser, K. A.; Patterson, J. E.; Zeitler, J. A.; Gordon, K. C.; Rades, T. *Eur. J. Pharm. Sci.* **2009**, *37*, 492–498.

Hancock, B. C.; Shamblin, S. L.; Zografi, G. *Pharm. Res.* **1995**, *12*, 799–806.

Taylor, L. S.; Zografi, G. *Pharm. Res.* **1997**, *14*, 1691–1698.

Ivanisevic, I.; Bates, S.; Chen, P. *J. Pharm. Sci.* **2009**, *98*, 3373–3386.

Newman, A.; Engers, D.; Bates, S.; Ivanisevic, I.; Kelly, R. C.; Zografi, G. *J. Pharm. Sci.* **2008**, *97*, 4840–4856.

Baird, J. A.; Taylor, L. S. *Adv. Drug Deliv. Rev.* **2012**, *64*, 396–421.

Thybo, P.; Pedersen, B. L.; Hovgaard, L.; Holm, R.; Müllertz, A. *Pharm. Dev. Technol.* **2008**, *13*, 375–386.

Wegiel, L. A.; Mauer, L. J.; Edgar, K. J.; Taylor, L. S. *J. Pharm. Sci.* **2012**, *102*, 171–184.

Willart, J. F.; Descamps, M. *Mol. Pharm.* **2008**, *5*, 905–920.

Caron, V.; Tajber, L.; Corrigan, O. I.; Healy, A. M. *Mol. Pharm.* **2011**, *8*, 532–542.

Gerber, J. J.; Caira, M. R.; Lotter, A. P. *J. Crystallogr. Spectrosc. Res.* **1993**, *23*, 863–869.

Clas, S.-D.; Faizer, R.; O'Connor, R. E.; Vadas, E. B. *Int. J. Pharm.* **1995**, *121*, 73–79.

de Villiers, M. M.; Wurster, D. E.; Van der Watt, J. G.; Ketkar, A. *Int. J. Pharm.* **1998**, *163*, 219–224.

Sauer, B. B.; Kampert, W. G.; Neal Blanchard, E.; Threefoot, S. A.; Hsiao, B. S. *Polymer* **2000**, *41*, 1099–1108.

McPhillips, H.; Craig, D. Q.; Royall, P. G.; Hill, V. L. *Int. J. Pharm.* **1999**, *180*, 83–90.

Gupta, P.; Kakumanu, V. K.; Bansal, A. K. *Pharm. Res.* **2004**, *21*, 1762–1769.

Ambike, A. A.; Mahadik, K. R.; Paradkar, A. *Pharm. Res.* **2005**, *22*, 990–998.

Bhattacharya, S.; Suryanarayanan, R. *J. Pharm. Sci.* **2009**, *98*, 2935–2953.

Vasanthavada, M.; Tong, W.-Q.; Joshi, Y.; Kislalioglu, M. S. *Pharm. Res.* **2004**, *21*, 1598–1606.

Khougaz, K.; Clas, S.-D. *J. Pharm. Sci.* **2000**, *89*, 1325–1334.

Marsac, P. J.; Rumondor, A. C. F.; Nivens, D. E.; Kestur, U. S.; Stanciu, L.; Taylor, L. S. *J. Pharm. Sci.* **2010**, *99*, 169–185.

Gupta, P.; Bansal, A. K. *J. Pharm. Pharmacol.* **2005**, *57*, 303–310.

Kalaiselvan, R.; Mohanta, G. P.; Manna, P. K.; Manavalan, R. *Pharmazie* **2006**, *61*, 618–624.

Albers, J.; Alles, R.; Matthée, K.; Knop, K.; Nahrup, J. S.; Kleinebudde, P. *Eur. J. Pharm. Biopharm.* **2009**, *71*, 387–394.

Marsac, P. J.; Shamblin, S. L.; Taylor, L. S. *Pharm. Res.* **2006**, *23*, 2417–2426.

Forster, A.; Hempenstall, J.; Tucker, I.; Rades, T. *Int. J. Pharm.* **2001**, *226*, 147–161.

Sun, Y.; Tao, J.; Zhang, G. G. Z.; Yu, L. *J. Pharm. Sci.* **2010**, *99*, 4023–4031.

Craig, D. Q. M. *Int. J. Pharm.* **2002**, *231*, 131–144.

Bhandari, B. R.; Howes, T. *J. Food Eng.* **1999**, *40*, 71–79.

Zipp, G. L.; Rodriguez-Hornedo, N. *Int. J. Pharm.* **1993**, *98*, 189–201.

Dubois, J.-L.; Ford, J. L. *J. Pharm. Pharmacol.* **2011**, *37*, 494–495.

Ilevbare, G. A.; Liu, H.; Edgar, K. J.; Taylor, L. S. *Cryst. Growth Des.* **2012**, *12*, 3133–3143.

Gaucher, G.; Satturwar, P.; Jones, M. C.; Furtos, A.; Leroux, J. C. *Eur. J. Pharm. Biopharm.* **2010**, *76*, 147-158.

Delie, F.; Blanco-Prieto, M. J. *Molecules* **2005**, *10*, 65-80.

Shaji, J.; Patole, V. *Indian J Pharm Sci* **2008**, *70*, 269-277.

Hauss, D. J. *Adv. Drug Del. Rev.* **2007**, *59*, 667-676.

Lipinski, C. A. *J. Pharmacol. Toxicol. Methods* **2000**, *44*, 235-249.

Lipp, R. *The Innovator Pipeline: Bioavailability Challenges and Advanced Oral Drug Delivery Opportunities*, 2013.

Ting, J. M.; Navale, T. S.; Bates, F. S.; Reineke, T. M. *Macromolecules* **2014**, *47*, 6554-6565.

Wilson, M.; Williams, M. A.; Jones, D. S.; Andrews, G. P. *Ther. Deliv.* **2012**, *3*, 787-797.

Paudel, A.; Worku, Z. A.; Meeus, J.; Guns, S.; Van den Mooter, G. *Int. J. Pharm.* **2013**, *453*, 253-284.

Loftsson, T.; Brewster, M.; Másson, M. *Am. J. Drug Deliv.* **2004**, *2*, 261-275.

Dalsin, M. C.; Tale, S.; Reineke, T. M. *Biomacromolecules* **2013**, *15*, 500-511.

Ormes, J. D.; Zhang, D.; Chen, A. M.; Hou, S.; Krueger, D.; Nelson, T.; Templeton, A. *Pharm. Dev. Technol.* **2013**, *18*, 121-129.

Huang, Y.; Dai, W. G. *Acta Pharm. Sin. B* **2014**, *4*, 18-25.

Yin, L. G.; Hillmyer, M. A. *Mol. Pharm.* **2014**, *11*, 175-185.

Friesen, D. T.; Shanker, R.; Crew, M.; Smithey, D. T.; Curatolo, W. J.; Nightingale, J. A. *Mol. Pharm.* **2008**, *5*, 1003-1019.

Tanno, F.; Nishiyama, Y.; Kokubo, H.; Obara, S. *Drug Dev. Ind. Pharm.* **2004**, *30*, 9-17.

Mundargi, R. C.; Rangaswamy, V.; Aminabhavi, T. M. *J. Appl. Polym. Sci.* **2011**, *122*, 2244-2251.

Liu, S. Q.; Tong, Y. W.; Yang, Y. Y. *Biomaterials* **2005**, *26*, 5064-5074.

Yeh, J. C.; Hsu, Y. T.; Su, C. M.; Wang, M. C.; Lee, T. H.; Lou, S. L. *J. Biomater. Appl.* **2014**, *29*, 442-453.

Ohtake, S.; Wang, Y. J. *J. Pharm. Sci.* **2011**, *100*, 2020-2053.

Yamashita, S.; Matsuzawa, Y. *Atherosclerosis* **2009**, *207*, 16-23.

Sizovs, A.; Xue, L.; Tolstyka, Z. P.; Ingle, N. P.; Wu, Y.; Cortez, M.; Reineke, T. M. *J. Am. Chem. Soc.* **2013**, *135*, 15417-15424.

Xu, X.; Smith, A. E.; Kirkland, S. E.; McCormick, C. L. *Macromolecules* **2008**, *41*, 8429-8435.

Tale, S. R.; Yin, L.; Reineke, T. M. *Polym. Chem.* **2014**, *5*, 5160-5167.

Qian, F.; Huang, J.; Hussain, M. A. *J. Pharm. Sci.* **2010**, *99*, 2941-2947.

Uchiyama, H.; Tozuka, Y.; Imono, M.; Takeuchi, H. *Eur. J. Pharm. Biopharm.* **2010**, *76*, 238-244.

Baird, J. A.; Taylor, L. S. *Adv. Drug Del. Rev.* **2012**, *64*, 396-421.

Yin, L.; Dalsin, M. C.; Sizovs, A.; Reineke, T. M.; Hillmyer, M. A. *Macromolecules* **2012**, *45*, 4322-4332.

Sauer, B. B.; Kampert, W. G.; Neal Blanchard, E.; Threefoot, S. A.; Hsiao, B. S. *Polymer* **2000**, *41*, 1099-1108.

McPhillips, H.; Craig, D. Q.; Royall, P. G.; Hill, V. L. *Int. J. Pharm.* **1999**, *180*, 83-90.

Gupta, P.; Bansal, A. K. *J. Pharm. Pharmacol.* **2005**, *57*, 303-310.

Kalaiselvan, R.; Mohanta, G. P.; Manna, P. K.; Manavalan, R. *Die Pharmazie* **2006**, *61*, 618-624.

Albers, J.; Alles, R.; Matthee, K.; Knop, K.; Nahrup, J. S.; Kleinebudde, P. *Eur. J. Pharm. Biopharm.* **2009**, *71*, 387-394.

Gupta, P.; Kakumanu, V. K.; Bansal, A. K. *Pharm. Res.* **2004**, *21*, 1762-1769.

Vasanthavada, M.; Tong, W. Q.; Joshi, Y.; Kislalioglu, M. S. *Pharm. Res.* **2004**, *21*, 1598-1606.

Tale, S. R.; Yin, L.; Reineke, T. M. *Poly Chem* **2014**, *5*, 5160-5167.

Lindenberg, M.; Kopp, S.; Dressman, J. *Eur. J. Pharm. Biopharm.* **2004**, *58*, 265-278.

Leuner, C.; Dressman, J. *Eur. J. Pharm. Biopharm.* **2000**, *50*, 47-60.

Vasconcelos, T.; Sarmento, B.; Costa, P. *Drug Discovery Today* **2007**, *12*, 1068-1075.

Rodier, E.; Lochard, H.; Sauceau, M.; Letourneau, J.; Freiss, B.; Fages, J. *Eur. J. Pharm. Sci.* **2005**, *26*, 184-193.

Loftsson, T.; Brewster, M. *J. Pharm. Sci.* **2012**, *101*, 3019-3032.

Konno, H.; Taylor, L. *J. Pharm. Sci.* **2006**, *95*, 2692-2705.

Won, D.; Kim, M.; Lee, S.; Park, J.; Hwang, S. *Int. J. Pharm.* **2005**, *301*, 199-208.

Ohara, T.; Kitamura, S.; Kitagawa, T.; Terada, K. *Int. J. Pharm.* **2005**, *302*, 95-102.

Friesen, D.; Shanker, R.; Crew, M.; Smithey, D.; Curatolo, W.; Nightingale, J. *Mol. Pharm.* **2008**, *5*, 1003-1019.

Desai, J.; Alexander, K.; Riga, A. *Int. J. Pharm.* **2006**, *308*, 115-123.

Urbanetz, N. *Eur. J. Pharm. Sci.* **2006**, *28*, 67-76.

Huang, J.; Wigent, R.; Bentzley, C.; Schwartz, J. *Int. J. Pharm.* **2006**, *319*, 44-54.

Shamma, R.; Basha, M. *Powder Technol.* **2013**, *237*, 406-414.

Di Martino, P.; Joiris, E.; Gobetto, R.; Masic, A.; Palmieri, G.; Martelli, S. *J. Cryst. Growth* **2004**, *265*, 302-308.

Tantishaiyakul, V.; Kaewnopparat, N.; Ingkatawornwong, S. *Int. J. Pharm.* **1999**, *181*, 143-151.

Zhang, X.; Sun, N.; Wu, B.; Lu, Y.; Guan, T.; Wu, W. *Powder Technol.* **2008**, *182*, 480-485.

Paradkar, A.; Ambike, A.; Jadhav, B.; Mahadik, K. *Int. J. Pharm.* **2004**, *271*, 281-286.

Thybo, P.; Pedersen, B.; Hovgaard, L.; Holm, R.; Mullertz, A. *Pharm. Dev. Technol.* **2008**, *13*, 375-386.

Nair, R.; Gonen, S.; Hoag, S. *Int. J. Pharm.* **2002**, *240*, 11-22.

Miller, D.; DiNunzio, J.; Yang, W.; McGinity, J.; Williams, R. *Drug Dev. Ind. Pharm.* **2008**, *34*, 890-902.

Vasanthavada, M.; Tong, W.; Joshi, Y.; Kislalioglu, M. *Pharm. Res.* **2005**, *22*, 440-448.

Bühler, V.; SpringerLink (Online service); Springer-Verlag Berlin Heidelberg: Berlin, Heidelberg, 2005.

Sekikawa, H.; Fujiwara, J.; Naganuma, T.; Nakano, M.; Arita, T. *Chem. Pharm. Bull.* **1978**, *26*, 3033-3039.

Yakou, S.; Yamazaki, S.; Sonobe, T.; Nagai, T.; Sugihara, M. *Chem. Pharm. Bull.* **1986**, *34*, 3408-3414.

Jachowicz, R. *Int. J. Pharm.* **1987**, *35*, 7-12.

Franco, M.; Trapani, G.; Latrofa, A.; Tullio, C.; Provenzano, M.; Serra, M.; Muggironi, M.; Biggio, G.; Liso, G. *Int. J. Pharm.* **2001**, *225*, 63-73.

Nam, I.; Bae, J.; Jee, K.; Lee, J.; Park, K.; Yuk, S. *Mol. Res.* **2002**, *10*, 115-121.

Dincer, S.; Rzaev, Z.; Piskin, E. *J. Polym. Res.* **2006**, *13*, 121-131.

Roy, D.; Brooks, W.; Sumerlin, B. *Chem. Soc. Rev.* **2013**, *42*, 7214-7243.

Ormes, J.; Zhang, D.; Chen, A.; Hou, S.; Krueger, D.; Nelson, T.; Templeton, A. *Pharm. Dev. Technol.* **2013**, *18*, 121-129.

Van den Mooter, G.; Wuyts, M.; Blaton, N.; Busson, R.; Grobet, P.; Augustijns, P.; Kinget, R. *Eur. J. Pharm. Sci.* **2001**, *12*, 261-269.

Zipp, G.; Rodriguezhornedo, N. *J. Phys. D: Appl. Phys* **1993**, *26*, B48-B55.

Bull, A. T.; Ward, A. C.; Goodfellow, M. *Microbiol. Mol. Biol. Rev.* **2000**, *64*, 573-606.

Grosdidier, S.; Totrov, M.; Fernandez-Recio, J. *Adv. Appl. Bioinform. Chem.* **2009**, *2*, 101-123.

Baltes, N. J.; Voytas, D. F. *Trends in Biotechnology, ASAP*

Szymanski, P.; Markowicz, M.; Mikiciuk-Olasik, E. *Int. J. Mol. Sci.* **2012**, *13*, 427-452.

Basavaraj, S.; Betageri, G. V. *Acta Pharm. Sin. B* **2014**, *4*, 3-17.

Hoelder, S.; Clarke, P. A.; Workman, P. *Mol. Oncol.* **2012**, *6*, 155-176.

Rosen, H.; Abribat, T. *Nat. Rev. Drug. Discov.* **2005**, *4*, 381-385.

Lipinski, C. A.; Lombardo, F.; Dominy, B. W.; Feeney, P. J. *Adv.Drug Deliv. Rev.* **2001**, *46*, 3-26.

Prentis, R. A.; Lis, Y.; Walker, S. R. *Br. J. Clin. Pharmacol.* **1988**, *25*, 387-396.

Stegemann, S.; Leveiller, F.; Franchi, D.; de Jong, H.; Linden, H. *Eur. J. Pharm. Sci.* **2007**, *31*, 249-261.

Strickley, R. G. *Pharm. Res.* **2004**, *21*, 201-230.

Loftsson, T.; Brewster, M.; Másson, M. *Am. J. Drug. Deliv.* **2004**, *2*, 261-275.

Loftsson, T.; Brewster, M. E. *J. Pharm. Sci.* **2012**, *101*, 3019-3032.

Serajuddin, A. T. *Adv.Drug Deliv. Rev.* **2007**, *59*, 603-616.

Leuner, C.; Dressman, J. *Eur. J. Pharm. Biopharm.* **2000**, *50*, 47-60.

Vasconcelos, T.; Sarmento, B.; Costa, P. *Drug Discov. Today* **2007**, *12*, 1068-1075.

Sareen, S.; Mathew, G.; Joseph, L. *Int. J. Pharm. Investig.* **2012**, *2*, 12-17.

Huang, Y.; Dai, W.-G. *Acta Pharm. Sin. B* **2014**, *4*, 18-25.

Re, M. I. *Drying Technol.* **2006**, *24*, 433-446.

Vehring, R. *Pharm. Res.* **2008**, *25*, 999-1022.

Hughey, J. R.; Keen, J. M.; Brough, C.; Saeger, S.; McGinity, J. W. *Int. J. Pharm.* **2011**, *419*, 222-230.

Ormes, J. D.; Zhang, D.; Chen, A. M.; Hou, S.; Krueger, D.; Nelson, T.; Templeton, A. *Pharm. Dev. Technol.* **2013**, *18*, 121-129.

Friesen, D. T.; Shanker, R.; Crew, M.; Smithey, D. T.; Curatolo, W. J.; Nightingale, J. A. *Mol. Pharm.* **2008**, *5*, 1003-1019.

Yin, L.; Hillmyer, M. A. *Mol. Pharm.* **2014**, *11*, 175-185.

Tanno, F.; Nishiyama, Y.; Kokubo, H.; Obara, S. *Drug Dev. Ind. Pharm.* **2004**, *30*, 9-17.

Rumondor, A. C.; Stanford, L. A.; Taylor, L. S. *Pharm. Res.* **2009**, *26*, 2599-2606.

Tajarobi, F.; Larsson, A.; Matic, H.; Abrahmsen-Alami, S. *Eur. J. Pharm. Biopharm.* **2011**, *78*, 125-133.

Qian, F.; Wang, J.; Hartley, R.; Tao, J.; Haddadin, R.; Mathias, N.; Hussain, M. *Pharm. Res.* **2012**, *29*, 2765-2776.

Ting, J. M.; Navale, T. S.; Bates, F. S.; Reineke, T. M. *ACS Macro Letters* **2013**, *2*, 770-774.

Islam, M. R.; Ahiabu, A.; Li, X.; Serpe, M. J. *Sensors* **2014**, *14*, 8984-8995.

Ward, M. A.; Georgiou, T. K. *Polymers* **2011**, *3*, 1215-1242.

Messing, R.; Schmidt, A. M. *Polym. Chem.* **2011**, *2*, 18-32.

Dalsin, M. C.; Tale, S.; Reineke, T. M. *Biomacromolecules* **2014**, *15*, 500-511.

Ting, J. M.; Navale, T. S.; Bates, F. S.; Reineke, T. M. *Macromolecules* **2014**, *47*, 6554-6565.

Nokhodchi, A.; Bolourtchian, N.; Dinarvand, R. *Int. J. Pharm.* **2003**, *250*, 85-97.

Zipp, G. L.; Rodriguezhornedo, N. *J. Phys. D: Appl. Phys.* **1993**, *26*, B48-B55.

Warren, D. B.; Bergstrom, C. A. S.; Benameur, H.; Porter, C. J. H.; Pouton, C. W. *Mol. Pharm.* **2013**, *10*, 2823-2848.

Schmatloch, S.; Meier, M. A. R.; Schubert, U. S. *Macromol. Rapid Commun.* **2003**, *24*, 33-46.

Barillaro, V.; Pescarmona, P. P.; Van Speybroeck, M.; Do Thi, T.; Van Humbeeck, J.; Vermant, J.; Augustijns, P.; Martens, J. A.; Van Den Mooter, G. *J. Comb. Chem.* **2008**, *10*, 637-643.

Xu, X. W.; Smith, A. E.; Kirkland, S. E.; McCormick, C. L. *Macromolecules* **2008**, *41*, 8429-8435.

Bauri, K.; Roy, S. G.; Arora, S.; Dey, R. K.; Goswami, A.; Madras, G.; De, P. *J. Therm. Anal. Calorim.* **2013**, *111*, 753-761.

Deng, K. L.; Tian, H.; Zhang, P. F.; Ren, X. B.; Zhong, H. B. *Express Polym. Lett.* **2009**, *3*, 97-104.

Gupta, P.; Kakumanu, V. K.; Bansal, A. K. *Pharm. Res.* **2004**, *21*, 1762-1769.

Miller, J. M.; Beig, A.; Carr, R. A.; Spence, J. K.; Dahan, A. *Mol. Pharm.* **2012**, *9*, 2009-2016.

Hancock, B. C.; Parks, M. *Pharm. Res.* **2000**, *17*, 397-404.

Vandecruys, R.; Peeters, J.; Verreck, G.; Brewster, M. E. *Int. J. Pharm.* **2007**, *342*, 168-175.

Yamashita, T.; Ozaki, S.; Kushida, I. *Int. J. Pharm.* **2011**, *419*, 170-174.